LAKE SEDIMENT RECORDS EXAMINING THE SPATIAL AND TEMPORAL CONNECTIONS OF HUMAN ACTIVITY AND CLIMATE CHANGE IN SOUTHWESTERN CHINA

by

Aubrey L. Hillman

B.S., University of Maryland Baltimore County, 2009

B.A., University of Maryland Baltimore County, 2009

M.S., University of Pittsburgh, 2011

Submitted to the Graduate Faculty of the

Kenneth P. Dietrich School of Arts and Sciences in partial fulfillment

of the requirements for the degree of

Doctor of Philosophy

University of Pittsburgh

2015

UNIVERSITY OF PITTSBURGH

DIETRICH SCHOOL OF ARTS AND SCIENCES

This thesis was presented

by

Aubrey L. Hillman

It was defended on

March 27, 2015

and approved by

Daniel Bain, Ph.D., Assistant Professor, Geology and Planetary Science

Emily Elliott Ph.D., Associate Professor, Geology and Planetary Science

Brian Stewart, Ph.D., Associate Professor, Geology and Planetary Science

Loukas Barton, Ph.D., Assistant Professor, Anthropology

Dissertation Director: Mark Abbott, Ph.D., Professor and Chair, Geology and Planetary Science

LAKE SEDIMENT RECORDS EXAMINING THE SPATIAL AND TEMPORAL CONNECTIONS OF HUMAN ACTIVITY AND CLIMATE CHANGE IN SOUTHWESTERN CHINA

Aubrey Hillman, Ph.D.

University of Pittsburgh, 2015

In regions of the world with long histories of human occupation, both natural environmental change and anthropogenic activities have impacted lake sediment dynamics over several millennia. The Yunnan Plateau of southwestern China is primarily impacted by the Indian Summer Monsoon (ISM) whose variability controls hydrologic balance. Despite the importance of the ISM as a critical water resource, we lack continuous terrestrial records of the ISM over a wide enough spatial gradient to understand its variability over multi-decadal time scales. Yunnan also has an extensive history of settlement, agriculture, and mineral resource extraction next to lakes, creating challenges in separating the impacts of recent disturbance from earlier activities. This dissertation will 1) establish records of anthropogenic impacts to lake sediment dynamics, 2) create records of hydrologic balance from lakes to understand ISM variability over the Holocene/Pleistocene, and 3) examine the intersection between climate variability and human activity around lakes to examine societal responses to changing water availability.

Utilizing a multi-proxy approach, including sedimentology and stratigraphy, stable isotopes of authigenic carbonate minerals and organic matter, and trace element geochemistry, this research characterizes the nature, timing, and magnitude of both anthropogenic disturbance and climate variability to four lakes in Yunnan: Xing Yun, Erhai, Chenghai, and Dian. Results

show that prior to ~2,000 years BP, shifts in hydrologic balance are generally in phase with insolation forcing. Several abrupt drops in ISM strength are inferred over the Holocene and agree with other records of ISM variability from the Tibetan Plateau. Over the last 2,000 years, records of climatic change are overwritten by pre-industrial human activities including soil erosion, eutrophication, heavy metal pollution, and hydrologic modification. The scale of such activities is either equal or greater than modern-day impacts, suggestive of a several millenia legacy that likely contributes to contemporary environmental challenges.

TABLE OF CONTENTS

PREFACE XXVII

1.0 INTRODUCTION 1

1.1 OBJECTIVES 1

1.1.1 Research Aims 1

1.1.2 Research Questions 4

1.1.3 Hypotheses 6

1.2 REGIONAL SETTING 7

1.2.1 Geology 7

1.2.2 Climate 10

1.3 HUMAN HISTORY OF THE YUNNAN PROVINCE 18

1.4 LACUSTRINE SEDIMENTS AS ENVIRONMENTAL ARCHIVES 22

2.0 XING YUN LAKE 28

2.1 REGIONAL SETTING 29

2.2 MATERIALS AND METHODS 31

2.2.1 Core collection 31

2.2.2 Age Control 31

2.2.3 Geochemistry 32

2.3 RESULTS AND DISCUSSION 34

2.3.1 Core Chronology 34

2.3.2 Sedimentology 37

2.3.3 Geochemistry 44

2.3.3.1 Unit I- Pre-human disturbance 44

2.3.3.2 Transition period 46

2.3.3.3 Unit II- Intensive human disturbance.. 51

2.4 CONCLUSION 57

3.0 XING YUN LAKE- LONG CORE.. 58

3.1 BACKGROUND 60

3.1.1 Regional Setting 60

3.1.2 Previous Paleoclimate Studies 62

3.2 MATERIALS AND METHODS 66

3.2.1 Core collection.. 66

3.2.2 Age Control 66

3.2.3 Geochemistry 67

3.3 RESULTS.. 69

3.3.1 Core Chronology.. 69

3.3.2 Sedimentology and Geochemistry 73

3.3.2.1 Unit I- >50 to 42 ka 76

3.3.2.2 Unit II- 42 to 33 ka.. 76

3.3.2.3 Unit III- 33 to 17 ka 77

3.3.2.4 Unit IV- 7.8 to 1.5 ka.. 77

3.3.2.4.1 Subunit I- 7.8 to 6.6 ka.. 79

3.3.2.4.2 Subunit II- 6.6 to 4.7 ka ... 81
3.3.2.4.3 Subunit III- 4.7 to 2.95 ka ... 81
3.3.2.4.4 Subunit IV- 2.95 to 1.5 ka ... 82
3.4 DISCUSSION ... 82
3.4.1 Unit I- >50 to 42 ka ... 82
3.4.2 Unit II- 42 to 33 ka ... 84
3.4.3 Unit III- 33 to 17 ka ... 85
3.4.4 Unit IV- 7.8 to 1.5 ka ... 89
3.4.4.1 Subunit I- 7.8 to 6.6 ka ... 93
3.4.4.2 Subunit II- 6.6 to 4.7 ka ... 96
3.4.4.3 Subunit III- 4.7 to 2.95 ka ... 97
3.4.4.4 Subunit IV- 2.95 to 1.5 ka ... 99
3.5 CONCLUSION ... 100
4.0 ERHAI LAKE ... 103
4.1 REGIONAL SETTING ... 105
4.2 ARCHAEOLOGICAL AND HISTORICAL CONTEXT ... 108
4.3 MATERIALS AND METHODS ... 110
4.3.1 Core Collection ... 110
4.3.2 Age Control ... 112
4.3.3 Geochemistry ... 113
4.4 RESULTS ... 115
4.5 DISCUSSION ... 119

4.5.1 Early Metallurgy ... 120
4.5.2 Peak in Lead Pollution ... 123
4.5.3 Modern Pollution ... 129
4.6 CONCLUSIONS ... 129
5.0 DIAN LAKE ... 131
5.1 REGIONAL SETTING ... 134
5.2 MATERIALS AND METHODS ... 138
5.2.1 Core Collection ... 138
5.2.2 Age Control ... 139
5.2.3 Geochemistry ... 139
5.3 RESULTS ... 142
5.3.1 Geochronology and Sedimentology of Transect Cores ... 142
5.3.2 Geochemistry of A-12 Cores ... 151
5.3.2.1 Unit I- 17-8.5 ka ... 153
5.3.2.2 Unit II- 8.5 to 4 ka ... 153
5.3.2.3 Unit III- 4 to 2 ka ... 154
5.3.2.4 Unit IV- 2 ka to present ... 156
5.4 DISCUSSION ... 158
5.4.1 Geochronology and Sedimentology of Transect Cores ... 158
5.4.2 Geochemistry of A-12 Cores ... 162
5.4.2.1 Unit I- Late Pleistocene and Pleistocene-Holocene transition ... 162
5.4.2.2 Unit II- Early to Middle Holocene ... 166

5.4.2.3 Unit III- Middle to Late Holocene lake level changes 168

5.4.2.4 Unit IV- Late Holocene intensive human disturbance 170

5.5 CONCLUSIONS 172

6.0 CHENGHAI LAKE 175

6.1 REGIONAL SETTING.. 176

6.2 MATERIALS AND METHODS 182

6.2.1 Core Collection 182

6.2.2 Age Control 182

6.2.3 Geochemistry 183

6.3 RESULTS 185

6.3.1 Geochronology 185

6.3.2 Geochemistry 187

6.3.2.1 Unit I- 1150-1360 AD 190

6.3.2.2 Unit II- 1360-1700 AD 194

6.3.2.3 Unit III- 1700 AD-present 194

6.4 DISCUSSION 195

6.4.1 Isotopic Interpretation 195

6.4.2 Unit I- Anthropogenic Disturbance 197

6.4.3 Unit II- Landscape Stability 200

6.4.4 Unit III- Hydrologic modification 203

6.5 CONCLUSION 207

7.0 CONCLUSIONS 209

7.1 THE NATURE OF ANTHROPOGENIC IMPACTS TO YUNNAN LAKES 209

7.2 ISM VARIABILITY RECORDED IN YUNNAN LAKES 214

7.3 LINKING HUMAN AND ENVIRONMENTAL CHANGE 216

BIBLIOGRAPHY 219

LIST OF TABLES

Table 1-1- Lakes selected for study 4

Table 1-2- Monthly average temperature, precipitation, oxygen isotope values, and deuterium values from 1986-2003 at Kunming GNIP station (25°1’N, 102°40’E, 1892 m) (IAEA/WMO, 2014). 12

Table 2-1- AMS Radiocarbon Dates for samples from Xing Yun 35

Table 2-2- Down-core ^{210}Pb activities, ^{214}Pb activities, cumulative weight flux, and constant rate of supply (CRS) sediment ages. 36

Table 2-3- Monthly average temperature, precipitation, and oxygen isotope values at Dongge Cave (25°17’N, 108°50’E, 680 m) (Dykoski et al., 2005).. 42

Table 3-1- AMS Radiocarbon Dates for samples from Xing Yun 72

Table 3-2- Spearman rho correlation coefficients between July insolation at 20°N and metal concentrations. Metal concentrations were linearly interpolated at 1,000 year time steps before calculating a correlation coefficient. Coefficients that are statistically significant ($p < 0.05$) are highlighted in bold. 83

Table 4-1- Ore bodies of northwestern Yunnan displayed in Figure 4-1 (Hou et al., 2007; Bureau of Geology and Mineral Resources of Yunnan Province, 1990). 105

Table 4-2- AMS radiocarbon dates for samples from Erhai Cores A-09 and C-12. 112

Table 4-3- Down-core ^{210}Pb activities, ^{214}Pb activities, cumulative weight, and CRS sediment ages from Core A-09. 113

Table 4-4- Pearson product-moment correlation coefficient between metals and reference factors over the pre-pollution time period (2700 BC-200 AD) (185-254 cm). The high correlation coefficients between Al, Mg, organic matter and metals of interest demonstrates that Al, Mg, and organic matter are appropriate reference factors from which to calculate EFs as they can explain some component of weathering. 120

Table 5-1- Core collection details 138

Table 5-2- AMS radiocarbon dates for samples from Dian cores 143

Table 6-1- Monthly average temperature, precipitation, and oxygen isotope values at Lijiang (26°53'N, 100°14'E, 2400 m) 178

Table 6-2- AMS radiocarbon dates for samples from Chenghai Core A-12. 186

Table 6-3- Down-core ^{210}Pb activities, ^{214}Pb activities, cumulative weight, and CRS sediment ages from Chenghai Core A-12. 186

Table 6-4- Monthly average temperature, precipitation, and oxygen isotope values at Dongge Cave (25°17'N, 108°50'E, 680 m) (Dykoski et al., 2005) 196

LIST OF FIGURES

Figure 1-1- A- map of China with Yunnan highlighted. B- Lakes selected for study in the eastern half of Yunnan- Erhai and Chenghai. C- Lakes selected for study in the western half of Yunnan- Dian and Xing Yun. Geologic map adapted from Meng and Li, 1970 and fault map adapted from Wang et al., 1998. 3

Figure 1-2- The Asian Summer Monsoon system: ISM = Indian Summer Monsoon, EASM = East Asian Summer Monsoon. Numbered locations of paleoclimate records from China discussed in this dissertation. 11

Figure 1-3- Water isotope samples from selected lakes in Yunnan, groundwater from ~2 m deep next to Dian (orange triangle), precipitation collected from a rainstorm at Dian in August 2014 (pink triangle), the annual weighted mean of modern rainfall for Kunming from GNIP station data (blue diamond). GMWL = Global Meteoric Water Line. LEL = Local Evaporation Line. 17

Figure 1-4- All known ore deposits in Yunnan (Kamitani et al., 2007) with place names mentioned in this chapter. 19

Figure 2-1- A- Locations of Xing Yun Lake (star), Dongge Cave (diamond); B- Yunnan lakes near Kunming; C- Xing Yun Lake (1721 m elevation) with 200 m contour intervals. Coring location in this study is marked by the circle. Coring location from Hodell et al., 1999 is marked X. 30

Figure 2-2- Age-depth model and 95% confidence intervals. ^{210}Pb (green circles), radiocarbon (red squares), gastropod shell dates (blue triangles), all with 2 sigma error bars. Gastropod shell dates exhibit a relatively consistent 1,100 year offset from terrestrial macrofossils and were excluded from the age model. ^{210}Pb age model detail is displayed in the inset...... 37

Figure 2-3- Proxies by depth. A- Weight percent organic matter (green circles), calcium carbonate (blue solid line), and residual mineral matter (red dotted line); B- Percent organic carbon (blue solid line), percent organic nitrogen (black dotted line); C- Carbon to nitrogen ratio (blue solid line), nitrogen to phosphorus ratio (black dotted line); D- Carbon isotope values of organic matter (blue solid line), nitrogen isotope values of organic matter (black dotted line); E- Oxygen isotopic composition of Xing Yun calcite- Drive 1 (blue), Drive 2 (red), Drive 3 (green), Drive 4 (purple); F- Carbon isotopic composition of Xing Yun calcite- Drive 1 (blue), Drive 2 (red), Drive 3 (green), Drive 4 (purple); G- Concentration of phosphorus (blue solid line), aluminum (black dotted line); H- Concentration of lead (blue solid line) and mercury (black dotted line).. 38

Figure 2-4- A- Weight percent organic matter (green circles), calcium carbonate (blue solid line), and residual mineral matter (red dotted line); B- Percent organic carbon (blue solid line), percent organic nitrogen (black dotted line); C- Carbon to nitrogen ratio (blue solid line), nitrogen to phosphorus ratio (black dotted line); D- Carbon isotope values of organic matter (blue solid line), nitrogen isotope values of organic matter (black dotted line); E- Oxygen isotopic composition of Xing Yun calcite (blue solid line), Dongge Cave (green circles); F- Carbon isotopic composition of Xing Yun calcite; G- Concentration of phosphorus (blue solid line), aluminum (black dotted line); H- Concentration of lead (blue solid line) and mercury (black dotted line). The gray bar is the initiation of human disturbance on the lake; the dotted lines are the establishment and decline of the Nanzhao Kingdom; the white with gray bars are the establishment and decline of the Yuan Dynasty; the red bar is the establishment of the Ming and decline of the Qing Dynasty. 40

Figure 2-5- SEM image of euhedral calcite from Xing Yun A-09 D1 4 cm. 43

Figure 2-6- A- Hodell's original $\delta^{18}O$ record from 8,000 years BP to present based on bulk sediment radiocarbon dates and gastropod shell dates. B- Hodell's adjusted $\delta^{18}O$ record and our new, high-resolution $\delta^{18}O$ record (in blue) with an age model based on terrestrial macrofossils. Our record shows that Hodell's original record is offset by several thousand years and that the low resolution sampling overlooked several abrupt shifts in oxygen isotopes. 45

Figure 2-7- Oxygen isotopes of calcite plotted against A- phosphorus, B- aluminum, C- lead, and D- mercury. Twentieth century values have been removed as they are anomalously high in phosphorus. The time period from 1500 BC-500 AD is represented by red circles, 500-800 AD by purple diamonds, 800-1120 AD by blue squares, and 1120-1900 AD by green triangles. These plots demonstrate that the change in lake level from 500-800 AD did not cause a significant change in metal concentrations. Similarly, an increase in metals from 800-1120 AD occurred while $\delta^{18}O$ values were relatively stable at -7‰, indicating the increase in concentrations of metals is unrelated to lake level changes. 48

Figure 2-8- Lead isotopes of Xing Yun through time and relevant ore bodies in southwestern China. A- $^{206}Pb/^{204}Pb$ and $^{207}Pb/^{204}Pb$. B) $^{206}Pb/^{204}Pb$ and $^{208}Pb/^{204}Pb$. C) $^{207}Pb/^{204}Pb$ and $^{208}Pb/^{204}Pb$. Xing Yun lead isotopes change through time, but do not match the isotopic composition of any nearby ore bodies. 49

Figure 2-9- Total pollution inventories for A- phosphorus (P), B- lead (Pb), C- mercury (Hg). Total P, Pb, and Hg inventories were calculated as the product of dry sediment inventory (g/m^2) and element concentration (mg/g). Concentrations within core intervals lacking data were estimated using linear interpolation between measurements. Intervals were summed and divided by time period (in centuries). 55

Figure 2-10- Concentrations of fecal 5β-stanols from Xing Yun that increase in the uppermost sediments dating to 1940 AD. 56

Figure 3-1- Locations of paleoclimate records from Yunnan discussed in this chapter. Inset- locations of other paleoclimate records from China discussed in this chapter. G = Guilya ice cap, D = Dunde ice cap, AC = Ahung Co, PC = Paru Co Lake, DC = Dongge Cave, SC = Sanboa Cave, HC = Hulu Cave, TC = Tianmen Cave, MC = Mawmluh Cave. 59

Figure 3-2- Xing Yun Lake (1721 m elevation) with 200 m contour intervals. Coring location in this study is marked by the circle. Coring location from Hodell et al., 1999 is marked X. 61

Figure 3-3- Map of Xing Yun Lake (1721 m elevation) and Fuxian Lake (1723 m elevation) with 200 m contour intervals. Green shaded area is the surface area of Xing Yun if the lake were 25 m higher than present day. Purple shaded area is the surface area of Xing Yun and Fuxian if the Xing Yun were 100 m higher than present day. 65

Figure 3-4- Age-depth model with 95% confidence intervals. ^{210}Pb dates (green triangles), radiocarbon dates (blue circles), excluded radiocarbon dates (red squares), all with 2 sigma error bars. A hiatus was modeled at 512.5 cm. The age of the bottom 2.6 m of the record have been extrapolated assuming constant sedimentation rate. 71

Figure 3-5- MIS = Marine Isotope Stage; A) Weight percent organic matter (green circles) and carbonate (blue dotted line); Weak extractions in black solid circles (left axes) and strong extractions in red dotted squares (right axes): B) Magnesium concentration; C) Iron concentration; D) Titanium concentration; E) Average summer (June, July, and August) insolation at 20°N. After 50,000 years BP, sediment age is extrapolated back in time, assuming a constant sedimentation rate. Peaks in summer insolation correspond to increases in strongly bound lithogenic metals. 75

Figure 3-6- The Holocene portion of the record divided into four subunits. A) Weight percent organic matter (green circles) and carbonate (blue dotted line); B) Oxygen isotope values of carbonate with average summer insolation at 20°N; C) Carbon isotopes of carbonate; D) Carbon isotopes of organic matter; E) Nitrogen isotopes of organic matter; F) Carbon to nitrogen ratio; G) Weight percent organic carbon (blue solid line) and organic nitrogen (black dotted line). The pink shaded bar indicates the period of anthropogenic impact (see Chapter 2.0)... 78

Figure 3-7- A) C/N versus $\delta^{13}C_{org}$ with a linear regression from 3,800 years BP to present (R^2 = 0.43, $p < 0.001$). 7,900 to 3,800 years BP were excluded from the regression; B) C/N versus $\delta^{15}N$ with a linear regression through the entire dataset (R^2 = 0.65, $p < 0.001$); C) $\delta^{13}C_{org}$ versus $\delta^{15}N$ with a linear regression from 3,800 years BP to present (R^2 = 0.47, $p < 0.001$). 7,900 to 3,800 years BP were excluded from the regression. 80

Figure 3-8- Sediment composition of Xing Yun from A) this study and B) Whitmore et al., 1994 with organic matter (green dots), carbonate (blue solid line), and residual mineral matter (red dotted line); C) total nitrogen (blue dotted line) and phosphorus (green solid line) from Whitmore et al., 1994; D) proportion of hypereutrophic diatoms (green), eutrophic diatoms (blue), and mesotrophic diatoms (gray) from Whitmore et al., 1994. The remainder of the percentage of diatoms was composed of either oligotrophic or unknown diatoms. A comparison of the sediment composition of this study in panel A and Whitmore's previous study in panel B shows close correspondence. 88

Figure 3-9- Comparison of this study and Hodell et al., 1999 for A) weight percent carbonate and B) oxygen isotope values by depth. The two records are similar though the record from the Hodell et al., 1999 study has a higher sedimentation rate.. 90

Figure 3-10- A) Xing Yun weight percent carbonate; B) Xing Yun carbon isotope values of organic matter; C) Paru Co weight percent biogenic silica (Bird et al., 2014); D) Ahung Co lake level reconstruction (Morrill et al., 2006); E) Western tropical Pacific SST reconstruction from Mg/Ca of benthic forminifera (MD98-2181) (Stott et al., 2007); F) Tianmen Cave oxygen isotope values (Cai et al., 2012); G) Dongge Cave oxygen isotope values (Wang et al., 2005). The gray shaded bars indicate pronounced drops in Xing Yun organic carbon isotopes indicative of drops in primary productivity and coincident with noted drops in ISM strength and Western Pacific SST. 95

Figure 4-1- A- China with Yunnan Province shaded in gray. Erhai (square) with dominant wind direction; B- Major ore bodies (see Table 4-1) and archaeological sites Haimenkou and Yinsuodao in relation to Dali and Erhai; C- Erhai and coring locations A-09, B-09, and C-12. Previous coring locations by Dearing et al., 2008 marked by Xs. Geologic map adapted with permission from Searle et al., 2010. 104

Figure 4-2- Dearing et al., 2008 polynomial age model for Erhai sediment cores (collection locations marked in Figure 4-1). Unpublished ^{210}Pb data (black square), paleomagnetic features from Hyodo et al., 1999 (purple circles), terrestrial macrofossil radiocarbon dates (blue triangles), bulk sediment radiocarbon dates from Hyodo et al., 1999 (green inverted triangles), and shell radiocarbon dates from Hyodo et al., 1999 (red diamonds). 107

Figure 4-3- Total sediment depths of cores from sites A-09, B-09, and C-12 (locations marked in Figure 4-1) and overlapping sections. Terrestrial macrofossil radiocarbon dates marked with white stars (see Table 4-2). 111

Figure 4-4- Age-depth model with 95% confidence intervals. ^{210}Pb dates (green circles) and radiocarbon dates (red squares), with 2 sigma error bars. ^{210}Pb dates with 2-sigma error bars in inset. 116

Figure 4-5- Left panel: reference factors measured in the C-12 cores. A- weight percent organic matter, B- concentrations of aluminum (Al), C- concentrations of magnesium (Mg). Right panel: concentrations of metals measured in the C-12 cores. D- copper (Cu), E- lead (Pb), F- silver (Ag), G- cadmium (Cd), and H- zinc (Zn). 117

Figure 4-6- Lead concentrations by depth for Cores A-09, B-09, and C-12. The increase in Pb occurs at a similar depth and is of a similar magnitude in all three cores, despite their different locations and depths in the lake. Core B-09 is too short to capture the entire increase in Pb. 118

Figure 4-7- A- Archaeological periods, Yunnan cultural periods in white boxes, and Chinese dynasties in black boxes. Anthropogenic EFs for organic matter (solid line), aluminum (dashed line), and magnesium (dotted line) for B- copper (Cu), C- lead (Pb), D- silver (Ag), E- cadmium (Cd), and F- zinc (Zn) from Cores C-12. Shading from 1100-1400 AD corresponds to the increased concentrations of Pb, Ag, Cd, and Zn during the time period of the Yuan Dynasty (the Mongols)... 121

Figure 4-8- Results of the age uncertainty analysis with 95% confidence intervals. Age uncertainties were calculated using a 10,000 iteration Monte Carlo simulation varied between the radiocarbon 2-sigma calibrated age uncertainties (Huybers and Wunch, 2004; Marcott et al., 2013). The uncertainty between the age-control points was modeled as a random walk with a "jitter" value of 200... 123

Figure 4-9- Comparison between this study and results from Dearing et al., 2008. A- Archaeological periods, Yunnan cultural periods in white boxes, and Chinese dynasties in black boxes; B- concentrations of lead (Pb) from this study (black dashed line); C- concentrations of lead (Pb) from Dearing et al., 2008 (blue solid line); D- concentrations of copper (Cu) from this study (black dashed line); E- concentrations of copper (Cu) from Dearing et al., 2008 (blue solid line). The timing and magnitude of geochemical changes differs significantly between the two studies... 128

Figure 5-1- A- Locations of other paleoclimate archives discussed in text. G = Guilya ice cap, D = Dunde ice cap, AC = Ahung Co, PC = Paru Co Lake, DC = Dongge Cave, SC = Sanboa Cave, HC = Hulu Cave, TC = Tianmen Cave, MC = Mawmluh Cave; B- Locations of Yunnan lakes discussed in text; C- Map of Dian with bathymetry (1 m contours) adapted from Zhang et al., 1996. Coring locations A-12 and B-12 indicated by black circle. Previous coring location in Sun et al., 1986 study denoted by the X. Coring locations of C-14 through F-14 in box at southern end of the lake. For more detail, see Figure 5-2.132

Figure 5-2- Details of the southern end of Dian shown in the box in Figure 5-1. A- Coring locations indicated by black circles along X-X' transect. Star indicates site of soil sampling location. B- Bathymetric profile of lake water depth, coring locations, and approximate length of collected sediment along X-X' transect... 133

Figure 5-3- Age-depth models with 95% confidence intervals, radiocarbon dates (blue circles) with 2 sigma error bars, and excluded radiocarbon dates (red crosses). Moving left to right with decreasing water depth: Cores A-12, D-14, E-14, F-14, and C-14. 146

Figure 5-4- Sedimentology and weight percent organic matter, carbonate material, and residual mineral matter. Moving left to right with decreasing water depth: Cores A-12, D-14, E-14, F-14, and C-14. 149

Figure 5-5- Magnetic susceptibility profiles for all cores on each individual age model (see Figure 5-3). Moving top to bottom with decreasing water depth: Cores A-12, D-14, E-14, F-14, and C-14. Many of the features of the magnetic susceptibility profiles are similar between coring sites- similarities are highlighted with gray shaded bars. 150

Figure 5-6- Stratigraphic column of core A-12. For color key, see Figure 5-4 caption. A- Weight percent organic matter (green circles) and calcium carbonate (blue solid line); B- Percent organic carbon (blue solid line), percent organic nitrogen (black dotted line); C- Carbon to nitrogen ratio (blue solid line) of organic matter, nitrogen to phosphorus ratio (black dotted line); D- Carbon isotope values of organic matter (blue solid line), nitrogen isotope values of organic matter (black dotted line); E- Concentrations of strongly bound aluminum (blue solid line) and iron (black dotted line); F- Magnetic susceptibility; G- Average summer (June, July, August) insolation at 20°N (Berger, 1978). The red shaded bar in Unit IV represents the initiation of anthropogenic impact on the lake. 152

Figure 5-7- Scanning electron microscopy (SEM) images of calcite from Dian D-14 cores. A) Calcite from D14 D1 130 cm showing massive anhedral cystal forms; B) Euhedral calcite from D14 D1 30 cm. 155

Figure 5-8- Proxies from A-12 cores over the last 2,000 years with significant historical events noted as well as Yunnan cultural and Chinese dynastic transitions. A- Weight percent organic matter (green circles), calcium carbonate (blue solid line), and residual mineral matter (red dotted line); B- Percent organic carbon (blue solid line), percent organic nitrogen (black dotted line); C- Carbon to nitrogen ratio (blue solid line), nitrogen to phosphorus ratio (black dotted line); D- Carbon isotope values of organic matter (blue solid line), nitrogen isotope values of organic matter (black dotted line); E- Concentrations of weakly bound lead (blue solid line), phosphorus (black dotted line); F- Concentrations of weakly bound aluminum (blue solid line) and titanium (black dotted line); G- Magnetic susceptibility. The gray bar indicates the initiation of human disturbance on the lake and the red bar indicates the period of the most intense eutrophication and human impact. 157

Figure 5-9- Organic isotope data from A-12 cores divided into the four units. A) C/N versus $\delta^{13}C_{org}$ with linear regression equation ($R^2 = 0.56$, $p < 0.001$). Data from the last 300 years were excluded from the regression; B) C/N versus $\delta^{15}N$; C) $\delta^{13}C_{org}$ versus $\delta^{15}N$.................. 164

Figure 5-10- Concentrations of fecal 5β-stanols from Dian A-12 cores that begin to increase around 500 years BP. 171

Figure 6-1- A- Locations of Chenghai Lake (square) and Dongge Cave (circle); B- Locations of Yunnan lakes mentioned in text as well as the city of Lijiang and the archaeological site Haimenkou; C- Map of Chenghai Lake with shaded topographic relief from ASTER Global DEMs. Coring locations indicated by black circles. Bathymetric data (10 meter contour intervals) from Wan et al., 2005. 179

Figure 6-2- Age-depth model with 95% confidence intervals. ^{210}Pb dates (green circles), radiocarbon dates (blue squares), excluded radiocarbon date (red circle), all with 2 sigma error bars. ^{210}Pb dates with 2-sigma error bars in inset. 187

Figure 6-3- Scanning electron microscopy (SEM) images of euhedral aragonite from Chenghai A-12 cores. 189

Figure 6-4- Isotopic covariance of Chenghai for three time periods; Unit I (1100-1360 AD) in red, Unit II (1360-1700 AD) in green, and Unit III (1700-2012 AD) in blue. 191

Figure 6-5- A- Oxygen isotopic composition of aragonite from Chenghai in blue, oxygen isotopic composition from Dongge Cave in green; C- Carbon isotopic composition of aragonite; C- Carbon to nitrogen ratio; D- Carbon isotopic composition of organic matter (blue solid line), nitrogen isotopic composition of organic matter (black dotted line); E- Concentration of copper (blue solid line), concentration of lead (black dotted line); F- Magnetic susceptibility. 192

Figure 6-6- Concentrations of weakly bound metals from Chenghai. A) Al, B) Co, C) Fe, D) Ti, E) Zn. 193

Figure 6-7- Comparison between our study (blue circles) and Jinglu et al., 2004 (red squares). A) $\delta^{18}O_{carb}$, B) $\delta^{13}C_{carb}$, C) $\delta^{13}C_{org}$. There is good relatively agreement between this study and the previous study prior to 1900 AD. 201

Figure 6-8- A) C/N versus δ^{15}N with a linear regression (R_2 = 0.53, $p < 0.001$). Data from 1980-2010 AD has anomalously high C/N and δ^{15}N values and was excluded from the regression; B) C/N versus $\delta^{13}C_{org}$ showing no relationship. 203

Figure 6-9- Weight percent organic matter estimated from LOI 550 (green circles) and weight percent aragonite estimated from LOI 1000 (dashed blue line). 206

Figure 7-1- Soil map of A) Western Yunnan and B) Eastern Yunnan. Adapted from Fengrang, 1990.. 212
Figure 7-2- The conceptual framework integrating humans, climate, and the environment (Brenner et al., 2002). 217

LIST OF EQUATIONS

Equation 2-1 (Kim and O'Neil, 1997) 43

Equation 4-1 (Weiss et al., 1999) 114

Equation 4-2 (Weiss et al., 1999) 114

Equation 6-1 (Kim et al., 2007) 197

PREFACE

As a runner I often think about the parallels between getting a PhD and running a marathon. They both require painfully long (often lonely) hours praticing your craft and the importance of persistence in the face of heart-crushing difficulty cannot be overstated. And there are the fun parts too. Like the sheer joy when I discovered that Mongol silver smelting was responsible for the lead pollution peak at Erhai at 2 AM alone in a hotel room in Lanzhou in the middle of winter. Or when I led a coring expedition to Dian Lake on a rickety fishing boat with only 3 fishermen who spoke neither Chinese nor English with only the vaguest idea of what we were trying to accomplish.

And like running a marathon, a PhD is exceedingly difficult to finish without a great deal of support and encouragement from your friends and family. Absolutely none of this work would have been possible without the help, reassurance, and advising of Mark Abbott. I don't think I will ever be able to adequately thank him enough for how much he has done for me and for all of the opportunities that he gave me. I also owe a enormous debt to JunQing Yu of the Qinghai Institute of Salt Lakes who provided us with logistical and technical support every time we went to China. A huge thank you goes out to my committee members Dan Bain, Emily Elliott, Brian Stewart, and Loukas Barton for their helpful comments and feedback on many aspects of this project.

I don't think I would have survived grad school without the moral support of my labmates Dave Pompeani and Matt Finkenbinder who were sounding boards for my ideas, emphathizers with my frustrations, and overall fantastic friends. Other people who provided essential laboratory support, fieldwork support, advice, and feedback include Byron Steinman, Colin Cooke, Darren Larsen, Bruce Finney, Pratigya Polissar, Katie Redling, TzeHuey Chiou-Peng, Alice Yao, Lauren Ledin, Bill Harbert, Ashley Albert, Stevie Perdziola, Adam Ofstun, Sage Lincoln, Alex Beatty, Jordan Abbott, ChunLiang Gao, and probably several others I am forgetting.

Much of this work was funded by grants from the National Natural Science Foundation of China (NSFC grants 40571173, 40871008, and 41171171), National Science Foundation EAR/IF 0948366, the Andrew Mellon Foundation, the Hewlett Foundation, two Geological Society of America graduate student grants, the Henry Leighton Memorial Fellowship, and the University of Pittsburgh International Studies Fund.

Lastly, I want to thank my parents and my husband Justin who provided unceasing support and encouragement. I have to imagine that when Justin and I met 10 years ago, he could have never envisioned trekking to a wet chemistry lab in the snow at 10:00 at night on Superbowl Sunday to help me shut down an ICP-MS. But he has never let me down.

1.0 INTRODUCTION

1.1 OBJECTIVES

1.1.1 Research Aims

Lakes in Yunnan Province of southwestern China have persistent and severe water quality problems related to rapid population growth and industrialization, which have placed great demands on freshwater and agricultural resources (Wang et al., 2012b; Whitmore et al., 1997). Today, many lakes in this region are heavily impacted by deforestation, soil erosion, agriculture, urbanization, and industrialization (Whitmore et al., 1994a). As a result of these activities, many lakes on the Yunnan plateau are now eutrophic (Li et al., 2007; Liu et al., 2012) and have high concentrations of toxic metals in their sediments (Zeng and Wu, 2009). Despite an increasing awareness of the negative landscape-scale impacts arising from these disturbances, problems associated with water pollution, sediment quality, and environmental degradation are likely to persist or worsen as the population expands.

However, it is increasingly apparent that some lakes on the Yunnan plateau may have been impacted by anthropogenic activities for centuries (e.g., Dearing et al., 2008; Shen et al., 2005). In Yunnan, a region that has a long history of human occupation, agriculture, and mining, questions remain regarding which lakes may have been impacted prior to the 20th century, the nature of the impact, and how anthropogenic effects can be differentiated from other controls such as climate change. Assessment of the relative influence of anthropogenic and climate forcing on the lake systems of this region has not been the main focus of most environmental investigations. **Therefore aim of this dissertation is to assess the timing, magnitude, and rate of anthropogenically driven environmental change in the context of natural climate variability for lakes in the Yunnan Province.**

Lakes in Yunnan can answer questions regarding long-term environmental change and the geochemical variations associated with human disturbance. Many of these lakes are situated near historically major centers of population **(Figure 1-1)** and have long, continuous records of sedimentation that total several thousand meters in some cases (Wang et al., 1998). This project focuses on two lakes (Erhai and Chenghai) in the western part of Yunnan, near the city of Dali, and two lakes (Xing Yun and Dian) in the east-central part of Yunnan, near the city of Kunming (**Table 1-1 and Figure 1-1**).

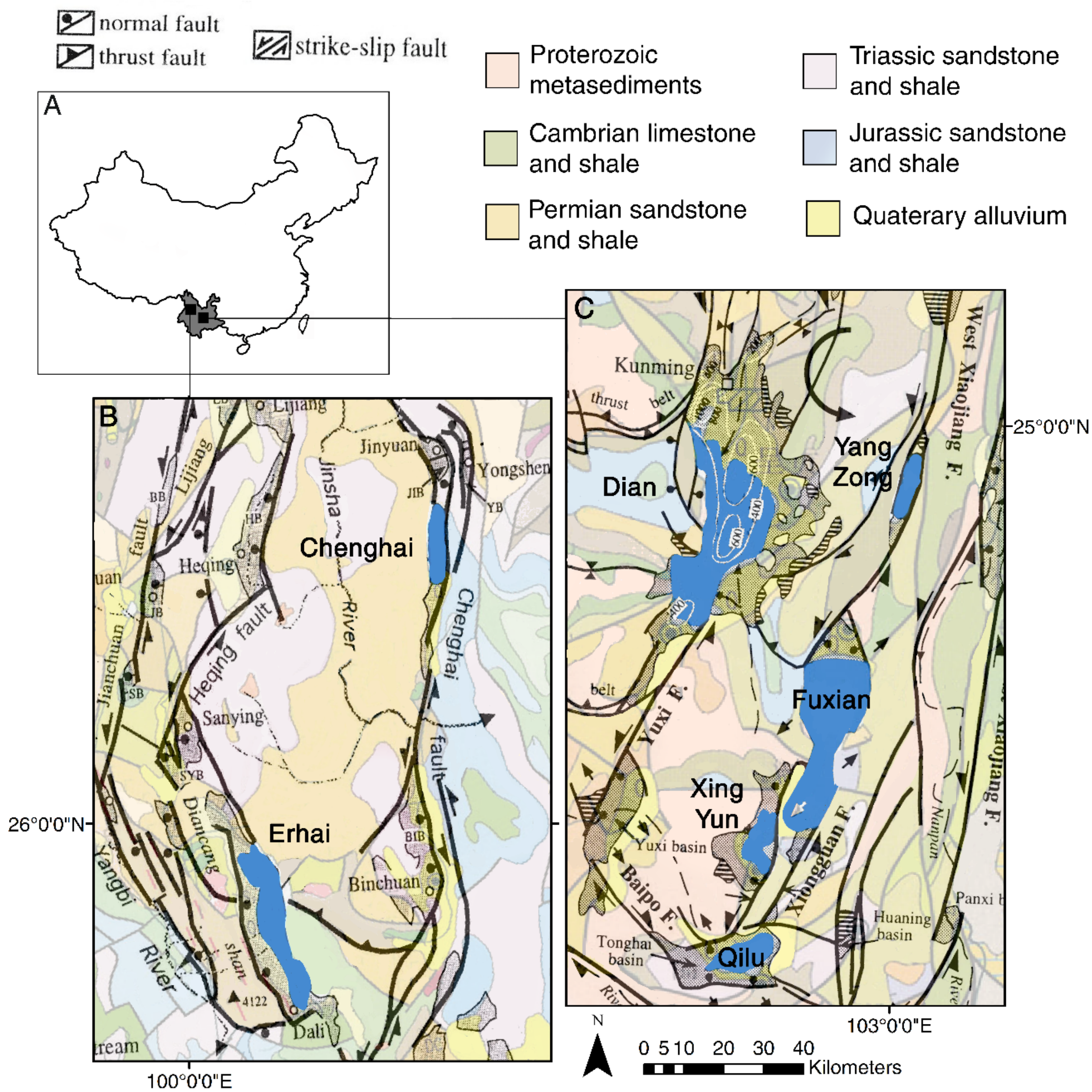

Figure 1-1- A- map of China with Yunnan highlighted. B- Lakes selected for study in the eastern half of Yunnan- Erhai and Chenghai. C- Lakes selected for study in the western half of Yunnan- Dian and Xing Yun. Geologic map adapted from Meng and Li, 1970 and fault map adapted from Wang et al., 1998.

Table 1-1- Lakes selected for study

Lake	Latitude	Longitude	Elevation (m)	Maximum Depth (m)	Surface Area (km^2) (*1*)	Catchment Area (km^2) (*1*)	CA/SA
Xing Yun	24°20'N	102°46'E	1783	11	35	383	10.94
Dian	24°47'N	102°43'E	1888	6	303	2920	9.64
Chenghai	26°33'N	100°39'E	1502	35	75	318	4.24
Erhai	25°48'N	100°10'E	1964	21	250	2565	10.26

1. (Li et al., 2007)

1.1.2 Research Questions

The research questions this dissertation seeks to address are as follows:

1) How have pre-industrial human activities on the Yunnan Plateau contributed to modern day limnological challenges such as industrial pollution, eutrophication, land use change, and hydrologic modification? Yunnan is a borderland region in southwestern China noted for rich mineral deposits, but inadequately documented metallurgical history. Additionally, the origins of rice agriculture in Yunnan are murky (Fuller, 2012) and thus the earliest use of agricultural terracing and associated land-use change remains unknown. As multiple previous studies have demonstrated (Brenner, 1983; Carson et al., 2014; Cooke et al., 2009; O'Hara et al., 1993; Pompeani et al., 2013; Rosenmeier et al., 2002), the scale of pre-industrial land-use change around the globe may be substantial and have multiple limnological consequences. The scale and timing of such activities remains ill-constrained in Yunnan due to insufficient archaeological and historical records (Allard, 1998; Yao and Zhilong, 2012); thus it is difficult to place present-day environmental challenges into an appropriate context.

2) What is the timing and nature of abrupt shifts in moisture associated with Indian Summer Monsoon (ISM) variability in the Pleistocene and Holocene? The ISM dominates the climate of Yunnan and people who live in regions of high-population density affected by the ISM base their livelihood on the timely arrival of the monsoon to deliver enough water to sustain agriculture and hydroelectric power. However, there is an inadequate understanding of how the ISM interacts with climate phenomena such as the El Niño Southern Oscillation (ENSO) (Turner and Annamalai, 2012) as well as how the ISM relates to the East Asian Summer Monsoon (EASM) (Cheng et al., 2012a; Clemens et al., 2010). In order to improve our understanding of the nature of rapid shifts in moisture balance, a long-term perspective of the ISM from terrestrial archives is necessary.

3) What role has hydroclimate played in human settlement and subsistence practices? Numerous studies worldwide have viewed climate change as a driver of societal upheaval (Binford et al., 2000; Buckley et al., 201; Cullen et al., 2000; Hodell et al., 2001; Zhang et al., 2008a), though typically this work has been limited by climate records that are too spatially distant or of low temporal resolution to make direct links with the archaeological record. Moreover, proxy records themselves may be influenced by anthropogenic activities as changes in pollen assemblages or charcoal abundance may reflect human-induced land-use change (D'Anjou et al., 2012). Nonetheless, as societies in Asia remain vulnerable to monsoonal variability in the context of future climate change (Lal et al., 2011), understanding societal adaptation to hydroclimate variation remains crucial. While it can be difficult to connect paleoclimate information to changing human land-use strategies, this work seeks to bridge the gap between archaeology and paleolimnology by investigating anthropogenic manipulations to lake basins in the context of changing monsoon variability.

1.1.3 Hypotheses

With the above research objectives in mind, the hypotheses are as follows:

1) There will be spatial and temporal differences in the initiation of human modification to lakes with those in the eastern section being earlier and more intense. The eastern and western sections of Yunnan have differing archaeological traditions and political histories of development (Elvin et al., 2002; Higham, 1996) with settlement occurring first around Dian Lake (Yao and Zhilong, 2012). Therefore we hypothesize that Dian will record the earliest anthropogenic impact. Additionally, the regional Dian kingdom was centered around the eastern section of Yunnan thus we hypothesize that human activity associated with agriculture and land use change will be most intense in the surrounding lakes.

2) Limnological characteristics, such as surface area and catchment area, will determine the nature of anthropogenic impact with smaller, shallower lakes responding more sensitively. Each of the paired lakes in the eastern and western sections have differing characteristics with two of them (Erhai and Dian) having large surface areas and catchment areas and two of them (Xing Yun and Chenghai) having small surface areas and catchment areas (**Table 1-1**). We hypothesize that Xing Yun and Chenghai will be the most disturbed systems and that Erhai and Dian will be the least disturbed due to their large size and dilution of anthropogenic impacts.

3) Hydroclimate shifts on the Yunnan Plateau will be similar in both timing and magnitude compared to shifts recorded on the Tibetan Plateau and Indian subcontinent. We expect that proxy measurements of ISM variability will broadly agree with lake records from the Tibetan Plateau (Bird et al., 2014; Morrill et al., 2006) and speleothem records from the Indian subcontinent (Berkelhammer et al., 2010; Cai et al., 2012), though many of these archives are not continuous through the Holocene. However, we expect to see shifts in the ISM that are distinct from those of the EASM as recorded in speleothems such as Dongge and Hulu Caves (Wang et al., 2005; Wang et al., 2001).

4) Due to the heavy reliance on the ISM for annual precipitation, periods of reduced monsoon variability will coincide with societal changes over the late Holocene. While it is difficult to find paleoclimate records in this region of the world undisturbed by people, we will use other paleoclimate records such as Dongge Cave (Dykoski et al., 2005) and Paru Co (Bird et al., 2014), to see if periods of aridity coincide with inferred land use or limnological changes.

1.2 REGIONAL SETTING

1.2.1 Geology

Eastern/central Yunnan is part of the Yangzi platform that is composed by of low-grade Proterozoic metamorphic rocks (Wang et al., 1998) and late Permian Emeishan continental flood basalts that resulted in extensive copper-chalcocite ore deposits (Zhang et al., 2009) (**Figure 1-1**). Western Yunnan has the same Permian flood basalts that surround Kunming but the geologic history is considerably more complicated. During the late Mesozoic a collage of crustal fragments came together but the subsequent deformation has been so complex that the origin of these fragments still remains unknown (Wang and Burchfiel, 1997). The Diancangshan metamorphic rock complex juts up against the western side of Erhai and by 4 million years, extensive erosion of these rocks began, possibly due to the activation of a nearby fault system (Wang et al., 1998). As a result of extensive weathering, red palaeosols rich in Al, Fe, and Ti are widespread in Yunnan and have been tentatively dated as being 1 million years old (Lu et al., 2015).

Yunnan has a complicated tectonic history related to the collision of India and Eurasia roughly 50 million years ago. Numerous strike-slip faults cut across the landscape to accommodate the convergence between India and Asia (Molnar and Tapponnier, 1975; Royden et al., 2008). As a result of these strike-slip faults, there are numerous pull apart basins, such as Fuxian, Xing Yun, Chenghai, and Qilu (Wang et al., 1998). Pull-apart basins form when an area is bound by two non-continuous normal faults and experiences tension (Kearney et al., 2009). In a pull-apart basin there may be multiple centers of deposition that change through time (Cohen, 2003). Other basins in Yunnan such as Erhai and Dian are caught on the extensional corner of a rotating crustal block, causing subsidence and more irregular shapes (Wang et al., 1998).

An extensive study of Yunnan fault systems can be found in Wang et al., 1998 and what follows is a brief summary of their work. Western Yunnan is dominated by the Dali fault system, which may be considered an extension of the Red River fault (RRF) that runs throughout much of southwestern China and down into Vietnam. Displacement on the RRF is temporally and spatially variable with the greatest displacement along the northern sections of the fault and almost no displacement on the southeast portions (Schoenbohm et al., 2006). The RRF currently has a slip rate of 1-5 mm/year though Pliocene slip rates were much higher. On the western side, Erhai is bound by an east-dipping normal fault that is part of the RRF. Sedimentary deposits in Erhai are estimated to be 2,000 m thick and originate from the Early Pleistocene. Chenghai lies on the Chenghai fault, a left-lateral branch of the RRF. The Chenghai fault shows evidence of recent activity as it has laterally displaced the lower branch of the Jinsha River by ~3 m. Sedimentary deposits in Chenghai are estimated to be 1,200 m thick.

Nearly all of the lakes in central-eastern Yunnan are formed from the extensive Xianshuihe-Xiaojiang fault (XXF) system. Much of the crustal deformation in Yunnan is currently being taken up by the XXF. All of the lake basins associated with the XXF date to the early Pleistocene but the sedimentary deposits vary greatly in terms of thickness. Based on the fact that no basins appear to be older than the early Pleistocene, Wang et al., 1998 estimate that the XXF system is 2-4 million years old and that the average long term slip rate is 15-30 mm/year. However, that is twice the slip rate that has been observed by field study and GPS measurements (Allen et al., 1991; King et al., 1997). A possible explanation is that slip rates have slowed down with time. Alternatively, the estimates of the age of the lake basins may be incorrect, especially since sedimentary deposit thicknesses are widely variable and have only been dated using one or two fossils or sparse paleomagnetic data. Improved age control on these sedimentary deposits and more extensive seismic surveys would need to be undertaken to determine which scenario is correct. Sedimentary deposits in Dian are greater than 1,000 m thick and are from the early Pleistocene. Estimates of sedimentary deposit thickness in Xing Yun are unknown however Fuxian is estimated to have 163 m of sediment that dates to the Pleistocene.

1.2.2 Climate

The Asian Summer Monsoon is due to the seasonal cycle of insolation that results in thermal contrasts between land and sea that drives atmospheric circulation and convective moisture. Twice a year this atmospheric circulation switches and creates distinct wet summers and dry winters in affected regions. The monsoon system is closely tied to the Intertropical Convergence Zone (ITCZ) as the northward progression of the ITCZ during the Northern Hemisphere summer accompanies the onset of the summer monsoon winds and results in increased moisture flux reaching the continent (Fleitmann et al., 2007). The Asian Monsoon system can be broken into two components- the Indian Summer Monsoon (ISM) where moisture originates from the Bay of Bengal and the East Asian Summer Monsoon (EASM) where moisture originates from the South China Sea (**Figure 1-2)**. It is difficult to define strict spatial barriers between these two systems (Cheng et al., 2012a) though some researchers have suggested 105°E as a possible division (Wang et al., 2003).

In Yunnan 70% of the average annual precipitation falls in the months of June-September (**Table 1-2**) and most of that precipitation is associated with the ISM (Araguás-Araguás et al., 1998). During the monsoonal season, which reaches its peak in July and August, land-ocean thermal gradients drive vigorous convection, resulting in greater moisture transfer from more distal sources. As moisture is transported over longer distances, heavier oxygen isotopes fall out first so that the remaining water in the air mass becomes more and more depleted in ^{18}O. This results in precipitation falling on the landscape with relatively lower $\delta^{18}O$ values (Cheng et al., 2012a). GNIP station data for Kunming shows that the precipitation with the lowest $\delta^{18}O$ and δD values occur during the summer months and are associated with the ISM (**Table 1-2**).

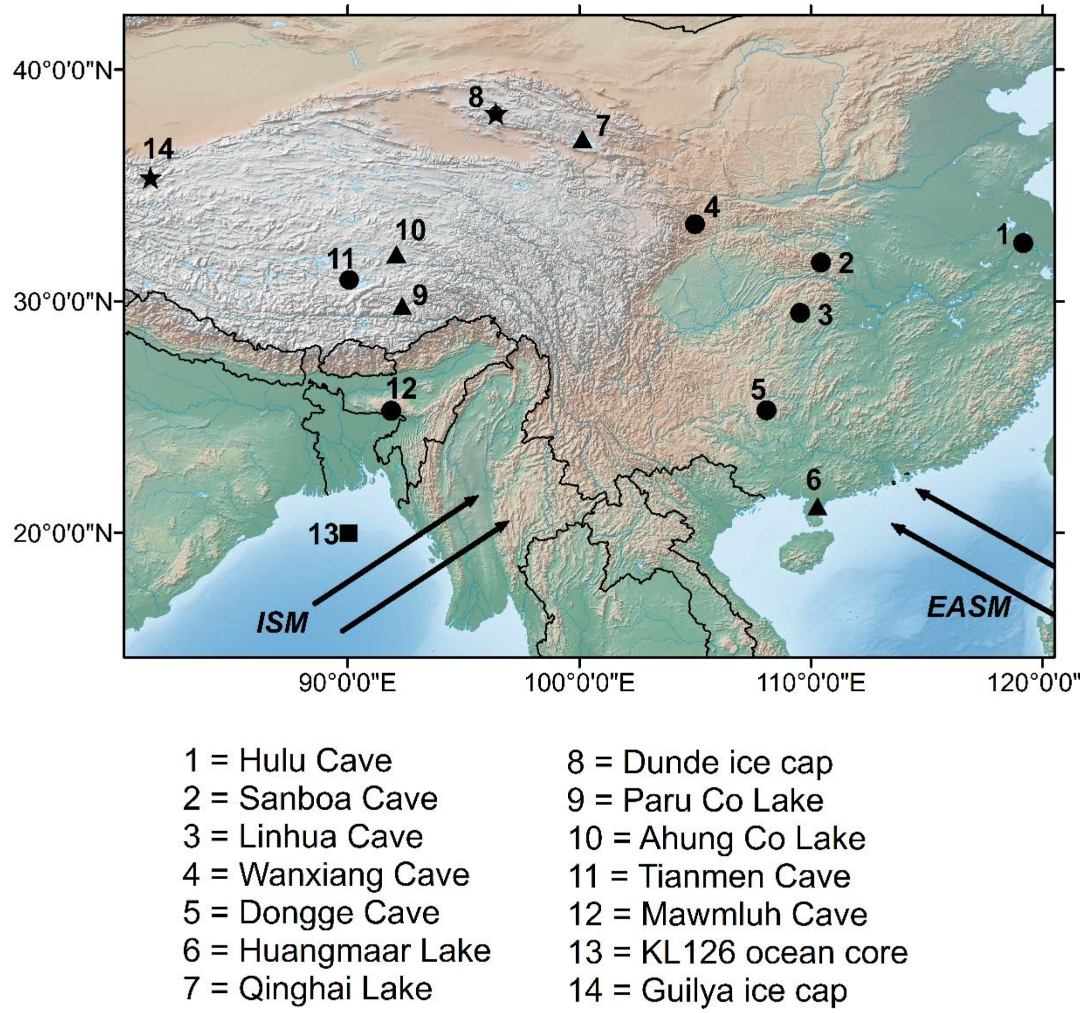

Figure 1-2- The Asian Summer Monsoon system: ISM = Indian Summer Monsoon, EASM = East Asian Summer Monsoon. Numbered locations of paleoclimate records from China discussed in this dissertation.

Table 1-2- Monthly average temperature, precipitation, oxygen isotope values, and deuterium values from 1986-2003 at Kunming GNIP station (25°1'N, 102°40'E, 1892 m) (IAEA/WMO, 2014).

	Jan	Feb	Mar	April	May	June	July	Aug	Sept	Oct	Nov	Dec
Average Temperature (°C)	8.9	10.8	14.3	17.7	19.1	20.3	20.0	19.8	18.2	16.2	12.3	9.0
Average Precipitation (mm)	19.4	13.7	16.8	20.9	97.2	191.2	209.2	194.6	107.9	84.2	34.8	11.2
$\delta^{18}O$ (‰VSMOW)	-4.32	-3.15	-3.51	-3.01	-5.42	-8.16	-12.37	-13.1	-10.75	-10.49	-8.58	-5.15
δD (‰VSMOW)	-30.6	-21.5	-29.8	-18.8	-39.3	-58.1	-84.3	-89.1	-75.6	-71.2	-58.7	-37.2

Average weighted $\delta^{18}O$ (‰VSMOW) = -9.86

Average weighted δD (‰VSMOW) = -68.22

Records of both the ISM and EASM have been extensively documented using speleothems. In particular, how the EASM has changed over the last several hundred thousand years has been investigated in great detail with a number of speleothems from interior China (Cosford et al., 2008; Dykoski et al., 2005; Wang et al., 2005; Wang et al., 2008; Wang et al., 2001; Zhang et al., 2008a). This work established that on millenial time-scales, the Asian Monsoon is controlled by precessional forcing- the variation in the global distribution of summer insolation due to changes in the orientation of Earth's orbital axis. The driving cause of this variation is the latitudinal migration of the ITCZ in response to changes in the amount of summer insolation (Fleitmann et al., 2007). Multiple records such as Dongge, Hulu, Sanboa, Linhua, Wanxiang, Mawmluh, and Tianmen Caves (**Figure 1-2)** show a strong connection between average summer insolation and $\delta^{18}O$ values as archived in speleothem calcite. As solar insolation increases, the land-ocean thermal gradient increases, driving increased monsoonal activity and moisture transport over longer distances, leading to lower $\delta^{18}O$ values in precipitation falling on the land (Yuan et al., 2004). While other mechanisms have been proposed to explain the tight connection between variations in $\delta^{18}O$ values and monsoon strength, including rainfall amount (Neff et al., 2001), moisture source (Maher and Thompson, 2012), and seasonality of precipitation (Wang et al., 2001), broad scientific consensus is that $\delta^{18}O$ values in speleothem calcite reflect upstream air mass processes (Hu et al., 2008; LeGrande and Schmidt, 2009; Liu et al., 2014).

Over centennial and decadal time-scales, researchers have suggested that abrupt drops in monsoon strength are related to Northern Hemisphere temperatures, Southern Hemisphere temperatures, and/or Pacific sea surface temperature (SST) gradients, but the relative importance of each of these factors is still debated. Many of the aforementioned speleothem records show sudden reductions in monsoon strength correspond closely to Heinrich events, periods of increased sea ice melting in the North Atlantic (Broecker et al., 1992). These events also cause reduced North Atlantic deep water formation that modeling studies suggest may cause colder temperatures across Eurasia and a reduced land-sea thermal gradient leading to a weaker monsoon (Morrill et al., 2003). Colder temperatures in the North Atlantic may also lead to a southward shift of the ITCZ (Cheng et al., 2012a). Alternatively, some researchers have suggested that the strength of the ISM in particular could be controlled by Southern Hemisphere temperatures as warm temperatures in the Southern Ocean led to less transquatorial flow and weaker winds (Cai et al., 2006; Zhisheng et al., 2011).

The impact of Pacific SSTs is mainly through El Niño Southern Oscillation (ENSO) and the Indian Ocean Dipole (IOD). During an El Niño event, warm SSTs in the eastern Pacific cause the Walker circulation cell that drives atmospheric convection to shift eastward. This causes subsidence in the western Pacific, anomolously warm SSTs in the Indian Ocean, and a weakened ISM (Kumar et al., 1999). This relationship has been observed in modern meterological data but has weakened in recent decades, possibly due to warming on the Eurasian continent driving an increased thermal gradient between land and sea (Kumar et al., 1999). Positive IOD events cause an anomolous increase in SSTs in the Bay of Bengal and a decrease in the southwestern Pacific near Sumatra (Abram et al., 2008). This has the overall effect of weakening the ISM and when IOD events coincide with El Niño events, the effect is enhanced (Abram et al., 2007). The Pacific Decadal Oscillation (PDO), whose positive phase results in anomolously cool SSTs in the Northern Pacific, causes warmer SSTs in the Indian Ocean and also results in a weaker ISM (Krishnan and Sugi, 2003).

There is still considerable debate about whether the ISM and the EASM respond to precessional forcing synchronously and similarly (Cheng et al., 2012a; Clemens et al., 2010). In part, this is due to a lack of continuous terrestrial hydroclimate records of the ISM. Speleothem records of the ISM such as Tianmen (Cai et al., 2012), Mawmlah (Berkelhammer et al., 2012), and Dandak (Sinha et al., 2007) Caves (**Figure 1-2)** do not continuously span the Holocene or are located spatially distant from the main component of the ISM on the Arabian Peninsula (Fleitmann et al., 2003). Other than speleothems, very few terrestrial records of the ISM exist over the Holocene. Many lake records on the Tibetan Plateau, such as Ahung Co, are also discontinuous through the Holocene (**Figure 1-2**).

The Guilya ice cap from the Tibetan Plateau (**Figure 1-2)** records substantial variations in $\delta^{18}O$ values over the last 125 ka related to moisture variability (Thompson et al., 1998). Abrupt variations in $\delta^{18}O$ values between 33 and 15 ka were hypothesized to be related to Dansgaard-Oeschger events, periods of rapid warming followed by gradual cooling on time-scales of approximately 1,500 years. Late Pleistocene and Holocene-scale climate was less well-constrained due to the absence of an absolute dating chronology, however the Last Glacial Maximum (LGM) was thought to be 18±1 ka. The Dunde ice cap from the northern Tibetan Plateau produced a higher resolution record of the ISM through the Holocene (Thompson et al., 1989). Increased dust deposition occurred from 30 to 10 ka, with an abrupt increase at 10.75 ka. Holocene optimal warmth inferred from $\delta^{18}O$ values occurred between 8 and 6 ka. More recently, a lake sediment record from Paru Co on the Tibetan Plateau demonstrated several significant drops in ISM strength at 7.2 and 5.2 ka using hydrogen isotopes of leaf waxes (Bird et al., 2014). The authors proposed that these abrupt events were due to century-scale variability of the IOD.

While these three records have done much to advance our understanding of the ISM expressed on the Tibetan Plateau, population density is quite low. By contrast, lakes situated on the Yunnan Plateau of China are essential water resources for both urban and rural areas, have population densities between 250-999 persons/km^2 (Center for International Earth Science Information Network, 2000), and are vital hydrologic resources for the Pearl, Red, and Yangtze River Basins.

Water isotope samples demonstrate the sensitivity of lakes on the Yunnan Plateau to hydroclimate variation (**Figure 1-3**). GNIP station data from 1986-2003 was used to calculate the annual weighted mean isotopic composition of modern rainfall for Kunming (**Table 1-2 and Figure 1-3**). A sample of groundwater taken in 2014 from 2 m below the surface on the southeastern shore of Dian Lake (24°42'25.77"N, 102°41'21.81"E) plots very close to the annual weighted mean of modern rainfall (**Figure 1-3)**. Water samples from various lakes in Yunnan (**Figure 1-1**) were collected in the summers of 2009, 2012, and 2014 and analyzed for $\delta^{18}O$ and δD. A plot of $\delta^{18}O$ versus δD reveals substantial variation in the isotopic composition of the lake waters (**Figure 1-3**). Erhai is isotopically closer to the annual weighted mean of modern rainfall for Kunming than the other lakes, though it still plots to the right of the Global Meteoric Water Line (GMWL) on the Local Evaporation Line (LEL), suggesting that some portion of water loss occurs through evaporation. Lakes Xing Yun, Fuxian, Dian, and Chenghai lie further to the right of the isotopic composition of Kunming rainfall, having higher values of both $\delta^{18}O$ and δD. This suggests that substantial water loss occurs through evaporation and that these lakes are closed basins.

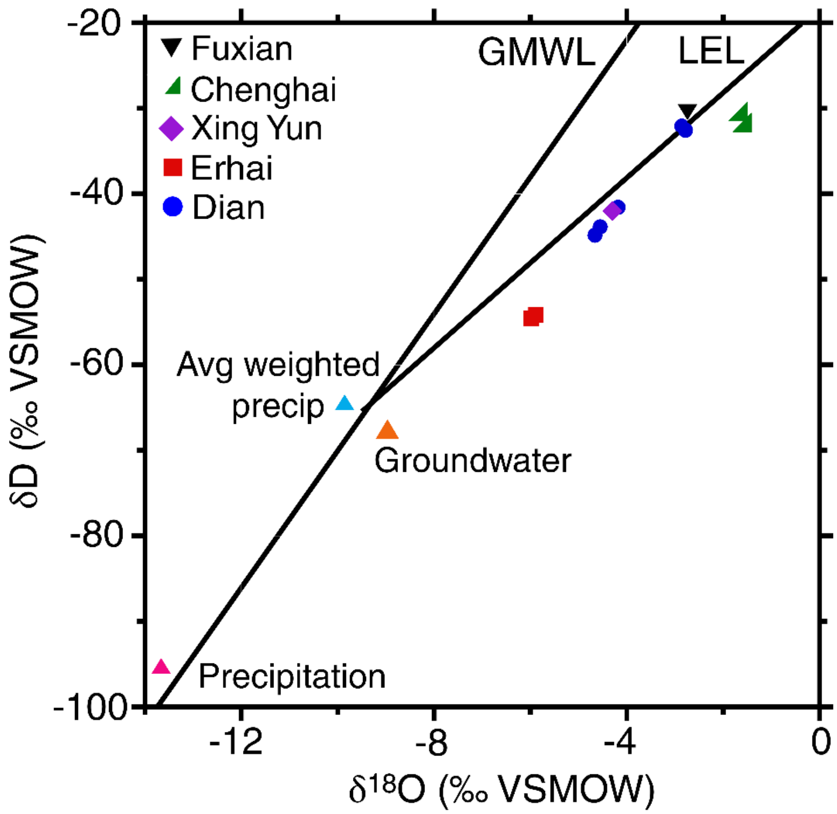

Figure 1-3- Water isotope samples from selected lakes in Yunnan, groundwater from ~2 m deep next to Dian (orange triangle), precipitation collected from a rainstorm at Dian in August 2014 (pink triangle), the annual weighted mean of modern rainfall for Kunming from GNIP station data (blue diamond). GMWL = Global Meteoric Water Line. LEL = Local Evaporation Line.

The ISM is the most dominant aspect of Yunnan climate as temperature in this region is generally stable throughout the year and winters are mild. The climate is defined as warm temperate with a dry winter and a warm summer (designated Cwb in the Köppen-Geiger classification system) (Kottek et al., 2006). Land clearance for agriculture is extensive around both Kunming and Dali, but in less impacted areas, subtropical conifer and evergreen broad-leafed forests predominate (Li and Walker, 1986).

1.3 HUMAN HISTORY OF THE YUNNAN PROVINCE

Yunnan has a long history of human occupation, with Neolithic settlement around lake basins occurring sometime between 10,000 and 3,500 years BP (Sun et al., 1986). Archaeological investigations of early agriculture in the region produced controversial evidence that Yunnan may have been a center of rice domestication (Fuller, 2012). The earliest definitive evidence for rice cultivation dates to 4,500-4,000 years BP, though archaeobotanical work has been limited (Fuller, 2012). Nonetheless, the great genetic diversity of rice from Yunnan suggests that it was an important center of rice cultivation (Zhang et al., 2007).

Yunnan has rich deposits of metals including copper, tin, lead, gold, silver, and iron, many of which were mined and processed near the city of Dali, in the western half of the province, and Gejiu mine, 200 km south of Kunming (Golas, 1999; Pirajno, 2013) (**Figure 1-4)**. Early habitation sites and associated metal artifacts are understudied relative to later, more abundant sites associated with the Dian culture of 400 BC-100 AD (Chiou-Peng, 2008, 2009). As a result, little is known about metalworking activities during the period of earliest habitation, especially around Kunming, the capital of Yunnan.

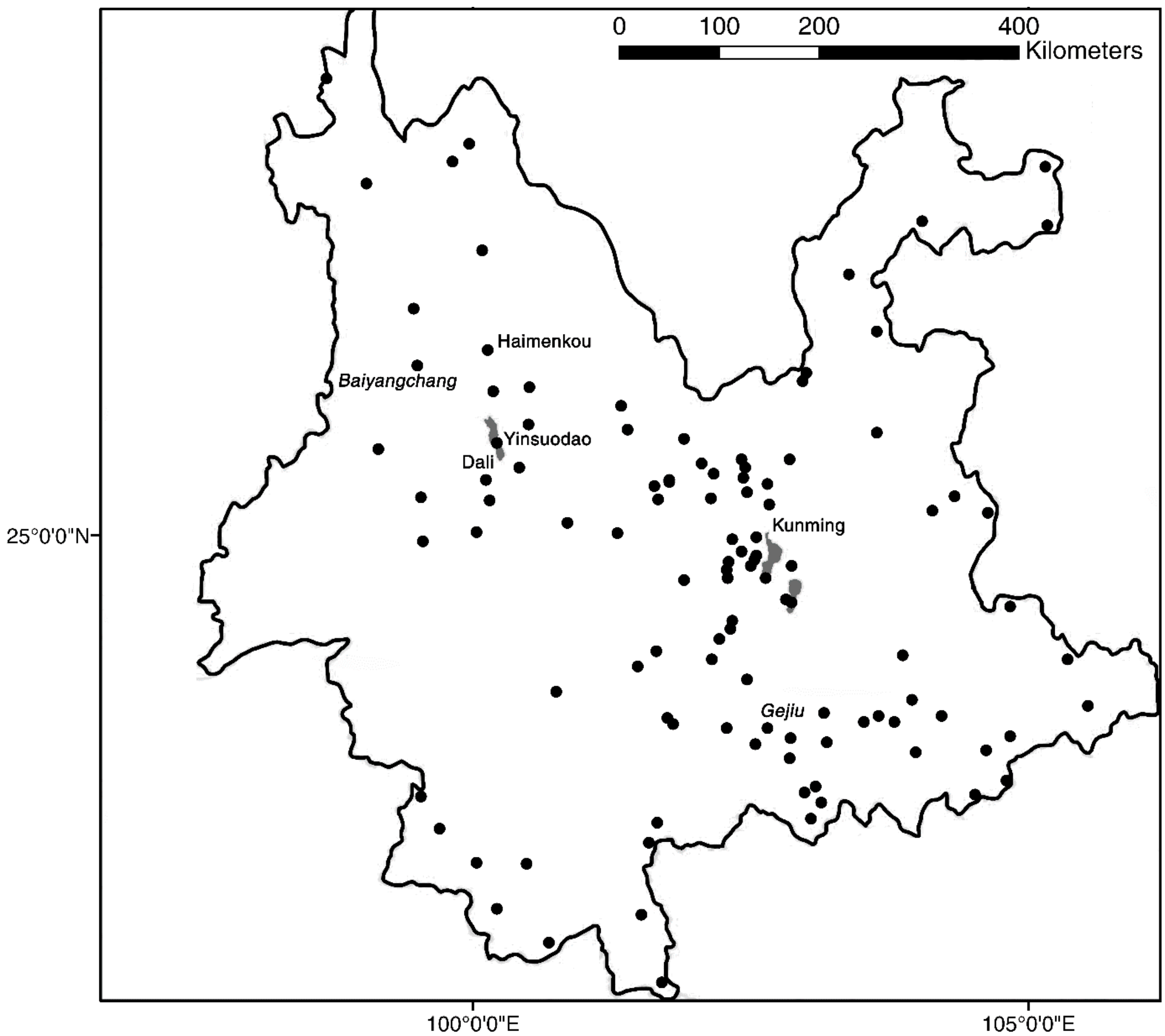

Figure 1-4- All known ore deposits in Yunnan (Kamitani et al., 2007) with place names mentioned in this chapter.

The earliest metallurgical activity in western Yunnan, in particular, has been a subject of debate due to a lack of dated artifacts and the absence of geochemical records of smelting activities. There may have been metal smelting and/or production facilities in the vicinity of Dali (Cui and Wu, 2008). Copper-based metalworking as early as 2nd millennium BC was found at the Haimenkou site (Yunnan Provincial Institute of Cultural Relics and Archaeology, 2009b; Min, 2013), located near Lake Jian, ~50 km north of Erhai, and at its contemporaneous site, Yinsuodao (Yunnan Provincial Institute of Cultural Relics and Archaeology, 2009a), on the southeastern shore of Erhai. Shared metallurgical features as well as artifact types indicate that these two sites were part of a 2nd and 1st millennia BC technological complex in western Yunnan that was linked to ore deposits along the Jinsha (upper Yangzi) valleys north and east of Erhai (Min, 2013). Moreover, lead isotope studies of Yunnan ores point to the possibility that the Baiyangchang ore body supplied materials for metal production at Haimenkou (Cui and Wu, 2008). Concurrent with the rise of hierarchical societies in western Yunnan during the first half of the 1st millennium BC, the progressing copper-based industry at sites near Haimenkou witnessed an increasing output of cultivation implements in addition to prestige goods (Chiou-Peng, 2011). Many of these metal objects became the prototypes of bronze (a mixture of copper and tin) in the Dian culture (ca. 350 BC-100 AD) located near Lake Dian in eastern Yunnan (Chiou-Peng, 2009).

Dian archaeological excavations suggest that by 700 BC copper materials were already being used (Yao and Zhilong, 2012) and that during the florescent stages of the Dian culture (200-50 BC), abundant bronze artifacts in conjunction with silver and gold objects were utilized. Although little evidence has been made available to explain how and where metal ores were exploited for the Dian communities, ancient texts in combination with modern lead isotope data point to several locales associated in the Gejiu polymetallic ore bodies in southern Yunnan, including Jianshui, Gejiu, and Mengzi deposits as possible sources (Cui and Wu, 2008). There is strong evidence indicating the existence in early 1st millennium AD of ore processing facilities at Gejiu (Dai and Zhang, 1998) as well as remains of accumulated ancient metal debris at the adjacent Jiansui and Mengzi deposits (Cui and Wu, 2008).

After the Dian people, various kingdoms and cultural traditions arose around Kunming, operating independently from the Chinese dynasties of the time. This independence limited the number and availability of historical records (Allard, 1998). Archaeological discoveries have filled in some gaps in written history, but have thus far been relatively limited. As bronze artifacts remained in vogue in Yunnan even after iron was introduced into the region toward the end of the 1st millennium BC, copper, tin, lead, and silver, likely continued to be extracted from these southern mines (Dai and Zhang, 1998) and used in parallel with many other ore deposits dispersed all over Yunnan (Zhang, 2000).

With the invasion of the Yuan Dynasty (the Mongols) in 1253 AD, the Dali Kingdom (an expansion of the previous regional Nanzhao government) was conquered and Yunnan nominally became part of Chinese territory (Giersch, 2009). Yunnan became well-known for its silver and copper deposits and mining and metal resource extraction was an integral part of the Yunnan economy (Yang, 2009). The Ming (ca. 1368-1644 AD) and the Qing (ca. 1644-1911 AD) Dynasties that followed heavily exploited the mineral resources of Yunnan for copper and silver, but historical records are insufficient and the true extent of this activity is unknown (Yang, 2009). The population of Yunnan increased dramatically during the Ming and Qing Dynasties as Han immigrants settled in great numbers to work in the mines (Lee, 1982).

Numerous studies have focused on recent changes in water and sediment quality (Liu et al., 2010; Zhang et al., 2010) and have attempted to document the changes associated with modern human disturbance through analysis of lacustrine sediment cores (Brenner et al., 1991; Whitmore et al., 1994a). However, bulk sediment radiocarbon measurements and hard-water reservoir effects made it difficult to constrain the timing of observed geochemical changes, thereby limiting this earlier work. Few studies of lake sediment cores from around Kunming have expressly examined the long-term effects of anthropogenic disturbance.

1.4 LACUSTRINE SEDIMENTS AS ENVIRONMENTAL ARCHIVES

Lacustrine sediments provide a geochemical archive of changes to the lake, its watershed, and the overlying atmosphere at a variety of spatial and temporal scales. The concentration and stable isotopic composition of organic matter, the stable isotopic composition of authigenic carbonate, and trace element geochemistry can offer insight into changes in lake trophic status, carbon cycling, hydrologic balance, and land use change. Combined, these proxies can provide an understanding of natural climate variability, past human-environment interactions, and limnological responses to landscape alterations.

To assess lake trophic status as well as nutrient loading arising from human activities, we focus on weight percent organic matter, weight percent carbon and nitrogen, the ratio of carbon to nitrogen (C/N), the ratio of nitrogen to phosphorus (N/P), and the stable isotopic composition of both carbon ($\delta^{13}C_{org}$) and nitrogen ($\delta^{15}N$) in organic matter. These proxies are not without their limitations and post-depositional loss of carbon and especially nitrogen may change C/N ratios as sediments are buried (Galman et al., 2008). Post-depositional loss may also affect the isotopic composition of organic carbon and nitrogen with increases and decreases of 1-2‰, respectively (Galman et al., 2009). With these caveats in mind, these variables are interpreted within the context of other sedimentological changes.

Weight percent carbon when paired with $\delta^{13}C_{org}$ can provide information on primary productivity. Lighter isotopes of carbon tend to be preferentially incorporated into organic matter; however, with increased productivity, ^{12}C gradually becomes depleted and ^{13}C starts to be utilized, driving up $\delta^{13}C_{org}$ values (Hodell and Schelske, 1998). When $\delta^{13}C_{org}$ values are interpreted in the context of C/N values, it can indicate the source of the organic matter being preserved in the lake (i.e. terrestrial or aquatic) (Meyers, 1994). Terrestrial organic matter typically has higher values of C/N (>14) while aquatic organic matter has lower values of C/N (<10) (Meyers and Laillier-verges, 1999).

While a full review of nitrogen isotopes is beyond the scope of this chapter, in general, $\delta^{15}N$ is a function of naturally-occurring reactive nitrogen sourced from biological fixation, lightning, and forest fires (Elliott and Brush, 2006). Controls on $\delta^{15}N$ can be complicated by many factors including primary productivity, nitrification, denitrification, ammonification, and volatilization. Lighter isotopes of nitrogen are preferentially used in biochemical and inorganic processes, leaving the remaining pool of nitrogen relatively enriched in ^{15}N. Determining the process is responsible for shifts in $\delta^{15}N$ in lakes is further complicated by post-depositional loss, inorganic nitrogen adsorbed by clay surfaces, and diatom nitrogen (Talbot, 2001). Additionally, modern day processes such as NO_x deposition from fossil fuel combustion and fertilizer and sewage runoff have perturbed the natural nitrogen cycle and isotopic signature (Kendall et al., 2007). Nonetheless, when used in conjunction with other proxies such as $\delta^{13}C_{org}$, weight percent nitrogen, and C/N, $\delta^{15}N$ values in lake sediments can give insight into trophic level shifts (Talbot et al., 1984), primary productivity (Brenner et al., 1999), cultural eutrophication (Hollander et al., 1992), and sewage inputs (Elliott and Brush, 2006). The ratio of nitrogen/phosphorus (N/P) in combination with $\delta^{15}N$ values can also be used to infer trophic status since eutrophic lakes and lakes with a high percentage of agricultural and sewage runoff have low N/P ratios (<6) (Downing and McCauley, 1992).

To assess changes in hydrologic balance, we rely on the stable isotopic composition of authigenic carbonate minerals that form in the water column and settle to the lake bottom, thereby archiving the lake water isotopic composition. While not all lakes precipitate carbonate minerals suitable for this analysis, where appropriate, the mineral of interest can be isolated and analyzed for its isotopic composition to estimate how water balance has changed through time. When lake levels rise and fall, the bathymetric characteristics of the lake change, which can alter the proportion of water lost through evaporation and change the isotopic composition of the lake water. To determine whether the cause of changes in water balance are due to natural climate variability or human modification of hydrology, it is necessary to compare our records to independent, well-established, nearby records of paleoclimate. Dongge Cave has been used to reconstruct variations in the strength of the monsoon over the Holocene and is situated in the Guizhou province of southwestern China, 530 km northeast of Yunnan (Wang et al., 2005). While some aspects of the Dongge Cave interpretation have been disputed by some researchers (Dayem et al., 2010; Maher and Thompson, 2012) and it may be more heavily influenced by the EASM (Araguás-Araguás et al., 1998), it is the closest record of monsoon variability that is unaffected by human activity.

To assess land use change, we rely on weight percent organic matter, carbonate, and residual mineral matter, magnetic susceptibility, and trace element geochemistry. Sediment may be delivered to lakes from surrounding watershed soils and is generally rich in elements such as aluminum, magnesium, and titanium (O'Hara et al., 1993). Concentrations of these metals, both weakly and strongly bound to the sediments, may be used to reconstruct erosional activities, however, mining and metalworking activities may also contribute to metal loadings on the landscape through atmospheric transport and may enter the lake system at a later time (see below). Magnetic susceptibility is often used as a proxy for the proportion of sediment derived from magnetic sources, such as basalt (Dearing et al., 2008), but may also indicate secondary processes such as burning, fossil fuel combustion, soil formation, and digenesis (Dearing, 1999). Since many of the lake catchments selected for study in Yunnan include basaltic bedrock (Bureau of Geology and Mineral Resources of Yunnan Province, 1990), we primarily interpret magnetic susceptibility to indicate erosional processes occurring within watersheds, in conjunction with the concentration of the aforementioned lithogenic elements. Changes in weight percent organic matter, carbonate, and residual mineral matter may also aid in the interpretation of these proxies.

Lastly, to assess the relative intensity of metalworking processes such as smelting, we rely on concentrations of elements weakly bound to the sediment. Metallurgical activity in China relied on a process known as cupellation. Ores of interest, usually silver and gold, were heated in low temperature ovens which caused lead oxides to form from ore impurities (Murowchick, 1989). These lead oxides would be volatized and transported in the atmosphere until being deposited by wet and dry fallout onto the landscape and lakes. Once in the water column, metals, such as lead, adsorb onto clay particles and organic matter and are deposited on the lake bottom forming layers that archive smelting history of the region. Lake sediments are sensitive enough to record very low intensity trace metal emissions, such as those produced by early pre-industrial efforts (Abbott and Wolfe, 2003; Renberg et al., 1994). There are several caveats to this approach (see above) and the concentrations of weakly bound metals must always be interpreted in the context of other erosional proxies.

We use an integrated approach to establish age control. These methods include: 1) ^{137}Cs measurements to anchor the 1963 cesium peak produced from atmospheric testing of nuclear weapons (Lima et al., 2005), 2) ^{210}Pb assays to constrain the upper sediments for the last 100-150 years (Appleby and Oldfield, 1983), and 3) accelerator mass spectrometry (AMS) ^{14}C measurements on charcoal and identifiable terrestrial macrofossils. Samples such as leaves and charcoal were targeted for dating because they are less subject to transport and reworking. Additionally, radiocarbon measurements made on discrete macrofossils are less subject to hard-water effects than bulk sediment or shell dates, which often appear several thousand years too old (Taylor, 1978). However, larger macrofossils such as pieces of wood may lie on the landscape and be subject to reworking (Abbott and Stafford, 1996); thus the eventual transport of such material into the lake may make sediments appear older than their true age of deposition. The interpretation of these dates should be considered within the context of other dates.

What follows in the next five chapters is a presentation of results from four lakes in the Yunnan province (**Table 1-1**). The late Holocene portion of Xing Yun Lake is presented in Chapter 2.0 while the Pleistocene and early-middle Holocene portion is presented in Chapter 3.0. Erhai Lake is presented in Chapter 4.0, Dian Lake is presented in Chapter 5.0, and Chenghai Lake is presented in Chapter 6.0. Chapter 2.0 was published in *Quaternary Science Reviews* in 2014, Chapter 4.0 was published in *Environmental Science and Technology* in 2015, and Chapter 6.0 is currently being prepared for publication. Since individual chapters are either published or intended for publication, they may contain redundancies in the introductory text and methods.

2.0 XING YUN LAKE

Rapid Environmental Change during Dynastic Transitions in Yunnan Province, China

Here, we present a 3,500-year sediment record from Xing Yun Lake, approximately 70 km south of Kunming, the capital of Yunnan. Xing Yun is a lake with a simple catchment and is located in a region containing several well-studied climate records. Additionally, a burial site, Lijiashan, associated with the Dian culture is located within the watershed of Xing Yun (Higham, 1996), making it ideal to investigate the long-term effects on lake sediment geochemistry associated proximal human activity. To reconstruct changes in land-use, lake-level management, and mineral resource extraction, we rely on measurements of sediment composition (% organic, carbonate, and mineral matter as well as magnetic susceptibility), the concentration and isotopic composition of organic carbon and nitrogen (%C, %N, $\delta^{13}C_{org}$, and $\delta^{15}N$), the oxygen and carbon isotopic composition of authigenic calcite ($\delta^{18}O_{carb}$ and $\delta^{13}C_{carb}$), and the concentrations of weakly bound metals (Al, P, Pb, and Hg) in sediment. We use these analyses to investigate the timing and magnitude of environmental changes at Xing Yun Lake in the context of anthropogenic activities that coincide closely with periods of cultural transition. We find that after 500 AD, isotopic and geochemical variations archived in the sediments are primarily the result of human activities such as land use change, hydrologic modification, and cultural eutrophication.

2.1 REGIONAL SETTING

Xing Yun Lake (24°10'N, 102°46'E) is a shallow (Z_{max}: 11 m) and eutrophic lake (Liu et al., 2012) with a surface area of 34 km^2 and a watershed area of 383 km^2. The lake catchment contains large flat sections of land used for rice agriculture. The western side of the catchment is dominated by slate and phyllite and the eastern side is composed of sandstone, shale, and limestone (Bureau of Geology and Mineral Resources of Yunnan Province, 1990). The lake's only surficial outflow is the Ge River, which drains into deep Fuxian Lake; however, today several dams exist on the Ge River, regulating water flow. The annual weighted $\delta^{18}O$ mean of modern rainfall for Kunming is -9.86‰ VSMOW (**Table 1-2**) and the $\delta^{18}O$ value of a water sample taken from the lake in 2009 is -4.3‰ VSMOW, suggesting that substantial water loss from Xing Yun occurs through evaporation (**Figure 1-3**).

The hydrologic and isotopic sensitivity of Xing Yun to changes in precipitation associated with the ASM was previously explored by Hodell et al., 1999 using a 12.5 m sediment core collected near the southern end of the lake at a water depth of 7 meters (**Figure 2-1**). Grain size, magnetic susceptibility, and oxygen isotopic values of authigenic carbonate were measured. The Hodell et al. 1999 study suggested that from 20,000 to 12,000 years BP, lake water $\delta^{18}O$ values decreased, indicating an increase in the strength of the ASM, and that from 8,000 years BP to present, $\delta^{18}O$ values increased in response to a weakening ASM. These isotopic shifts occurred in conjunction with changes in Northern Hemisphere summer insolation, similar to conclusions drawn from the Dongge Cave record (Wang et al., 2005). Notably however, the chronology of the Hodell et al. 1999 Xing Yun $\delta^{18}O$ record was constrained by bulk sediment and gastropod shell radiocarbon dates, which are subject to hard-water effects (Deevey et al., 1954). Further, the low sampling resolution (5-6 cm) makes the $\delta^{18}O$ transitions appear abrupt and uneven, a consequence that precludes a direct comparison to the Dongge Cave record (which has a much higher temporal resolution) and makes it difficult to constrain the timing of abrupt shifts in $\delta^{18}O$ values. The Hodell et al. 1999 study acknowledged the possibility of recent anthropogenic disturbance (last 250 years) on Xing Yun, but did not address the possibility of impacts on the lake by earlier human activity.

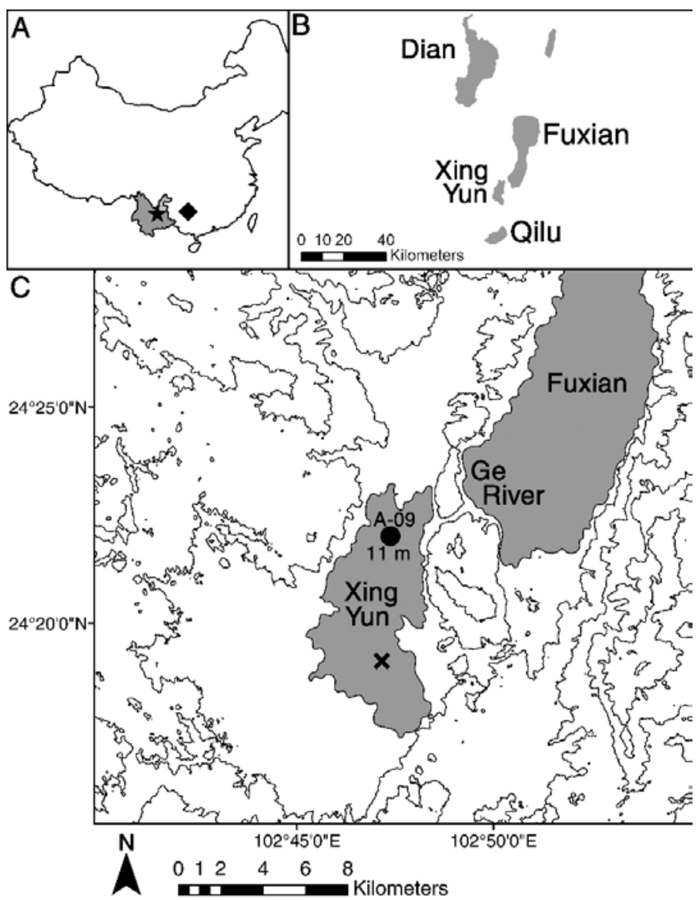

Figure 2-1- A- Locations of Xing Yun Lake (star), Dongge Cave (diamond); B- Yunnan lakes near Kunming; C- Xing Yun Lake (1721 m elevation) with 200 m contour intervals. Coring location in this study is marked by the circle. Coring location from Hodell et al., 1999 is marked X.

2.2 MATERIALS AND METHODS

2.2.1 Core collection

Four overlapping cores from Xing Yun were collected in 2009 from the deepest part of the lake (11 m) (**Figure 2-1)**, forming a composite record of 317 cm. Core D-1 was recovered using a 5.5-cm diameter piston core with a removable polycarbonate tube and measures 133.5 cm. A steel barrel Livingston corer (Wright et al., 1984) was used to collect three overlapping cores (D-2, D-3, and D-4) from below this depth. These three Livingston sections were extruded in the field and measure 92 cm, 96 cm, and 63 cm, respectively. An Aquatic Research percussion core measuring 75 cm was taken from the same location, and the upper 56 cm were extruded in the field at 0.5-cm intervals.

2.2.2 Age Control

Radiocarbon ages were measured on seven terrestrial macrofossils and three gastropod shells. Samples were analyzed at Keck Center for Accelerator Mass Spectrometry at the University of California Irvine. Prior to analysis, samples were pretreated using a standard acid, base, acid procedure (Abbott and Stafford, 1996). The resulting ages were calibrated using CALIB 6.0 and the INTCAL09 calibration curve (Reimer et al., 2009). The upper 11 cm of the gravity core were lyophilized and analyzed for ^{210}Pb and ^{214}Pb activities by direct gamma (γ) counting in a broad energy germanium detector (Canberra BE-3825) at the University of Pittsburgh.

2.2.3 Geochemistry

Water content and bulk density were measured at 2 cm intervals using 1 cm^3 samples. Weight percent organic matter and carbonate content within these same samples was determined by loss-on-ignition (LOI) analysis at 550°C and 1000°C, respectively (Dean, 1974). Sediment core magnetic susceptibility was measured on split cores using a Bartington® Instruments Ltd. ME2EI surface-scanning sensor equipped with a TAMISCAN-TSI automatic logging conveyer.

Weight percent nitrogen, weight percent organic carbon, $\delta^{15}N$, $\delta^{13}C_{org}$, and atomic C/N ratio were measured at 2-cm intervals. Samples were covered in 1 M HCl for 24 hours to dissolve carbonate minerals and rinsed. Samples were then lyophilized and analyzed at Idaho State University using an ECS 4010 (Elemental Combustion System 4010) interfaced to a Delta V mass spectrometer through the ConFlo IV system. Organic carbon isotopes are expressed in conventional delta (δ) notation as the per mil (‰) deviation from the Vienna Peedee Belemnite standard (VPDB) whereas nitrogen isotopes are reported relative to atmospheric N_2.

Cores were sampled continuously at 0.5-cm intervals for analysis of the oxygen and carbon isotopic composition of carbonate minerals. Samples were disaggregated with 7% H_2O_2 and sieved through a 63-µm screen to remove biological carbonates derived from ostracod and gastropod shells. Samples were soaked in a 50% bleach and 50% DI water mixture for 6-8 hours, rinsed, and lyophilized. Bulk carbonate samples were reacted in ~100% phosphoric acid at 90°C and measured using a dual-inlet GV Instruments, Ltd. (now Isoprime, Ltd) IsoPrime™ stable isotope ratio mass spectrometer and MultiPrep™ inlet module at the Regional Stable Isotope Laboratory for Earth and Environment Science Research at University of Pittsburgh. Oxygen and carbon isotope results are expressed in conventional delta (δ) notation as the per mil (‰) deviation from VPDB. One sigma analytical uncertainties are within ±0.10‰. Replicate measurements of $\delta^{18}O_{carb}$ and $\delta^{13}C_{carb}$ of Xing Yun sediment had an average standard deviation of 0.10 and 0.20‰ (VPDB), respectively.

Weakly sorbed metal concentrations were measured at 6-cm intervals between 317 cm and 53 cm; above 53 cm depth, samples were measured at 1–3 cm intervals. All samples were lyophilized and homogenized prior to analysis. Elements were extracted by reacting samples with 10 mL of 1 M HNO_3 for ~24 hours (Graney et al., 1995). The supernatant was extracted and diluted before measurement on an inductively coupled plasma mass spectrometer (ICP-MS); samples below 260 cm depth were measured on a Perkin-Elmer NeXION 300x ICP-MS at the University of Pittsburgh and samples above 260 cm were measured on a Perkin-Elmer Sciex Elan 6000 ICP-MS at the University of Alberta. Duplicates were run on every 10th sample and were within 5% of each other. Blanks were run every 10 samples and were consistently below detection limits of interest. Lead isotopes were extracted by reacting samples with 10 mL of 1 M HMO_3 overnight and measured on an MC-ICP-MS at Yale University. Measurement of total Hg was undertaken using a DMA80 direct mercury analyzer at Yale University. Standard reference materials (Mess-3) included in each run were within 10% of certified values.

Five samples were analyzed for organic biomarker compounds at the Lamont-Doherty Earth Observatory Organic Geochemistry Lab through intervals of interest, following the methods outlined in Polissar and Freeman, 2010. Freeze-dried sediments were extracted with a Dionex Accelerated Solvent Extraction (ASE) system. Two to 5 g of dried sediment were placed in the stainless-steel sample holders and extracted at 100°C and 1000 psi with 10% (v/v) methanol/dichloromethane with a total volume of 50 mL. These total lipid extracts (TLEs) were evaporated to near dryness with N_2 in a Turbovap solvent evaporator and transferred to 4 mL borosilicate vials with Teflonlined caps. All remaining solvent was then evaporated and the TLE stored in a few drops of hexane at 4°C. TLEs were separated into aliphatic (F1), ketone/alcohol/acid (F2), and polar (F3) fractions with silica gel column chromatography. Silica gel was transferred in hexane to the SPE column and the column then rinsed twice with 6 mL hexane. The TLE was loaded on the column in 100 μL hexane and the F1, F2, and F3 fractions eluted with 5 mL of 10% dichloromethane in hexane, 8 mL ethyl acetate, and 5 mL methanol. Compounds were characterized by gas chromatography–mass spectrometry (GC–MS) using an Agilent 6890 GC with a split/ splitless injector operated in splitless mode at 300°C, a DB-5 column (0.25 mm i.d., 0.25 lm film thickness, 30 m length), 2.0 cm^3 min1 He flow and programmed heating of the oven from 60 to 170°C at 15°C/min, and to 320°C at 5°C/min, and an Agilent 5973 quadrapole mass spectrometer. Compounds were identified by elution time, comparison with published spectra, and authentic standards.

2.3 RESULTS AND DISCUSSION

2.3.1 Core Chronology

Radiocarbon ages were measured on seven terrestrial macrofossils and three gastropod shells, the latter of which provide an estimate of the hard-water effect. Dates from the gastropods are approximately 1,100 years older than the terrestrial macrofossil ages (**Table 2-1**). This offset is consistent with the radiocarbon reservoir age previously noted in Xing Yun and other Yunnan lakes (Hodell et al., 1999; Whitmore et al., 1994a; Xu and Zheng, 2003). The upper 11 cm of the percussion core were dated using the constant rate of supply (CRS) ^{210}Pb age model method (**Table 2-2)** (Appleby and Oldfield, 1983). An age-depth model for the Xing Yun sediment record was developed using the ^{210}Pb ages and calibrated macrofossil radiocarbon dates (**Figure 2-2**). A third order polynomial was used to produce an age model using the *clam* 2.1 code (Blaauw, 2010) in the statistical software package "R" (R Development Core Team, 2008). Uncertainty (2σ) associated with the age-depth model is generally limited to ±60 years. The composite record of 317 cm spans 3,500 years.

Table 2-1- AMS Radiocarbon Dates for samples from Xing Yun

UCI Number	Composite Core Depth (cm)	Sample Type	^{14}C age (BP)	±	Median Probability Calibrated Age (yr AD/BC)	2σ Calibrated Age Range (yr AD/BC)
71481	35.5	Wood	110	25	1838	1954-1682
71482	37.5	Charcoal	110	50	1827	1954-1673
84722*	42.5	Gastropod Shell	1245	20	739	863 - 685
71483	59	Charcoal	130	25	1826	1953 - 1677
84866	145	Charcoal	1060	25	988	1022 - 898
84723*	222.5	Gastropod Shell	3000	25	-1252	-1130 - -1372
84867	250	Wood	2105	20	-129	-54 - -191
84724*	259.5	Gastropod Shell	3285	20	-1566	-1508 - -1615
84815	263	Charcoal	2220	20	-277	-204 - -378
122325	310.5	Charcoal	3070	15	-1350	-1299 - -1407

* denotes date excluded from age model due to reservoir effect

Table 2-2- Down-core ^{210}Pb activities, ^{214}Pb activities, cumulative weight flux, and constant rate of supply (CRS) sediment ages.

Depth (cm)	^{210}Pb activity, Bq-g^{-1}	1σ Error ^{210}Pb activity	^{214}Pb activity, Bq-g^{-1}	1σ Error ^{214}Pb activity	Cumulative Weight Flux, g cm^{-2}	CRS age (yr AD/BC)	1σ Error Age
0.5-1.0	0.2500	0.0335	0.1120	0.0097	0.09	2008	2.08
1.0-1.5	0.2270	0.0318	0.0745	0.0087	0.15	2006	2.14
3.0-3.5	0.2180	0.0343	0.0767	0.0088	0.46	1996	2.39
4.0-4.5	0.2020	0.0280	0.0660	0.0072	0.66	1988	2.64
5.0-5.5	0.1770	0.0249	0.0583	0.0064	0.91	1976	2.98
6.0-6.5	0.1140	0.0170	0.0623	0.0057	1.09	1971	3.19
7.0-7.5	0.1310	0.0163	0.0614	0.0048	1.28	1963	3.67
8.0-8.5	0.1100	0.0158	0.0656	0.0053	1.50	1954	4.10
9.0-9.5	0.0998	0.0134	0.0663	0.0048	1.70	1947	4.62
10.0-10.5	0.1030	0.0128	0.0672	0.0047	1.92	1936	5.68
11.0-11.5	0.0876	0.0091	0.0556	0.0048	2.15	1919	8.22

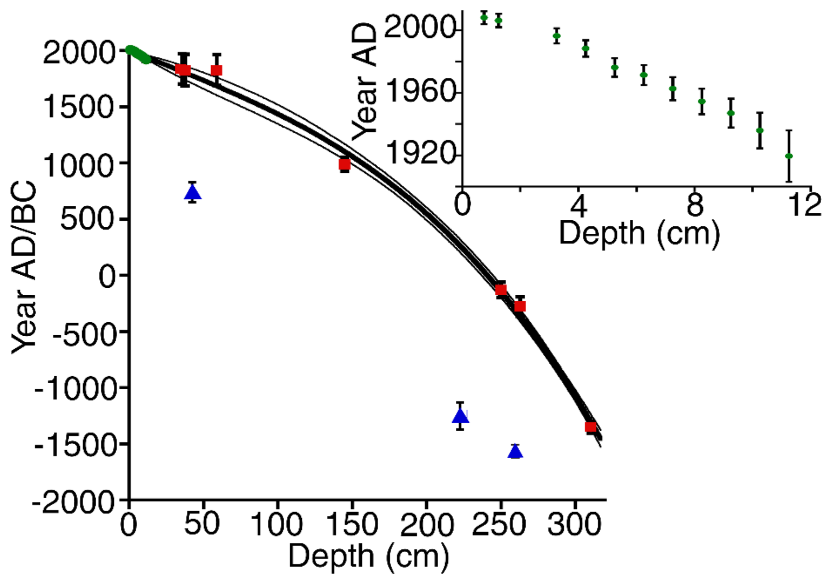

Figure 2-2- Age-depth model and 95% confidence intervals. ^{210}Pb (green circles), radiocarbon (red squares), gastropod shell dates (blue triangles), all with 2 sigma error bars. Gastropod shell dates exhibit a relatively consistent 1,100 year offset from terrestrial macrofossils and were excluded from the age model. ^{210}Pb age model detail is displayed in the inset.

2.3.2 Sedimentology

Two distinct sedimentological units characterize the Xing Yun sediment record. Unit I, (317-200 cm) spans 1500 BC-500 AD and is composed of ~50% carbonate, 40% mineral matter, and 10% organic matter (**Figures 2.3 and 2.4**). The transition from Unit I into II (200-157 cm) spans 500-1000 AD and is characterized by a marked increase in residual mineral content, decrease in carbonate, and little change in organic matter. Unit II (157-0 cm) spans 1000 AD-present and mainly consists of iron-rich red clays and silts that are low in both calcium carbonate (<10%) and organic matter (10–20%) content; the color and composition of these Unit II sediments match closely with catchment soils. These sedimentological units also broadly correspond to geochemical changes.

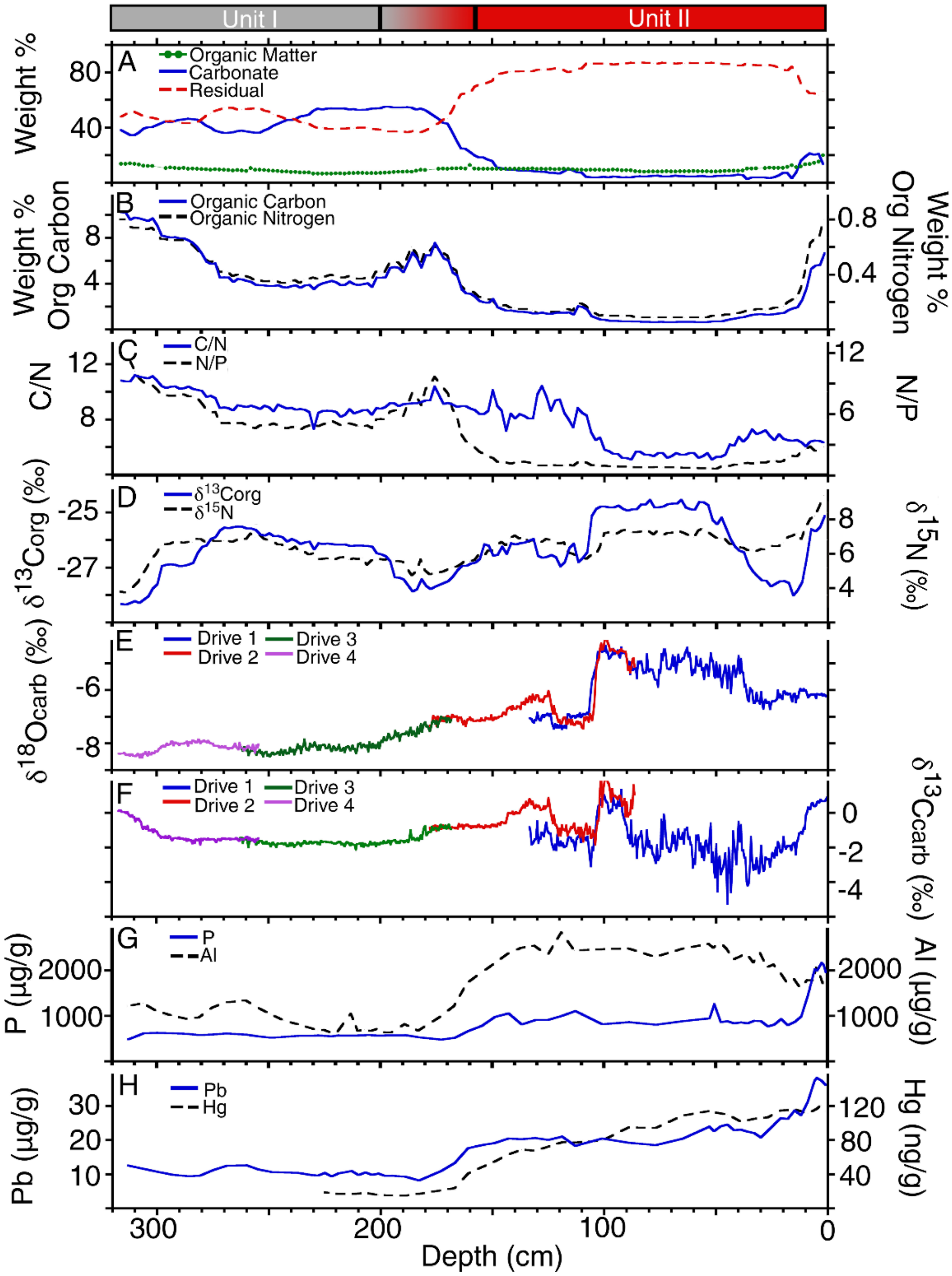

Figure 2-3- Proxies by depth. A- Weight percent organic matter (green circles), calcium carbonate (blue solid line), and residual mineral matter (red dotted line); B- Percent organic carbon (blue solid line), percent organic nitrogen (black dotted line); C- Carbon to nitrogen ratio (blue solid line), nitrogen to phosphorus ratio (black dotted line); D- Carbon isotope values of organic matter (blue solid line), nitrogen isotope values of organic matter (black dotted line); E- Oxygen isotopic composition of Xing Yun calcite- Drive 1 (blue),

Drive 2 (red), Drive 3 (green), Drive 4 (purple); F- Carbon isotopic composition of Xing Yun calcite- Drive 1 (blue), Drive 2 (red), Drive 3 (green), Drive 4 (purple); G- Concentration of phosphorus (blue solid line), aluminum (black dotted line); H- Concentration of lead (blue solid line) and mercury (black dotted line).

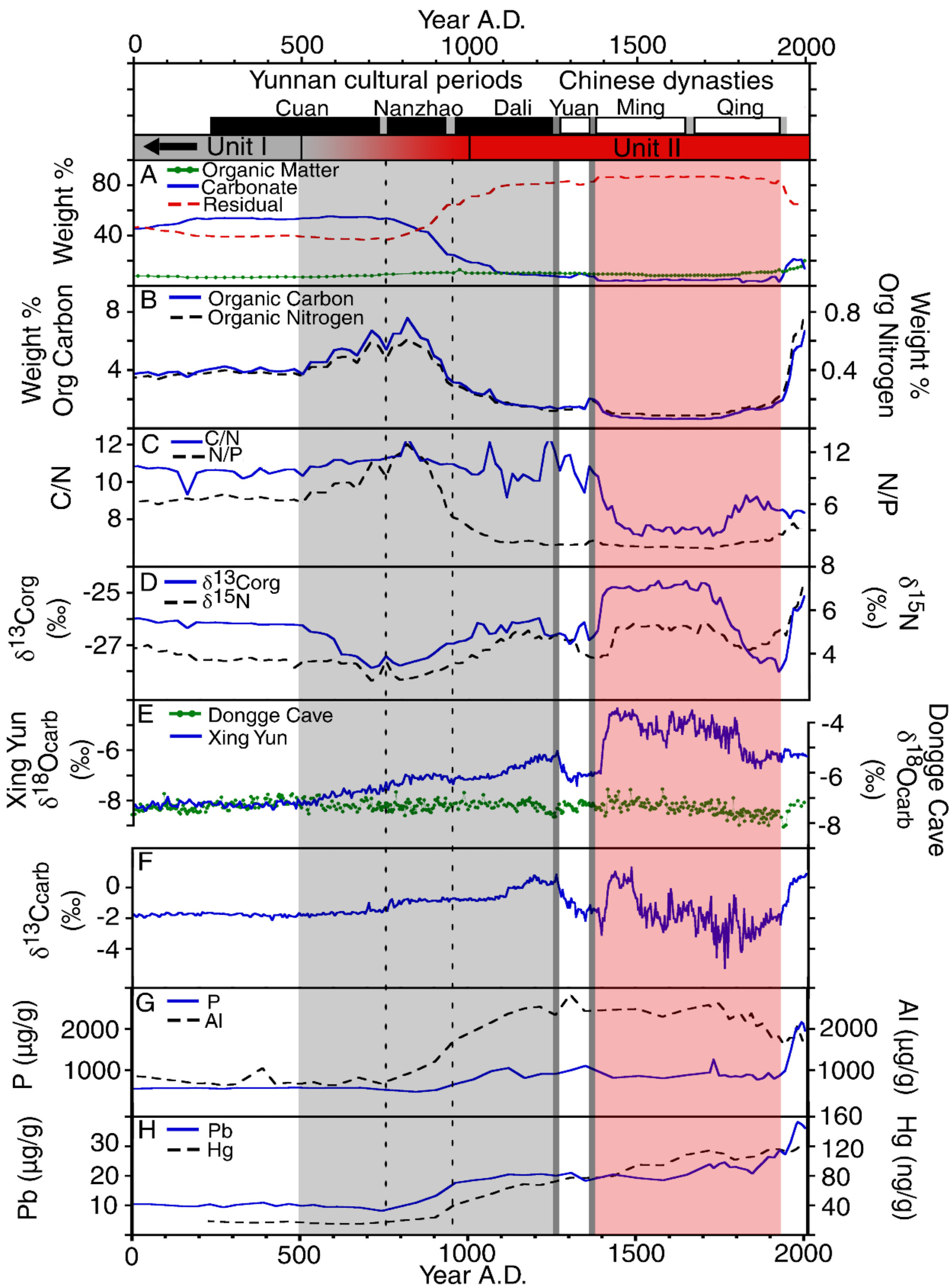

Figure 2-4- A- Weight percent organic matter (green circles), calcium carbonate (blue solid line), and residual mineral matter (red dotted line); B- Percent organic carbon (blue solid line), percent organic nitrogen (black dotted line); C- Carbon to nitrogen ratio (blue solid line), nitrogen to phosphorus ratio (black dotted line); D-

Carbon isotope values of organic matter (blue solid line), nitrogen isotope values of organic matter (black dotted line); E- Oxygen isotopic composition of Xing Yun calcite (blue solid line), Dongge Cave (green circles); F- Carbon isotopic composition of Xing Yun calcite; G- Concentration of phosphorus (blue solid line), aluminum (black dotted line); H- Concentration of lead (blue solid line) and mercury (black dotted line). The gray bar is the initiation of human disturbance on the lake; the dotted lines are the establishment and decline of the Nanzhao Kingdom; the white with gray bars are the establishment and decline of the Yuan Dynasty; the red bar is the establishment of the Ming and decline of the Qing Dynasty.

We interpret $\delta^{18}O_{carb}$ to primarily reflect changes in the lake water balance. Xing Yun water samples suggest that a large portion of lake water is lost through evaporation (**Figure 1-3**), so lake water isotopes should reflect the balance between precipitation and evaporation (P/E). When lake levels rise or fall, the bathymetric characteristics of the lake (volume, surface area, etc.) change and alter the proportion of water lost through evaporation, which in turn alters the isotopic composition of the remaining lake water (Leng and Marshall, 2004; Steinman et al., 2010; Steinman and Abbott, 2013). Authigenic calcite minerals that form in the Xing Yun water column (and settle to the lake bottom) archive the lake water isotopic composition. By isolating the authigenic calcite and analyzing its isotopic composition, we can estimate how lake levels have changed through time.

Stable isotopes in speleothem carbonate at Dongge Cave in the Guizhou province, 530 km northeast of Xing Yun (Wang et al., 2005) (**Figure 2-1**), were used to reconstruct variations in the strength of the EASM over the Pleistocene and Holocene. We use the Dongge Cave record as our primary comparative dataset because of the cave's proximity to Xing Yun, the similarity in climate (**Tables 1.2 and 2.3**), and the well-dated, high-resolution nature of the record.

Table 2-3- Monthly average temperature, precipitation, and oxygen isotope values at Dongge Cave (25°17'N, 108°50'E, 680 m) (Dykoski et al., 2005).

	Jan	Feb	Mar	April	May	June	July	Aug	Sept	Oct	Nov	Dec
Average Temperature (°C)	5.2	9.9	11.3	16.3	19.7	22.1	23.5	22.8	20.8	16.4	11.4	7.2
Average Precipitation (mm)	29.8	36.7	55.7	135.7	237.8	305.4	324.2	292.3	124.8	116.4	61.8	32.5
$\delta^{18}O$ (‰VSMOW)	-4.72	-3.45	-4.47	-2.82	-5.16	-7.99	-12.42	-9.67	-12.48	-10.06	-6.99	-5.43

Average weighted $\delta^{18}O$ (‰VSMOW) = -8.33

Samples taken at even intervals within Units I and II were analyzed using X-ray diffraction (XRD). XRD analysis identified calcite as the primary carbonate mineral in all the samples (**Figure 2-5)**. We calculated the theoretical $\delta^{18}O$ value of calcite using **Equation 2-1**:

$$\mathbf{1000}\boldsymbol{ln\alpha}(\text{Calcite-H}_2\text{O})\ \mathbf{=18.03(10^{3}T^{-1})-32.42}$$

Equation 2-1 (Kim and O'Neil, 1997)

where T = 20°C (the mean June, July, August temperature of Kunming). Given the observed $\delta^{18}O$ value of -4.3‰ VSMOW from the water sample collected in 2009, the $\delta^{18}O$ value of calcite precipitated during the summer should be -6.5‰ VPDB. This value is very close to the $\delta^{18}O$ value of calcite in the surface sediments (-6.2‰), supporting our assertion that the calcite is authigenic and that it precipitates in isotopic equilibrium with the lake water.

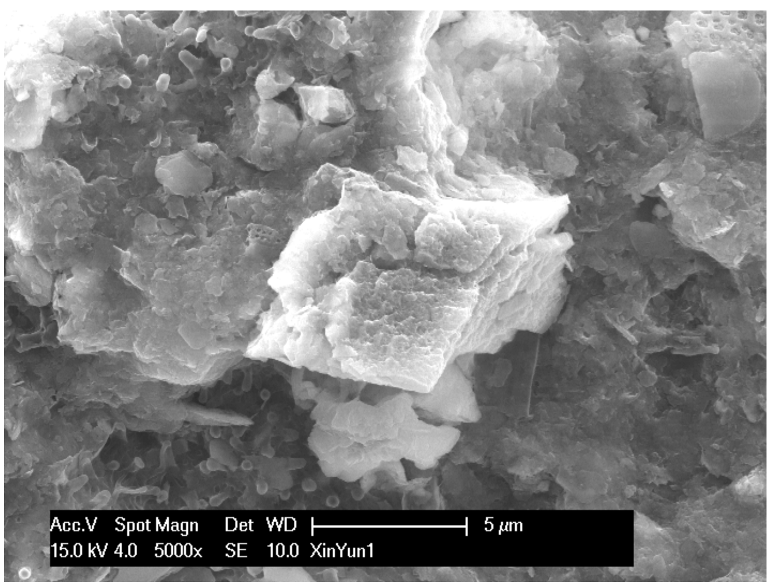

Figure 2-5- SEM image of euhedral calcite from Xing Yun A-09 D1 4 cm.

2.3.3 Geochemistry

2.3.3.1 Unit I- Pre-human disturbance

Within Unit I, some of the proxies (%C, %N, C/N, N/P, $\delta^{13}C_{org}$, $\delta^{15}N$, and Al) exhibit slight shifts, particularly from 280-240 cm (680 BC-5 AD) (**Figure 2-3**). This time period corresponds with the Dian culture (400 BC-100 AD); these slight changes may indicate early, but minimal, land use change. However, in the context of the full record, these geochemical variations are minimal and are not accompanied by any sedimentological changes (e.g., sediment color or % residual mineral matter). Since many of the other proxies are stable prior to 500 AD, we focus our attention on the last 2,000 years (**Figure 2-4**).

Trace metal concentrations are steady and low in this interval ($P_{average}$: 600±30 µg/g; $Pb_{average}$: 10±1 µg/g; $Hg_{average}$: 20±1 ng/g). Notably, the oxygen isotopic composition of the authigenic calcite is highly stable, averaging -8.2±0.2‰. This is ~1‰ lower than the average $\delta^{18}O$ value (-7.4±0.2‰ over the past 3,500 years) of a speleothem from Dongge Cave (Wang et al., 2005). The difference between the Xing Yun and Dongge Cave $\delta^{18}O$ values can be explained by disparity in the annual weighted $\delta^{18}O$ means of modern rainfall in these two regions, which are offset by ~1.5‰ (**Tables 1.2 and 2.3**). This suggests that Xing Yun was an overflowing, hydrological open system prior to 500 AD and that the calcite precipitated during this time primarily records the oxygen isotopic composition of regional rainfall (with secondary influence by lake water temperature) (Kim and O'Neil, 1997; Leng and Marshall, 2004). This portion of the record agrees well with previous analyses of Xing Yun $\delta^{18}O_{carb}$ values, when accounting for the aforementioned reservoir effect of 1,100 years (Hodell et al., 1999) (**Figure 2-6**).

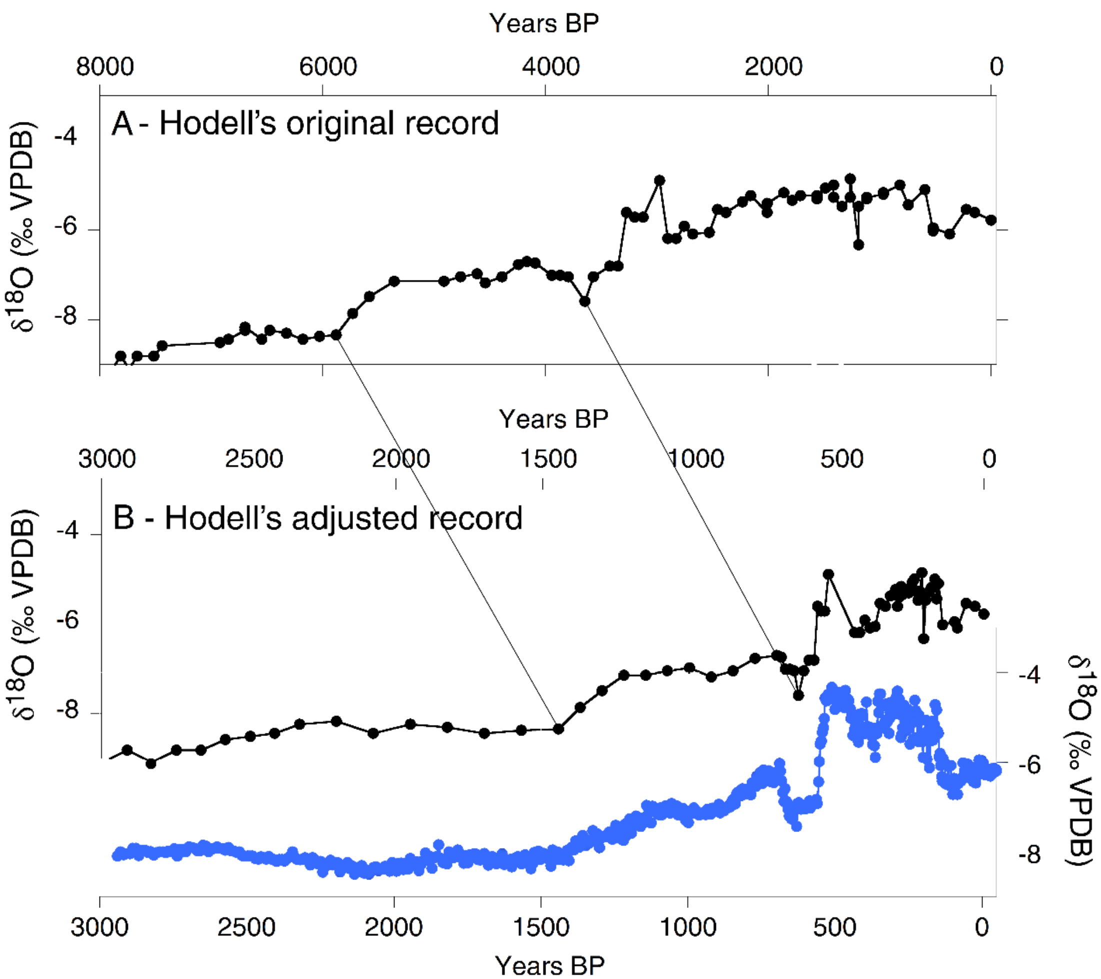

Figure 2-6- A- Hodell's original δ^{18}O record from 8,000 years BP to present based on bulk sediment radiocarbon dates and gastropod shell dates. B- Hodell's adjusted δ^{18}O record and our new, high-resolution δ^{18}O record (in blue) with an age model based on terrestrial macrofossils. Our record shows that Hodell's original record is offset by several thousand years and that the low resolution sampling overlooked several abrupt shifts in oxygen isotopes.

Our results indicate that anthropogenic impact on the lake was relatively limited prior to ~500 AD. This is despite a well-known burial site associated with the Dian culture within Xing Yun's watershed (Higham et al., 2011) and historical indication of rice agriculture in Yunnan since the Han Dynasty (ca. 200 BC) (Herman, 2002). This also contrasts with a previous paleolimnological study of Erhai Lake, located ~300 km to the northwest of Xing Yun, which found palynological evidence for landscape modification as early as the middle Holocene (Dearing et al., 2008). Archaeological and historical evidence indicate that the political and cultural traditions around Xing Yun were different from those of Erhai, near which there are no Dian burial sites (Elvin et al., 2002; Higham, 1996).

2.3.3.2 Transition period

The transition from Units I to Unit II, which spans the period from 500 to 1000 AD, is marked by substantial shifts in most of the proxies (**Figure 2-4**). Percent carbon and nitrogen roughly double before declining, and $\delta^{13}C_{org}$ and $\delta^{15}N$ shift briefly towards lower values before increasing by 1‰ and 2‰ respectively. Additionally, gradual increases in the $\delta^{18}O_{carb}$ and $\delta^{13}C_{carb}$ values occur at the beginning of this transition. Around 800 AD, P, Pb, and Hg concentrations roughly double while Al concentrations increase by ~3-fold. These geochemical changes occur in conjunction with increased mineral matter and decreased carbonate content. A plot of $\delta^{18}O$ values versus concentrations of phosphorus, aluminum, lead, and mercury (**Figure 2-7**) reveal that changes in the concentrations of metals occurred independently from changes in lake level. The change in water level from 500-800 AD did not cause a significant change in metal concentrations. In particular, we note the transition across $\delta^{18}O$ values of -7‰ where metal concentrations increase while lake level remains relatively constant. This occurs from 800-1120 AD and demonstrates that the increase in metals at this time is unrelated to lake level. A concomitant shift in lead isotopes (**Figure 2-8**) indicates a change in the source of lead. However, the isotopic composition of ores from various mines in southwestern China (Chang and Zhu, 2002; Cheng et al., 2012b; Xue et al., 2007; Zhang et al., 2006; Zhou et al., 2001) does not match the isotopic composition of the lake sediments at this time; therefore the source of lead cannot be directly ascribed to any particular mineral deposit and further supports the conclusion that the lead was likely washed in from erosional activity.

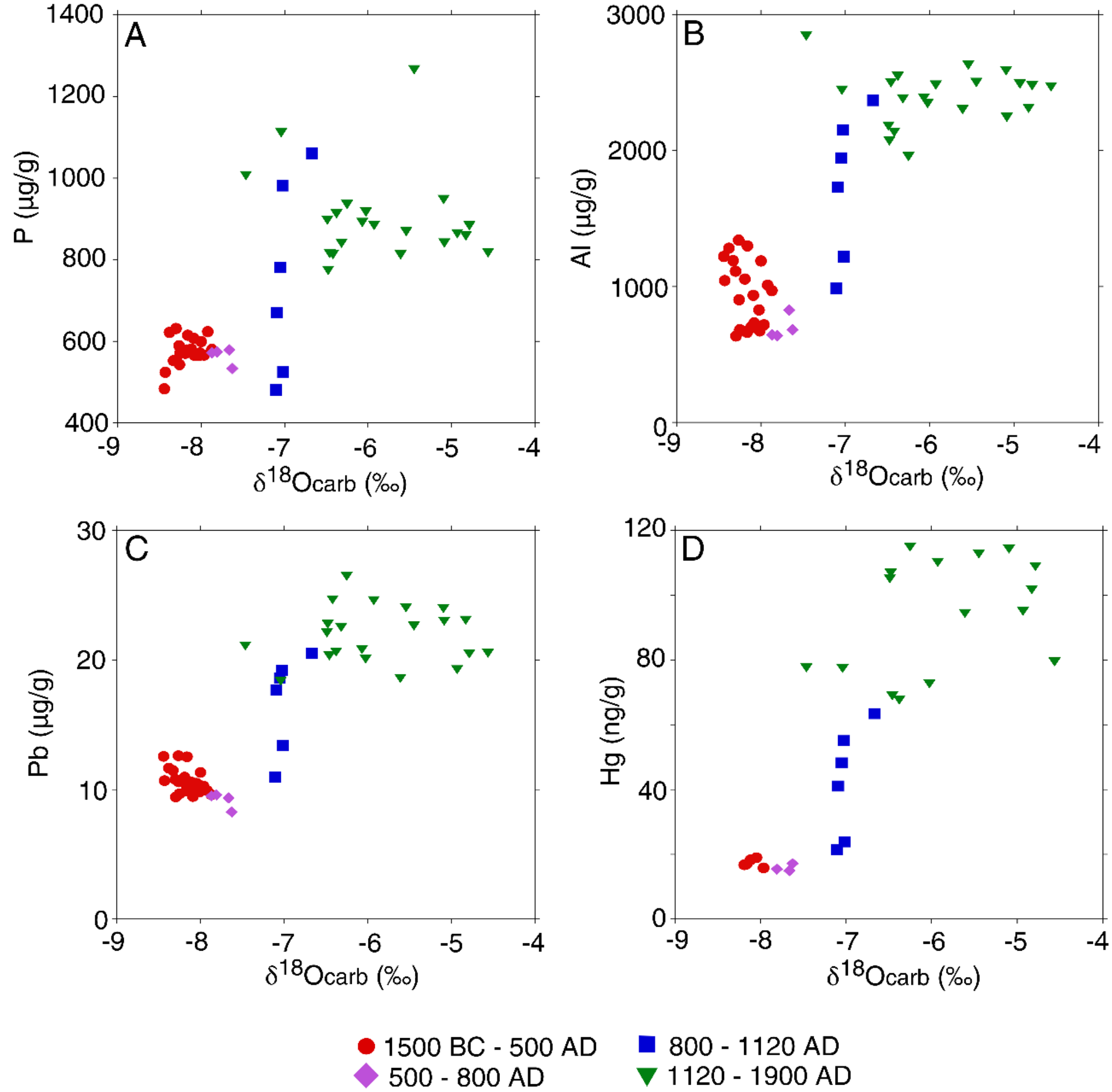

Figure 2-7- Oxygen isotopes of calcite plotted against A- phosphorus, B- aluminum, C- lead, and D- mercury. Twentieth century values have been removed as they are anomalously high in phosphorus. The time period from 1500 BC-500 AD is represented by red circles, 500-800 AD by purple diamonds, 800-1120 AD by blue squares, and 1120-1900 AD by green triangles. These plots demonstrate that the change in lake level from 500-800 AD did not cause a significant change in metal concentrations. Similarly, an increase in metals from 800-1120 AD occurred while $\delta^{18}O$ values were relatively stable at -7‰, indicating the increase in concentrations of metals is unrelated to lake level changes.

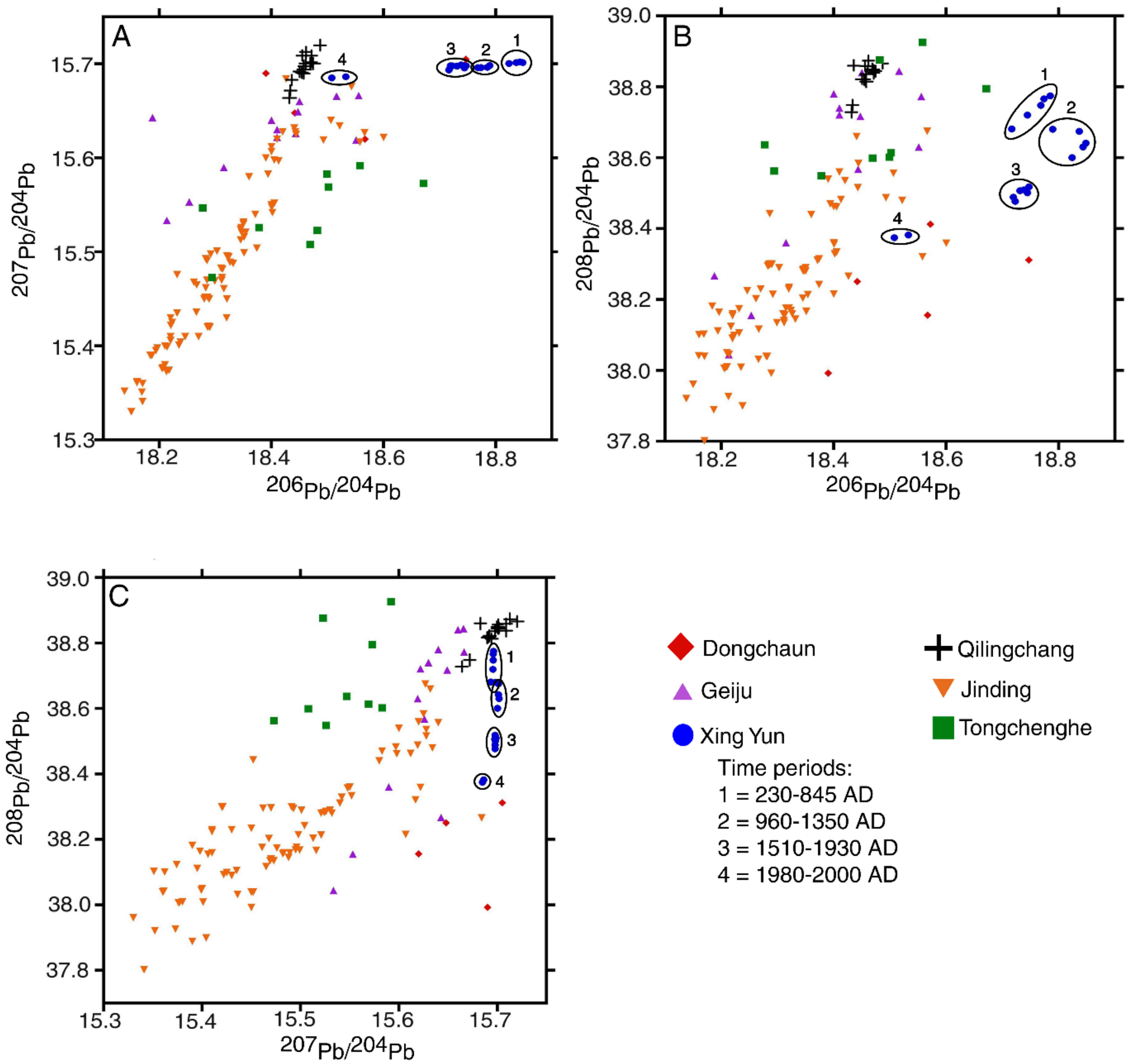

Figure 2-8- Lead isotopes of Xing Yun through time and relevant ore bodies in southwestern China. A- $^{206}Pb/^{204}Pb$ and $^{207}Pb/^{204}Pb$. B) $^{206}Pb/^{204}Pb$ and $^{208}Pb/^{204}Pb$. C) $^{207}Pb/^{204}Pb$ and $^{208}Pb/^{204}Pb$. Xing Yun lead isotopes change through time, but do not match the isotopic composition of any nearby ore bodies.

The transition between Units I and II exhibits many of the biogeochemical fingerprints commonly ascribed to eutrophication. For example, a two-fold increase in P, which limits phytoplankton growth in many lakes, is contemporaneous with a decrease in %C and N/P ratio and increases in $\delta^{13}C_{org}$ and $\delta^{15}N$. Lakes heavily impacted by eutrophication typically have high fertilizer and sewage inputs that are characterized by higher $\delta^{15}N$ values (Brenner et al., 1999), high sediment $\delta^{13}C_{org}$ values, and low N/P ratios (Schindler et al., 2008). Our conclusion is further supported by a previous analysis of the diatom community composition that documented an increase in the proportion of hypereutrophic and eutrophic diatom species (from 60 to >80%) during this transition (Whitmore et al., 1994a). However, the timing of this transition in the previous study was thought to be around 2,500 years BP. Bulk sediment radiocarbon measurements combined with large hard-water reservoir effects led to limited age control; the results presented here demonstrate that this transition actually occurred >1,000 years later.

The gradual increase in $\delta^{18}O_{carb}$ values likely resulted in part from catchment water diversion for agriculture and a consequent decrease in water throughflow to the Ge River leading to longer residence times and increased enrichment of the heavy isotopes of oxygen by evaporation. While Dongge Cave records an abrupt and brief decrease in monsoon strength at 400 AD (Wang et al., 2005), the gradual, prolonged nature of the increase in $\delta^{18}O_{carb}$ values at Xing Yun, the difference in timing, and the other geochemical changes that co-occurred with this shift suggests that a decrease in the strength of the monsoon likely had little influence on the drop in lake level. Combined, these data indicate that intensive land-use within Xing Yun's watershed, probably dominated by agriculture activities, began between 500 and 1000 AD. The lagged increase in Al, P, Pb, and Hg suggests that initial land-use activities were limited in scope, and were not aimed at exploiting mineral resources within Xing Yun's watershed.

The onset of intensive land-use – as indicated by the rapid deposition of red, iron-rich clays, decrease in carbonate, increase in P, Pb, and Hg concentrations, and increase in magnetic susceptibility – occurred soon after the regional establishment of the Nanzhao Kingdom (~700 AD) (**Figure 2-4**). This sedimentological transition was noted in the previous study of Xing Yun, but was dated to 1000 BC (Hodell et al., 1999) because of the large uncorrected hard-water reservoir effects. Studies of other Yunnan lakes, including Qilu (Brenner et al., 1991) and Dian (Sun et al., 1986) (**Figure 2-1**), also noted this transition and attributed it to the onset of 20th Century industrialization, though these studies acknowledged that the timing of this transition was unclear. Our more accurately dated sediment record places this transition into a more reliable temporal context. Additionally, the timing of this matches quite closely with a period of enhanced erosion and landscape disturbance at Erhai (Shen et al., 2005). The characteristics of Xing Yun sediments from this time, namely, a low organic carbon content and high residual mineral matter content composed primarily of catchment soils, are similar to those from Guatemalan lakes known to have been impacted by human deforestation and erosion (Binford et al., 1987; Brenner, 1983) supporting our hypothesis that the transition from Unit I to II was caused by anthropogenic activities.

2.3.3.3 Unit II- Intensive human disturbance

The ~100 years (1270–1380 AD) that include the Yuan Dynasty, better known as the Mongols, are marked by a clear departure from the last ~700 years in many of the proxies (**Figure 2-4)**. In general, $\delta^{18}O_{carb}$, $\delta^{13}C_{org}$, and $\delta^{15}N$ values are lower and %C and C/N values are higher than in sediment from adjacent time periods. These shifts occur over several decades or less, and are not matched by changes in either regional land-use or mineral extraction, as indicated by stable inputs of Al, P, Pb, and Hg, or monsoon intensity, as recorded by the Dongge

Cave $\delta^{18}O$ record (Wang et al., 2005). We suggest that these changes reflect lake-level management during this period; historical data confirm that the Mongols implemented a series of regional political changes, including the construction of dams and artificial reservoirs near Kunming largely for transportation purposes (Herman, 2002). Lower $\delta^{18}O_{carb}$ values therefore likely reflect some combination of higher lake levels and/or greater water throughflow at Xing Yun during this time.

Wet-rice agriculture, which requires the routine flooding and drying of flat fields (Bray, 1986), became widespread in Yunnan shortly after the Ming defeated the Mongols in 1368 AD (Herman, 2002). Trenching of the Ge River to control Xing Yun water levels took place multiple times during the Ming and early Qing Dynasties, resulting in a water level drop of ~4 m (Wang, 1994). Our sediment core suggests that these changes in regional cultural activity at the Mongol-Ming transition had important limnological consequences. Sediment %C, C/N, N/P, $\delta^{18}O_{carb}$, and $\delta^{13}C_{org}$ rapidly shift to values (1%, 8, 1, -4‰, and -25‰, respectively) that are unprecedented within the sediment record (**Figure 2-4**). The low %C, C/N, and N/P values indicate eutrophic conditions, and high Al, P, and $\delta^{15}N$ values suggest that soil erosion, manure, and sewage inputs supplied nutrients to the lake. The combination of lower lake levels and eutrophic conditions likely accelerated the remineralization of autochthonous organic matter in this broad shallow lake, limiting organic carbon preservation.

This time period also encompasses the Little Ice Age, which was characterized by a weakened monsoon and decreased precipitation across much of southwestern China (Morrill et al., 2003). Changing climate during this period may have reduced catchment water availability (leading to lower lake levels) and exacerbated eutrophication. The Dongge Cave record indicates an abrupt and brief drop in the strength of the monsoon at 1500 AD (Wang et al., 2005). However, the drop in monsoon strength occurs slightly later and is much shorter in duration than the changes in the Xing Yun record. Since historical records confirm intentional manipulation of lake level (Wang, 1994), and since other geochemical changes occur with the shift in $\delta^{18}O_{carb}$ values (C/N, N/P, $\delta^{13}C_{org}$, and $\delta^{15}N$), we attribute the majority of lake-level change to human activity, including catchment water diversion for agriculture. The high variability in $\delta^{18}O_{carb}$ and $\delta^{13}C_{carb}$ values during this period suggests that the lake was more hydrologically closed, lake levels were likely on average lower than during prior periods (Steinman et al., 2010), and that lake level and water use were managed. This rapid shift to higher $\delta^{18}O_{carb}$ values is present in the earlier study of Xing Yun, but the low sampling resolution makes the exact timing difficult to discern, and the large hard-water effect makes it appear ~1,000 older (Hodell et al., 1999).

The onset of wet-rice agriculture and lake-level management during this time period was likely enhanced by regional population expansion within Yunnan as more Han Chinese immigrants moved into the province to work in the mines (Durand, 1960). The intensification of erosional activity is reflected in the Xing Yun sediment record as the concentrations of Pb and Hg remained high during the Ming Dynasty (**Figure 2-4**), which (though it spanned only ~300 years), accounts for 28%, 28%, and 32% of the total P, Pb, and Hg deposited in the lake, respectively (**Figure 2-9**).

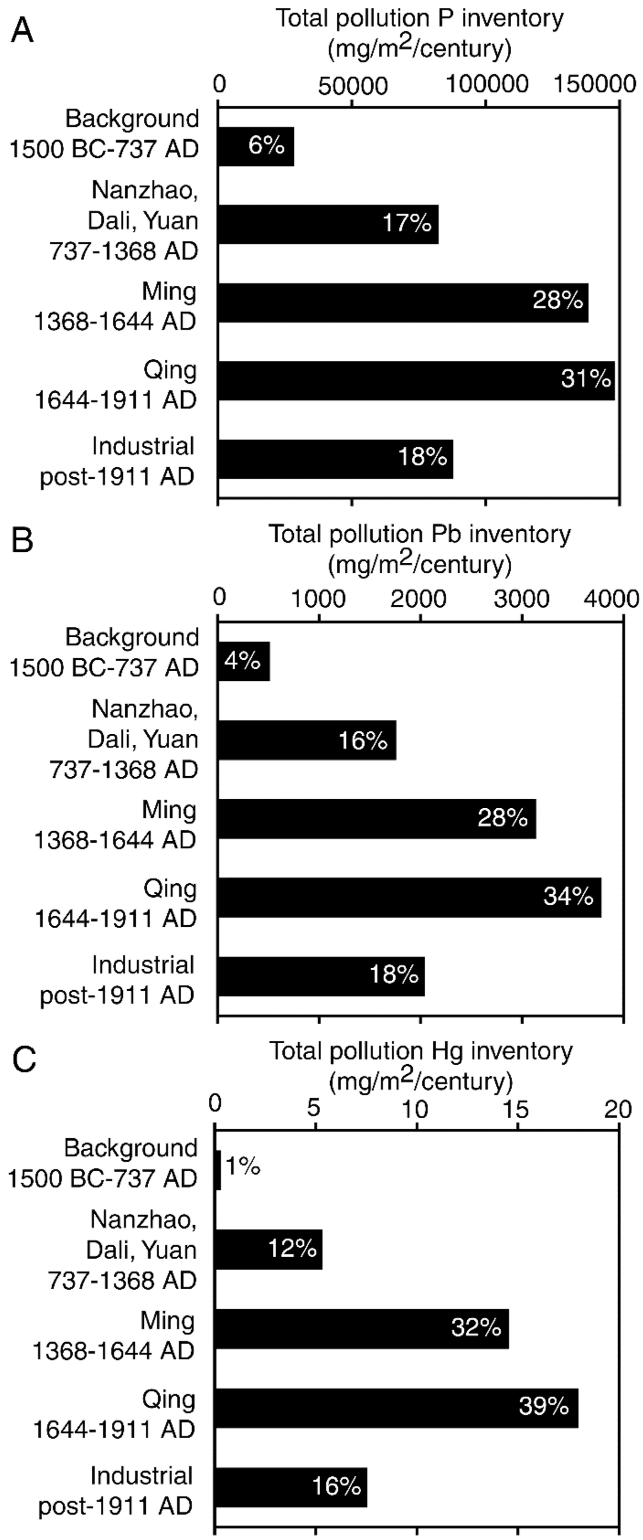
A
Total pollution P inventory
(mg/m2/century)
0
50000
100000
150000
Background
1500 BC-737 AD
6%
Nanzhao,
Dali, Yuan
737-1368 AD
17%
Ming
1368-1644 AD
28%
Qing
1644-1911 AD
31%
Industrial
post-1911 AD
18%
B
Total pollution Pb inventory
(mg/m2/century)
0
1000
2000
3000
4000
Background
1500 BC-737 AD
4%
Nanzhao,
Dali, Yuan
737-1368 AD
16%
Ming
1368-1644 AD
28%
Qing
1644-1911 AD
34%
Industrial
post-1911 AD
18%
C
Total pollution Hg inventory
(mg/m2/century)
0
5
10
15
20
Background
1500 BC-737 AD
1%
Nanzhao,
Dali, Yuan
737-1368 AD
12%
Ming
1368-1644 AD
32%
Qing
1644-1911 AD
39%
Industrial
post-1911 AD
16%

Figure 2-9- Total pollution inventories for A- phosphorus (P), B- lead (Pb), C- mercury (Hg). Total P, Pb, and Hg inventories were calculated as the product of dry sediment inventory (g/m^2) and element concentration (mg/g). Concentrations within core intervals lacking data were estimated using linear interpolation between measurements. Intervals were summed and divided by time period (in centuries).

Substantial biogeochemical shifts also occurred in Xing Yun shortly after the transition from the Ming to Qing Dynasty (1644 AD). The rate of carbon burial increased and coincided with a decrease in extractable Al, suggesting decreased erosion and landscape stabilization (**Figure 2-4**). Changes in the C/N and N/P ratios and decreases in $\delta^{13}C_{org}$ and $\delta^{15}N$ may indicate a reduction of eutrophic conditions due to agricultural and water management changes. This is reflected in the shift to lower $\delta^{18}O_{carb}$ values, and presumably higher lake levels, approximately 75 years after the shifts in other variables. Once again, the rapid nature of this transition and the lack of a clear connection to any change in monsoon strength (Wang et al., 2005) suggests that this rise in lake level was likely driven by human activities. The total pollution index for P, Pb, and Hg reached the highest levels during this time period, indicating the intensification of erosional activities and/or metal resource extraction. The Qing Dynasty accounts for 31%, 34%, and 39% of total P, Pb, and Hg, respectively, deposited in the lake (**Figure 2-9**).

Post-Qing sediments (1911 AD-present) are characterized by the highest $\delta^{13}C_{org}$ (-25‰) and $\delta^{15}N$ (7‰) values, increases in %C and %N, and high inputs of Al, P, Pb, and Hg (**Figure 2-4**). Our conclusion is further supported by analysis of fecal 5β-stanols, including coprostinol and epi-coprostanol, which show an increase in concentration beginning around this period (**Figure 2-10**). These compounds can be used as indicators of fecal contamination in modern aquatic environments (Leeming and Nichols, 1996), and have been used as evidence of human occupation of a watershed (D'Anjou et al., 2012). Our results suggest high inputs of sewage to the lake. Lead isotopes also attain their lowest values during this latest interval (**Figure 2-8**), suggestive of deposition from leaded gasoline (Graney et al., 1995). Xing Yun entered a unique state during the 20th century; however, in the context of entire sediment record, the total pollution index for P, Pb, and Hg is relatively low compared to previous time periods (**Figure 2-9**). The 20th century accounts for only 18%, 18%, and 16% of total P, Pb, and Hg, respectively, deposited in the lake. Thus, while the rate of current change in Xing Yun water and sediment quality is unprecedented, the current level of pollution is not, indicating that modern increases in eutrophication and water quality degradation are part of a much longer legacy of human alteration to the Xing Yun lake catchment system.

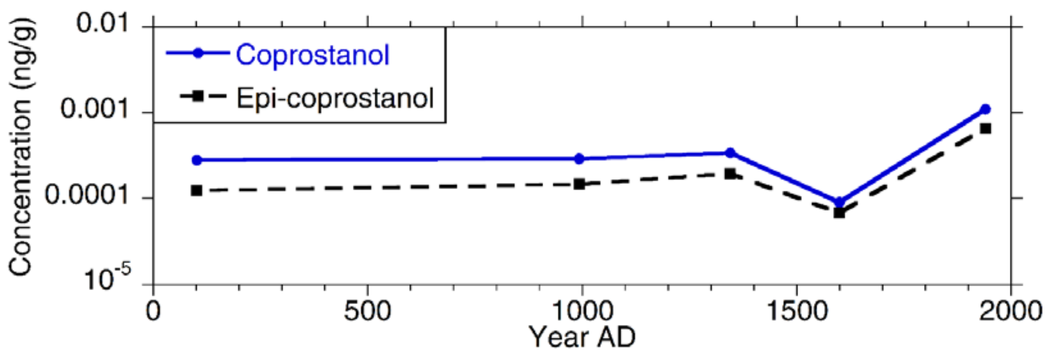

Figure 2-10- Concentrations of fecal 5β-stanols from Xing Yun that increase in the uppermost sediments dating to 1940 AD.

2.4 CONCLUSION

The 3,500-year, multi-proxy lake sediment record presented here reveals that substantial alterations to Xing Yun Lake and its watershed co-occurred with several cultural and dynastic transitions and that impacts of human modification of the lake and its watershed were greater than that of climate change. The record implies that each group of people altered the lake-catchment system in a different way and to a different degree. Furthermore, the often abrupt nature of these transitions suggests that anthropogenic manipulations were rapid, occurring within years to decades. Although water quality deterioration was thought to be a relatively recent phenomenon, this study indicates that human actions have profoundly affected the lake for >1,500 years. The role of climatic change and variability in the strength of the monsoon may have contributed to the observed changes, but we find that the primary driver of shifts in lake level and trophic status over the past 2,000 years was anthropogenic activity. The differences among the various organic matter and geochemical proxies illustrate that, at times, nutrient loading associated agricultural activities varied independently from erosional inputs associated with other land use changes.

Our temporally higher resolution study reveals anthropogenically driven changes that earlier investigations on lakes in the Kunming region did not adequately identify due to either limited chronological constraint (Brenner et al., 1991; Sun et al., 1986; Whitmore et al., 1994a) or a lack of focus on the short-term, abrupt nature of change (Hodell et al., 1999). This study underscores the need for additional lake sediment studies in regions characterized by a historically complex and variable relationship between humans and the environment to provide context for current environmental issues.

3.0 XING YUN LAKE- LONG CORE

Indian Summer Monsoon Variability through the Holocene and Pleistocene in Yunnan China as Recorded in Lake Sediments

Here, we present a sediment record from Xing Yun Lake that spans >50,000 years BP and is one of the oldest continuous terrestrial records of the Indian Summer Monsoon (ISM). Xing Yun is located in a region containing several well-studied climate records that span the Holocene and Pleistocene including caves (Dykoski et al., 2005; Wang et al., 2005) and lake sediments (Chen et al., 2014; Cook et al., 2011; Cook et al., 2012; Hodell et al., 1999) (**Figure 3-1**). Chapter 2.0 focused on the late Holocene portion of the record in the context of human activity and modification to the lake-catchment system. This chapter will focus on the natural climate variability of the Pleistocene and early to middle Holocene. To examine sediment dynamics over the Pleistocene, we rely on measurements of weight percent organic, carbonate, and mineral matter and trace element geochemistry including the concentrations of both weakly and strongly bound metals. To examine hydroclimate variability and primary productivity through the Holocene, we rely on measurements of the oxygen and carbon isotopic composition of authigenic calcite ($\delta^{18}O_{carb}$ and $\delta^{13}C_{carb}$) and the content and stable isotopic composition of organic carbon and nitrogen ($\delta^{13}C_{org}$ and $\delta^{15}N$).

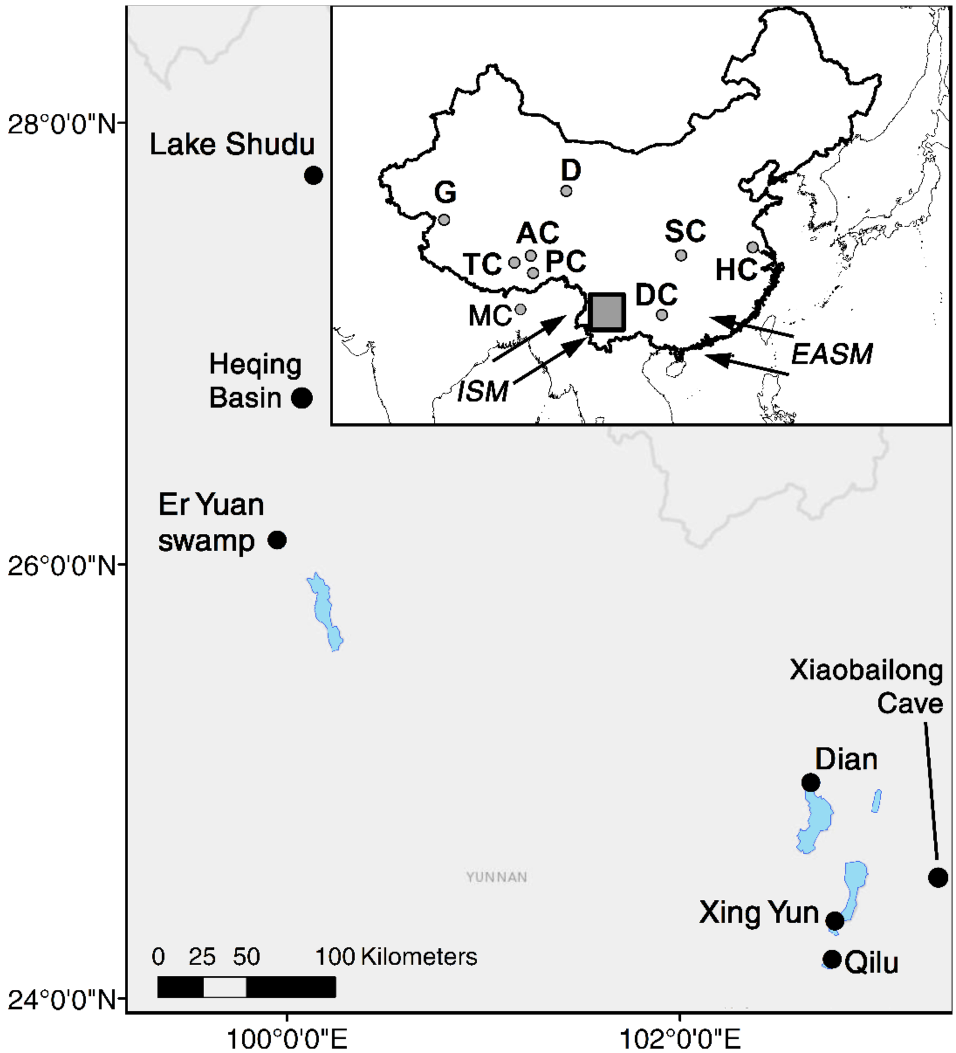

Figure 3-1- Locations of paleoclimate records from Yunnan discussed in this chapter. Inset- locations of other paleoclimate records from China discussed in this chapter. G = Guilya ice cap, D = Dunde ice cap, AC = Ahung Co, PC = Paru Co Lake, DC = Dongge Cave, SC = Sanboa Cave, HC = Hulu Cave, TC = Tianmen Cave, MC = Mawmluh Cave.

3.1 BACKGROUND

3.1.1 Regional Setting

The ISM provides water to over a billion people and comprises the western component of the larger Asian Summer Monsoon (ASM) system which also includes the East Asian Summer Monsoon (EASM). Regions affected by ISM include not just the Indian sub-continent, but extend across parts of Africa and Southeast Asia. People who live in these regions base their livelihood on the timely arrival of the ISM to deliver enough water to sustain agriculture and hydroelectric power. The ISM is projected to increase in strength but become more variable in both timing and magnitude due to future climate change (Lal et al., 2011). However, there is an inadequate understanding of how this system interacts with other climate phenomena such as the El Niño Southern Oscillation (ENSO) (Turner and Annamalai, 2012) as well as how the ISM relates to the EASM- how they function together as a whole and separately as independent units. Therefore, a long-term perspective of the intensity of the ISM can provide information about the nature of rapid shifts in moisture balance. Moreover, this perspective needs to originate from regions of high population density most affected by the ISM with essential water resources for both urban and rural areas.

Xing Yun Lake (24°10'N, 102°46'E) lies on the Yunnan Plateau of southwestern China, approximately 50 km south of Kunming, the capital of the province and a rapidly expanding urban and industrial center. 70% of the average annual precipitation falls in the months of June-September associated with the ISM (**Table 1-2**) and temperature in this region is moderate throughout the year with mild winters and cool summers (Kottek et al., 2006). Xing Yun is a shallow (Z_{max}: 11 m) and eutrophic lake (Liu et al., 2012) with a surface area of 34 km^2 and a watershed area of 383 km^2 (**Figure 3-2**). The lake catchment contains large flat sections of land used for rice agriculture. The western side of the catchment is dominated by slate and phyllite and the eastern side is composed of sandstone, shale, and limestone (Bureau of Geology and Mineral Resources of Yunnan Province, 1990). The lake's only surficial outflow is the Ge River, which drains into deep Fuxian Lake; however, today several dams exist on the Ge River, regulating water flow. The only surficial outlet for Fuxian is the Nanpan River on the northeast side of the lake, which ultimately drains into the Pearl River. Both Xing Yun and Fuxian are pull-apart basins separated by a horst and bound by normal faults (Wang et al., 1998) (**Figure 1-1**).

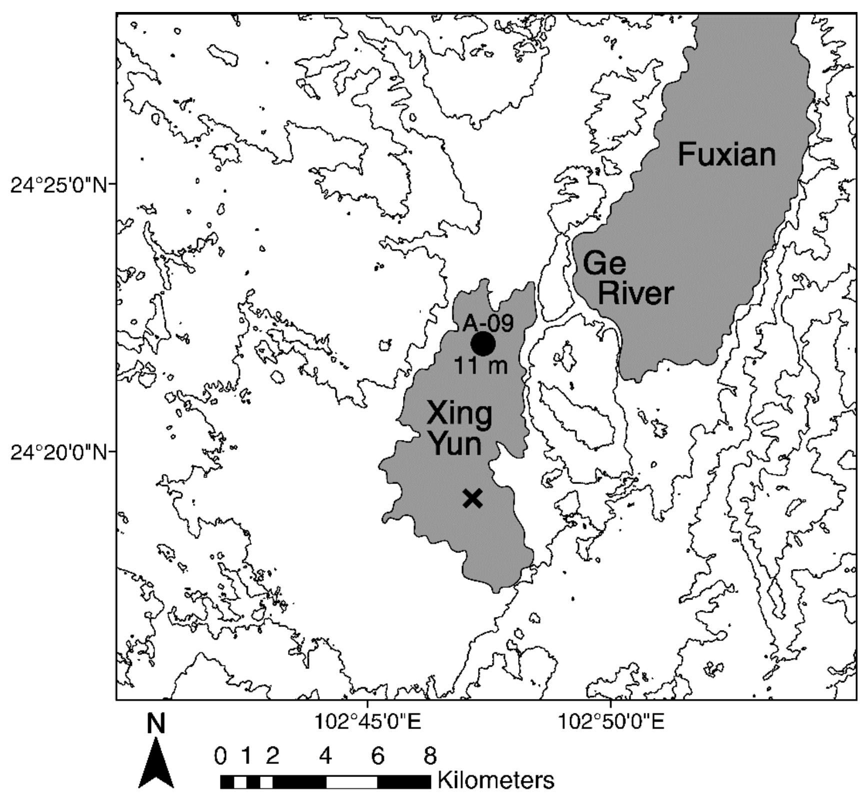

Figure 3-2- Xing Yun Lake (1721 m elevation) with 200 m contour intervals. Coring location in this study is marked by the circle. Coring location from Hodell et al., 1999 is marked X.

The annual weighted $\delta^{18}O$ mean of modern rainfall for Kunming is -9.86‰ VSMOW with lower $\delta^{18}O$ values occurring during the summer months during the monsoon season (**Table 1-2**). The $\delta^{18}O$ value of a water sample taken from Xing Yun in 2009 is -4.3‰ VSMOW, suggesting that substantial water loss from the lake occurs through evaporation (**Figure 1-3**). Thus, the $\delta^{18}O$ values of authigenic carbonate material that forms in the water column during the summer months records not only the isotopic composition of precipitation resulting from the ISM, but also the effects of evaporation on the isotopic composition of the lake water (P-E balance).

3.1.2 Previous Paleoclimate Studies

Due to the potential for continuous climate records, previous lake sediment work was performed in Yunnan in the 1980's and 1990's, though much of it was limited by reliance on one set of proxy data and/or poor age control (Brenner et al., 1991; Sun et al., 1986; Whitmore et al., 1994b). Previous analysis on sediment cores from both Xing Yun and Qilu (Hodell et al., 1999) found that the lakes were sensitive to changes in monsoon strength over the last 50,000 years. Using grain size and magnetic susceptibility, Hodell found evidence of relatively warm temperatures from 50 to 41 ka and declining temperatures from 41 to 12 ka. Stable oxygen isotopes of carbonate material were measured on both lakes and were generally found to track insolation, evidence that the ISM broadly responds to insolation forcing over long time scales as recorded in lake sediments. However, this study suffered from several problems: 1) reliance on bulk sediment radiocarbon dates and gastropod shell dates that are subject to hard-water effects and may appear several thousand years too old (Deevey et al., 1954) (see Chapter 2.0 for more details), 2) analysis of bulk carbonate material for isotopic analysis that may include biogenic material that is subject to vital effects (Leng and Marshall, 2004), and 3) low sampling resolution of this carbonate material that precludes a direct comparison with most other paleoclimate records and limits our understanding of century-scale shifts in monsoon intensity.

More recently, research on Lake Shudu on the northern border of Yunnan found deglaciation in the catchment occurring by 22.6 ka, followed by cold and dry conditions with several abrupt, step-wise warmings occurring from 17.7 to 17.4 and 11.9 to 10.5 ka (Cook et al., 2011; Cook et al., 2012). However, the Holocene portion of this lake sediment record was lost and further details on Holocene ISM strength are not available.

In a collaborative study with our Chinese colleagues at Lanzhou University, working on a parallel set of cores from Xing Yun, pollen and grain size were analyzed from 36.4 to 13.4 ka (Chen et al., 2014). From 36.4 to 29.2 ka, grain size was low and there was a high percentage of coniferous tree pollen, suggesting a wet climate and a relatively strong monsoon. From 29.2 to 17.6 ka, grain size increased and drought-resistant, broad-leaved trees increased, indicative of lower lake levels and a gradually drying climate associated with the Last Glacial Maximum (LGM). From 17.6 to 13.4 ka, a decrease in cold-tolerant conifers suggested warmer conditions associated with deglaciation. While these trends broadly agree with insolation changes and with changes in the EASM, there are some notable exceptions, particularly around 33 ka when the ISM was weak despite high summer insolation and the EASM did not drop in strength until ~29 ka. This raises questions regarding the potential differences in timing of shifts in the ISM versus the EASM.

A stratigraphic profile from a coal mine on the western side of the Xing Yun catchment is at an elevation of 1820 m, approximately 100 m higher than the surface of the modern-day lake.

Several meters of lacustrine sediments are interrupted by three peat units, that have been radiocarbon dated to >40,000, 30,200±1500, and 19,478±500 years BP (Yu et al., 2001). These sequences suggest deepwater phases interrupted by periods of lower lake level, though the water level necessary for this peat deposition is uncertain. The deposition of several meters of lacustrine sediment provides evidence that Xing Yun was once ~100 m higher than present-day, which would necessitate that the Nanpan River was dammed (**Figure 3-3**). A water level of this height would have connected Xing Yun and Fuxian into one large lake with a surface area of 487.7 km^2, 12 times the surface area of Xing Yun today.

A stratigraphic profile of the terrace between Xing Yun and Fuxian on the Ge River at 1745 m elevation shows a coarsening-upwards sequence of lacustrine black clay, fine silts and sands, and coarse sand and gravel with cross-bedding. While the entirely of this sequence has not been radiocarbon dated, the lacustrine clay has a date of 11,831±415 years BP, evidence that towards the early Holocene, Xing Yun was ~25 m higher than present-day.

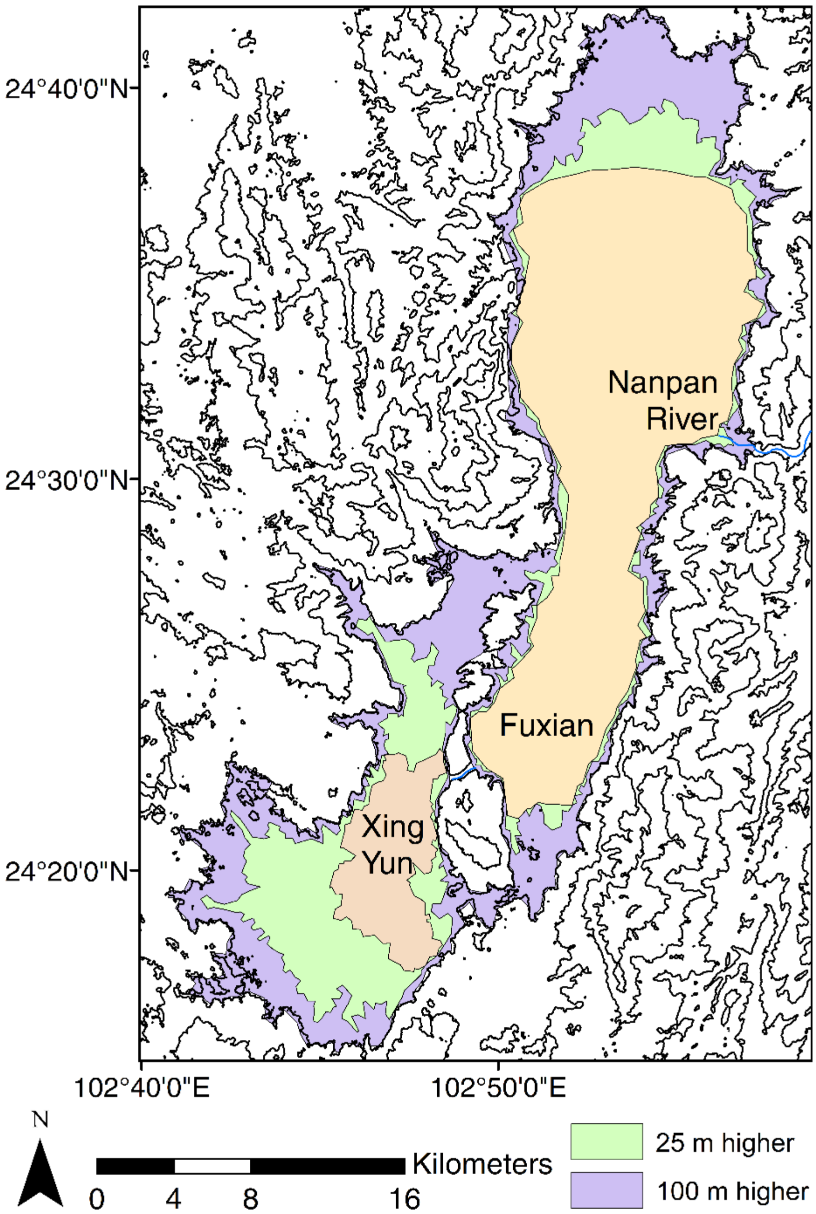

Figure 3-3- Map of Xing Yun Lake (1721 m elevation) and Fuxian Lake (1723 m elevation) with 200 m contour intervals. Green shaded area is the surface area of Xing Yun if the lake were 25 m higher than present day. Purple shaded area is the surface area of Xing Yun and Fuxian if the Xing Yun were 100 m higher than present day.

Since none of this work has been updated with more precise estimates or ages of lake level change, there is a clear need to reassess lake level fluctuations in the context of ISM variability over multi-millennial time scales. This study builds upon previous work by Hodell et al., 1999 and Whitmore et al., 1994 by relying on an age model created from AMS radiocarbon dates on terrestrial macrofossils and taking a multi-proxy approach with higher sampling resolution.

3.2 MATERIALS AND METHODS

3.2.1 Core collection

Five cores from Xing Yun were collected in 2008 from the deepest part of the lake (11 m) (**Figure 3-2**) using a UWITEC coring system with removable polycarbonate tubes, forming a composite record of 12.79 m. Core D-1 measures 2.65 m, D-2 measures 2.49 m, D-3 measures 2.33 m, D-4 measures 2.71 m, and D-5 measures 2.60 m. None of the drives are overlapping. Additional cores from the same location were collected in 2009 using a steel barrel Livingston corer (Wright et al., 1984)- see Chapter 2.0 for more details. The 2008 and 2009 cores were correlated on the basis of visible stratigraphy and sediment composition.

3.2.2 Age Control

Radiocarbon ages were measured on fifteen terrestrial macrofossils from the 2008 cores and seven terrestrial macrofossils from the 2009 cores. Samples were analyzed at Keck Center for Accelerator Mass Spectrometry at the University of California Irvine. Prior to analysis, samples were pretreated using a standard acid, base, acid procedure (Abbott and Stafford, 1996). The resulting ages were calibrated using CALIB 7.0 and the INTCAL13 calibration curve (Reimer et al., 2013).

3.2.3 Geochemistry

Weight percent organic matter and carbonate content was determined every 2 cm by loss-on-ignition (LOI) analysis at 550°C and 1000°C, respectively (Dean, 1974). Samples for X-ray diffraction (XRD) analysis were taken every 50 cm from 0-5.00 m, lyophilized, and ground by hand. The samples were prepared as back-filled cavity mounts and analyzed using a Phillips X'Pert MPD diffractometer.

From a depth of 0-5.14 m, cores were sampled at 0.5-2.0 cm intervals for analysis of the oxygen and carbon isotopic composition of carbonate minerals. Samples were disaggregated with 7% H_2O_2 and sieved through a 63-μm screen to remove biological carbonates derived from ostracod and gastropod shells. Samples were soaked in a 50% bleach and 50% DI water mixture for 6-8 hours, rinsed, and lyophilized. Bulk carbonate samples were reacted in ~100% phosphoric acid at 70°C. Samples above 3.1 m depth were measured using a dual-inlet GV Instruments, Ltd. (now Isoprime, Ltd) IsoPrime™ stable isotope ratio mass spectrometer and MultiPrep™ inlet module at the Regional Stable Isotope Laboratory for Earth and Environment Science Research at University of Pittsburgh. Samples from 3.10 to 5.14 m depth were measured using an automated carbonate preparation device (KIEL-III) coupled to a gas-ratio mass spectrometer (Finnigan MAT 252) at the University of Arizona. Oxygen and carbon isotope results are expressed in conventional delta (δ) notation as the per mil (‰) deviation from

VPDB. One sigma analytical uncertainties are within ±0.10‰ for $\delta^{18}O_{carb}$ and ±0.08‰ for $\delta^{13}C_{carb}$.

From a depth of 0-5.14 m, cores were sampled at 4 cm intervals for analysis of weight percent nitrogen, weight percent organic carbon, $\delta^{15}N$, and atomic C/N ratio. Samples were covered in 1 M HCl for 24 hours to dissolve carbonate minerals, rinsed, and lyophilized. Samples above 3.10 m depth were analyzed at Idaho State University using an ECS 4010 (Elemental Combustion System 4010) interfaced to a Delta V mass spectrometer through the ConFlo IV system. Samples from 3.10-5.14 m depth were analyzed at the University of Arizona using a continuous-flow gas-ratio mass spectrometer (Finnigan Delta PlusXL) coupled to an elemental analyzer (Costech). Organic carbon isotopes are expressed in conventional delta (δ) notation as the per mil (‰) deviation from the Vienna Peedee Belemnite standard (VPDB) whereas nitrogen isotopes are reported relative to atmospheric N_2. One sigma analytical uncertainties are within ±0.10‰ for $\delta^{13}C_{org}$ and ±0.20‰ for $\delta^{15}N$.

Weakly sorbed metal concentrations were measured at 5 cm intervals. All samples were lyophilized and homogenized prior to analysis. Elements were extracted by reacting samples with 10 mL of 1 M HNO_3 for ~24 hours (Graney et al., 1995). Concentrations of elements in the residual mineral matter portion were measured at 10 cm intervals and strong extractions were performed using aqua regia (3:1 mixture of hydrologic and nitric acid) (Tokalioğlu et al., 2000). Sediment was extracted overnight, evaporated down, and re-dissolved in a 10% nitric solution. The supernatant from both weak and strong extractions was diluted before being measured on an inductively coupled plasma mass spectrometer (ICP-MS) at the University of Pittsburgh. Duplicates were run on every 10th sample and were generally within 10% of each other. Blanks were run every 10 samples to check for bleed through and were consistently below detection limits of interest.

3.3 RESULTS

3.3.1 Core Chronology

Radiocarbon ages were measured on fifteen terrestrial macrofossils from the 2008 cores and seven terrestrial macrofossils from the 2009 cores (**Table 3-1**). A composite age-depth model for the Xing Yun sediment record was developed using the ^{210}Pb ages from the 2009 cores (see Chapter 2.0) and calibrated macrofossil radiocarbon dates (**Figure 3-4**). Six radiocarbon dates were discarded. Three samples were gastropod shells and subject to a hard-water effect (Deevey et al., 1954) (see Chapter 2.0 for more details). One sample from 776.5 cm was comprised of mixed material (wood and charcoal) and was anomalously young, suggesting that it may have been contaminated by modern carbon during sampling and pre-treatment. Two samples from 1030.5 and 1255.5 cm were beyond the limits of radiocarbon dating (>50,000 years BP).

A second-order polynomial regression was used to produce an age model using the *clam* 2.2 code (Blaauw, 2010) in the statistical software package "R" (R Development Core Team, 2008). Due to the large gap in ages between samples from 504.5 and 519.5 cm, a hiatus was modeled at 514 cm (further details can be found below in section 3.4.4). Uncertainty (2σ) associated with the age-depth model is generally ±200 years and increases to ±2500 years after ~7 m. The upper 10.18 m spans 50,000 years and the bottom 2.6 m of the record span beyond the limits of radiocarbon dating.

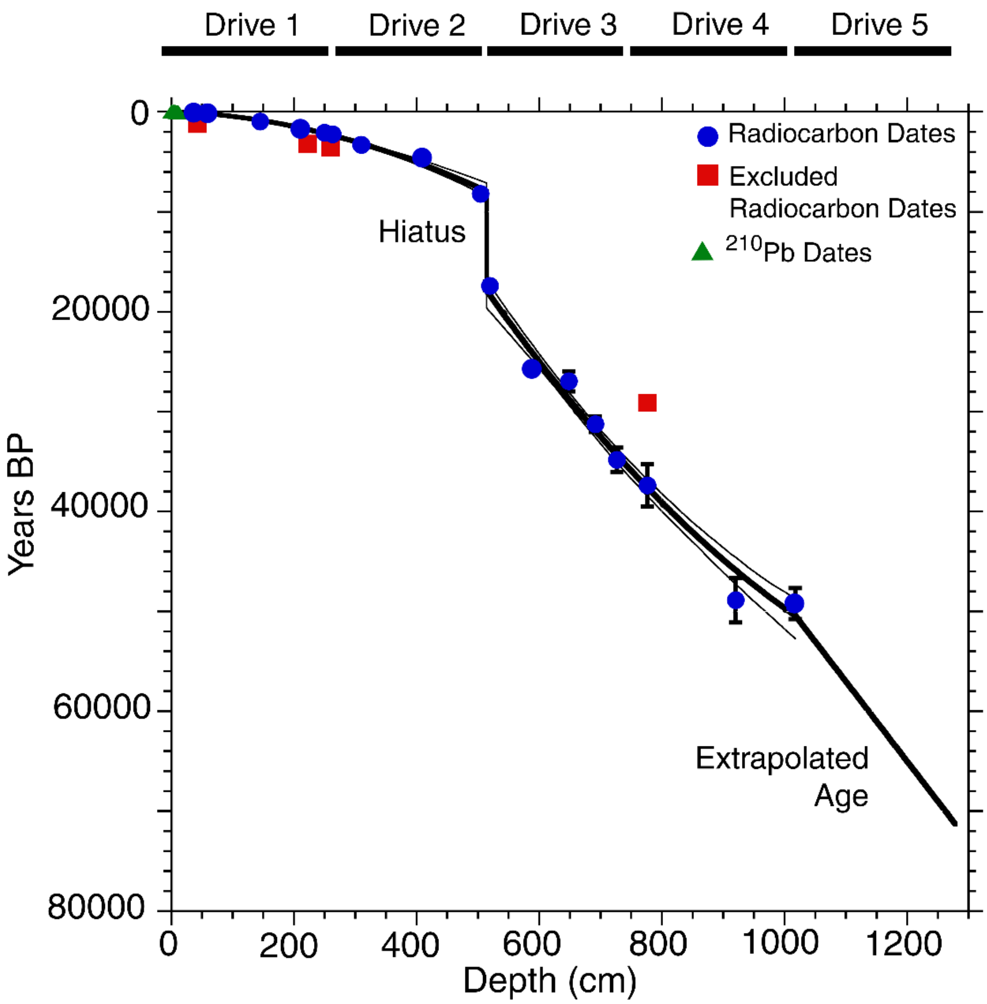

Figure 3-4- Age-depth model with 95% confidence intervals. ^{210}Pb dates (green triangles), radiocarbon dates (blue circles), excluded radiocarbon dates (red squares), all with 2 sigma error bars. A hiatus was modeled at 512.5 cm. The age of the bottom 260 cm of the record have been extrapolated assuming constant sedimentation rate.

Table 3-1- AMS Radiocarbon Dates for samples from Xing Yun

UCI Number	Composite Core Depth (cm)	Sample Type	^{14}C age (BP)	±	Median Probability Calibrated Age (year BP)	2σ Calibrated Age Range (years BP)
71481	35.5	Wood	110	25	112	-4 to 268
71482	37.5	Charcoal	110	50	123	-4 to 277
84722*	42.5	Gastropod Shell	1245	20	1211	1087 to 1265
71483	59	Charcoal	130	25	124	-3 to 273
84866	145	Charcoal	1060	25	962	928 to 1052
141232	210.5	Leaf	1785	35	1707	1616 to 1817
84723*	222.5	Gastropod Shell	3000	25	3202	3080 to 3322
84867	250	Wood	2105	20	2079	2004 to 2141
84724*	259.5	Gastropod Shell	3285	20	3516	3458 to 3565
84815	263	Charcoal	2220	20	2227	2154 to 2328
141233	309	Wood	3065	20	3290	3215 to 3349
122325	310.5	Charcoal	3070	15	3300	3249 to 3357
141234	408.5	Charcoal	4080	20	4564	4448 to 4796
141235	504.5	Leaf	7375	35	8200	8049 to 8343
141236	519.5	Charcoal	14290	70	17408	17157 to 17619
152036	588.5	Charcoal and wood	21410	100	25747	25620 to 25869
141237	648.5	Charcoal	22660	220	26962	26426 to 27432
152037	691.5	Wood	27380	270	31260	30898 to 31670
141238	726.5	Charcoal	30900	290	34817	34235 to 35428

Table 3-1 (continued)

141239*	776.5	Charcoal and wood	25090	140	29129	28777 to 29496
152038	825.5	Wood	33190	420	37398	36327 to 38467
141240	920.5	Wood	48600	2500	48883	47766 to 50000
141241	1017.5	Wood	51500	3600	49225	48450 to 50000
141242*	1030.5	Charcoal and wood	>49500			
141362*	1255.5	Charcoal	>49500			

* denotes dates excluded from age model

3.3.2 Sedimentology and Geochemistry

Along the entire 12.79 m record, there are abundant large gastropods of the species *Margarya melanioides*, which are endemic to Yunnan lakes and have a slight preference for deep water conditions (Song et al., 2013). Within the lower 10 m of the record (see Chapter 2.0 for results and interpretation on the upper ~3 m), there are two distinct sedimentologies. From a depth of 12.80 to 5.14 m, corresponding to at least 50 ka to 17 ka, sediments are homogenous, brown/gray fine-grained clay with no visible stratigraphy or lithological changes. Sediments are composed of ~10% organic matter and 90% residual mineral matter with the exception of an interval from 7.60-7.50 m, when carbonate content increases to 40% (**Figure 3-5**).

During the transition from Drive 3 to 2, at a depth of 5.14 m, sediment abruptly changes to homogenous green/brown clay comprised of between 20 and 40% carbonate material, 10% organic matter, and 50 to 70% residual mineral matter. A gradual transition to gray clay takes place at a depth of ~4 m. This clay has a higher carbonate content of between 50 and 60%. In the upper 2 m, corresponding to the last 1,500 years, carbonate material abruptly declines and sediments are composed of red, iron-rich very fine-grained clay (see Chapter 2.0 for more details). X-ray diffraction and scanning electron microscopy confirm that the carbonate material from the upper 5.14 m of core is euhedral calcite (**Figure 2-5**), strongly suggesting that this material precipitated directly in the water column and that the stable isotopic composition of the calcite will archive the stable isotopic composition of the lake water at the time of formation (Leng and Marshall, 2004). On the basis of trace element geochemistry and the stable isotopic composition of this calcite, we divide the record into four units, with the last unit, the Holocene portion of the record, having four subunits.

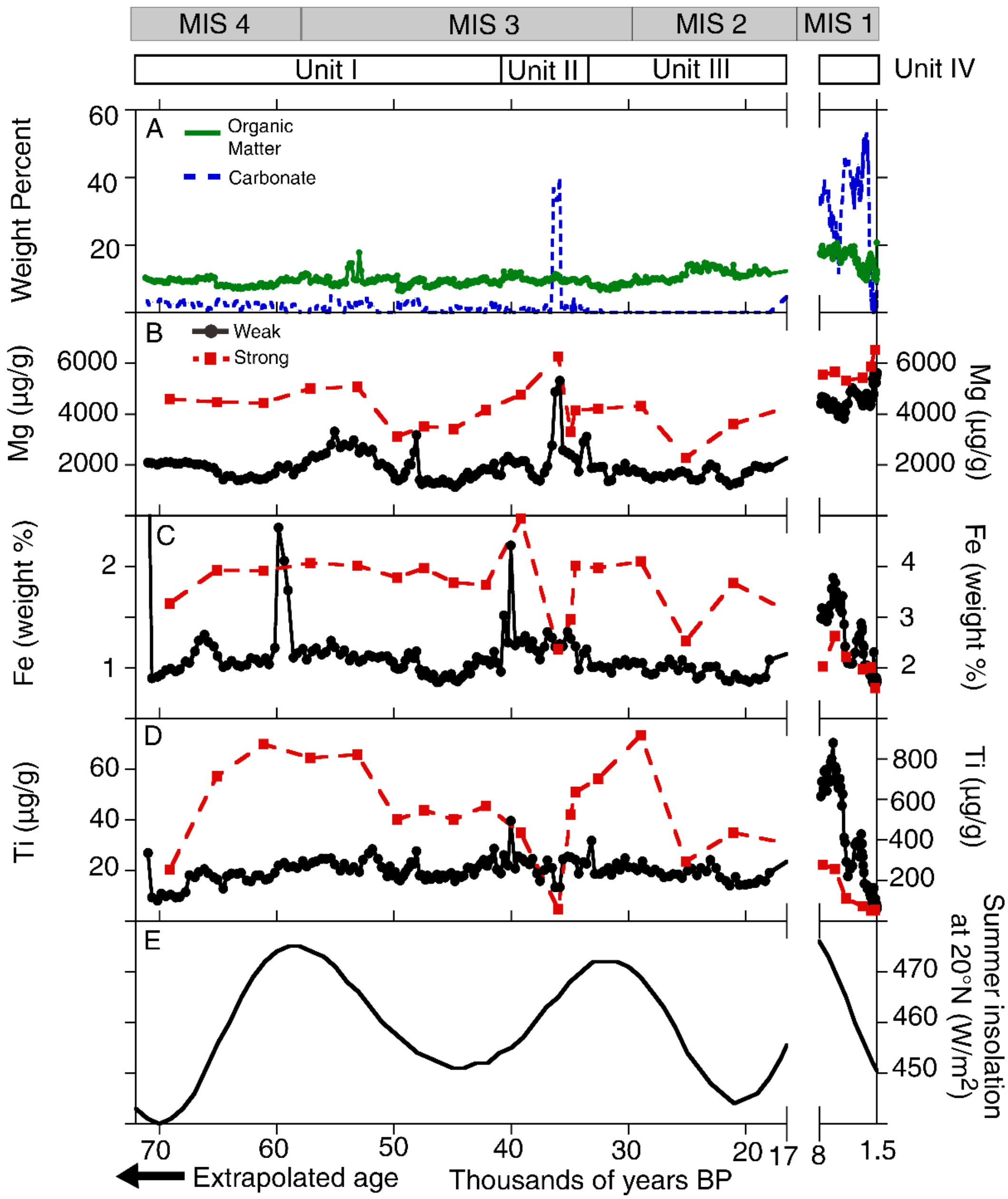

Figure 3-5- MIS = Marine Isotope Stage; A) Weight percent organic matter (green circles) and carbonate (blue dotted line); Weak extractions in black solid circles (left axes) and strong extractions in red dotted squares (right axes): B) Magnesium concentration; C) Iron concentration; D) Titanium concentration; E) Average summer (June, July, and August) insolation at 20°N. After 50,000 years BP, sediment age is extrapolated back in time, assuming a constant sedimentation rate. Peaks in summer insolation correspond to increases in strongly bound lithogenic metals.

3.3.2.1 Unit I- >50 to 42 ka

Unit I spans a total depth of 12.79 to 8.40 m, corresponding to an age greater than 50 ka to 42 ka and encompassing Marine Isotope Stages (MIS) 4 and 3 (**Figure 3-5**). For the purposes of data presentation on an age-depth scale, the age of the sediments from 12.79 to 10.18 m have been extrapolated back in time, assuming a constant sedimentation rate. From an estimated age of 70 to 60 ka, weakly bound Mg concentrations are stable at an average of 1800±300 µg/g, approximately double by 55 ka, and then decline back to an average of 1600±400 µg/g by 43 ka. Strongly bound Mg concentrations follow similar trends but are 30-50% higher. Weakly bound Fe concentrations are stable and low at an average of 0.5% with the exception of 11.35-11.25 m, corresponding to an estimated age of 60 to 59 ka, where they reach a peak of 2%. Strongly bound Fe is stable at 4% during the entirety of Unit I. Weakly bound Ti is stable at an average of 19±4 µg/g, however strongly bound Ti increases 4-fold from 200 to 800 µg/g from 70 to 60 ka and declines to 500 µg/g from 60 to 42 ka.

3.3.2.2 Unit II- 42 to 33 ka

Unit II spans from a depth of 8.40 to 7.10 m, corresponding to an age of 43 to 33 ka and MIS 3 (**Figure 3-5)**. Weakly bound Fe and Ti double at ~40 ka and thereafter slowly decline to concentrations that are similar to Unit I. This is followed by an increase in carbonate content from 0 to 40% and weakly and strongly bound Mg concentrations that triple at a depth of 7.60 to 7.50 m, corresponding to an age of 36.5 to 35.5 ka. Coincident with these increases are decreases in the strongly bound concentrations of Fe and Ti by 50%. Weight percent organic matter remains roughly the same at 12%.

3.3.2.3 Unit III- 33 to 17 ka

Unit III spans from a depth of 7.10 to 5.14 m, corresponding to an age of 33 to 17 ka and MIS 3 and 2. Concentrations of weakly bound Mg, Fe, and Ti are low and stable at an average of 1600±200 μg/g, 4800±600 μg/g, and 19±3 μg/g, respectively (**Figure 3-5)**. Concentrations of strongly bound Mg, Fe, and Ti increase by 30%, 100%, and 100%, respectively, at 30 ka and thereafter decline to some of the lowest values in the entire preceding units. Additionally, weight percent organic matter slowly increases from ~9% to 15%.

3.3.2.4 Unit IV- 7.8 to 1.5 ka

From a total depth of 5.14 to 2.04 m, corresponding to an age of 7.8 to 1.5 ka, we divide the unit into four subunits (**Figure 3-6**).

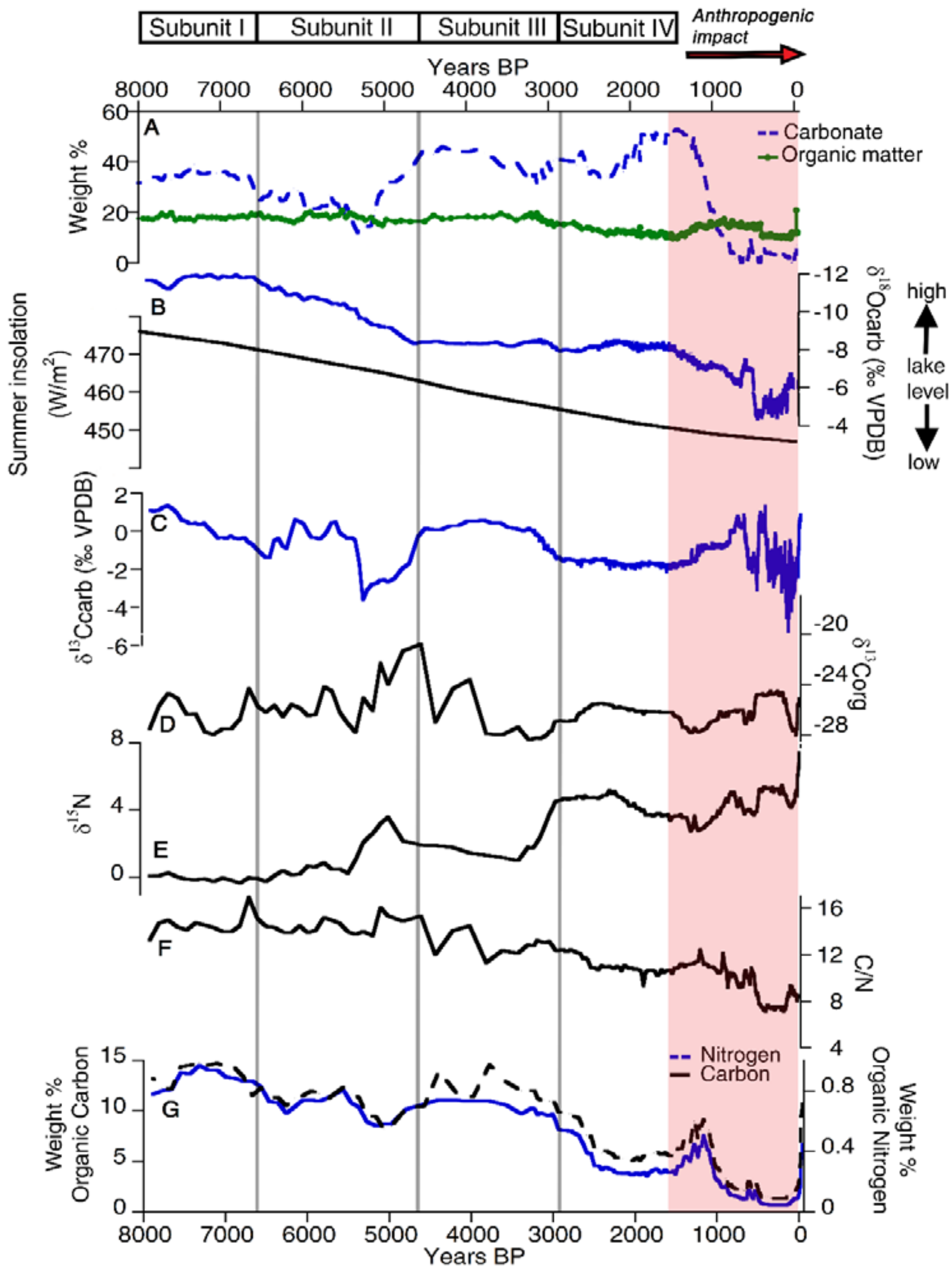

Figure 3-6- The Holocene portion of the record divided into four subunits. A) Weight percent organic matter (green circles) and carbonate (blue dotted line); B) Oxygen isotope values of carbonate with average summer insolation at 20°N; C) Carbon isotopes of carbonate; D) Carbon isotopes of organic matter; E) Nitrogen isotopes of organic matter; F) Carbon to nitrogen ratio; G) Weight percent organic carbon (blue solid line) and organic nitrogen (black dotted line). The pink shaded bar indicates the period of anthropogenic impact (see Chapter 2.0).

3.3.2.4.1 Subunit I- 7.8 to 6.6 ka

Composition of the sediment is stable with ~20% organic matter and between 30-40% carbonate (**Figure 3-6)**. $\delta^{18}O_{carb}$ values are stable at -11.7‰ while $\delta^{13}C_{carb}$ values show a gradual trend towards lower values from 1.0‰ to -1.0‰. $\delta^{13}C_{org}$ values are variable ranging from -24 to -28‰ and reaching minimum values at 7.1 ka. $\delta^{15}N$ and C/N are stable at 0.0‰ and 13, respectively. C/N and $\delta^{15}N$ values exhibit a negative relationship throughout the entirety of the record (**Figure 3-7**).

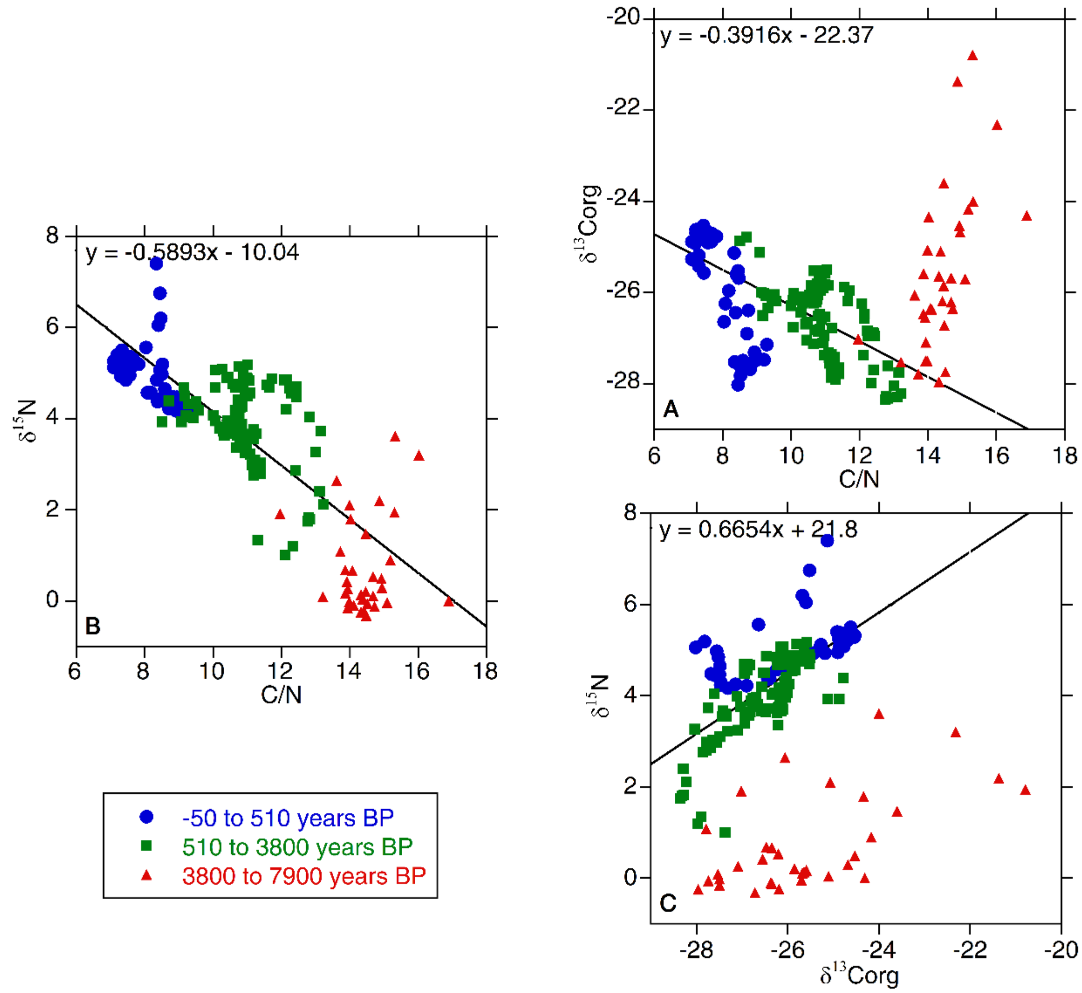

Figure 3-7- A) C/N versus $\delta^{13}C_{org}$ with a linear regression from 3,800 years BP to present ($R^2 = 0.43$, $p < 0.001$). 7,900 to 3,800 years BP were excluded from the regression; B) C/N versus $\delta^{15}N$ with a linear regression through the entire dataset ($R^2 = 0.65$, $p < 0.001$); C) $\delta^{13}C_{org}$ versus $\delta^{15}N$ with a linear regression from 3,800 years BP to present ($R^2 = 0.47$, $p < 0.001$). 7,900 to 3,800 years BP were excluded from the regression.

3.3.2.4.2 Subunit II- 6.6 to 4.7 ka

Weight percent organic matter is stable throughout this interval, though weight percent carbonate declines from 30% to a minimum of 12% at 5.4 ka (**Figure 3-6)**. Thereafter, weight percent carbonate increases to 40% by the end of the subunit. $\delta^{18}O_{carb}$ gradually increases from -11.7 to -8.5‰. $\delta^{13}C_{carb}$ is highly variable, decreasing by about 1‰ at the beginning of the unit and increasing by 2‰ from 6.5 to 6.1 ka. From 6.1 to 5.3 ka, values decrease by 4‰ to a minimum of -3.6‰. At the end of the subunit, values begin to increase to -2.0‰. The dips and increases in inorganic carbon isotopes match closely with changes in weight percent carbonate. $\delta^{15}N$ values increase from 0.0 to 3.6‰ while C/N remains stable at an average of 14.5. $\delta^{13}C_{org}$ values are more variable but in general increase to -20.8‰ by the end of the unit.

3.3.2.4.3 Subunit III- 4.7 to 2.95 ka

Weight percent organic matter is stable throughout this interval, though weight percent carbonate gradually declines from 40 to 30% (**Figure 3-6)**. $\delta^{18}O_{carb}$ values are very stable with an average of -8.4±0.1‰. At the beginning of the subunit, $\delta^{13}C_{carb}$ increases to 0.5‰ and remains stable until 3.2 ka before declining to -1.0‰ by the end of the subunit. Weight percent organic carbon declines by 2% while organic nitrogen remains stable. $\delta^{15}N$ values decline by 1‰ from 4.7 to 3.4 ka before increasing by 3‰ at the end of the unit. $\delta^{13}C_{org}$ and C/N values are variable but generally decrease by about 7‰ and 3, respectively. C/N and $\delta^{13}C_{org}$ have a negative relationship after 3.9 ka (**Figure 3-7)**.

3.3.2.4.4 Subunit IV- 2.95 to 1.5 ka

Throughout this subunit, organic matter content slowly declines from 20 to 10% and carbonate content slowly increases from 30 to 50% (**Figure 3-6)**. Both $\delta^{18}O_{carb}$ and $\delta^{13}C_{carb}$ are stable with an average of -8.2±0.2‰ and -1.7±0.2‰, respectively. C/N values slowly decline to a minimum of 10 while $\delta^{13}C_{org}$ slowly increases to -26.2‰. $\delta^{15}N$ values are stable at 5‰ before declining to 3.5‰ at 1.8 ka.

3.4 DISCUSSION

3.4.1 Unit I- >50 to 42 ka

Because sediments from 12.79 to 10.18 m are too old to date by means of radiocarbon, we have extrapolated back from the last reliable radiocarbon date at 10.18 m to the base of the core, assuming a constant sedimentation rate. There are obvious limitations to this approach, thus we make only tentative conclusions about the data during this timeframe. Prior to 40 ka, sedimentological evidence from a terrace ~100 m higher than present-day lake level shows evidence of lacustrine deposits (Yu et al., 2001). On the basis of this indication, for all of Unit I Xing Yun was likely 100 m higher and connected to Fuxian.

Both the ISM and the EASM system have been shown to respond summer insolation, which is predominantly controlled by precessional forcing (Cheng et al., 2012a). The catchment of Xing Yun is composed of red palaeosols whose weathering would result in high proportions of Al, Fe, and Ti being delivered to the lake (Lu et al., 2015). Notably, prior to 17 ka, the Spearman rho correlation coefficients between average summer insolation at 20°N (defined here as June, July, and August) and the strongly bound concentrations of Mg, Fe, and Ti are 0.41, 0.35, and 0.70, respectively (**Table 3-2**).

During the period of maximum summer insolation at 59 ka, the ISM was strongest, resulting in higher lake levels, more precipitation, higher weathering rates within the Xing Yun catchment, and increased delivery of lithogenic metals to the core site (**Figure 3-5)**. Conversely, the trough of summer insolation at 44 ka resulted in a weaker ISM, lower lake levels, less precipitation, lower weathering rates, and decreased delivery of lithogenic metals to the core site. Radiocarbon dates from a peat deposit on the nearby lacustrine terrace are dated to >40 ka (Yu et al., 2001). While we cannot definitively conclude that the peat was deposited during this period of potentially lower lake levels at 44 ka, this interpretation would fit with the metal concentration data.

Table 3-2- Spearman rho correlation coefficients between July insolation at 20°N and metal concentrations. Metal concentrations were linearly interpolated at 1,000 year time steps before calculating a correlation coefficient. Coefficients that are statistically significant ($p < 0.05$) are highlighted in bold.

	Weakly bound Mg	Weakly bound Fe	Weakly bound Ti	Strongly bound Mg	Strongly bound Fe	Strongly bound Ti
July insolation at 20°N	0.228	**0.469**	**0.487**	**0.422**	**0.595**	**0.735**
Weakly bound Mg		**0.609**	**0.497**	**0.475**	0.198	0. 190
Weakly bound Fe			**0.541**	**0.665**	**0.333**	0.221
Weakly bound Ti				0.202	**0.444**	0.226
Strongly bound Mg					**0.512**	**0.288**
Strongly bound Fe						**0.687**
Strongly bound Ti						

3.4.2 Unit II- 42 to 33 ka

Unit II is marked by brief peaks in Fe and Ti (**Figure 3-5)** as well as other elements such as P, Mn, As, and Sn (not shown) at 40 ka. This is followed 5,000 years later by increases in carbonate content and Mg. While it is difficult to make definitive conclusions with the limited dataset, a possible explanation is that these changes are the result of dramatic lake level fluctuations. Iron and manganese are sensitive to changes in the oxidation/reduction conditions of the water column (Davidson, 1993). The sudden precipitation of both strongly and weakly bound iron in the sediments may indicate a more oxidizing environment associated with abruptly lower lake levels. Authigenic carbonate material is also often dissolved in anoxic, reducing environments (Dean, 1999). The sudden preservation of such material from 36.5 to 35.5 ka may further indicate oxidizing conditions resulting from lower lake levels.

A similar increase in carbonate content from 0 to 20% was also found at nearby Qilu Lake from 40 to 37 ka that was hypothesized to be a result of warm temperatures and increased monsoon strength (Hodell et al., 1999). However, the timing of this event at both Xing Yun and Qilu corresponds closely with Heinrich Event 4 (38 ka), which was recorded as an abrupt weakening in the ISM in nearby Xiaobailong Cave (Cai et al., 2006) (**Figure 3-1)** and may have contributed to lake level lowering. An alternative explanation is that the observed geochemical changes may be driven by tectonic activity or may be associated with nearby ore deposits. Estimates of fault activity, past slip rates, and relevant ore geochemistry that would allow to test these possibilities currently do not exist.

During this time, summer insolation gradually increases and reaches a peak at 33 ka (**Figure 3-5)**. A literature review of lake sediment records from monsoonal Central Asia found that roughly 70% of records indicated moderately wet conditions from 43 to 37.6 ka BP as a result of a strengthened ISM (Herzschuh, 2006). However, it is during Unit II that the relationship between strongly bound metals and summer insolation is the weakest. A possible explanation for this is the persistence of Northern Hemisphere glaciers, even through this interstadial period. Results from modeling studies that simulated late MIS 3 showed that the monsoon system may have had reduced sensitivity to insolation forcing due to these large glaciers (deMenocal and Rind, 1993). Palynological analysis on the parallel set of cores from Xing Yun also inferred a relatively weak monsoon from 36.4 to 34 ka that was attributed to a strengthened Walker Circulation in the Pacific (Chen et al., 2014).

3.4.3 Unit III- 33 to 17 ka

Summer insolation at 20°N gradually declines to a minimum at 21 ka before gradually increasing to a maximum at 10 ka. Concentrations of strongly bound Mg, Fe, and Ti broadly follow similar trends, declining to minimum concentrations at ~25 ka before beginning to increase towards the end of the unit (**Figure 3-5)**. Evidence for lower lake levels may be found from the deposition of peat at the nearby terrace at ~20 ka (Yu et al., 2001). An additional peat layer was dated to ~30 ka, however there is no evidence of lower lake levels at this time in our record.

These changes roughly correspond to the timing of the LGM at 21 ka, however the exact timing and nature of the LGM in southwestern China is debated (Herzschuh, 2006). Due to lower sea levels, the Sunda Shelf was exposed and likely led to a weaker Walker circulation cell in the Indian Ocean (DiNezio and Tierney, 2013) and contributed to a weakened monsoon. However, a literature review found that lakes in Western China show evidence of higher than present-day levels during the LGM whereas lakes in Eastern China appear to be lower than present-day; records from Yunnan lie along the geographic dividing line (Yu et al., 2003). On the basis of modeling, the authors concluded that precipitation was likely decreased across much of China but that evaporation was stronger in the east than the west. Individual regional studies in Yunnan generally show cold and dry conditions but the timing of the transition out of the LGM varies widely. Evidence for full glaciation of Lake Shudu (**Figure 3-1)** was not observed and the catchment was completely deglaciated by at least 22.5 ka despite its high altitude (3630 m) (Cook et al., 2011). Similarly, Lugu Lake (3870 m) was never fully glaciated but diatom assemblages show evidence of cold and dry conditions associated with the LGM persisting until 18 ka (Wang et al., 2014). Palynological evidence from Xing Yun does not suggest climate amelioration until 17.6 ka (Chen et al., 2014). Conversely, the $\delta^{13}C$ values of n-alkanes from Heqing paleolake (**Figure 3-1)** show evidence of increased aquatic productivity throughout the LGM suggesting moderately warm conditions that persisted until 15 ka (Zhang et al., 2004).

While the proxy data from this study cannot expressly address temperature or aridity, previous research on sediment cores from Xing Yun from roughly the same location in the lake focused on organic matter and carbonate content, total nitrogen, total phosphorus, and diatom assemblages (Whitmore et al., 1994b). Changes in weight percent organic matter and carbonate take place at roughly the same depth as those in our core (**Figure 3-8)**. Few radiocarbon measurements on bulk sediment dates led to limited age control and the depth of 8 m was thought to be approximately 11.4 ka. Our new age model based on terrestrial macrofossils suggests that sediment at this depth is actually much older (~40 ka). However, on the basis of very similar stratigraphic changes, we use the previous study's diatom assemblage analysis to support our conclusions. From a depth of 7.5 to 5.0 m, which our study suggests is approximately 35-17 ka, a high proportion of benthic and eutrophic diatoms were found, that the authors interpreted as evidence of low lake levels (Whitmore et al., 1994b) (**Figure 3-8**). This suggests sustained aridity at Xing Yun until 17 ka.

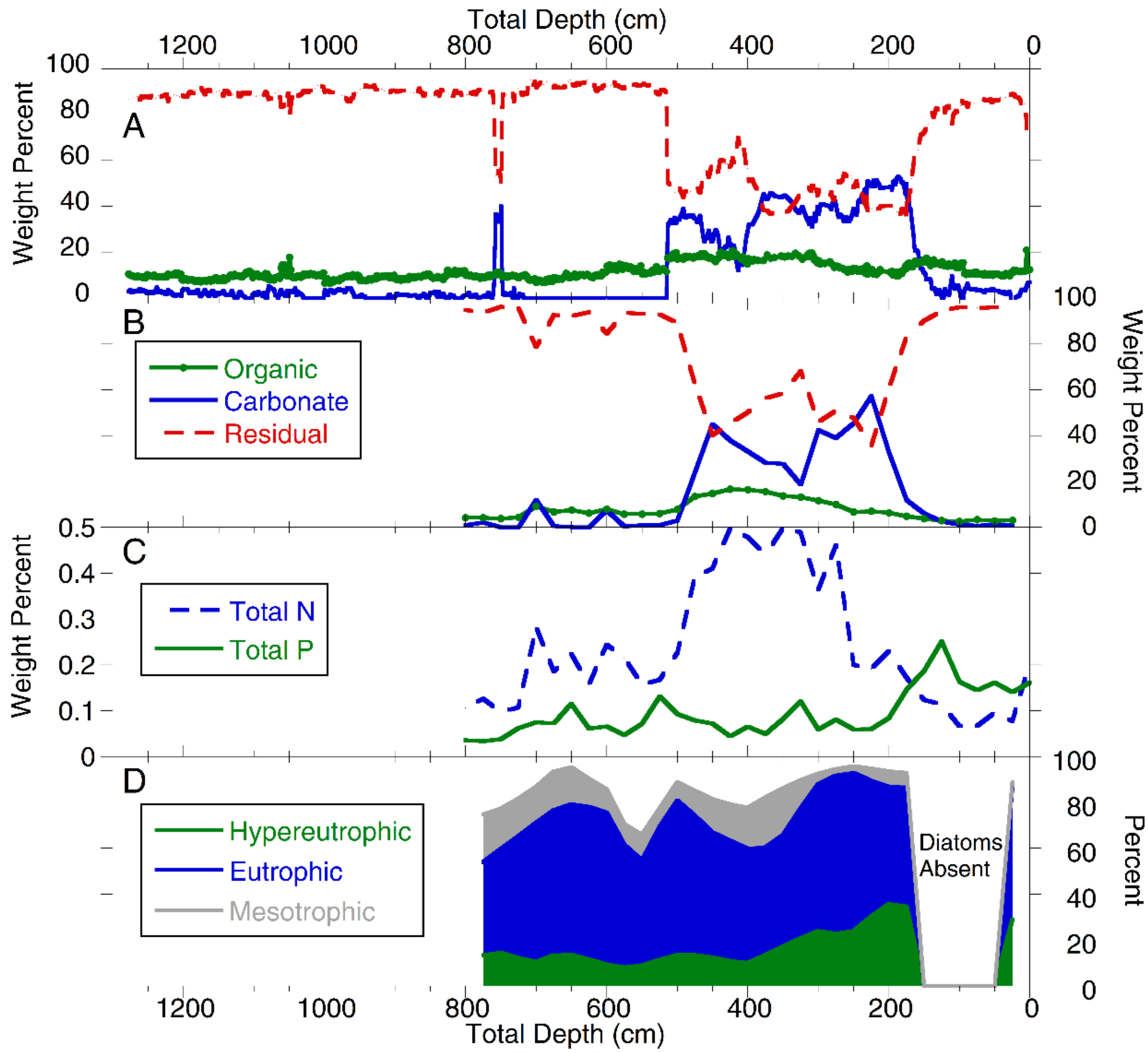

Figure 3-8- Sediment composition of Xing Yun from A) this study and B) Whitmore et al., 1994 with organic matter (green dots), carbonate (blue solid line), and residual mineral matter (red dotted line); C) total nitrogen (blue dotted line) and phosphorus (green solid line) from Whitmore et al., 1994; D) proportion of hypereutrophic diatoms (green), eutrophic diatoms (blue), and mesotrophic diatoms (gray) from Whitmore et al., 1994. The remainder of the percentage of diatoms was composed of either oligotrophic or unknown diatoms. A comparison of the sediment composition of this study in panel A and Whitmore's previous study in panel B shows close correspondence.

3.4.4 Unit IV- 7.8 to 1.5 ka

Unit IV is marked by a major sedimentological change- the deposition of authigenic euhedral calcite. Carbonate content changes as well as $\delta^{18}O_{carb}$ values are roughly similar to the previous study of Xing Yun by Hodell et al., 1999 when matched by depth (**Figure 3-9**). Notable differences include a longer sequence of red, iron-rich clay at the top, a longer sequence of moderate carbonate content averaging 30% from the depth of 4.5 to 6.0 m, and a much longer sequence of high carbonate content (>50%) from the depth of 6.0 to 8.0 m. A possible reason for this is that the coring location in the previous study was on a shelf at a water depth of approximately 7 m **(Figure 3-2)**. Sedimentation rates in this location are likely higher, leading to a greater accumulation of carbonate material over roughly the same time interval.

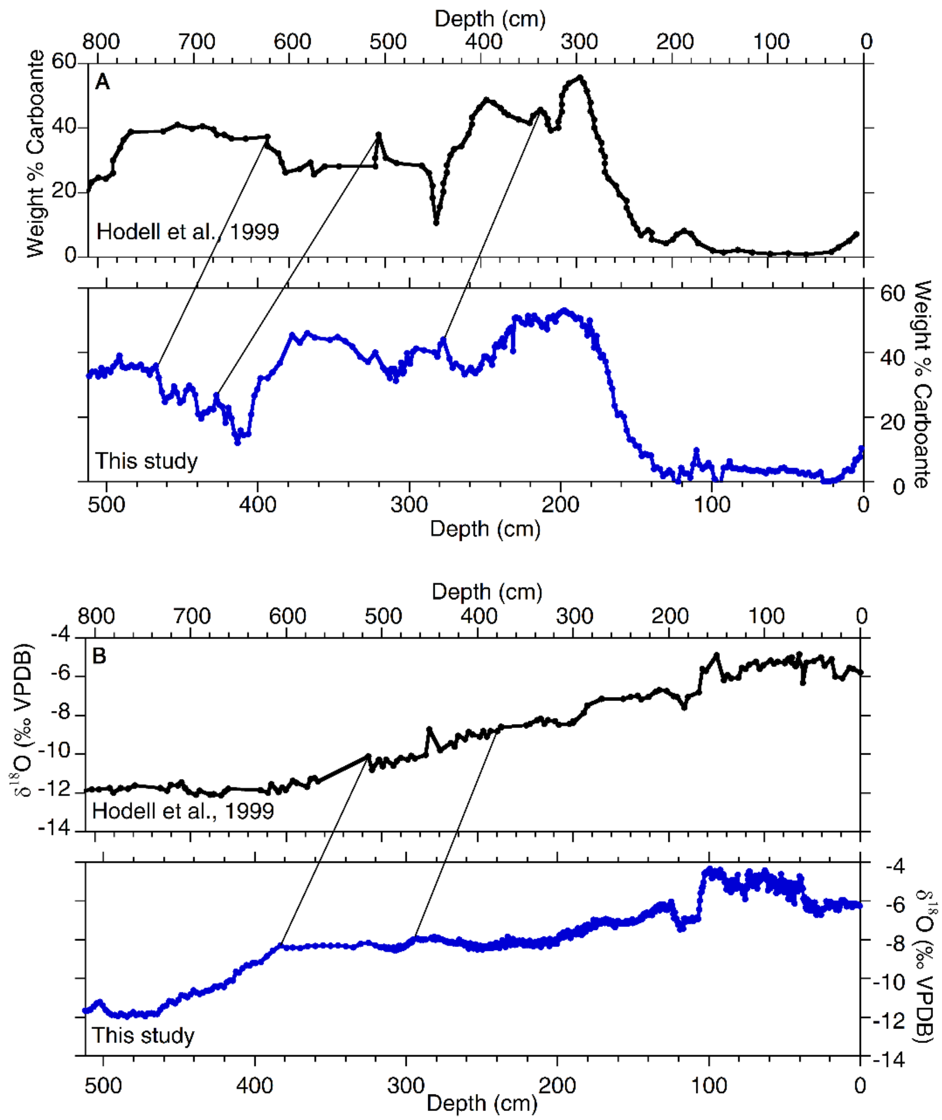

Figure 3-9- Comparison of this study and Hodell et al., 1999 for A) weight percent carbonate and B) oxygen isotope values by depth. The two records are similar though the record from the Hodell et al., 1999 study has a higher sedimentation rate.

The abrupt transition into Unit IV at 5.14 m takes place at a core break, between Drive 3 and 2. The radiocarbon results of terrestrial macrofossils from our sediment cores at the top of Drive 3 and the base of Drive 2 reveal a gap of ~9,000 years that roughly corresponds to the MIS 2/1 boundary (within 3,000 years) (**Figure 3-8**). Previous study of Xing Yun revealed a similarly abrupt transition from sediments composed primarily of residual mineral matter to carbonate rich sediments (Hodell et al., 1999; Whitmore et al., 1994b) (**Figures 3.8 and 3.9**). The Whitmore et al., 1994 study also showed an abrupt increase in variables such as total nitrogen and phosphorus, percentage of planktonic diatoms, and percentage of eutrophic diatoms (**Figure 3-8**). Our colleagues at Lanzhou also noted a hiatus in sedimentation occurring at a similar depth, though the timing is slightly different with their radiocarbon ages being ~4,000 years younger (Chen et al., 2014). Given the abrupt nature of the sedimentological transition as well as the gap in radiocarbon ages, we infer an unconformity between these two units.

According to the Hulu, Dongge, and Sanbao Cave records (**Figure 3-1)**, beginning around 18 ka, ASM strength began dropping, reaching a minimum at ~16 ka, and then gradually increasing to a peak at ~10 ka with an abrupt drop occurring from 13 to 11 ka corresponding to the Younger Dryas cold event (Dykoski et al., 2005; Wang et al., 2008; Wang et al., 2001). The parallel set of cores analyzed at Lanzhou noted that sediments just below 5.14 m had a larger grain size and signaled the beginning of a palynological transition to more drought-resistant broadleaved trees indicative of drier climate conditions (Chen et al., 2014). Palynological and aquatic productivity analyses from 22.6 to 17.7 ka at Lake Shudu (**Figure 3-1)** also suggested cold and dry conditions (Cook et al., 2011). Palynological analysis at the Er Yuan swamp as well as Dian lake also found evidence of cold and dry conditions until 16-15 ka, followed by fluctuating climate conditions of short summers with long, dry winters until 10 ka (Lin et al., 1986; Sun et al., 1986). However, the timing of maximum cold and arid conditions at all of the aforementioned sites is not precisely the same as the unconformity in our Xing Yun record, nor does climate variability explain why sedimentation resumed at 7.8 ka.

Paleoclimate records do not converge to suggest a single, clear climate driven cause of the unconformity, so we hypothesize that this event may be due to tectonic activity since Xing Yun is a pull-apart basin and there are extensive fault systems in the region (**Figure 1-1**). If Fuxian and Xing Yun were once connected into one large lake that was 100 m higher, the Nanpan River would been dammed (**Figure 3-3**). If movement along one of the many faults near the lakes occurred and removed the dam, a catastrophic event would have taken place. This may also have been erosive and may account for the unconformity. After 7.8 ka, sediments were preserved again and Xing Yun was a much different lake as it was much smaller and lower due to the absence of a dam on the Nanpan River. This could account for the dramatically different character of the sediment.

The lack of carbonate material prior to 7.8 ka may have been due to deepwater conditions. Deep lakes with anoxic bottom waters may not preserve carbonate material due to the decomposition of organic matter and low pH, leading to the dissolution of carbonate (Dean, 1999). This also explains the relatively low, constant proportion of organic matter throughout the entire core, despite vegetation and temperature changes that would have influenced primary productivity over these long time scales. If a dramatic change in the geomorphology of the lake basin occurred after 17 ka, lake levels may have been low enough to permit the preservation of carbonate material. This interpretation is supported by the termination of lacustrine sediment and peat layers from a terrace 100 m higher than present-day lake levels and the termination of lacustrine sediment from a terrace 25 m higher than present-day lake levels between Xing Yun and Fuxian at ~11.8 ka (Yu et al., 2001). While we cannot definitively prove the above scenario, the proposed hypothesis best fits all of the available evidence that has been collected. Further study on fault slip rates and events would need to be undertaken to provide more support for this interpretation.

3.4.4.1 Subunit I- 7.8 to 6.6 ka

The $\delta^{18}O_{carb}$ values through this interval suggest stable, high lake levels, broadly in agreement with previous records of a strong EASM from Dongge Cave (Wang et al., 2005) and a strong ISM from Tianmen Cave (Cai et al., 2012) due to relatively high average summer insolation in the early to mid-Holocene. C/N values in the range of 13 to 15 suggest a greater terrestrial contribution of organic matter to Xing Yun, possibility as a result of increasing rainfall and runoff. The relatively constant C/N values prior to 4.7 ka suggest that changes in organic matter source cannot account for the variations in $\delta^{13}C_{org}$ values. Changes in $\delta^{13}C_{org}$ values could be driven by soil organic carbon input, but this is not supported by the C/N values nor the declining weight percent carbon and nitrogen throughout the Holocene. With a more terrestrial source of organic matter influencing the carbon isotopic composition, vegetational shifts could also cause the observed changes in $\delta^{13}C_{org}$ values. However, CMIP5 modeling studies of vegetation changes in Southeast Asia found that the relative proportion of C4 grasses for the past 21 ka only varied by 10-20% with the most substantial changes taking place in the LGM (Thomas et al., 2014). This suggests that vegetational shifts were not large enough in the Holocene to explain all of the observed variation in $\delta^{13}C_{org}$ values at Xing Yun. Additionally, palynological analysis at nearby Dian Lake (**Figure 3-1**) found that the most substantial shifts in vegetational assemblages occurred from 9.5 to 8 ka (Sun et al., 1986), prior to the beginning of the Xing Yun Holocene sediment record.

Therefore, we interpret changes in $\delta^{13}C_{org}$ values in the Xing Yun record to primarily reflect primary productivity. Lighter isotopes of carbon tend to be preferentially incorporated into organic matter and leaves the remaining dissolved inorganic carbon (DIC) pool relatively enriched in ^{13}C (McKenzie, 1985). However, with increased productivity the supply of ^{12}C may be depleted leading to increased $\delta^{13}C_{org}$ values over time (Schelske and Hodell, 1995). $\delta^{13}C_{org}$ values may further increase as a result of rapid algal growth resulting in less discrimination between ^{12}C and ^{13}C (Brenner et al., 1999). Conversely, decreases in $\delta^{13}C_{org}$ values may reflect declining primary productivity and may account for the decreases in $\delta^{13}C_{carb}$ and $\delta^{13}C_{org}$ in the early to mid-Holocene at Xing Yun. The correspondence between Xing Yun weight percent carbonate, Xing Yun $\delta^{13}C_{org}$ values, and Paru Co weight percent biogenic silica throughout much of the Holocene suggests that this interpretation may be plausible (**Figure 3-10)**.

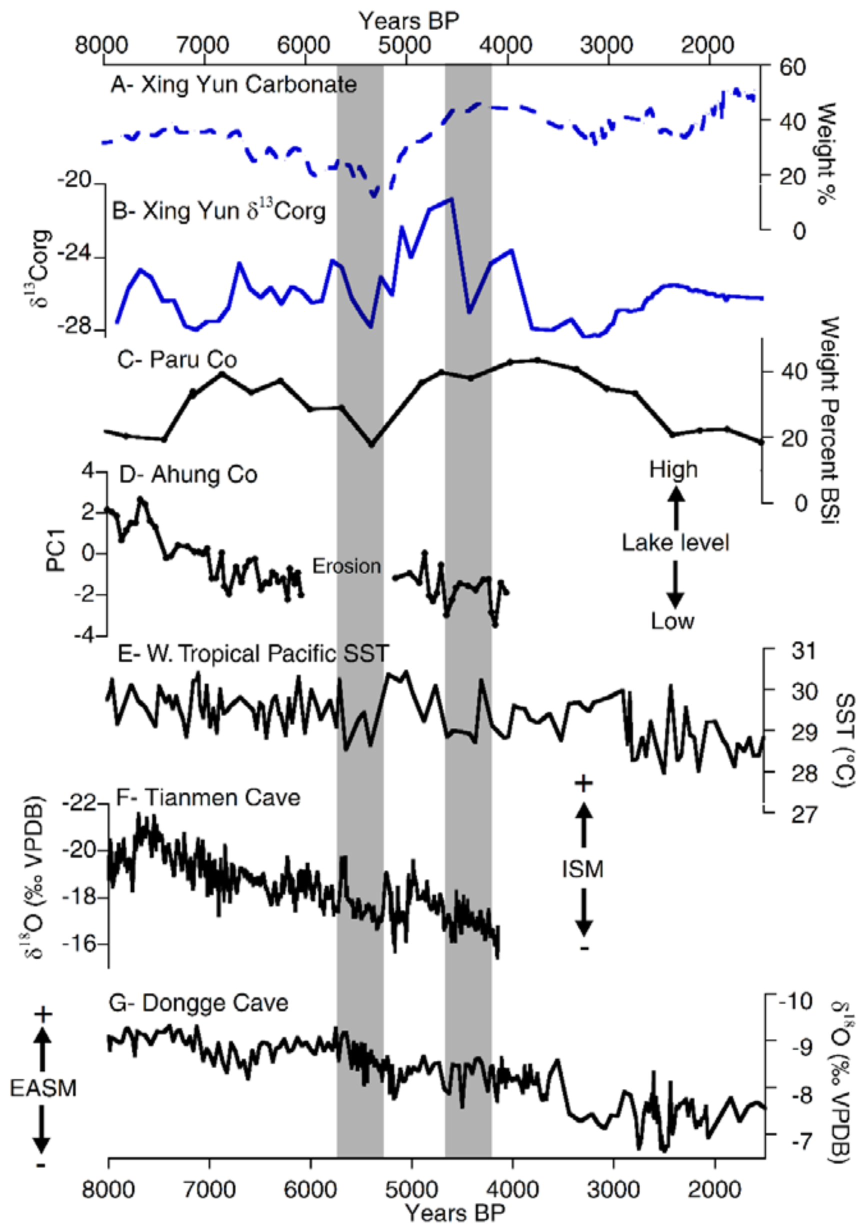

Figure 3-10- A) Xing Yun weight percent carbonate; B) Xing Yun carbon isotope values of organic matter; C) Paru Co weight percent biogenic silica (Bird et al., 2014); D) Ahung Co lake level reconstruction (Morrill et al., 2006); E) Western tropical Pacific SST reconstruction from Mg/Ca of benthic forminifera (MD98-2181) (Stott et al., 2007); F) Tianmen Cave oxygen isotope values (Cai et al., 2012); G) Dongge Cave oxygen isotope values (Wang et al., 2005). The gray shaded bars indicate pronounced drops in Xing Yun organic carbon isotopes indicative of drops in primary productivity and coincident with noted drops in ISM strength and Western Pacific SST.

3.4.4.2 Subunit II- 6.6 to 4.7 ka

Subunit II is marked by a pronounced trend towards higher $\delta^{18}O_{carb}$ values and highly variable $\delta^{13}C_{carb}$ values. The sustained trend towards higher $\delta^{18}O_{carb}$ values, coupled with declining solar insolation, suggests increased aridity driving lower lake levels. While records of the EASM show that optimal moisture conditions persisted until 5 ka, ISM records from the Tibetan Plateau show a decrease in optimal moisture beginning around 7 ka (Herzschuh, 2006). The previous study by Whitmore et al., 1994 found a higher proportion of eutrophic and hypereutrophic taxa and increased weight percent organic nitrogen from a depth of 4.6-3.6 m, corresponding to approximately 6.5 to 4 ka on the basis of our new age model, that they also interpreted to suggest lower lake levels (**Figure 3-8**).

The high variability in $\delta^{13}C_{carb}$ values suggests substantial changes to the DIC pool. These changes in $\delta^{13}C_{carb}$ values closely follow changes in weight percent carbonate, which suggests that the isotopic composition of inorganic carbon is directly linked to carbonate precipitation, since changes in carbonate content tend to slightly lead changes in $\delta^{13}C_{carb}$ values. This may be caused by changes in primary productivity because increased photosynthetic activity results in the drawdown of dissolved CO_2, forcing the precipitation of inorganic carbonate (Kelts and Hsu, 1978). This interpretation is supported by the close correspondence between $\delta^{13}C_{org}$ and weight percent carbonate during this subunit. Once again, the consistent C/N values through this time period suggest that changes in the isotopic composition of organic carbon is likely not linked to inputs arising from soil erosion. However, increased productivity would force the remaining DIC pool in the lake to have more ^{13}C, which is reflected in the

$\delta^{13}C_{carb}$ values. Therefore we infer a period of slightly increased productivity from 6.6 to 5.6 ka and substantially increased productivity from 5.1 to 4.7 ka.

These periods are interrupted by an abrupt drop in weight percent carbonate, $\delta^{13}C_{carb}$, and $\delta^{13}C_{org}$ at 5.3 ka. Several other lake records from the Tibetan Plateau show changes around the same time with a drop in biogenic silica at Paru Co around 5.3 ka (Bird et al., 2014) and a period of no sedimentation and erosion at Ahung Co from 6 to 5.8 ka (Morrill et al., 2006) (**Figure 3-10)**. Western Pacific SSTs reconstructed from ocean core MD98-2181 (6°17'60''N, 125°49'12''E) noticeably drop at 5.4 ka (Stott et al., 2007) and ODP site 723 in the Arabian Sea (18°3'5''N, 57°36'34''E) shows a decrease in *G. bulloides* from 6 to 5.3 ka, indicative of cooler ocean conditions, that the authors linked to Bond event 4 (Gupta et al., 2002). Reconstructed SSTs from throughout the Mentawai Islands also show cooling, suggestive of a positive phase IOD event (Abram et al., 2009). Bird et al., 2014 interpreted this to be a period of increased monsoon strength on the Tibetan Plateau due to an increased thermal gradient from ocean cooling. Changes in ISM strength are not recorded in Xing Yun oxygen isotopes, however the shift in the carbon cycle of the lake does suggest that productivity dropped possibly due to cooler temperatures.

3.4.4.3 Subunit III- 4.7 to 2.95 ka

The relatively stable $\delta^{18}O_{carb}$ values through this interval suggest steady lake levels, likely substantially lower than the previous two subunits, but not wildly fluctuating or changing. The hydrologic balance of the lake reaches a steady state that persists until 1.5 ka when human activities perturb the natural stability (see Chapter 2.0). Increased evaporation leads to degassing of CO_2 and the preferential removal of lighter ^{12}C atoms, leaving the remaining lake water relatively enriched in ^{13}C (Li and Ku, 1997). Atmospheric CO_2 has $\delta^{13}C$ values of around -8‰ and lake water that is in equilibrium with atmospheric CO_2 will have values between 1-3‰ (Leng and Marshall, 2004), close to the average carbon isotopic composition through this unit (0.5‰). The loss of CO_2 may cause precipitation of carbonate minerals (Ito, 2001) and could account for the high proportions of carbonate material through this interval. Lower lake levels are also supported by an increase in eutrophic and hypereutrophic diatom taxa (Whitmore et al., 1994b).

A synthesis of abrupt changes in the entire Asian monsoon system over the Holocene found statistically significant aridity from 5 to 4.5 ka (Morrill et al., 2003) and there is evidence from nearby Dian Lake (see Chapter 5.0) of lower lake levels during this time period as well. Mawmulh (Berkelhammer et al., 2012) and Tianmen Caves (Cai et al., 2012) (**Figure 3-10**) both record an abrupt decrease in ISM strength and stop precipitating carbonate material after 4 ka. Several lakes on the Tibetan Plateau, including Lake Qinghai (Lister et al., 1991), Bangong Co (Gasse et al., 1996), Selin Co (Gu et al., 1993), and Ahung Co (Morrill et al., 2006), suggest the beginning of substantially drier conditions and Ahung Co was desiccated after 4 ka (**Figure 3-10)**. The abrupt drop in $\delta^{13}C_{org}$ values at Xing Yun at 4.5 ka coincides closely with a drop in Western Pacific SSTs (**Figure 3-10**), similar to what was observed at 5.3 ka. Ocean cores from the Soledad Basin off the coast of Mexico display a shift to warmer SSTs and a more El Niño-like mean state after 4 ka (Marchitto et al., 2010). A more El Niño-like mean state beginning in the mid to late Holocene has been observed in multiple other oceanic records (Rein et al., 2005; Stott et al., 2004). We suggest a connection between decreases in primary productivity at Xing Yun and cooler Western Pacific SSTs due to more El Niño-like conditions.

The otherwise slow decline in weight percent carbon, nitrogen, and C/N values at Xing Yun may be due to a shift in the trophic state of the lake. These changes may be linked to declining summer insolation values and a weaker ISM washing less terrestrial organic matter into the lake. A plot of C/N versus $\delta^{15}N$ values shows a negative relationship and a similar relationship can be seen for C/N versus $\delta^{13}C_{org}$ after 3.8 ka (**Figure 3-7)**. Changes in $\delta^{15}N$ may also be linked to increasing aridity since decreasing precipitation has been shown to increase both soil and foliar $\delta^{15}N$ (Amundson et al., 2003; Craine et al., 2009). This phenomenon is still being investigated but several explanations have been proposed including increased gaseous nitrogen loss, less dependence on mycorrhizal fungi, and less efficient nitrogen recycling with decreased moisture (Amundson et al., 2003; Craine et al., 2009).

3.4.4.4 Subunit IV- 2.95 to 1.5 ka

The lowest average summer insolation values occur in the late Holocene resulting in a generally weak monsoon and substantial aridity recorded in lake sediments throughout China (Zhang et al., 2011). This subunit in Xing Yun is marked primarily by a noticeable decline in $\delta^{13}C_{carb}$ values without a concomitant decline in $\delta^{18}O_{carb}$ values as well as declining weight percent organic matter, carbon, nitrogen, and C/N. This is indicative of a continued shift in the trophic status of the lake without considerable drops in lake level. Continued low lake levels and more eutrophic conditions may have accelerated the remineralization of organic matter in this broad shallow lake, limiting organic preservation. Increased primary productivity is supported by $\delta^{13}C_{org}$ and $\delta^{15}N$ values that increase at the beginning of this subunit.

Notably, biogenic silica from Paru Co declines and Western Pacific SSTs decrease during this time (**Figure 3-10**). The relationship between Western Pacific SST and Xing Yun $\delta^{13}C_{org}$ is no longer present and some other variable began exerting a control on the isotopic composition of the carbon pool of the lake. The sudden negative relationship between C/N and $\delta^{13}C_{org}$ during this time suggests while previously, $\delta^{13}C_{org}$ values were controlled by factors other than organic matter source, after 3.8 ka $\delta^{13}C_{org}$ values were being driven by variations in the proportions of aquatic and terrestrial organic matter. While nearby archaeological sites consisting of shell mounds, settlement structures, and rice remains date to 4 to 3 ka (Yao, 2010), there is no definitive evidence of human activity perturbing the lake until 1.5 ka. However, anthropogenic impacts may partially explain why Western Pacific SSTs and Xing Yun $\delta^{13}C_{org}$ values suddenly appear anti-correlated.

3.5 CONCLUSION

This sediment record from Xing Yun Lake is one of the oldest terrestrial records of the ISM that is continuous through the Holocene. As such, it provides an unprecedented look into what was driving hydroclimate variability associated with the ISM as expressed in southwestern China. The Pleistocene portion of our record is limited by macrofossils that are too old to date by means of AMS radiocarbon dating. Future work to establish a more reliable chronology may include the use of paleomagnetic secular variation or U-Th dating of gastropods.

However, on the basis of relatively linear sedimentation rates, we demonstrate a relationship between July insolation at 20°N and the weakly and strongly bound concentrations of several lithogenic metals including Mg, Fe, and Ti over an estimated time period of 70,000 years. The ISM responded in a linear, rapid fashion to changes in summer insolation, causing increased weathering and increased delivery of sediments derived from the catchment to the lake coring site. This is broadly similar to what other studies have found regarding the EASM and the ISM over the Holocene and we have demonstrated that this relationship holds over much longer time scales than previously investigated. This simple relationship weakens from 42 to 33 ka, possibly due to large Northern Hemisphere ice sheets causing a muted response of the monsoon system to solar insolation. Future work on sediment from this portion of the record will include the analysis of the hydrogen isotopic composition of *n*-alkane leaf waxes (δD_{wax}) derived from terrestrial and aquatic plants. While δD_{wax} can be influenced by multiple processes such as biosynthetic factors, when changes in vegetation can be constrained, these measurements are well correlated with mean precipitation δD values (Polissar and Freeman, 2010; Sachse et al., 2012). Measurements of δD_{wax} will be a powerful tool for understanding variations in the strength of the ISM as well as the impacts of evaporation on lake hydrology.

The Xing Yun sediment record is interrupted by a 9,000 year unconformity from 17 to 8 ka, which may be due to the desiccation of the lake resulting from exceptionally dry climatic conditions, an erosive event resulting from tectonic activity, or some combination of both. Further study including seismic surveys, transect cores, or longer sediment records from adjacent lakes such as Fuxian may provide some context to the observed unconformity.

The resumption of sedimentation at Xing Yun occurs in the early to middle Holocene and is marked by the sudden preservation of carbonate material. Isotopic analysis of this calcite reveals substantial (4-6‰) changes in both carbon and oxygen. Oxygen stable isotopes suggest a transition to lower lake levels beginning around 6.6 ka, similar to what other lake sediment studies from the Tibetan Plateau record. Lake levels as reflected in $\delta^{18}O_{carb}$ values reach a steady state by 4.7 ka even though other paleoclimate records show that the ISM continued to decline in strength. Carbon stable isotopes of both carbonate material and organic matter are considerably more variable, particularly from 6.6 to 4.7 ka. These changes closely track weight percent carbonate as well as weight percent biogenic silica from Paru Co Lake on the Tibetan Plateau. This suggests that both carbonate precipitation and $\delta^{13}C_{carb}$ values are controlled by primary productivity. Prior to 2.95 ka, decreased primary productivity at Xing Yun is linked to cooler Western Pacific SSTs, demonstrating the importance of the tropics on controlling the climate of southwestern China over multi-decadal timescales. Weight percent carbon, nitrogen, and C/N show a slow, gradual trend towards lower values in concert with declining summer insolation. Lower lake levels may have driven a shift towards more eutrophic conditions and shifts in primary productivity can be seen in the $\delta^{13}C_{org}$ and $\delta^{15}N$ values with a notable increase at 2.95 ka. The Xing Yun record is one of the first continuous terrestrial hydroclimate records of the ISM through the Holocene and shows broad agreement with previous paleoclimate studies from the Tibetan Plateau.

4.0 ERHAI LAKE

The Environmental Legacy of Copper Metallurgy and Mongol Silver Smelting Recorded in Yunnan Lake Sediments

Lake Er (Erhai) is located in the northwest portion of Yunnan with the modern city of Dali situated on the southern shores of the lake (**Figure 4-1**). Erhai is ideally situated to answer questions about the history of mineral resource use in Yunnan since historically there were metal smelting and production facilities in the vicinity of Dali (Cui and Wu, 2008) and modern day nickel, copper, and platinum metal mining takes place on the eastern side of the lake at the Huangcaoba mine (Kamitani et al., 2007). Today, a number of ore bodies are mined in western Yunnan including the Mrchangjing and Zhacun gold mines, the Yongping copper mine, and the lead and zinc mine of Jinding (Pirajno, 2013) (**Table 4-1 and Figure 4-1**). Here, we present a 4,500 year record of smelting and mining from Erhai using the concentrations heavy metals in sediment. Lake sediment geochemistry has been used elsewhere in the world to reconstruct metal inputs related to mining and metalworking (Bindler et al., 2012; Renberg et al., 1994), yet relatively few records of this type exist in China (Jin et al., 2013; Lee et al., 2008).

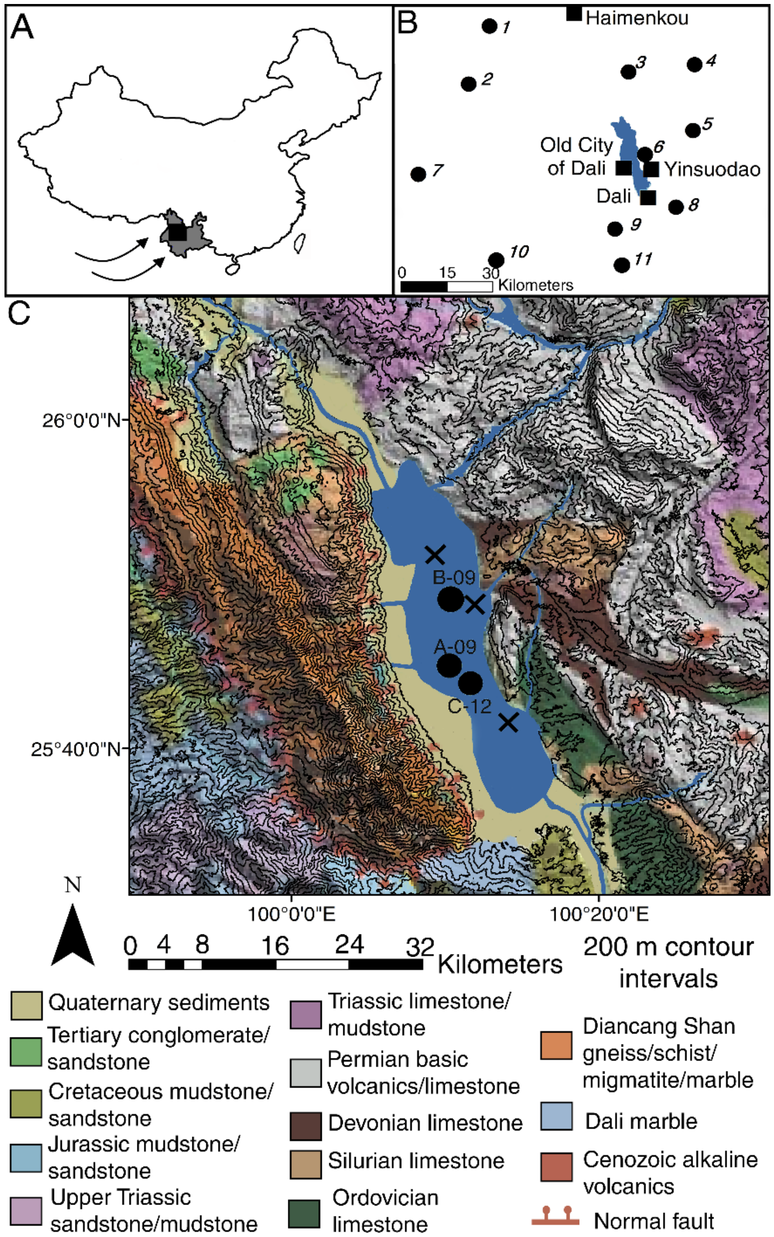

Figure 4-1- A- China with Yunnan Province shaded in gray. Erhai (square) with dominant wind direction; B- Major ore bodies (see Table 4-1) and archaeological sites Haimenkou and Yinsuodao in relation to Dali and Erhai; C- Erhai and coring locations A-09, B-09, and C-12. Previous coring locations by Dearing et al., 2008 marked by Xs. Geologic map adapted with permission from Searle et al., 2010.

Table 4-1- Ore bodies of northwestern Yunnan displayed in Figure 4-1 (Hou et al., 2007; Bureau of Geology and Mineral Resources of Yunnan Province, 1990).

Number in figure 1	Name	Deposit
1	Jinding	Pb, Zn, Sr, Gypsum
2	Baiyangchang	Co, Cu, Ag
3	Beiya	Au
4	Heqing	Mn
5	Baofengsi	Pb, Zn, Pyrite
6	Huangcaoba	Ni, Cu, Platinum Group Metals
7	Tiechang	Sn
8	Mrchangjing	Au
9	Shihuangchang	As
10	Yongping	Cu, Co
11	Zhacun	Au

4.1 REGIONAL SETTING

Erhai (25°47'N, 100°11'E, 1964 m elevation) is a relatively deep (maximum depth: 21.5 m) lake with a catchment area of 2,560 square kilometers (Whitmore et al., 1997) (**Figure 4-1**). The Diancang Shan Mountains, on the western side of the catchment, are composed of high-grade metamorphic rocks such as gneiss and schist and are bound by a normal fault (Bureau of Geology and Mineral Resources of Yunnan Province, 1990; Searle et al., 2010). The northern and eastern sections of the catchment are composed of Quaternary sediments, Permian basic volcanics and limestones, and Triassic sandstones and mudstones (Bureau of Geology and

Mineral Resources of Yunnan Province, 1990; Searle et al., 2010). The lake receives inflow from 38 streams and outflows through the Xier River to the south (Whitmore et al., 1994a). The Erhai basin is connected to Southeast Asia via the Red and Mekong Rivers. Since 1980, algal blooms, eutrophication, and other water and sediment quality issues have been noted (Liu et al., 2012; Wang et al., 2012b). Previous research on Erhai sediment cores found that lake levels varied by only 1-3 m over the late Holocene (Yu et al., 2001). While this is a tectonically active region and several earthquakes have occurred historically (Allen et al., 1984), the small fluctuations in lake level suggest that over the last several thousand years, tectonic activity had a limited impact on water levels.

Previous research on sediment cores from Erhai by Dearing et al., 2008 included palynological analysis and measurements of grainsize, magnetic properties, and geochemistry. They identified a rise in metalworking at 1400 BC with an increase in the concentration of copper from 12 to 14 μg/g (Dearing et al., 2008). Additionally, an increase in lead concentration at 550 AD from 4 to 14 μg/g was inferred to represent a change from bronze to silver metalworking. However, this previous study relied on an age model based on a combination of radiocarbon measurements on bulk sediment and shell material, both of which are subject to reservoir effects, and correlation with paleomagnetic features from three cores recovered from different locations in the lake (Hyodo et al., 1999; Xu and Zheng, 2003; Yang et al., 2005) (**Figures 4.1 and 4.2**). Shell material and bulk sediment are subject to radiocarbon reservoir effects, where ancient carbon from carbonate rocks and soils is incorporated into samples, making them appear older than the true age of deposition (Deevey et al., 1954). Other research on Yunnan lakes has identified a pronounced reservoir effect of several thousand years from bulk sediment dates (Brenner et al., 1991; Whitmore et al., 1994b). Because limestone exists in the

Erhai catchment (Bureau of Geology and Mineral Resources of Yunnan Province, 1990), bulk sediment and shell radiocarbon dates should be avoided. Additionally, several age reversals appear in the sediment profile, but these were disregarded in the age model, which relied on a polynomial line of best fit drawn through all of the dates (**Figure 4-2**). It should also be noted in the Dearing et al., 2008 study that the three cores were separated by as much as 20 km and some of the cores were collected from the deepest part of the lake while others were collected along the shoreline where there are significantly different sediment accumulation rates (**Figure 4-1**). Given the potential issues with the Dearing et al., 2008 age model there is a clear need to reassess the findings using radiocarbon measurements on identifiable terrestrial macrofossils that are unaffected by reservoir effects.

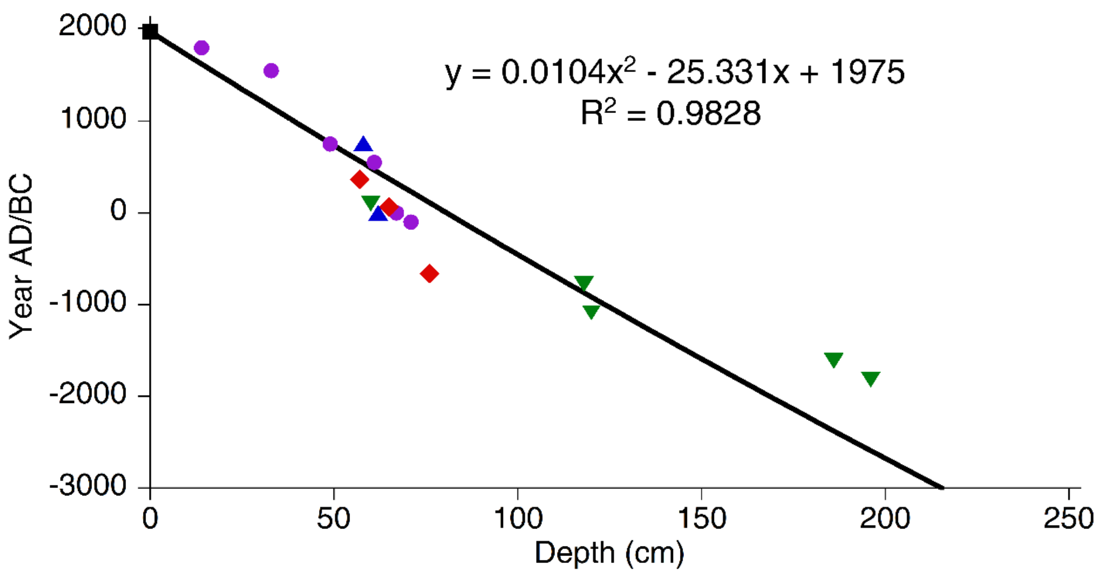

Figure 4-2- Dearing et al., 2008 polynomial age model for Erhai sediment cores (collection locations marked in Figure 4-1). Unpublished ^{210}Pb data (black square), paleomagnetic features from Hyodo et al., 1999 (purple circles), terrestrial macrofossil radiocarbon dates (blue triangles), bulk sediment radiocarbon dates from Hyodo et al., 1999 (green inverted triangles), and shell radiocarbon dates from Hyodo et al., 1999 (red diamonds).

4.2 ARCHAEOLOGICAL AND HISTORICAL CONTEXT

The results of archaeological excavations and palynological analysis suggest that Erhai's lakeshores were occupied during the Neolithic (Wan, 2013). One of these Neolithic/Bronze Age settlements is the Yinsuodao shell midden on the southeastern shore (Yunnan Provincial Institute of Cultural Relics and Archaeology, 2009b) (**Figure 4-1**). Metal slag and complex copper and bronze artifacts found there date to no later than 1200 BC (Yunnan Provincial Institute of Cultural Relics and Archaeology, 2009b; Cui, 2014), suggesting that metal production existed in the area during the middle of the 2nd millennium BC. Similar evidence of copper-based metalworking as early as 2nd millennium BC was found at the Haimenkou site (Yunnan Provincial Institute of Cultural Relics and Archaeology, 2009b; Min, 2013), located near Lake Jian, ~50 km north of Erhai (**Figure 4-1**). Elemental analyses of materials from these two sites indicate that copper was the earliest metal to be used in western Yunnan (Cui, 2014). Alloyed bronzes made of mixtures of copper and tin were later used, but pure copper items were used in Yunnan throughout the Bronze Age (Chiou-Peng, 2011). Prior to the middle of the 1st millennium BC, lead was usually a trace metal (<5%) in standard bronze recipes (Chiou-Peng, 2011). Archaeological materials from the Erhai region show influence from the Eurasian steppes (Cui, 2014); however, due to the lack of archaeological data marking the transition between Neolithic and Bronze ages in Yunnan, and the absence of geochemical records associated with smelting activities near Erhai, the timing of the earliest metallurgical activities in Yunnan remains unclear (Higham et al., 2011). The current interpretations of the beginnings of Yunnan metallurgy are particularly relevant to ongoing debates about the onset of metallurgy in Southeast Asia, a region that is geographically and culturally connected to Erhai through the Great Mekong exchange system (Higham et al., 2011; Min, 2013; White and Hamilton, 2009).

Similar metallurgical features and artifact types at Yinsuodao and Haimenkou indicate that the metal industry was part of the 2nd and 1st millennia BC technological complex in western Yunnan, which had close associations with ore deposits along the Jinsha (upper Yangzi) valleys north and east of Erhai (Min, 2013). Lead isotope studies of Yunnan ores suggest that the Baiyangchang ore body (**Figure 4-1**) was a source for metal production at Haimenkou (Cui and Wu, 2008). Many of these objects became the prototypes of bronze for the Dian culture (350 BC-100 AD) (Cui, 2014), located on the shores of Lake Dian, ~250 km southeast of Erhai. Bronze artifacts remained in vogue in Yunnan even after iron was introduced into the region towards the end of the 1st millennium BC. Copper, tin, lead, and silver probably continued to be extracted from these southern mines (Dai and Zhang, 1998) and used in parallel with other ore deposits widely dispersed over Yunnan (Zhang, 2000). An immense silver industry arose during the Nanzhao and Dali kingdoms of Yunnan (ca. 738-1253 AD) and during this time, silver utilitarian and religious objects were produced in parallel with iron and bronze utensils and weaponry (Zhang, 2000). With the invasion of the Yuan Dynasty (the Mongols) in 1253 AD, the Dali Kingdom was conquered and Yunnan nominally became part of Chinese territory (Giersch, 2009). The Yuan administration's mismanagement of Yunnan ore resources resulted in the decline of the copper industry (Han and Ke, 2007). Silver materials from large-scale mining activities in Yunnan were distributed nationwide, but the value of silver in Yunnan was severely deflated due to over-production (Han and Ke, 2007). The Ming (ca. 1368-1644 AD) and Qing (ca. 1644-1911 AD) Dynasties that followed heavily exploited the mineral resources of Yunnan for copper and silver, but historical records are insufficient and the true extent of this activity is unknown (Yang, 2009).

4.3 MATERIALS AND METHODS

4.3.1 Core Collection

To characterize the impact that metallurgy has had on the lake over the past several thousand years and attain more realistic estimates of the timing and scale of metalworking, we recovered sediment cores from three different locations in Erhai (A-09, B-09, and C-12 coring sites; **Figure 4-1**). We measured the sediment concentrations of a suite of weakly bound metals including copper, lead, silver, cadmium, zinc, titanium, aluminum, and magnesium. We focus our attention on lead because it has successfully been used to document early pre-industrial anthropogenic metallurgical activities (Abbott and Wolfe, 2003; Renberg et al., 1994) and is relatively immobile once deposited in lake sediments (Gallon et al., 2004); however, we supplement our interpretation using other metals.

In 2009, three cores were collected from Erhai at 25°44’34’’N, 100°11’44’’E (core site A-09) at a water depth of 11 m and one core was collected from 25°48’42’’N, 100°11’42’’E (core site B-09) at a water depth of 20 m (**Figure 4-1**). At site A-09, a 62 cm long core with an intact sediment-water interface was collected using a light weight percussion coring system (A-09 surf) (**Figure 4-3**). The upper 20 cm were sliced in the field at 0.5 cm intervals and used for geochemical analysis and ^{210}Pb dating. Deeper sediments (A-09 D-1 and D-2) were collected using a steel barrel Livingston corer (Wright et al., 1984). At site B-09, a 74 cm long surface core was recovered with an intact sediment-water interface using the percussion coring system (B-09 surf) (**Figure 4-3**) and the upper 20 cm were sliced in the field at 0.5 cm intervals and used for geochemical analysis and ^{210}Pb dating.

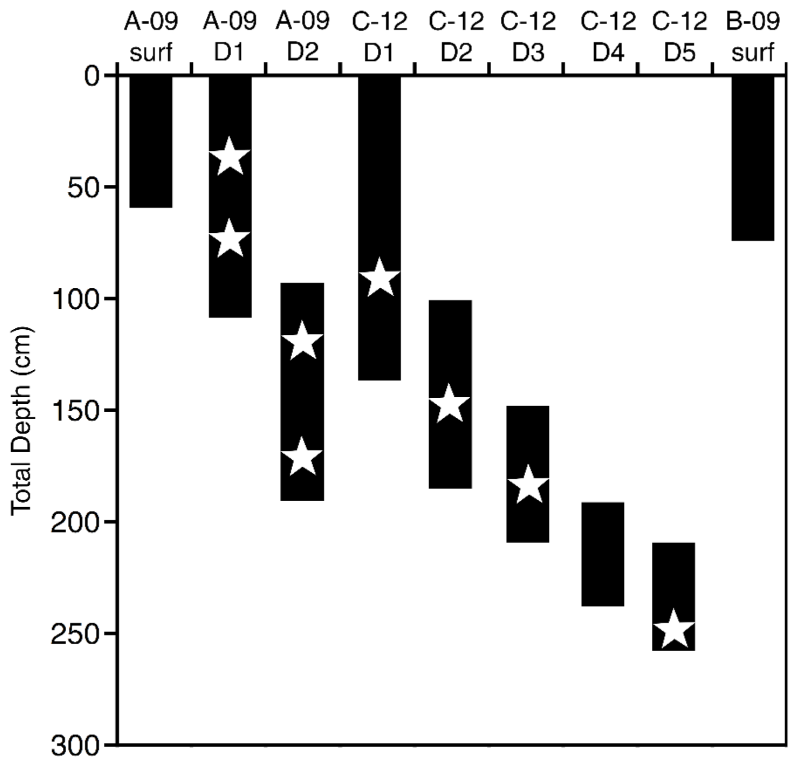

Figure 4-3- Total sediment depths of cores from sites A-09, B-09, and C-12 (locations marked in Figure 4-1) and overlapping sections. Terrestrial macrofossil radiocarbon dates marked with white stars (see Table 4-2).

In 2012, five core drives were collected at 25°43’38’’N, 100°12’01’’E (core site C-12) using a steel barrel Livingston corer (**Figure 4-1**) at a water depth of 11 m, forming a composite record of 259 cm (C-12 D1-D5) (**Figure 4-3**). Overlapping sections at all coring sites were identified based on field measurements and confirmed with stratigraphic correlation of geochemical data. Since core sites A-09 and C-12 are separated by <1 km and have a similar water depth, we combined the sediment cores from these two sites into one composite record using field notes and stratigraphic correlation of geochemical data.

4.3.2 Age Control

Eight radiocarbon ages of terrestrial macrofossils were measured on the A-09 and C-12 cores (**Table 4-2**). Terrestrial macrofossils, such as leaves and charcoal, were targeted for dating because they are less subject to transport and reworking, and unlike bulk sediment and shells they are not subject to hard-water effects (Taylor, 1978). These samples were pretreated using the standard acid, alkali, acid procedure (Abbott and Stafford, 1996), measured at the Keck Center for Accelerator Mass Spectrometry at the University of California Irvine, and calibrated using Calib 7.0 (Reimer et al., 2013). The upper 8 cm of Core A-09 was dated using a constant rate of supply (CRS) ^{210}Pb age model (Appleby and Oldfield, 1983) (**Table 4-3**). A smooth spline was used to produce an age model with the best fit using the clam 2.2 code (Blaauw, 2010) in the statistical software package "R"(R Core Development Team, 2008) (**Figure 4-4**).

Table 4-2- AMS radiocarbon dates for samples from Erhai Cores A-09 and C-12.

UCI Number	Composite Core Depth (cm)	Material	^{14}C age (BP)	Error ±	Median Probability Calibrated Age (yr AD/BC)	2σ Calibrated Age Range (yr AD/BC)
Cores A-09						
99742	39.5	Leaf	375	20	1494	1624-1449
99743	75	Wood	700	30	1286	1386-1262
99744	117	Charcoal	1520	70	529	648-406
99873	178	Charcoal	1790	40	235	342-128
Cores C-12						
131495	97.5	Charcoal	1135	20	926	779 - 981
122329	150.5	Leaf	1635	15	414	528 - 355
131496	188.5	Charcoal	1915	20	87	-2472 - -2571
122330	254.0	Charcoal	4000	20	-2532	-2472 - -2571

Table 4-3- Down-core ^{210}Pb activities, ^{214}Pb activities, cumulative weight, and CRS sediment ages from Core A-09.

Depth (cm)	^{210}Pb activity, Bq-g^{-1}	1σ Error ^{210}Pb activity	^{214}Pb activity, Bq-g^{-1}	1σ Error ^{214}Pb activity	Cumulative Weight, g cm^{-1}	CRS age (yr AD/BC)	1σ Error Age
Cores A-09							
0.0-0.5	0.3800	0.0610	0.0826	0.0191	0.0425	2003	1.64
1.0-1.5	0.3630	0.0421	0.0514	0.0069	0.1517	1998	1.79
2.0-2.5	0.2990	0.0338	0.0509	0.0053	0.2989	1993	2.02
3.0-3.5	0.1800	0.0203	0.0431	0.0037	0.5921	1985	2.38
4.0-4.5	0.2240	0.0269	0.0509	0.0051	0.8564	1974	3.05
5.0-5.5	0.1350	0.0176	0.0400	0.0040	1.1702	1963	3.94
6.0-6.5	0.1230	0.0145	0.0404	0.0034	1.4822	1950	5.63
7.0-7.5	0.1110	0.0109	0.0460	0.0040	1.8133	1932	9.18
8.0-8.5	0.0866	0.0066	0.0345	0.0033	2.1497	1910	17.83

4.3.3 Geochemistry

Water content, bulk density, and loss on ignition were measured at 2-cm intervals using 1 cm^3 samples. Samples were dried at 60°C for 48 hours to remove water. Weight percent organic matter and carbonate content was determined by loss-on-ignition (LOI) analysis at 550°C and 1000°C, respectively (Dean, 1974).

Half centimeter thick slices were sampled at 3 to 5 cm intervals on sediment cores from all three core sites. Half centimeter thick slices from the upper 30 cm of the C-12 cores were analyzed every 1 cm. All samples were lyophilized and homogenized. Elements were extracted using 6 mL of 1 M HNO_3 overnight, a standard method for extracting weakly bound trace metals from lake sediments (Graney et al., 1995). The supernatant was extracted and diluted before being measured on a Perkin Elmer NeXION 300X inductively coupled plasma mass spectrometer (ICP-MS) at the University of Pittsburgh. Duplicates were run every 20 samples and were generally within 10% of each other. Blanks were run every 20 samples to check for memory effects and were consistently far below the detection limit of the instrument.

To account for changes associated with sediment delivery and source to the watershed, we calculated anthropogenic enrichment factors based on the reference factors of aluminum (Al), and magnesium (Mg), and organic matter. By normalizing metal concentrations to Al and Mg, we can account for changes in erosion, runoff, and sediment source (Boës et al., 2011) since the Erhai catchment includes mafic igneous rocks, sandstones, and mudstones (**Figure 4-1**), whose weathering would result in high amounts of Al and Mg. Additionally, metals such as lead are commonly sorbed to organic matter, so changes in organic matter must be accounted for (Bindler et al., 2012; Boyle, 2002). The enrichment factor (EF) was calculated following the methods of (Weiss et al., 1999). For example, calculating the lead (Pb) EF is in **Equation 4-1**:

$$Pb\ EF = \frac{Pb\ sample}{Reference\ sample} \Big/ \frac{Pb\ background}{Reference\ background}$$

Equation 4-1 (Weiss et al., 1999)

where $Pb_{background}$ and $Reference_{background}$ is site-specific and is defined as the average concentration over the stable pre-anthropogenic period. The Pb EF is then used to calculate the Pb anthropogenic EF in **Equation 4-2**:

$$Pb\ anthropogenic\ EF = \ Pb\ sample - (Pb\ sample/Pb\ EF)$$

Equation 4-2 (Weiss et al., 1999)

4.4 RESULTS

Core C-12 is the focus of our discussion because it is closest to the old city of Dali and has the longest recovered sedimentary record, but we use cores A-09 and B-09 to support our conclusions. The results of the composite age model based on ^{210}Pb dating and 8 AMS radiocarbon dates on terrestrial macrofossils indicate that the C-12 cores span the last 4,500 years (**Figure 4-4**). Sedimentation rates from 2500 BC to 200 AD average 0.03 cm/year, increase to 0.30 cm/year from 200 to 450 AD, and from 450 AD to present remain stable at 0.11 cm/year. Sediments from all three sets of cores are homogenous dark brown/black fine silt and clay and are composed of 5-10% organic matter (**Figure 4-5**) with no detectable carbonate. We see no sedimentological evidence in the cores to suggest substantial variations in water level; thus we conclude that lake level changes have not played an important role in causing variations in metal concentrations in the past 4,500 years.

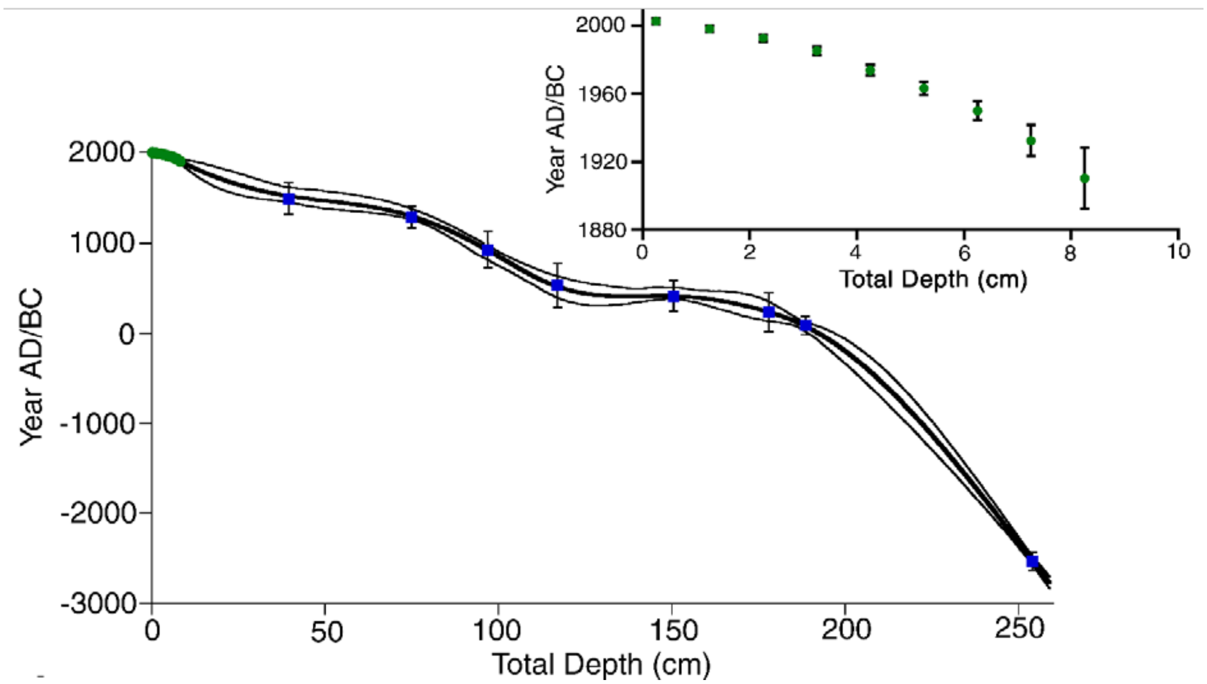

Figure 4-4- Age-depth model with 95% confidence intervals. ^{210}Pb dates (green circles) and radiocarbon dates (red squares), with 2 sigma error bars. ^{210}Pb dates with 2-sigma error bars in inset.

We focus our attention on the concentration of the metals copper (Cu), lead (Pb), silver (Ag), cadmium (Cd), and zinc (Zn) as these display the most variation (**Figure 4-5**). The concentrations of these metals, in particular Pb, are remarkably similar in terms of both stratigraphic depth and magnitude from all three coring sites though core B-09 is much shorter than A-09 and C-12 (**Figure 4-6**).

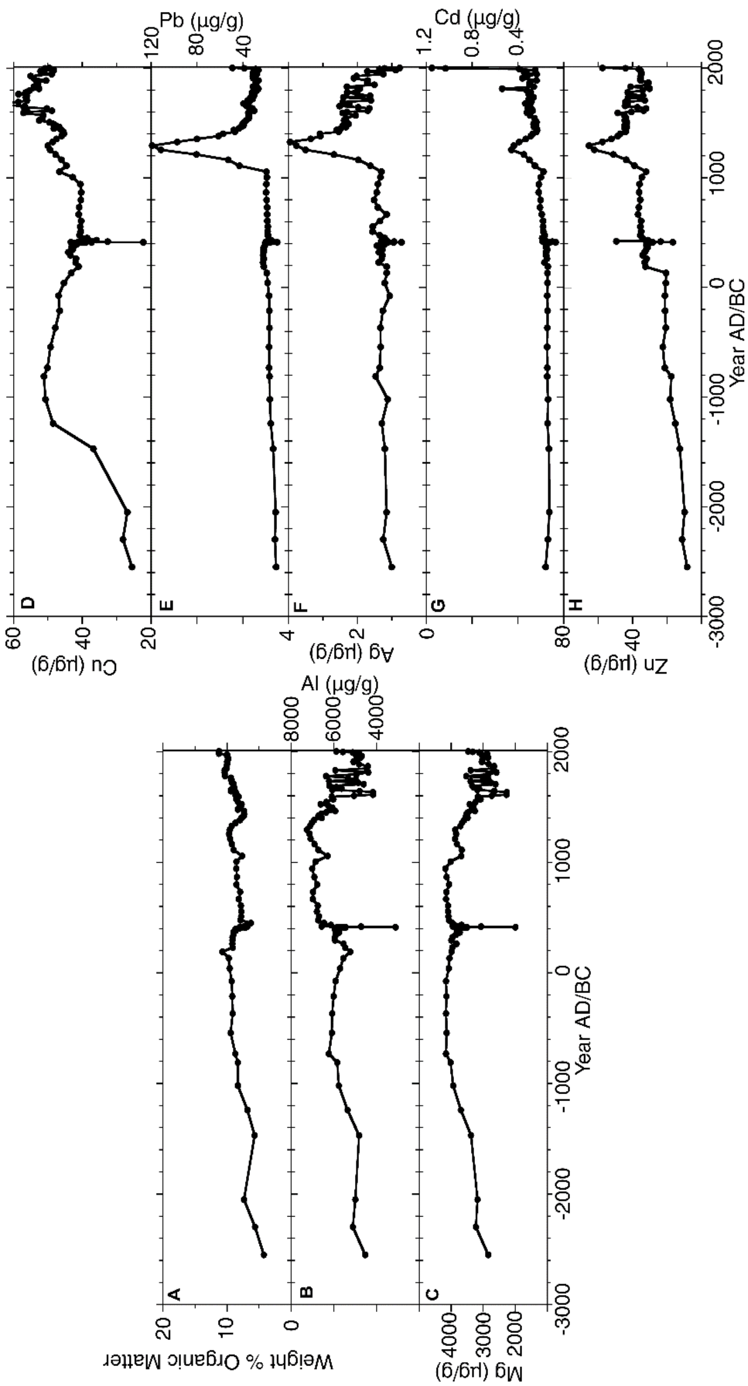

Figure 4-5- Left panel: reference factors measured in the C-12 cores. A- weight percent organic matter, B- concentrations of aluminum (Al), C- concentrations of magnesium (Mg). Right panel: concentrations of metals measured in the C-12 cores. D- copper (Cu), E- lead (Pb), F- silver (Ag), G- cadmium (Cd), and H- zinc (Zn).

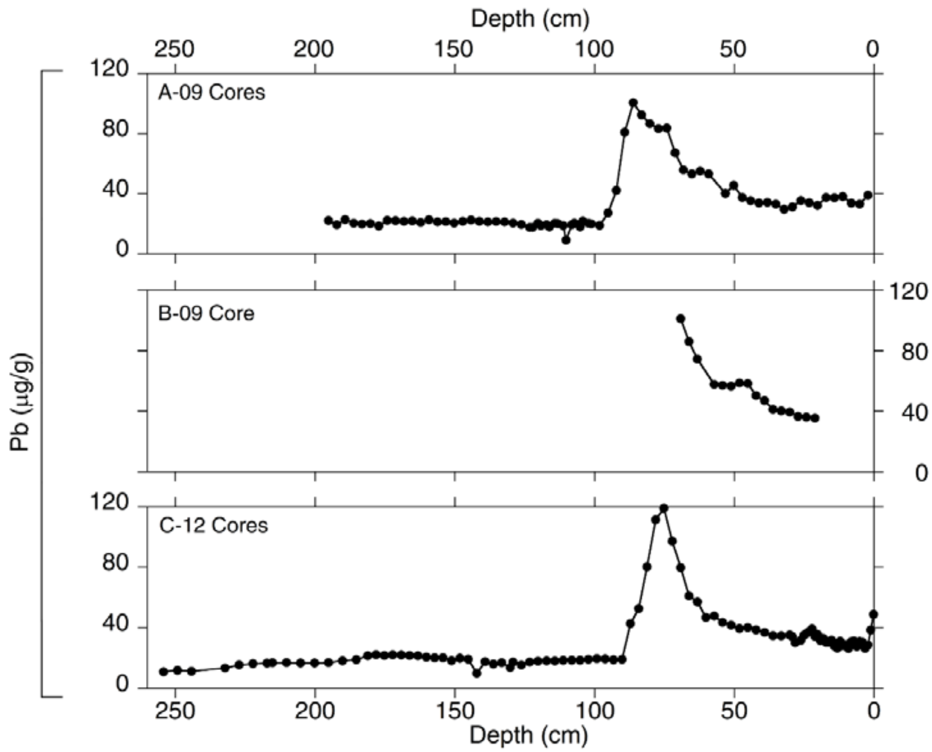

Figure 4-6- Lead concentrations by depth for Cores A-09, B-09, and C-12. The increase in Pb occurs at a similar depth and is of a similar magnitude in all three cores, despite their different locations and depths in the lake. Core B-09 is too short to capture the entire increase in Pb.

From 2500 BC to 200 AD, the concentrations of Pb, Ag, Cd, and Zn are low and stable, averaging 15.6, 1.2, 0.1, and 29.5 µg/g, respectively (**Figure 4-5)**. From 200 to 450 AD, concentrations double for all of the aforementioned elements. After 450 AD, the concentrations remain stable until 1100 AD. Beginning at 1100 AD, concentrations of Pb, Ag, Cd, and Zn increase and reach a peak at 1300 AD of 119.1, 3.8, 0.4, and 65.4 µg/g, respectively. From 1300 to 1980 AD, concentrations decline to 26.6 µg/g for Pb, 0.88 µg/g for Ag, 0.25 µg/g for Cd, and 35.7 µg/g for Zn. Over the last 30 years there are slightly higher concentrations of Pb, Ag, Cd, and Zn at 49.1, 0.8, 1.2, and 57.5 μg/g, respectively. Concentrations of Cu display different variations- from 2500-2000 BC, Cu averages 26.8±1 μg/g and nearly doubles to 51.1 μg/g beginning ~1500 BC (**Figure 4-5**). After a peak at 700 BC, concentrations decline to an average of 41.4 μg/g. At 1000 AD, concentrations increase to a peak of 66.2 μg/g at 1650 AD before declining to 49.5 μg/g in the last 10 years.

4.5 DISCUSSION

We calculated anthro EFs to account for changes in erosion, runoff, and sediment flux that may have impacted the delivery of metals to the lake. We acknowledge that the weak acid extraction performed on these samples does not represent the total lithogenic proportion of elements such as Al or Mg (Reimann and De Caritate, 2000); rather, we seek to normalize the concentrations of metals such as Pb to natural geogenic processes to account for variations in sediment transport. The high correlation coefficient between the chosen reference factors and metals of interest during the pre-pollution time period suggests that they can account part of metal content in the sample (**Table 4-4**). On the basis of the relatively stable and low concentrations of the reference elements (**Figure 4-5**), we define background levels as the time period from 2500 BC to 200 AD.

Table 4-4- Pearson product-moment correlation coefficient between metals and reference factors over the pre-pollution time period (2700 BC-200 AD) (185-254 cm). The high correlation coefficients between Al, Mg, organic matter and metals of interest demonstrates that Al, Mg, and organic matter are appropriate reference factors from which to calculate EFs as they can explain some component of weathering.

	Al	Mg	Organic Matter
Cu	0.9023	0.9426	0.8904
Pb	0.9579	0.8782	0.9660
Ag	0.8035	0.7448	0.5526
Cd	0.7270	0.6602	0.4702
Zn	0.9646	0.9914	0.9301

4.5.1 Early Metallurgy

From 2500 BC to 200 AD, the anthro EFs of Pb, Ag, Cd, and Zn were stable and less than 2, representing our best estimate of background variations arising from natural, non-anthropogenic sources (**Figure 4-7**). Natural sources of these metals include wind-blown dust, sea salt, volcanic emissions, and forest fires (Nriagu, 1989). Approximately 40-50% of Cd and 20-40% of Pb arise from volcanic emissions and 20-30% of Pb and Zn can be attributed to soil-derived dust; the remainder of natural emissions are primarily due to biogenic processes (Nriagu, 1989).

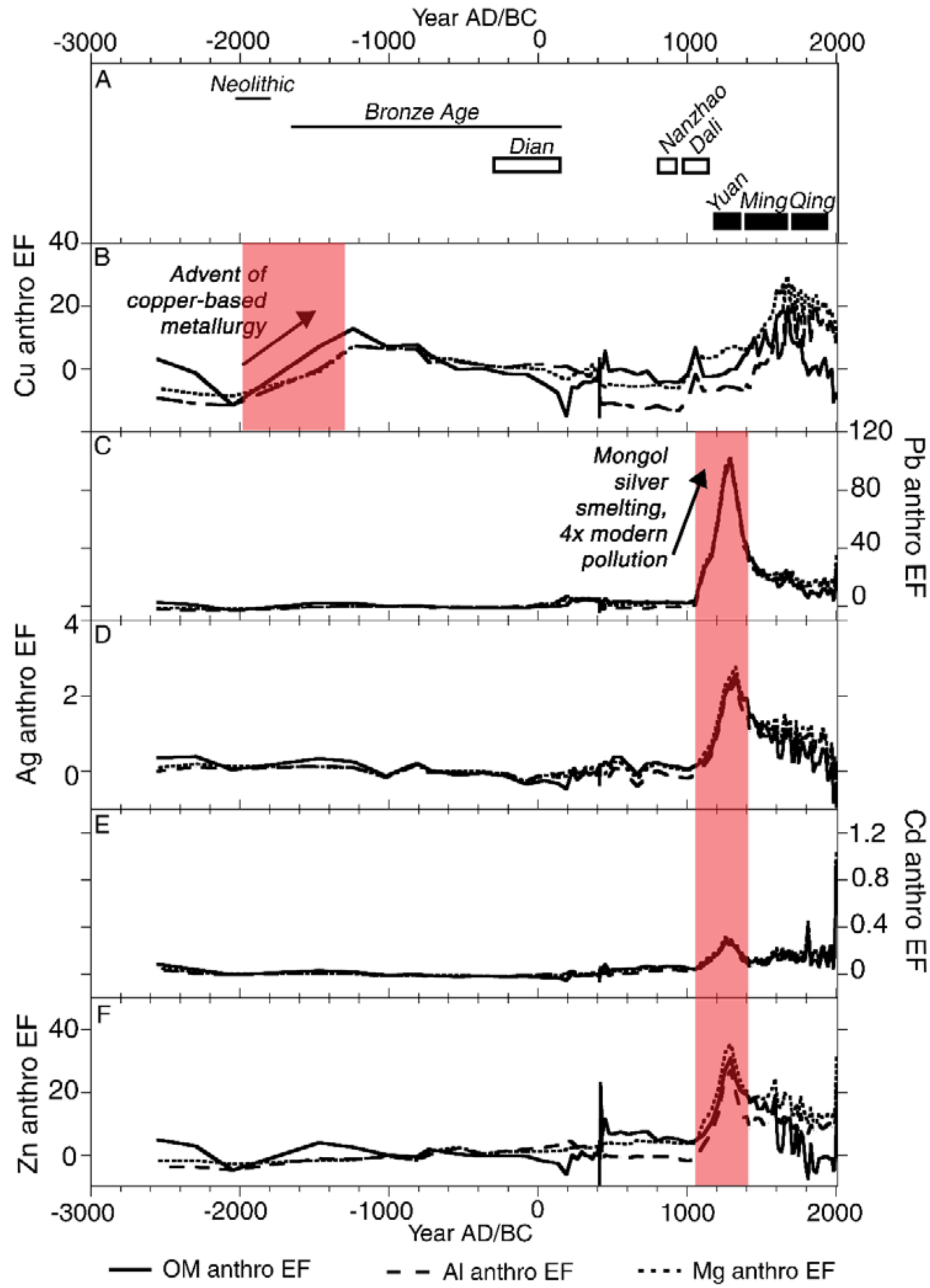

Figure 4-7- A- Archaeological periods, Yunnan cultural periods in white boxes, and Chinese dynasties in black boxes. Anthropogenic EFs for organic matter (solid line), aluminum (dashed line), and magnesium (dotted line) for B- copper (Cu), C- lead (Pb), D- silver (Ag), E- cadmium (Cd), and F- zinc (Zn) from Cores C-12. Shading from 1100-1400 AD corresponds to the increased concentrations of Pb, Ag, Cd, and Zn during the time period of the Yuan Dynasty (the Mongols).

From 200 to 450 AD, the anthro EFs of Pb, Ag, Cd, and Zn increase to between three and four. This is accompanied by a ten-fold increase in the sedimentation rate (**Figure 4-7**). We attribute these increases to be the result of greater sediment influx to the lake reflecting land use change that led to higher rates of erosion. Pottery models from grave sites on the shores of Erhai dating to the Han Dynasty (ca. 206 BC-220 AD) depict irrigated farming practices (Elvin et al., 2002), which suggests that Chinese-style agriculture first arose in these settlements beginning ~2,000 years ago. The initiation of this style of agriculture coincides closely with the land use change inferred in our record.

The Cu anthro EF from 2500-2000 BC is less than one (**Figure 4-7**), likely recording natural variability associated with biogenic emissions. Beginning at 1500 BC, Cu anthro EF increases to between 6 and 12. While our age control in this portion of the record is limited by a lack of a radiocarbon date directly at the increase, we performed age uncertainty analysis (**Figure 4-8**) and found that the timing of this event is ±400 years. Our interpretation is that this is caused by the initiation of copper-based metalworking around the lake, which archaeological research suggests began around this time (Yunnan Provincial Institute of Cultural Relics and Archaeology, 2009a). The lack of an increase in either Pb or Sn at 1500 BC concurs with archaeological records that initial metalworking techniques were primarily used for copper-making and were not associated with the production of complex bronze alloys combining more than two or three metals (Chiou-Peng, 2009). The absence of increases in other metals (e.g. Zn and Cd) suggests that this increase in copper was linked to atmospheric emissions. Small increases in Al, Mg, and organic matter (**Figure 4-5)** may be linked to the Cu increase, however the magnitude of change is much less than that of the Cu. Given that the beginnings of copper-based metallurgy during the 2nd millennium BC in Yunnan remains an open question (Higham et al., 2011; Min, 2013; White and Hamilton, 2009), our results lend substantial support to the initiation of this activity beginning by at least 1500 BC. These data not only add new dimensions to the history of Yunnan metals in the context of Eurasian metallurgy, but they will also be crucial for clarifying the much debated chronological issues related to the initiation of copper-based metallurgy in adjacent Southeast Asia.

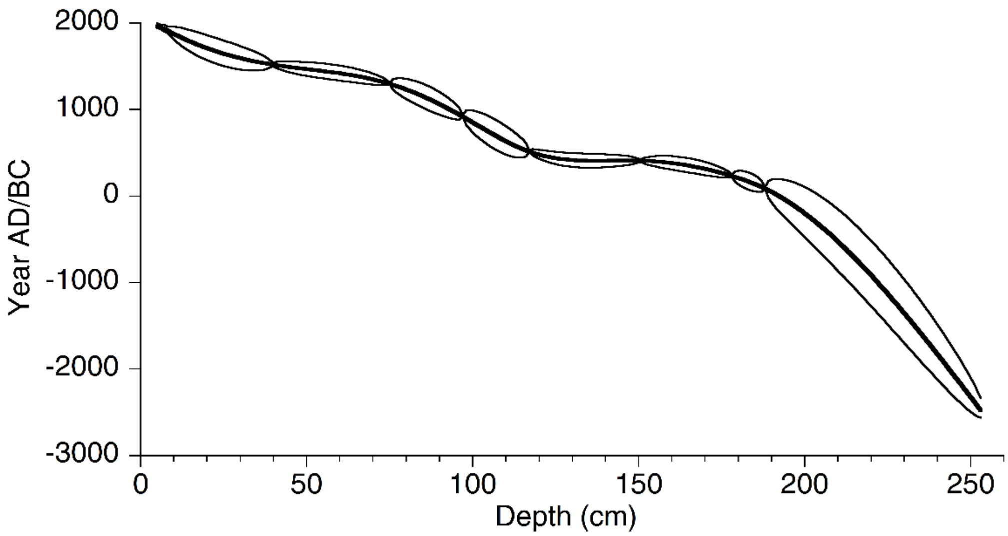

Figure 4-8- Results of the age uncertainty analysis with 95% confidence intervals. Age uncertainties were calculated using a 10,000 iteration Monte Carlo simulation varied between the radiocarbon 2-sigma calibrated age uncertainties (Huybers and Wunch, 2004; Marcott et al., 2013). The uncertainty between the age-control points was modeled as a random walk with a "jitter" value of 200.

4.5.2 Peak in Lead Pollution

The Pb anthro EF increases after 1100 AD, reaches a peak of 100±2 at 1300 AD, and declines to 30±2 by 1420 AD (**Figure 4-7**). Anthro EFs of silver, cadmium, and zinc follow similar trends (**Figure 4-7**). Argentiferous galena ((Pb, Ag) S) is a common ore in Yunnan and there are a large number of ore bodies situated close to Erhai (Golas, 1999; Pirajno, 2013) (**Figure 4-1**). The Baiyangchang ore body, 75 km northwest of Erhai, has rich deposits of silver with impurities of lead and zinc (Hou et al., 2007) and mining and exploitation of this deposit is a possible source of the observed increases in metals. Geochemical data that would allow us to confidently attribute this increase in metals to a particular ore body currently do not exist; however, this is a direction of future research. The peak of this enrichment corresponds to the Yuan Dynasty (1271-1368 AD), the Mongols, within the 95% confidence intervals of the age uncertainty (±30 years).

The Mongols established the first government operated silver mine in Yunnan in 1290 AD and by 1328 AD, taxes from silver production in Yunnan alone accounted for 47% of national tax revenue (Xue and Wu, 2002). The process of purifying the silver ores relied on a technique known as cupellation (Xue and Wu, 2002). The ores would be roasted in low temperature fires in a furnace that ensures sufficient oxygen flow (Needham and Gwei-Djen, 1971). As wood is combusted, lead monoxide and other metal oxides form from ore impurities and are volatized into ash, which can then be deposited on the land and water via wet and dry deposition. Since this metallurgical procedure requires large amounts of wood, it is reasonable to expect that deforestation would have occurred in the lake catchment. We see no sedimentological evidence of this, however previous study by Dearing et al., 2008 found a decrease in arboreal pollen coincident with the rise in lead. The sudden decline in lead pollution at Erhai is likely related to the end of the Mongol Dynasty in 1368 AD. Since silver mining was restricted during the beginning of the subsequent Ming Dynasty (Lu and Wang, 1998), this further contributed to the decline in lead emissions.

Our hypothesis is that these metals were primarily deposited in the lake via atmospheric transport. There is no accompanying change in the concentration of organic matter (constant at 8-10%) (**Figure 4-5**) or bulk density of the sediments (constant at 0.6-0.7 g/cm^3). Additionally, since metals such as Pb and Zn are generally not subject to remobilization from oxidation/reduction changes during sedimentation and compaction (Hamilton-Taylor and Davison, 1978), we do not believe that the increase in metals is not the result of variations in water chemistry. In a lake such as Erhai that has a large surface area and catchment, it is possible that sediment storage on floodplains and hillslopes can occur over several hundred years (Trimble, 1983), and that the remobilization of contaminated sediment can create peaks in metal concentration (Lecce et al., 2007). However, the narrow, high gradient fluvial systems in Erhai's catchment, especially on the western side near cores A-09 and C-12 (**Figure 4-1**), limits the potential for floodplain sediment storage. There is no contemporaneous change in sedimentation rate (**Figure 4-4**) or sedimentology, ruling out an increased influx of erosional material. While we cannot definitively reject the possibility of floodplain sediment storage in this system, the geochemical signal in the lake sediments seems more likely influenced by atmospheric deposition than remobilization of stored, contaminated sediments.

Lee et al., 2008 measured metal concentrations in lake sediments in central China and found an increase in lead from 1370-1470 AD, attributed to increased warfare and demand for manufacturing of weapons associated with the beginning of the Ming Dynasty (Lee et al., 2008). Yunnan has some of the largest zinc deposits in the world and the Ming Dynasty established at least 20 zinc smelting operations in southwestern China (Zhou et al., 2012). However, most of these activities took place in the latter half of the Ming Dynasty (~1500 AD) and many of the zinc smelters are almost 1,000 km east of Erhai (Zhou et al., 2012). Moreover, we can confidently attribute the spike in metal pollution to the Mongols as we have a radiocarbon date on a terrestrial macrofossil directly at the increase (**Table 4-2-** UCI#99743). Whatever zinc distillation activities may have impacted the lake, they were not as large compared to the silver smelting that was taking place during the time of the Mongols.

Our study differs significantly from previous work by Dearing et al., 2008 whose study of Erhai sediment cores found increases in Cu at 400 BC from 12 to 14 µg/g and Pb from 550 to 950 AD from 4 to 14 µg/g (**Figure 4-9**). The timing of these geochemical changes in the previous study is different, with the copper rise being at least 1000 years later and the lead rise being 700 years earlier. The differences in timing of these increases is significant, because the lead increase in the Dearing et al., 2008 study is incorrectly attributed to the Nanzhao and Dali kingdoms. Our results provide a more accurate chronology allowing us to attribute the source of the pollution to the Mongols, as well as pinpoint a specific process (silver smelting), that was responsible for the observed increases in metal concentrations. Since it is our hypothesis that these increases in metals are due to atmospheric emissions, this implies that deposition and metal loading also took place on the surrounding landscape. As deforestation and land use change has already led to soil loss within Erhai's catchment (Wang et al., 2004), the mobility of this soil, likely high in concentrations of lead, silver, zinc, and cadmium, may lead to further contamination problems.

Another discrepancy between this study and the previous work by Dearing et al., 2008 is the difference in magnitude of both copper and lead concentrations in the sediments. An increase of 2 µg/g of copper in the previous study is within the range of natural variability of sediment concentrations (**Figure 4-9**). The increase of 10 µg/g of lead is ten times less than the observed increase in this study. This is due to differing extraction techniques; however, the details of the extraction methods were not documented in the Dearing et al., 2008 study and it is unclear what strength and type of acid was used to measure the metals weakly sorbed to the sediments. Our work shows that the increases in metal concentrations were actually much more substantial. According to consensus-based sediment quality guidelines the concentrations of lead at 1300 AD (120 µg/g) approached the probable effect concentration of 128 µg/g, above which harmful effects are likely to be observed in freshwater organisms(MacDonald et al., 2000). A study of Idaho wetland sites documented that the persistence of lead in sediments impacted organisms several centuries after mining activity was reduced (Beyer et al., 1998). Similarly, we suggest that the elevated concentrations of lead due to the environmental legacy of Mongol silver mining has impacted the lake for several centuries.

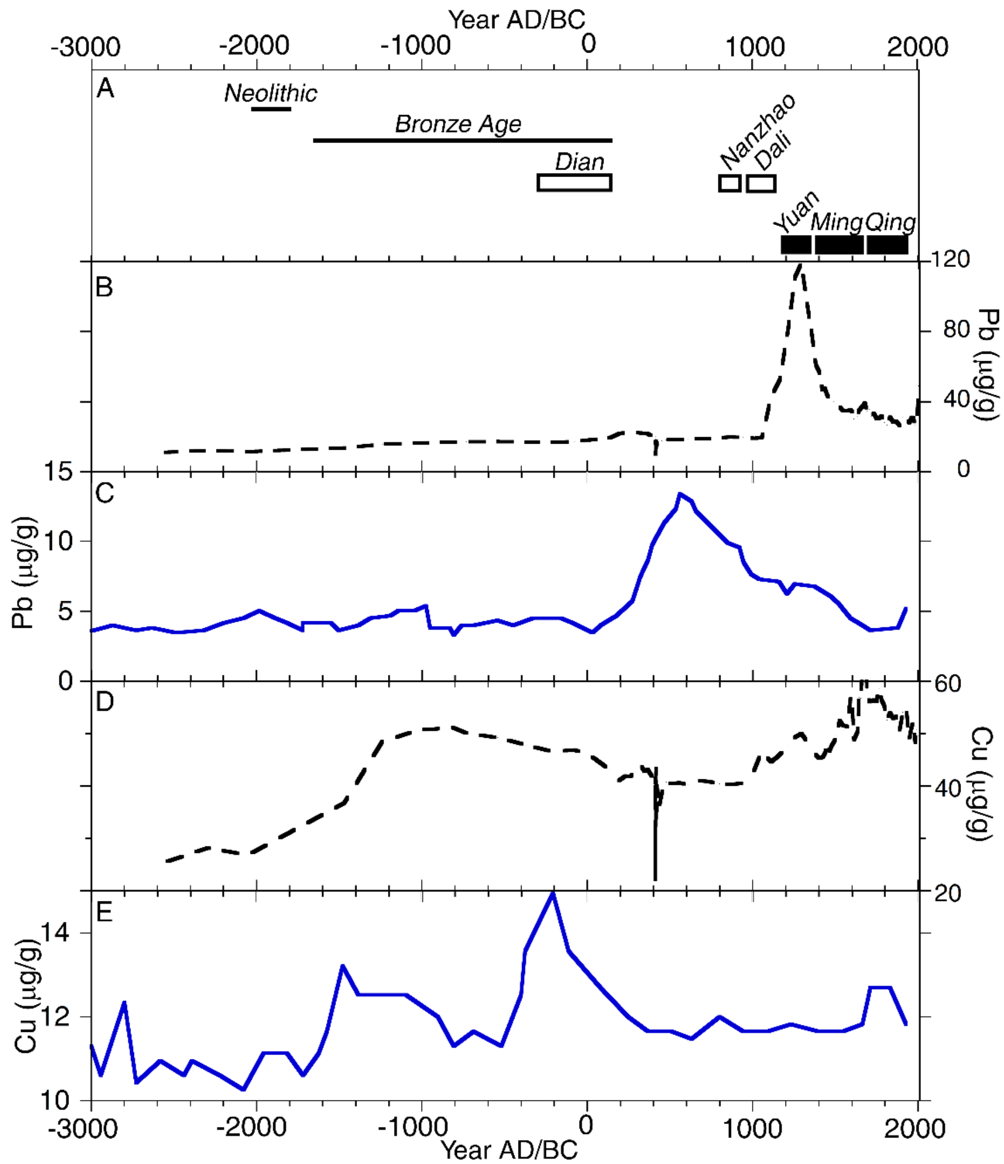

Figure 4-9- Comparison between this study and results from Dearing et al., 2008. A- Archaeological periods, Yunnan cultural periods in white boxes, and Chinese dynasties in black boxes; B- concentrations of lead (Pb) from this study (black dashed line); C- concentrations of lead (Pb) from Dearing et al., 2008 (blue solid line); D- concentrations of copper (Cu) from this study (black dashed line); E- concentrations of copper (Cu) from Dearing et al., 2008 (blue solid line). The timing and magnitude of geochemical changes differs significantly between the two studies.

4.5.3 Modern Pollution

Lead anthro EF declines from 30±2 in 1420 AD to 9±5 in 1980 AD (**Figure 4-7**). The Pb anthro EF in the top sediments deposited in the last 20 years increases to 30±4. Silver and Zn anthro EFs following similar trends of slowly declining at 1400 AD and increasing slightly after 1980 AD. It is only the Cd anthro EF that displays values five to six times higher in modern-day sediments than the past. Modern industrial activities near the lake include nickel, copper, and platinum mining (Kamitani et al., 2007). While these activities may contribute to the observed modern-day decline of sediment quality in the lake, the scale of these activities is small in comparison to the historical ones; the Pb anthro EF at 1300 AD is almost four times greater than modern pollution. This may be due to the larger scale of metallurgical operations in the historical period or the low efficiency of metallurgical procedures, which caused greater amounts of impurities to be volatized and delivered to the lake. Copper anthro EF reaches a peak of 25 in 1670 AD, during the Qing Dynasty (**Figure 4-7**). This roughly corresponds to the surge in Yunnan copper production associated with the Qing Dynasty's increase in the demand of copper for coinage (Yang, 2009). It is notable that the 20th and 21st century Cu anthro EF averages 8, despite copper mining currently occurring within the lake's watershed.

4.6 CONCLUSIONS

Our findings are unique- while pre-industrial pollution has been detected in lake sediments over many time periods and regions of the world, only a few studies have found pre-industrial pollution levels to be greater than modern (Abbott and Wolfe, 2003; Camarero et al.,

1998) and none of these have been in China. The long slow decline of lead concentrations to present day values may in part be influenced by the persistence of the historical lead pollution being reworked from lake sediments. Therefore, we suggest that modern pollution issues rest on a long history of decline in sediment quality at Erhai. This environmental legacy of silver smelting creates complications in accurately attributing the accumulation of heavy metals to specific modern-day processes as well as developing mitigation strategies.

5.0 DIAN LAKE

A 17,000 Year Multi-Proxy Study of Lake Level Change and Human Settlement Patterns in Southwestern China

This study focuses on Lake Dian in central Yunnan Province (**Figure 5-1**) next to the modern city of Kunming. Here, we present a 17,000 year record of both natural environmental change (pre-200 AD) and human impact to the lake (post-200 AD). To analyze changes in lake primary productivity and sediment delivery, we rely on measurements of sediment composition (% organic, carbonate, and mineral matter as well as magnetic susceptibility), the concentration and isotopic composition of organic carbon and nitrogen (%C, %N, $\delta^{13}C_{org}$, and $\delta^{15}N$), and the concentrations of both weakly and strongly bound metals (e.g. Al, Fe, P, Pb, and Ti) in sediment. These measurements were taken from a set of cores in the northern end of Dian in deep water conditions (**Figure 5-1)**. We couple these proxy measurements with a series of transect cores from the southern end of Dian moving from shallow to deep water conditions (**Figure 5-2**).

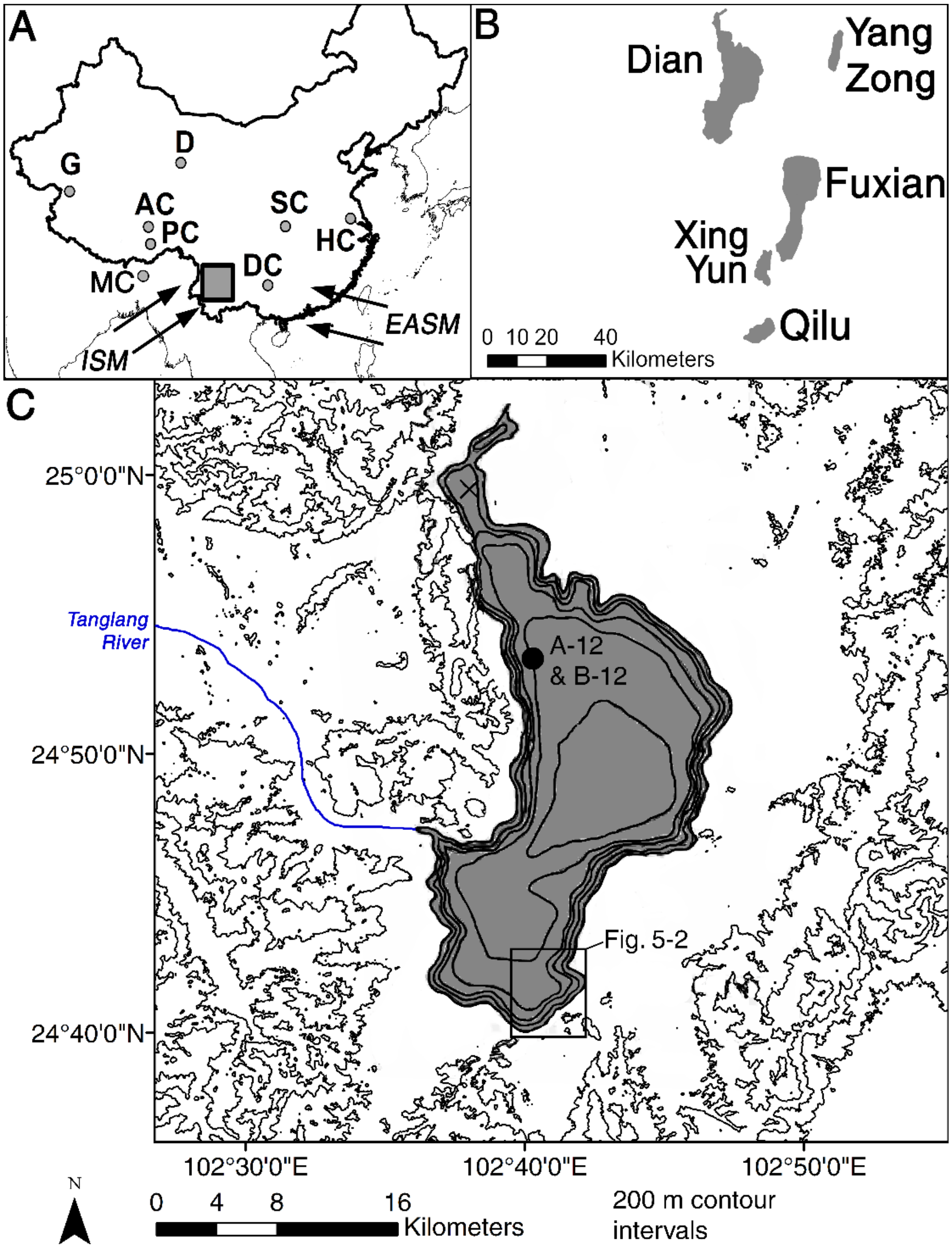

Figure 5-1- A- Locations of other paleoclimate archives discussed in text. G = Guilya ice cap, D = Dunde ice cap, AC = Ahung Co, PC = Paru Co Lake, DC = Dongge Cave, SC = Sanboa Cave, HC = Hulu Cave, TC = Tianmen Cave, MC = Mawmluh Cave; B- Locations of Yunnan lakes discussed in text; C- Map of Dian with bathymetry (1 m contours) adapted from Zhang et al., 1996. Coring locations A-12 and B-12 indicated by black circle. Previous coring location in Sun et al., 1986 study denoted by the X. Coring locations of C-14 through F-14 in box at southern end of the lake. For more detail, see Figure 5-2.

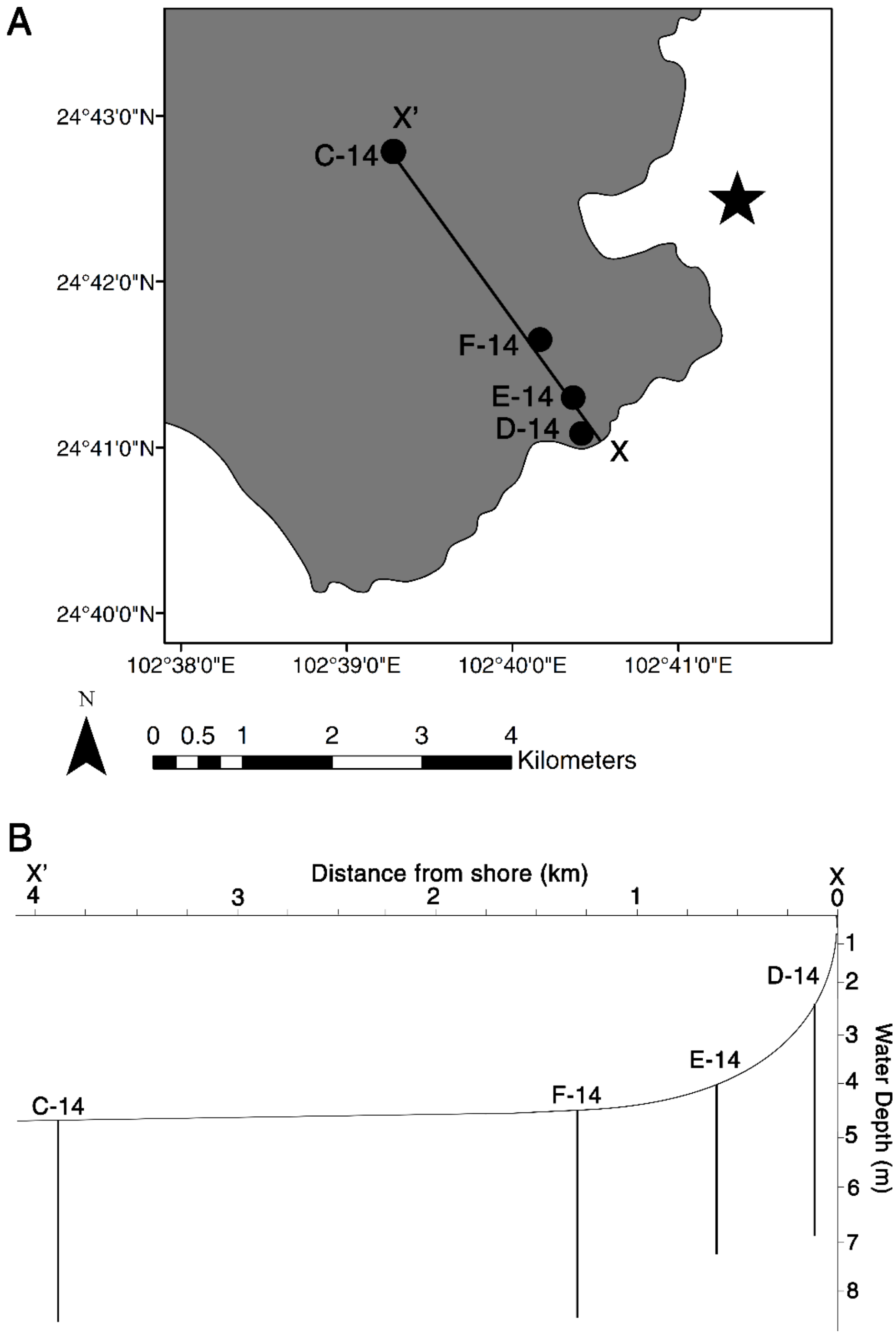

Figure 5-2- Details of the southern end of Dian shown in the box in Figure 5-1. A- Coring locations indicated by black circles along X-X' transect. Star indicates site of soil sampling location. B- Bathymetric profile of lake water depth, coring locations, and approximate length of collected sediment along X-X' transect.

5.1 REGIONAL SETTING

Dian is a large (SA = 300 km^2) and shallow lake (Z_{max} = 5 m, Z_{avg} = 4.4 m) (Li et al., 2007) that formed on the edge of a rotating crustal block caught on a left lateral strike-slip fault during the early Pleistocene (Wang et al., 1998). Estimates on the amount of rotation are 1-2°/million years (England and Molnar, 1990). Since the fault has been active for roughly 4-5 million years, this would produce a maximum of 8-10° of rotation. As rotation has increased through time, the size of Dian has been increasing, though not necessary at a gradual and/or continuous rate. Drilling indicates that there are several sub-basins beneath the lake separated by faults and there is evidence for active recent faulting along the western side of the lake (Wang et al., 1998).

Dian was formerly two separate lakes- Dian Caohai and Dian Waihai. Caohai was a small lake towards the north and Waihai was a much larger lake to the south (Li et al., 2007). They are now connected to form one lake though an artificial water gate that still separates the former barriers (Li et al., 2007). Dian has a large catchment area that includes the urban watershed of Kunming as well as several large, flat portions of land used for urban and agricultural activities (**Figure 5-1**). The catchment of Dian is composed mostly of Quaternary alluvium with small portions of sandstone, limestone, and shale (Bureau of Geology and Mineral Resources of Yunnan Province, 1990). Dian's only outflow is the artificial Tanglang River to the west (Whitmore et al., 1997) (**Figure 5-1**). Anthropogenic impact on the vegetation around Kunming has been extensive, but in less impacted areas, subtropical conifer forests predominate (Li and Walker, 1986).

Roughly 70% of precipitation in Yunnan falls between the months of June-September associated with the Indian Summer Monsoon (ISM) (IAEA/WMO, 2014) (**Table 1-2**).

Temperatures are generally mild, ranging between 9 to 20°C (IAEA/WMO, 2014) (**Table 1-2**). The oxygen stable isotopic composition of water samples collected from Dian in the summer of 2012 and 2014 range between -2.82‰ and -4.66‰ VSMOW, about 5-7‰ higher than the average weighted precipitation of Kunming (-9.5‰ VSMOW) (**Figure 1-3**), strongly suggesting that Dian loses the majority of water through evaporation. Previous research into the water quality of Yunnan lakes observed a lake water isotopic composition of -6.4‰ VSMOW for Dian (Whitmore et al., 1997), demonstrating that in the last 20 years, Dian has become increasingly enriched in heavy isotopes, likely due to evaporative modification. The average pH of Dian is around 9 but can range between 6.2 and 10.6 depending on the season and location (Yang et al., 2010).

Today the water quality of Dian is an increasingly pressing concern as it is a vital source of water for the people around Kunming yet is hypereutrophic (Whitmore et al., 1997; Yang et al., 2010) and contaminated with high levels of dichlorodiphenyltrichloroethanes (DDTs), polycyclic aromatic hydrocarbons (PAHs) (Guo et al., 2013), and heavy metals such as lead, mercury, and zinc (Zhang et al., 2008b). Despite its importance as an essential water resource, relatively little work has been done to characterize hydrologic balance through time. Dian is proximal to a number of other lakes (Yang Zong, Fuxian, Xing Yun, and Qilu) (**Figure 5-1**), making it part of an ideal set for comparisons in the spatial and temporal variability of both climate and the initiation of human impact.

Dian has been a population center for many thousands of years and archaeological evidence suggests that people settled around the lake as early as 10,000 years BP (Sun et al., 1986). Archaeological investigations on Neolithic and Bronze Age sites have been minimal, but there is some evidence to suggest that ores were extracted from the Gejiu ore deposits, 200 km south of Kunming, perhaps as early as 1,000-2,000 years BP (Cheng et al., 2012b; Cui and Wu, 2008). The Dian culture (ca. 400 BC-100 AD), known for their bronze artifacts (Chiou-Peng, 2008), was based around the lake and numerous archaeological sites have been found on the shores of the lake (Higham, 1996). Following the Dian culture, terraced agriculture and irrigation were introduced by the Han governor in 210 AD (Sun et al., 1986). The modern city of Kunming was established in 764 AD and was subject to repeated flooding problems (Sun et al., 1986). With the establishment of the Yuan Dynasty (ca. 1271-1368 AD), also known as the Mongols, canals were constructed throughout Yunnan (Sun et al., 1986). In 1273 AD, the Tanglang River was dug, causing lower lake levels and large flat areas of land to be exposed on the eastern side of the lake (Sun et al., 1986; Whitmore et al., 1997). Historical accounts record several episodes of drought that reportedly caused Dian to completely dry out by 1764 AD (Sun et al., 1986).

Sediment core work on Dian has thus far been relatively limited. Previous study of pollen in Dian sediments focused on analysis of two sediment cores from the northern end of the lake (**Figure 5-1**) (Sun et al., 1986). On the basis of pollen and sedimentology, the authors found that vegetation changed in response to monsoon intensity throughout the Pleistocene and Holocene. From 16 to 10.5 ka, sediment accumulation in the northern end of the shallow part of the lake increased. The authors interpreted this to reflect reduced water from inflowing rivers due to less precipitation. By 10 ka, colder and more humid conditions existed, transitioning to warmer conditions with a more equal distribution of rainfall throughout the year by 7 ka. Between 7 and 4.5 ka, terrestrial vegetation changes were not discernable, but aquatic vegetation changes suggested moderate swings in lake level between swamp and shallow open water conditions. By 4 ka, conditions at Dian were similar to today. This study found evidence of human disturbance by 1.5 ka and noted that although human settlements likely dated to 10 ka, there were no palynological indicators of this settlement. However, this study suffered from several problems: 1) reliance solely on palynological analysis, which records shifts in terrestrial vegetation but may not detect other land use changes associated with anthropogenic impact; 2) reliance on bulk sediment radiocarbon dates, that are subject to hard-water effects (Deevey et al., 1954); and 3) limited spatial coverage that focused solely on sediment cores from the shallow, northern part of the lake where initial settlement population density was not high (Yao and Zhilong, 2012).

An additional study that examined the mineralogy of Dian sediments found similar changes in lake level as the Sun et al. study, though the sediment cores were not dated and changes were noted on a total depth scale (Zhang et al., 1996). This study found that the surface sediments of Dian had a large proportion of goethite (>4 weight %) as well as pyrite and pyrrhotite (Zhang et al., 1996). Down core, additional minerals such as calcite and aragonite, were especially abundant during a period that was inferred to be the Holocene. On the basis on other sedimentological indicators, the authors believed that this indicated shallower lake levels than the preceding time period. However, extremely low sampling resolution prevented any further conclusions. This study aims to build upon the previous two studies with a more accurate age model based on terrestrial macrofossil radiocarbon dates and a multi-proxy approach focused on understanding within-lake environmental changes.

5.2 MATERIALS AND METHODS

5.2.1 Core Collection

In 2012, two sets of cores (A-12 and B-12) were collected from the northern end of the lake (**Table 5-1 and Figure 5-1**). In 2014, a series of four sets of transect cores were collected from the southern end of the lake (**Table 5-1, Figures 5.1 and 5.2)**. For cores B-12, D-14, and F-14, a piston corer was used to collect surface sediments that preserved the water-sediment interface. Below this level, a Livingston corer was used to collect deeper samples (Wright et al., 1984). For cores A-12, C-14, and E-14, the upper 30 cm of sediment was not preserved due to the high water content. In these locations, a Livingston corer was used to collect deeper samples (Wright et al., 1984).

Table 5-1- Core collection details

Core	Latitude	Longitude	Water Depth (m)	Distance from shoreline (km)	Composite length of record (m)
A-12	24°53’09’’N	102°40’02’’E	5.0	1.14	3.96
B-12	24°53’09’’N	102°40’02’’E	5.0	1.14	0.56
C-14	24°42’47’’N	102°39’17’’E	4.6	3.85	3.75
D-14	24°41’5’’N	102°40’25’’E	2.5	0.16	4.29
E-14	24°41’18’’N	102°40’22’’E	3.9	0.54	3.14
F-14	24°41’39’’N	102°40’10’’E	4.3	1.28	3.83

Soil samples were collected from approximately 24°42’25’’N, 102°41’22’’E at an archaeological excavation pit (**Figure 5-2)**. Sample 1 was taken 211 cm below the surface from a shell midden layer intermixed with red clay and archaeological artifacts, samples 2 and 3 were taken 286 and 288 cm below the surface in a sterile, red clay, and sample 4 was taken 316 cm below the surface in sterile, gley clay.

5.2.2 Age Control

Radiocarbon ages were measured on 26 terrestrial macrofossils (e.g. charcoal, leaves) from the cores. Intervals targeted for dating were chosen on the basis of stratigraphy and erosional features. Samples were analyzed at Keck Center for Accelerator Mass Spectrometry at the University of California Irvine. Prior to analysis, samples were pretreated using a standard acid, base, acid procedure (Abbott and Stafford, 1996). The resulting ages were calibrated using CALIB 7.0 and the INTCAL13 calibration curve (Reimer et al., 2013). The upper 20 cm of the B-12 and F-14 cores was lyophilized and analyzed for ^{210}Pb and ^{214}Pb activities by direct gamma (γ) counting in a broad energy germanium detector (Canberra BE-3825) at the University of Pittsburgh.

5.2.3 Geochemistry

Water content and bulk density were measured at 2 cm intervals using 1 cm^3 samples from all sets of cores. Weight percent organic matter and carbonate content within these same samples was determined by loss-on-ignition (LOI) analysis at 550°C and 1000°C, respectively (Dean, 1974). Sediment core magnetic susceptibility was measured on all split cores using a Bartington® Instruments Ltd. ME2EI surface-scanning sensor equipped with a TAMISCAN-TSI automatic logging conveyer.

Weight percent nitrogen, weight percent organic carbon, $\delta^{15}N$, $\delta^{13}C_{org}$, and atomic C/N ratio were measured at 2-cm intervals from the A-12 cores. Samples were covered in 1 M HCl for 24 hours to dissolve carbonate minerals and rinsed. Samples were then lyophilized and analyzed at Idaho State University using an ECS 4010 (Elemental Combustion System 4010) interfaced to a Delta V mass spectrometer through the ConFlo IV system. Organic carbon isotopes are expressed in conventional delta (δ) notation as the per mil (‰) deviation from the Vienna Peedee Belemnite standard (VPDB) whereas nitrogen isotopes are reported relative to atmospheric N_2.

Weakly sorbed metal concentrations were measured at 3-5-cm intervals on the A-12 cores. All samples were lyophilized and homogenized prior to analysis. Elements were extracted by reacting samples with 10 mL of 1 M HNO_3 for ~24 hours (Graney et al., 1995). Concentrations of elements in the residual mineral matter portion was measured at 5 to 10 cm intervals. Strong extractions were performed using aqua regia (3:1 mixture of hydrologic and nitric acid) (Tokalioğlu et al., 2000). Sediment was extracted overnight, evaporated down, and re-dissolved in a 10% nitric solution. The supernatant from both weak and strong extractions was diluted before being measured on an inductively coupled plasma mass spectrometer (ICP-MS) at the University of Pittsburgh. Duplicates were run on every 10th sample and were generally within 10% of each other. Blanks were run every 10 samples to check for bleed through and were consistently below detection limits of interest.

Five samples were analyzed for organic biomarker compounds at the Lamont-Doherty Earth Observatory Organic Geochemistry Lab from cores A-12 through intervals of interest, following the methods outlined in Polissar and Freeman, 2010. Freeze-dried sediments were extracted with a Dionex Accelerated Solvent Extraction (ASE) system. Two to 5 g of dried sediment were placed in the stainless-steel sample holders and extracted at 100°C and 1000 psi with 10% (v/v) methanol/dichloromethane with a total volume of 50 mL. These total lipid extracts (TLEs) were evaporated to near dryness with N_2 in a Turbovap solvent evaporator and transferred to 4 mL borosilicate vials with Teflonlined caps. All remaining solvent was then evaporated and the TLE stored in a few drops of hexane at 4°C. TLEs were separated into aliphatic (F1), ketone/alcohol/acid (F2), and polar (F3) fractions with silica gel column chromatography. Silica gel was transferred in hexane to the SPE column and the column then rinsed twice with 6 mL hexane. The TLE was loaded on the column in 100 μL hexane and the F1, F2, and F3 fractions eluted with 5 mL of 10% dichloromethane in hexane, 8 mL ethyl acetate, and 5 mL methanol. Compounds were characterized by gas chromatography–mass spectrometry (GC–MS) using an Agilent 6890 GC with a split/ splitless injector operated in splitless mode at 300°C, a DB-5 column (0.25 mm i.d., 0.25 lm film thickness, 30 m length), 2.0 cm^3 min1 He flow and programmed heating of the oven from 60 to 170°C at 15°C/min, and to 320°C at 5°C/min, and an Agilent 5973 quadrapole mass spectrometer. Compounds were identified by elution time, comparison with published spectra, and authentic standards.

Soil samples were sent to ALS Minerals Corporation where samples were dried and successively digested with perchloric, nitric, hydrofluoric, and hydrochloric acids (Method ME-ICP61). Samples were redissolved in hydrochloric acid and measured on an inductively coupled plasma-atomic emission spectrometry (ICP-AES).

5.3 RESULTS

5.3.1 Geochronology and Sedimentology of Transect Cores

Radiocarbon ages were measured on 26 terrestrial macrofossils (**Table 5-2)**. We attempted to date the upper 20 cm of the B-12 and F-14 cores using the constant rate of supply (CRS) ^{210}Pb age model method (Appleby and Oldfield, 1983), however, excess ^{210}Pb never reached background values in either core. We hypothesize this is because Dian is a shallow lake, subject to a great deal of mixing, which can cause disequilibrium of ^{210}Pb (Binford et al., 1993). Additionally, since we are not certain that sedimentation has been continuous (see section 5.4.1), ^{210}Pb age models may not be appropriate. Smooth spline age models were produced using the calibrated macrofossil radiocarbon dates using *clam* 2.2 code (Blaauw, 2010) in the statistical software package, "R" (R Core Development Team, 2008) (**Figure 5-3)**.

Table 5-2- AMS radiocarbon dates for samples from Dian cores

UCI Number	Composite Core Depth (cm)	Material	^{14}C age (BP)	Error ±	Median Probability Calibrated Age (yr BP)	2σ Calibrated Age Range (yr BP)
Dian A-12 Dates						
116862	36.5	Plants	795	35	713	672-810
116863	97.5	Plants and charcoal	1140	20	1027	974-1172
116864	147.5	Plants and charcoal	2940	35	3098	2976-3208
122328	272.0	Charcoal	10285	50	12064	11827-12380
116865	351.5	Charcoal	13110	60	15736	15457-15985
116866	354.5	Charcoal	12670	40	15093	14855-15310
Dian C-14 Dates						
152056	56.0	Charcoal	605	20	603	547-651
152057*	250.5	Leaf	3725	20	4064	3987-4149
152058	342.5	Charcoal and wood	2530	20	2627	2502-2743
Dian D-14 Dates						
152039	234.5	Charcoal	13180	100	15831	15457-16146
152040	274.5	Wood	16790	60	20252	20045-20465
152041	316.0	Wood	20470	90	24627	24435-24811
152042	336.5	Charcoal and wood	25950	360	30151	29342-30896
152043	380.25	Charcoal	>47100			
152044	385.5	Charcoal	>47300			
152045	400.75	Wood	>48000			

Table 5-2 (continued)

Dian E-14 Dates						
152046	124.0	Charcoal and wood	1710	15	1606	1561-1692
152047	210.0	Wood	13010	40	15574	15339-15766
152048	270.5	Wood	23610	140	27725	27491-27954
152049	293.5	Charcoal	26610	190	30845	30522-31121
152050	307.0	Wood	26590	240	30817	30366-31154
Dian F-14 Dates						
152051	92.0	Charcoal and wood	585	50	598	526-657
152052	152.0	Wood	2260	15	2312	2183-2341
152053	285.0	Charcoal and leaf	9580	40	10934	10742-11122
152054	320.5	Wood	10810	140	12726	12428-13038
152055	349.5	Wood	15275	50	18550	18395-18695

*denotes date excluded from age model

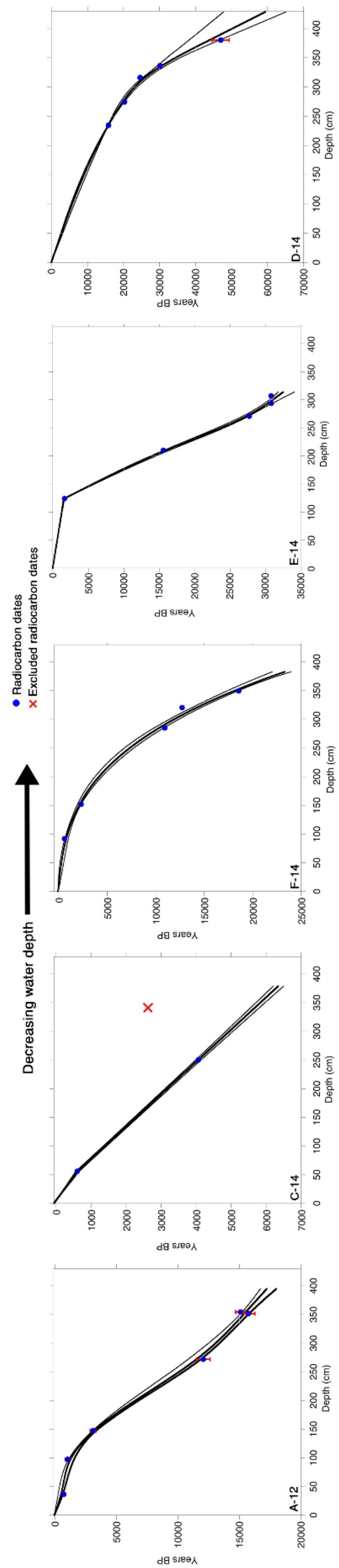
Decreasing water depth
Radiocarbon dates
Excluded radiocarbon dates
A-12
C-14
F-14
E-14
D-14
Years BP
Depth (cm)

Figure 5-3- Age-depth models with 95% confidence intervals, radiocarbon dates (blue circles) with 2 sigma error bars, and excluded radiocarbon dates (red crosses). Moving left to right with decreasing water depth: Cores A-12, D-14, E-14, F-14, and C-14.

The sediment from D-14, the shallowest coring site, spans beyond the limits of radiocarbon dating and an estimated age of 40 ka can be assigned to a total depth of 368 cm, though this is uncertain due to the lack of robust age control in this portion of the record (**Figure 5-3**). An unconformity at 385.5 cm is marked by coarse, yellow sand with pebbles transitioning to brown silt with an uneven surface (**Figure 5-4)**. The timing of this unconformity remains unknown as radiocarbon dates taken on either side are older than 47 ka. The end of two coarser sand deposits are dated to 20.3 and 25 ka and the deposition of a discrete silt layer at 234.5 cm is dated to 15.8 ka.

The base of the E-14 cores is dated to around 31 ka and is marked by a discrete sand layer (**Figure 5-4)**. The deposition of two more discrete sand layers are dated to 31 and 28 ka. Both the F-14 and C-14 cores have homogenous sedimentology with no sand or silt layers. However, even though both F-14 and C-14 sediment cores are around 380 cm in length, the base of the F-14 cores date to an estimated age of 23.3 ka.

The basal age of the C-14 cores is difficult to determine since we had to exclude the deepest radiocarbon date from the age model due to it being younger than anticipated. It is possible that this date was contaminated or that the radiocarbon age is a poor estimate of the true age of the sediments due to it being comprised of mixed material (wood and charcoal). The somewhat similar magnetic susceptibility profiles of the C-14 and A-12 cores (**Figure 5-5**) suggest that the basal date is the one that should be excluded, rather than the date from the middle of the C-14 cores (250.5 cm). The base of the C-14 cores date to an estimated age of 6.5

ka (**Figure 5-3)**, though this date is highly uncertain without a reliable radiocarbon date in this interval.

The upper 200 cm of all sediment cores display more similarities with homogenous, fine-grained gray/brown clay (**Figure 5-4)**. Along the entire length of the brown/gray clay units, there are abundant large gastropods of the species *Margarya melanioides*, which are endemic to Yunnan lakes and have a slight preference for deep water conditions (Song et al., 2013). After this unit, all cores have 50-100 cm of light, fine-grained clay that is roughly synchronous to an increase in carbonate content to 20%. This layer is dated to around 580 years BP in the F-14 cores and estimated to be 4,000 years BP in the A-12 cores based on the age model. All of the sediment cores also display 50-100 cm of red, fine-grained clay at the top (**Figure 5-4**) that is dated to 600 years BP in the C-14 cores and estimated to be 1,800 years BP in the A-12 cores based on the age model.

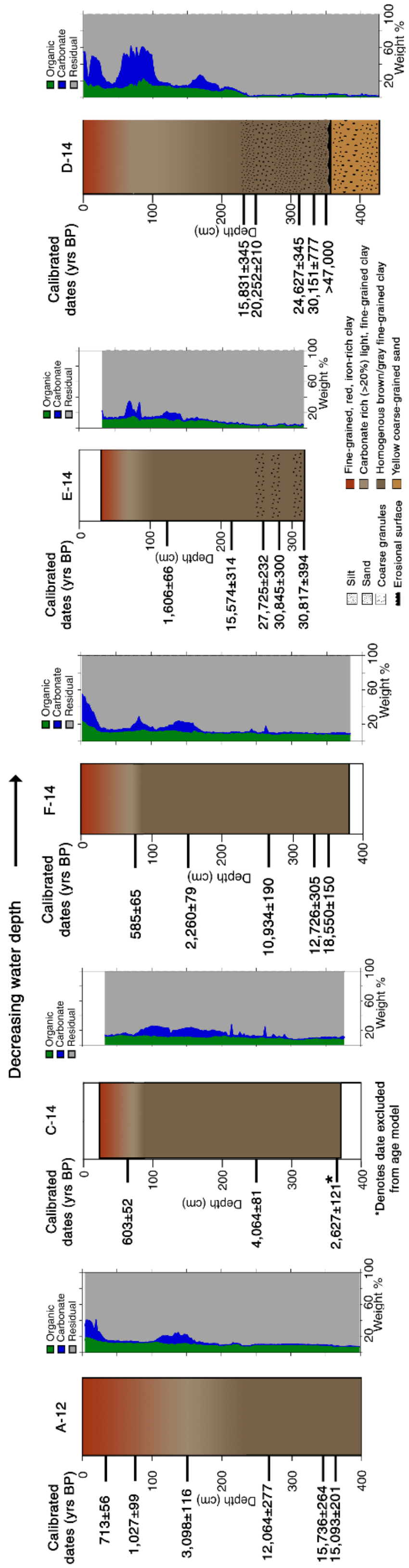
Decreasing water depth
A-12
C-14
F-14
E-14
D-14
Calibrated dates (yrs BP)
Depth (cm)
Weight %
Organic
Carbonate
Residual
713±56
1,027±99
3,098±116
12,064±277
15,736±264
15,093±201
603±52
4,064±81
2,627±121*
*Denotes date excluded from age model
585±65
2,260±79
10,934±190
12,726±305
18,550±150
1,606±66
15,574±314
27,725±232
30,845±300
30,817±394
15,831±345
20,252±210
24,627±345
30,151±777
>47,000
Silt
Sand
Coarse granules
Erosional surface
Fine-grained, red, iron-rich clay
Carbonate rich (>20%) light, fine-grained clay
Homogenous brown/gray fine-grained clay
Yellow coarse-grained sand

Figure 5-4- Sedimentology and weight percent organic matter, carbonate material, and residual mineral matter. Moving left to right with decreasing water depth: Cores A-12, D-14, E-14, F-14, and C-14.

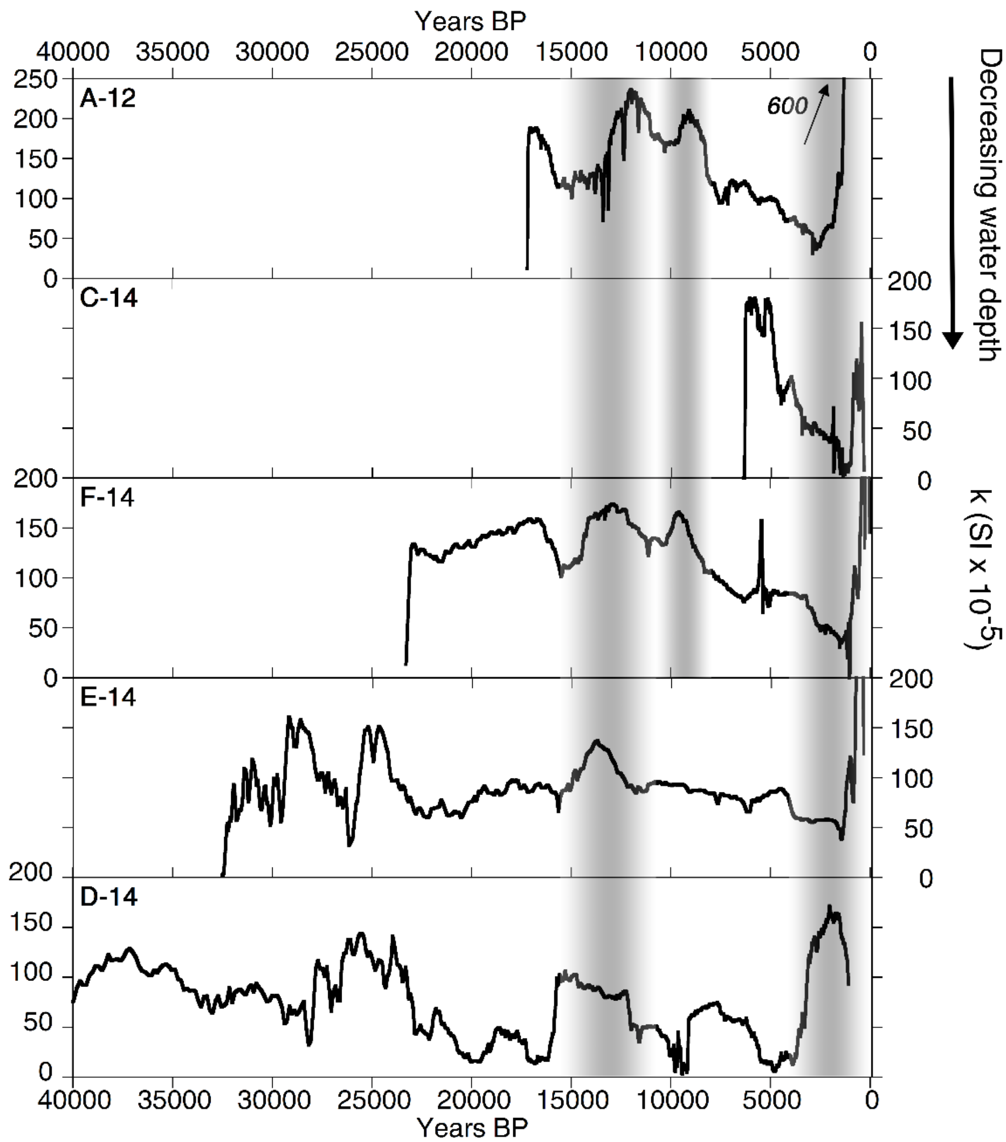

Figure 5-5- Magnetic susceptibility profiles for all cores on each individual age model (see Figure 5-3). Moving top to bottom with decreasing water depth: Cores A-12, D-14, E-14, F-14, and C-14. Many of the features of the magnetic susceptibility profiles are similar between coring sites- similarities are highlighted with gray shaded bars.

5.3.2 Geochemistry of A-12 Cores

The geochemical and isotopic data from the A-12 cores is divided into four units- Unit I from 17-8.5 ka, Unit II from 8.5 to 4 ka, Unit III from 4 to 2 ka, and Unit IV from 2 ka to present (**Figure 5-6**).

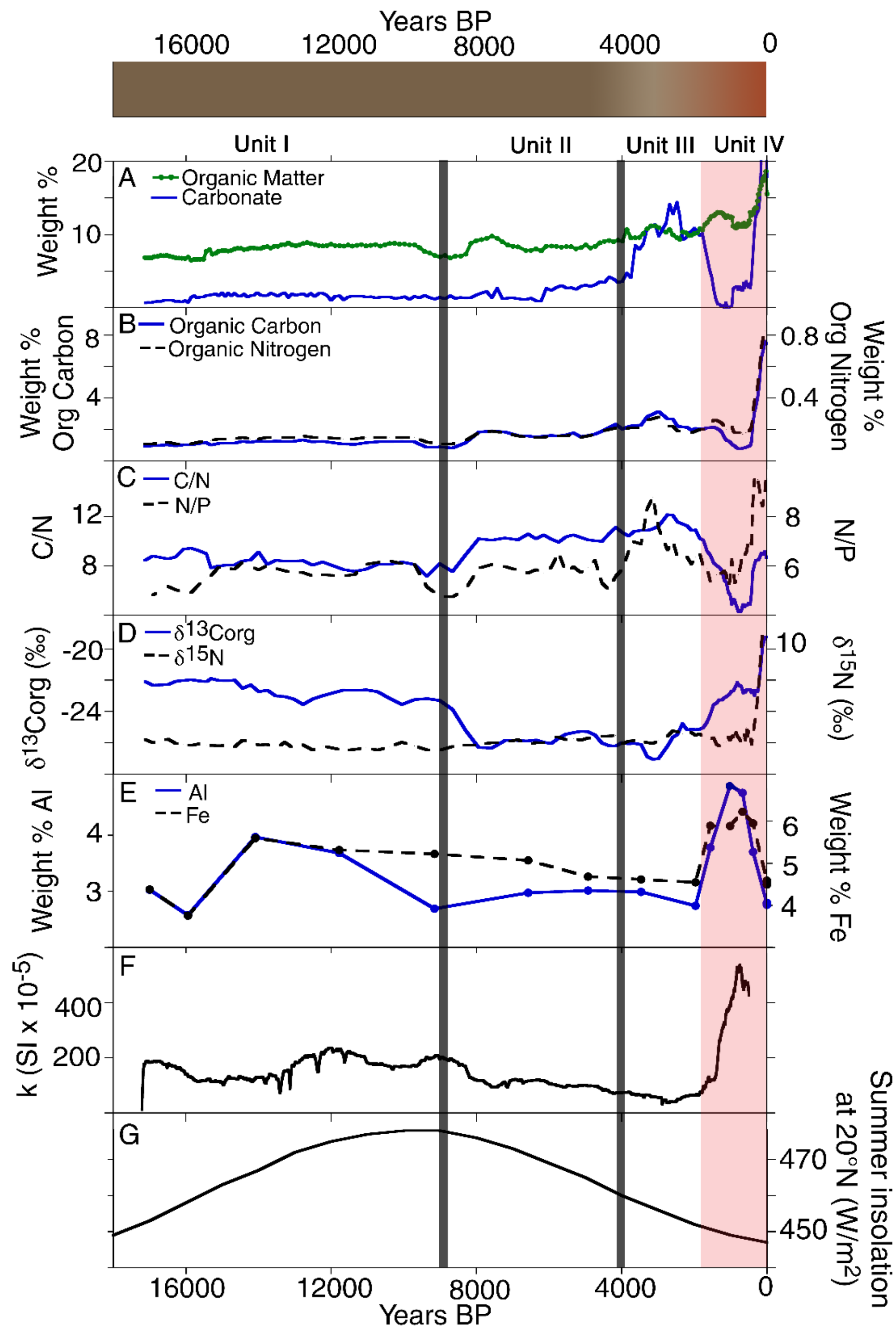

Figure 5-6- Stratigraphic column of core A-12. For color key, see Figure 5-4 caption. A- Weight percent organic matter (green circles) and calcium carbonate (blue solid line); B- Percent organic carbon (blue solid line), percent organic nitrogen (black dotted line); C- Carbon to nitrogen ratio (blue solid line) of organic matter, nitrogen to phosphorus ratio (black dotted line); D- Carbon isotope values of organic matter (blue

solid line), nitrogen isotope values of organic matter (black dotted line); E- Concentrations of strongly bound aluminum (blue solid line) and iron (black dotted line); F- Magnetic susceptibility; G- Average summer (June, July, August) insolation at 20°N (Berger, 1978). The red shaded bar in Unit IV represents the initiation of anthropogenic impact on the lake.

5.3.2.1 Unit I- 17-8.5 ka

Sediments in Unit I are composed of homogenous, fine, dark gray clay with no visible stratigraphy or lithologic changes (**Figure 5-6)**. Most proxies in this unit are steady and low. Organic matter, residual mineral matter, and carbonate average 8%, 91%, and 1%, respectively. Organic carbon and nitrogen average 1.1% and 0.2%, respectively. C/N and N/P values are stable at 8 and 4, respectively, and $\delta^{13}C_{org}$ and $\delta^{15}N$ values average -24.7‰ and 3.8‰, respectively. Both weakly and strongly bound Al and Fe as well as other metals (Mn, Cr- not shown) show an increase of ~30% and decrease over the period of 14 to 11 ka. Slightly later, magnetic susceptibility values roughly double from 13 to 11 ka.

5.3.2.2 Unit II- 8.5 to 4 ka

Sediments in Unit II are the same as those of Unit I- homogenous, fine, dark gray clay (**Figure 5-6**). Many of the proxies that were steady and low in Unit I continue to remain the same. Organic carbon and nitrogen average 2.0% and 0.2%, respectively, and are not significantly different from the previous subunit. Other proxies (C/N, N/P, and $\delta^{13}C_{org}$) exhibit shifts, particularly at 8.5 ka, though the timing of this transition is ill-constrained due to the lack of a radiocarbon age in this interval (**Figure 5-3**). C/N and N/P values increase to an average of 11 and 4, respectively, while $\delta^{13}C_{org}$ values decrease to an average of -27.9‰ and $\delta^{15}N$ values slightly increase to 4.2‰.

5.3.2.3 Unit III- 4 to 2 ka

Sediments in this unit are slightly lighter in color and composed of between 15 and 20 weight percent carbonate (**Figure 5-6**). Scanning electron microscopy (SEM) images from the D-14 cores show that this carbonate is calcite that is subhedral to anhedral (**Figure 5-7**). Since this unit is homogenous and of a similar thickness throughout the entire basin, we infer that the carbonate material from the A-12 cores is likely similar. N/P values increase to 7, primarily due to an increase in weight percent nitrogen from 0.2 to 0.3%. Additionally, $\delta^{13}C_{org}$ and $\delta^{15}N$ values decrease by about 2‰ and 0.5‰, respectively.

A- Dian D14 D1, 130 cm

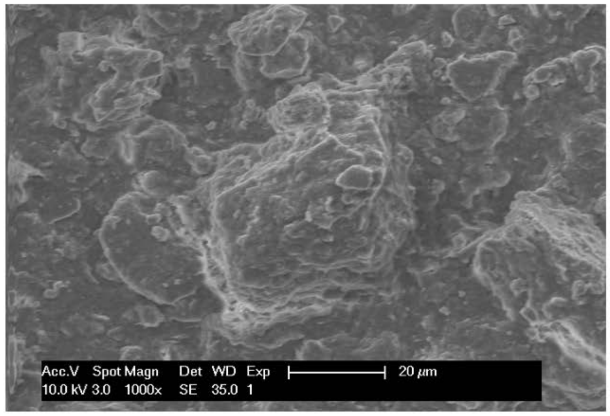

B- Dian D14 D1, 30 cm

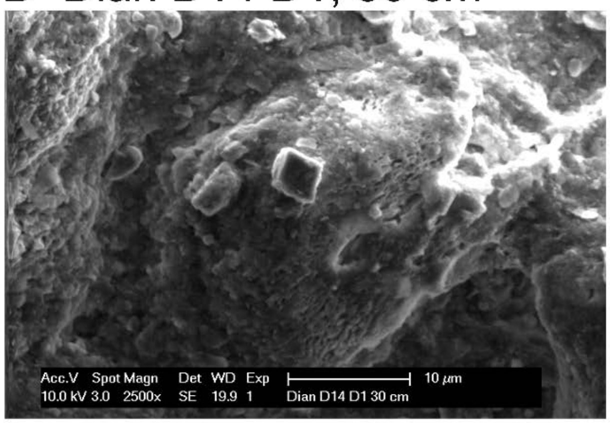

Figure 5-7- Scanning electron microscopy (SEM) images of calcite from Dian D-14 cores. A) Calcite from D14 D1 130 cm showing massive anhedral cystal forms; B) Euhedral calcite from D14 D1 30 cm.

5.3.2.4 Unit IV- 2 ka to present

This unit is primarily characterized by a sedimentological shift to the deposition of red, iron-rich clays as carbonate content decreases from 15% to <1%, residual mineral matters increases from 75% to 90%, and organic matter remains constant at 10% (**Figure 5-8)**. Sedimentation rates increase from a stable average of 0.02 cm/year to 0.07 cm/year. Concentrations of weakly bound Al, Ti, and Pb roughly double and P increases by ~50% at 200 AD. These geochemical changes occur in conjunction with C/N values that halve and a +3‰ shift in $\delta^{13}C$ values. Magnetic susceptibility values increase by 5-fold approximately 300 years later. The upper 30 cm of these sediment cores have higher proportions of carbonate material (>10%) and organic matter (>20%). SEM images show that this carbonate is calcite that is euhedral (**Figure 5-7**). These changes are accompanied by a two-fold increase in P, and a 4-fold increase in weight percent carbon and nitrogen. $\delta^{13}C_{org}$ and $\delta^{15}N$ values increase by 3‰ and 8‰, respectively. Concentrations of lead increase to a peak of 34µg/g.

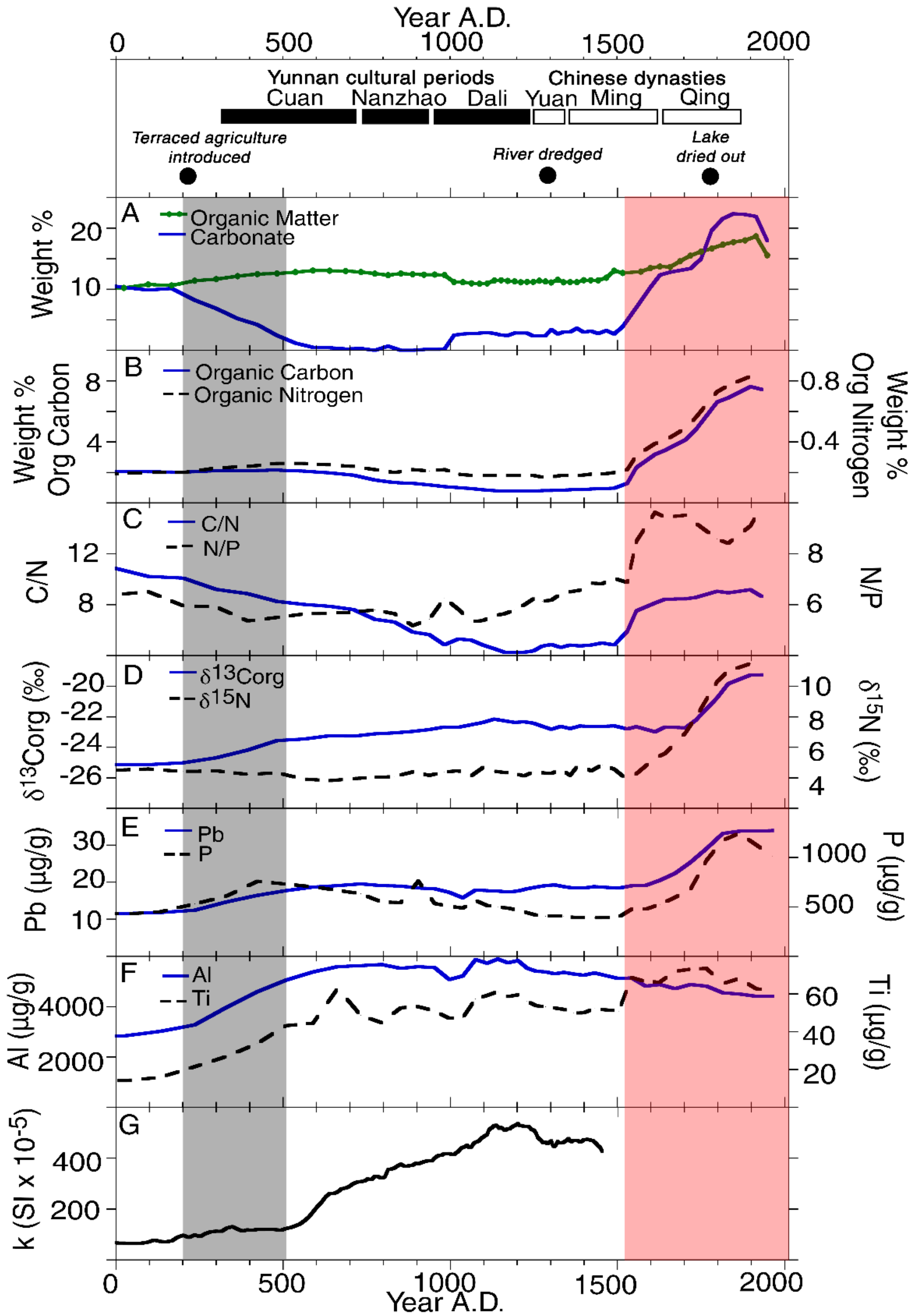

Figure 5-8- Proxies from A-12 cores over the last 2,000 years with significant historical events noted as well as Yunnan cultural and Chinese dynastic transitions. A- Weight percent organic matter (green circles), calcium

carbonate (blue solid line), and residual mineral matter (red dotted line); B- Percent organic carbon (blue solid line), percent organic nitrogen (black dotted line); C- Carbon to nitrogen ratio (blue solid line), nitrogen to phosphorus ratio (black dotted line); D- Carbon isotope values of organic matter (blue solid line), nitrogen isotope values of organic matter (black dotted line); E- Concentrations of weakly bound lead (blue solid line), phosphorus (black dotted line); F- Concentrations of weakly bound aluminum (blue solid line) and titanium (black dotted line); G- Magnetic susceptibility. The gray bar indicates the initiation of human disturbance on the lake and the red bar indicates the period of the most intense eutrophication and human impact.

5.4 DISCUSSION

5.4.1 Geochronology and Sedimentology of Transect Cores

The conclusions of the transect core study thus far are relatively limited without further proxy data or additional radiocarbon dates from the C-14 and D-14 cores. Conclusions are further complicated by an unclear understanding of the role that tectonics play in influencing sedimentation rates throughout the basin. Faults surrounding Dian are presently active (Wang et al., 1998) and the Yuxi fault runs directly through the southern part of the basin (**Figure 1-1)**. It is unknown if variable rates of slip on the multiple faults may have produced diachronous sedimentation or erosion. Additionally, with tectonic lakes a rise in lake level may not necessarily be indicative of changes in climate such as increased monsoon strength. The role that tectonics may play in influencing basin morphometry and accommodation space is particularly ill-constrained in Dian. Therefore, the discussion points that follow in regards to sedimentation, lake level, and climate are tentative.

Clear evidence for a low-stand in the D-14 cores occurs with the unconformity (**Figure 5-4**), but without another dating method, we cannot definitively conclude when this might have taken place. Extrapolating back to the base of the core assuming a constant sedimentation rate is not reasonable given that this shallow core site has experienced highly variable sedimentation rates through time, which the age model in the upper 300 cm shows (**Figure 5-3**). Evidence for a weaker ISM coincident with minimum average summer insolation at 20°N at 43 ka was tentatively found at Xing Yun Lake (see Chapter 3.0) and we speculate that low lake levels at Dian may be coincident with this.

The deposition of coarser material in both the D-14 and E-14 cores suggests a low-stand somewhere between 31 and 30 ka (**Figure 5-4)**. However, this interpretation is complicated by the radiocarbon dates from the bottom two silt layers in the E-14 cores being indistinguishable in age (**Table 5-2, Figures 5.3 and 5.4**). The sample from 293.5 cm is charcoal and likely represents the true age of deposition. The sample from 307 cm is wood that could have been re-worked but would be expected to produce an older age if this were the case. The wood may have been contaminated by modern carbon during sampling and pre-treatment but further radiocarbon samples would be needed to confirm this. Therefore we tentatively suggest that lake level may have dropped by several meters in order to produce the two successive silt layers. Summer insolation reaches a peak at 33 ka and would be expected to produce a strong ISM and high lake levels. However, an abrupt drop in monsoon strength was recorded in Hulu Cave (**Figure 5-1**) at ~30 ka that the authors interpreted to be a result of Heinrich Event 3 (Wang et al., 2001). Additionally, even through this interstadial period, the persistence of Northern Hemisphere glaciers may have dampened the response of the monsoon system to summer insolation (deMenocal and Rind, 1993), which was also observed at Xing Yun Lake (see Chapter 3.0).

Finer sediments in between the top and middle silt layers in the E-14 cores imply a higher lake level between 30 and 27 ka (**Figure 5-4**). However, this lake level rise was not high enough to alter the continued deposition of coarse silt at the D-14 site. After 24.5 ka, sediments in the D-14 cores gradually fine upwards, indicative of higher lake levels. This roughly corresponds to the timing of the Last Glacial Maximum (LGM) at 21 ka, however the exact timing and nature of the LGM in southwestern China is debated (Herzschuh, 2006). Due to lower sea levels, the Sunda Shelf was exposed and likely led to a weaker Walker circulation cell in the Indian Ocean (DiNezio and Tierney, 2013) and contributed to a weakened monsoon. However, a literature review found that lakes in Western China show evidence of higher than present-day levels during the LGM whereas lakes in Eastern China appear to be lower than present-day; records from Yunnan lie along the geographic dividing line (Yu et al., 2003). On the basis of modeling, the authors concluded that precipitation was likely decreased across much of China but that evaporation was stronger in the east than the west. This may partially account for the counterintuitive results that Dian lake levels rose during the LGM, but the possibility of tectonic activity cannot be discounted.

At some point, this period of higher lake levels was terminated and is marked by the abrupt transition from silt to sand at 290 cm in the D-14 cores (**Figure 5-4)**. The timing of this transition is unknown without a radiocarbon age in this interval. Another inferred lake level rise occurs from 20 to 15 ka with the fining upwards of D-14 sediments from coarse sand to silt to fine clay. Other lake sediment records from Yunnan also indicate climate amelioration with warmer and wetter conditions prevailing at Lugu after 18 ka (Wang et al., 2014), at Shudu after 17.1 ka (Cook et al., 2011), and at Xing Yun after 17.6 ka (Chen et al., 2014). The Hulu, Dongge, and Sanbao Cave records (**Figure 5-1)** show an abrupt drop in EASM strength at ~16 ka associated with Heinrich Event 1 (Dykoski et al., 2005; Wang et al., 2008; Wang et al., 2001) but there is no evidence of a rapid lake level drop associated with a weakening of the ISM in Dian.

Following these sedimentological changes, there are no additional sand or silt layers in either the D-14 or E-14 cores. One possibility is that sedimentation at these sites has not been continuous due to their shallowness. Additional radiocarbon dates at the top of these cores may answer this question. Alternatively, if sedimentation has been continuous, this implies that lake level changes in the Holocene have been of a smaller magnitude that those in the Pleistocene. The Pleistocene-Holocene transition at 11.5 ka is marked by a noticeable increase in monsoon strength throughout Asia (Herzschuh, 2006; Morrill et al., 2003). However, there are no sedimentological indicators in the transect cores that mark this transition. While these results are promising, further work needs to be done to definitively constrain lake levels in the southern Dian basin through the Pleistocene and Holocene.

Grain size in the upper 200 cm of all the cores is constant and clay-sized regardless of water depth. Notable differences include a thicker sequence of both the carbonate-rich fine-grained clay and the red, iron-rich clay in the D-14 and A-12 cores (**Figure 5-4)**. This is not unexpected at the D-14 site because of its proximity to the shoreline where more sediment may be transported to the site and deposited. The A-12 site is at a water depth of 5 m, deeper than the C-14 site, however it has a thicker package of sediments that also have older radiocarbon ages. For example, the initiation of carbonate deposition is estimated to be 4,000 years BP in the A-12 cores but 580 years BP in the F-14 cores (**Figure 5-4**). This may be due to an erroneous radiocarbon date from the F-14 core that was composed of charcoal and wood and may have been re-worked material. Alternatively, this may reflect localized changes in the hydrologic balance of Dian. The A-12 and F-14 sites are approximately 20 km apart and while the bathymetry of the basin is relatively simple (**Figure 5-1**), the large distance combined with the uncertain role of tectonics in affecting diachronous sedimentation may account for the large offset in ages.

The different ages in the initiation of the red clay deposition between the A-12 and the C-14 sites may reflect subtle differences in land use history. Our interpretation is that the red, iron-rich clay layer is the result of human activity (see section 5.4.2.4 below for further details). The A-12 site is located at the northern end of the basin, closest to the city of Kunming, where land use change likely was the most substantial and occurred the earliest with the introduction of terraced agriculture (Sun et al., 1986). Therefore, it is not unreasonable to speculate that land use change may have occurred earliest at the northern end of the lake and migrated down to the southern end over a period of several hundred years.

5.4.2 Geochemistry of A-12 Cores

5.4.2.1 Unit I- Late Pleistocene and Pleistocene-Holocene transition

Since the A-12 cores span the last 17,000 years and multiple types of proxy data were measured, we can make more firm conclusions about within-lake environmental changes. Sediments in Unit I cover the late Pleistocene and the Pleistocene-Holocene transition at 11.5 ka though there is no radiocarbon sample to date this transition (**Figure 5-3**). This unit is marked by the gradual decline in $\delta^{13}C_{org}$ values by -1.5‰. The carbon isotopic composition of organic matter within lake sediments may be influenced several factors including the relative proportions of C3 and C4 vegetation within the catchment. The decline of $\delta^{13}C_{org}$ values at Dian may imply a decrease in the relative proportion of C4 vegetation throughout this unit. CMIP5 modeling studies of vegetation changes in Southeast Asia found a higher abundance of C4 grasses during the LGM that declined through the Holocene (Thomas et al., 2014). While palynological analysis cannot distinguish between C3 and C4 plants, major vegetational changes were noted in Dian sediments at 9.5 ka with decreases in deciduous and humid evergreen trees (Sun et al., 1986). These changes in terrestrial vegetation over the Pleistocene and Pleistocene-Holocene transition may have impacted $\delta^{13}C_{org}$ values in Dian. However, the C/N values through this interval are suggestive of a more aquatic source of organic matter dominating the sediments rather than a terrestrial one (Meyers, 1994), suggesting that primary productivity may have exerted more of an influence on the carbon isotopic composition of the organic matter. A plot of $\delta^{13}C_{org}$ and C/N values from 17,000 to 300 years BP (**Figure 5-9)** shows a negative relationship demonstrating that more aquatic sources of organic matter have higher $\delta^{13}C_{org}$ values due to this influence of primary productivity.

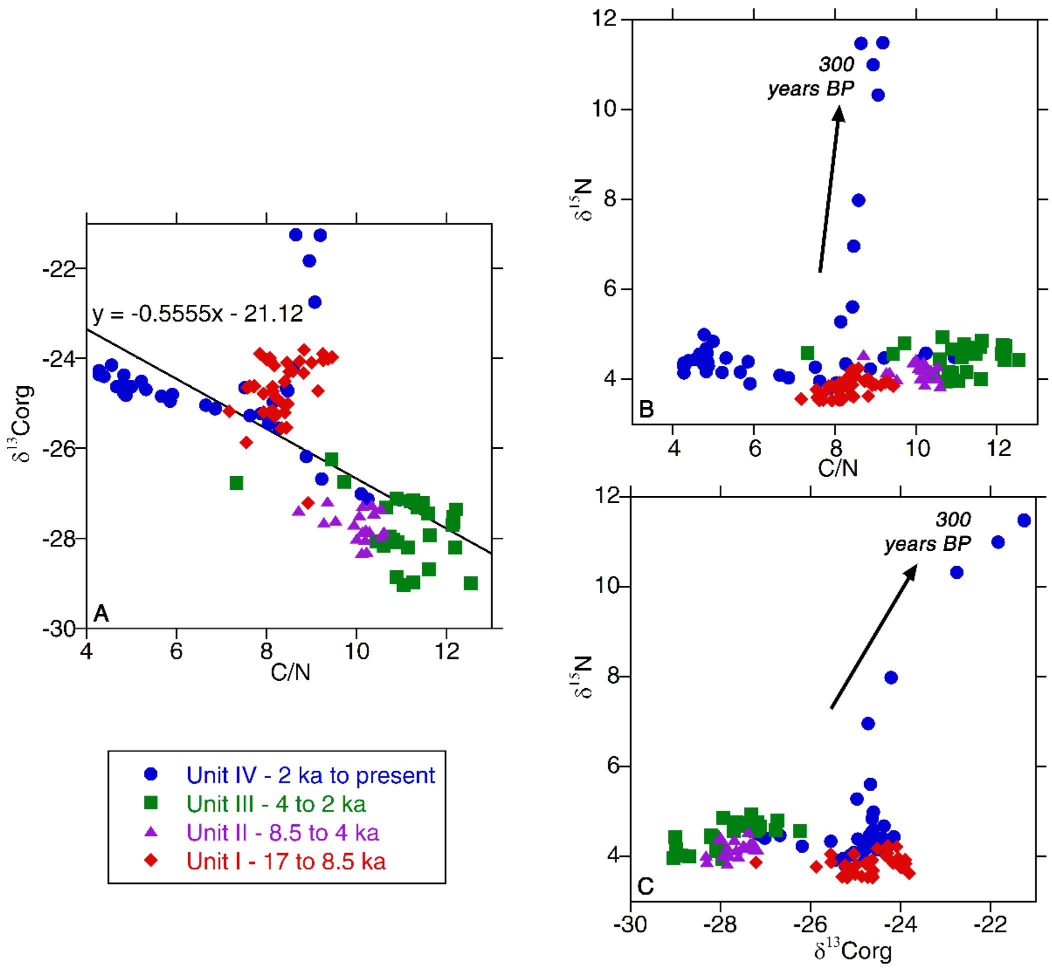

Figure 5-9- Organic isotope data from A-12 cores divided into the four units. A) C/N versus $\delta^{13}C_{org}$ with linear regression equation (R^2 = 0.56, p < 0.001). Data from the last 300 years were excluded from the regression; B) C/N versus $\delta^{15}N$; C) $\delta^{13}C_{org}$ versus $\delta^{15}N$.

N/P values are relatively low and close to the values expected for eutrophic lake sediments (Downing and McCauley, 1992). The relatively constant $\delta^{15}N$ values prior to 300 years BP (**Figure 5-9**) suggests that the source of nitrogen was not highly variable or that any fractionations were offset by complementary changes from different nitrogen sources. The Dian catchment was dominated by *Quercus*, *Pinus*, and *Tsuga* in the late Pleistocene (Sun et al., 1986) and expected N/P values for nutrient export in this deciduous/evergreen forest setting would be 60-70 (Downing and McCauley, 1992). Taken together, these results suggest that the majority of organic matter being preserved in Dian sediments was autochthonous and that the lake was relatively productive through this unit.

The increases in Al and Fe at 14 ka and later the increase in magnetic susceptibility at 13 ka roughly corresponds with the Younger Dryas, a global climate event that caused an abrupt weakening of the entire Asian monsoonal system from 13 to 11.5 ka (Herzschuh, 2006). This peak in magnetic susceptibility can be seen in several other Dian cores, most prominently in the E-14 and F-14 cores (**Figure 5-5**). During the Younger Dryas the East Asian Winter Monsoon (EAWM) became stronger (Yancheva et al., 2007) and increased aridity coupled with a stronger EAWM likely resulted in increased dust transportation (Wang et al., 2012a). There are potentially two sources of dust to Yunnan: the Tibetan Plateau to the west and the more northerly Chinese deserts (i.e. - Qaidam, Tengger, and Badain Juran). Geochemically, dust from the Tibetan Plateau tends to be enriched in aluminum, iron, and manganese oxides relative to other sources of Asian dust (Ferrat et al., 2011). Thus the geochemical changes in the Dian sediment cores may be due to increased dust delivered from the Tibetan Plateau.

On the other hand, increases in these metals may also result from increased lithogenic material being delivered to the core site. Total acid digestions indicate that soils on the southeastern side of the Dian catchment (**Figure 5-2**) are rich in elements such as Al, Fe, K, Mg, and Ti, particularly the red chromic luvisols that comprise the majority of the C soil horizon in the Dian catchment (Fengrang, 1990). Weathering and erosion of this soil material to the lake may explain the observed trace metal increases. A similar relationship between increased summer insolation and higher lithogenic metal concentrations was found over the past 50 ka at Xing Yun Lake (see Chapter 3.0). However, the timing of the increases in trace metals at Dian and the peak in summer insolation is off by several thousand years (**Figure 5-6**). This may also result from poor age control in the cores or more likely suggests that increased weathering associated with a stronger monsoon cannot account for the increases in Al and Fe.

Thus we infer a relatively warm and wet climate at Dian during the late Pleistocene and early Holocene was interrupted by a period of increased dust deposition arising from increased aridity during the Younger Dryas. This interpretation agrees well with previous conclusions from the palynological study of Dian (Sun et al., 1986) and has been observed in the Dunde and Guilya ice core records from the Tibetan Plateau (**Figure 5-1)** (Thompson et al., 1989; Thompson et al., 1998) and a variety of lake sediment records from central Asia (Herzschuh, 2006). The Pleistocene-Holocene transition at 11.5 ka is marked by a noticeable increase in monsoon strength throughout Asia (Herzschuh, 2006; Morrill et al., 2003) but there are no shifts in the Dian proxy data that show this transition.

5.4.2.2 Unit II- Early to Middle Holocene

In the previous study of Dian sediments, major vegetational shifts were observed at 8 ka with decreases in *Pinus*, *Quercus*, and other taxa associated with valley forests, that was interpreted to result from warmer winter temperatures and more equal annual rainfall distribution (Sun et al., 1986). The beginning of Unit II at 8.5 ka in our study is marked by shifts in organic matter proxies. The decrease in $\delta^{13}C_{org}$ values suggests that primary productivity decreased during this time (Schelske and Hodell, 1995). However, these changes may also result from soil organic carbon being washed into the lake as the accompanying higher C/N values are suggestive of a more terrestrial source of organic matter (Meyers, 1994). Increases in both weight percent organic carbon and nitrogen support this interpretation. The timing of these changes is similar to the 8.2 ka event, a global climate event marked by increased amounts of ice-rafted debris in the North Atlantic (Bond et al., 1997), a weaker ISM (Neff et al., 2001), and a weaker EASM (Wang et al., 2005). However there is not a subsequent recovery of the Dian proxies to pre-8.2 ka conditions, marking a shift or threshold response in the lake. This suggests that the abrupt but brief 8.2 ka event cannot account for the observed changes.

Instead we suggest that these changes are being driven by the gradual weakening of the monsoon system that peaks in strength at 10 ka and gradually decreases around 8 ka in concert with declining summer insolation (**Figure 5-6**). If lake levels gradually began dropping, more terrestrial organic matter along the shoreline may have been exposed and transported into the lake. Decreasing lake levels associated with a weaker ISM broadly agree with oxygen isotope records from Qunf Cave in southern Oman (Fleitmann et al., 2003) and Mawmluh Cave (Berkelhammer et al., 2012) (**Figure 5-1)** that both show increasing aridity by 8 ka. Lake records from the Tibetan Plateau including Ahung Co (Morrill et al., 2006) and Paru Co (Bird et al., 2014) (**Figure 5-1)** do not show evidence of arid conditions until 7.5 ka. Notably, the shifts in the Dian proxies occur when summer isolation values are still relatively high and this possible shift to drier conditions occurs earlier than would be expected. High effective moisture is found in some regions affected by the ISM until 5.5 ka (Herzschuh, 2006). Without a radiocarbon date in this interval, we cannot definitively constrain the timing of these changes and determine if the Dian limnological response leads or lags the peak in summer insolation.

5.4.2.3 Unit III- Middle to Late Holocene lake level changes

The previous study of Dian noted substantial increases in organic matter content at 4 ka (Sun et al., 1986). We suggest that the changes in organic matter proxies at 4 ka are the result of lower lake levels. Lower lake levels can lead to increased evaporation and loss of CO_2, which causes the precipitation of authigenic carbonate minerals (Kelts and Hsu, 1978). SEM photographs show that this carbonate is irregularly shaped aggregates of calcite approximately 10-20 µm in size (**Figure 5-7**). The subhedral shape does not necessarily imply that the calcite was not precipitated authigenically; these crystal forms, especially ones of such large size, can indicate either rapid growth or post depositional dissolution (Kelts and Hsu, 1978). Lower lake levels may also have caused increased wind turbulence and water column mixing, promoting the remineralization of organic matter and returning light isotopes to the surface, causing the observed shifts in $\delta^{13}C_{org}$ and $\delta^{15}N$ values (Talbot, 2001). However, the increases in weight percent carbon, nitrogen, N/P, and C/N are all indicative of a more terrestrial source of organic matter washing into the lake (Meyers and Laillier-verges, 1999). The lower $\delta^{13}C_{org}$ and $\delta^{15}N$ values may result from decomposing soil organic matter being transported into the lake due to the increased exposure of shoreline area associated with lake level drops (Hammarlund et al., 1997). However, without measurements of the carbon and nitrogen isotopic composition of soil samples in the Dian watershed, we are limited in our ability to definitively conclude this.

The inferred period of lower lake levels agrees well with the findings of previous studies. A synthesis of abrupt changes in the Asian monsoon system over the Holocene from a variety of proxy records found statistically significant aridity from 5 to 4.5 ka (Morrill et al., 2003). A rapid (<20 years) shift in oxygen isotope values at Mawmluh Cave indicative of drier conditions occurred at 4 ka with the cessation of calcite occurring at 3.5 ka (Berkelhammer et al., 2012) and Ahung Co Lake on the Tibetan Plateau (**Figure 5-1)** was completely desiccated by 4 ka (Morrill et al., 2006).

The cause of this aridity is still debated and may be linked to changes in tropical Pacific Ocean dynamics. The Pallcacocha lake record in Ecuador, which has been interpreted to reflect El Niño Southern Oscillation (ENSO) variability through the Holocene, does not show anything anomalous about 4 ka, though ENSO events become more frequent in the mid and late Holocene (Moy et al., 2002). SST reconstructions from the Soledad Basin off the coast of Mexico display a shift to warmer SSTs and a more El Niño-like mean state after 4 ka (Marchitto et al., 2010). A more El Niño-like mean state beginning in the mid to late Holocene has been observed in multiple other oceanic records (Rein et al., 2005; Stott et al., 2004). Additionally, coral records from the Mentawai Islands off the coast of Sumatra show cooler SSTs from 5.5 to 4.3 ka indicative of a persistently positive IOD phase (Abram et al., 2009). Both El Niño and positive IOD events have the effect of weakening the ISM and combined, may account for the widespread aridity in Asia at this time that previous researchers have suggested (Berkelhammer et al., 2012; Bird et al., 2014; Morrill et al., 2003). Alternatively, multiple speleothem records from the Arabian Peninsula show gradual drops in ISM strength as opposed to abrupt ones. The authors hypothesized that the reason for this is that lake records are especially sensitive to small alterations in P-E balance and that abrupt drops in lake level are not necessarily indicative of abrupt drops in monsoon strength (Fleitmann et al., 2007).

5.4.2.4 Unit IV- Late Holocene intensive human disturbance

The transition into Unit IV coincides closely with the introduction of terraced agriculture and irrigation according to historical records (Sun et al., 1986) as well as the establishment of the Cuan regional kingdom (ca. 320 AD) within the errors of the age model (**Figure 5-8**). The deposition of this layer takes place across the entire lake basin with the thickest and earliest dated deposits occurring in the A-12 cores (**Figure 5-5**). Previous study of Dian sediment cores noted similar changes and interpreted them as evidence of human impacts on the landscape (Sun et al., 1986). The timing of this transition in the previous study was thought to be around 500 AD, very close to the results presented here, despite bulk sediment radiocarbon measurements used in the previous study. Our interpretation is that this transition was caused by anthropogenic activities. Sedimentation rates increase at all coring sites and increase by almost 4-fold in the A-09 cores. Sediments exhibit many of the same characteristics noted in previous studies of Yunnan lake sediment cores: Xing Yun (Chapter 2.0), Qilu (Brenner et al., 1991), and Chenghai (Chapter 6.0). Previous work attributed these changes to the onset of intensive land-use and noted that the low organic carbon and high residual mineral matter content composed primarily of catchment soils is similar to what was found in Guatemalan lakes known to have been impacted by human deforestation and erosion (Binford et al., 1987; Brenner, 1983). The geochemical composition of these sediments matches closely with the composition of the red chromic luvisols in the C horizon from the soil profile on the southeastern side of the lake (**Figure 5-2**).

Additionally, similar to previous studies of Yunnan lakes, many of the shifts seen in the organic proxies beginning around 1560 AD can be attributed to cultural eutrophication. The increase in phosphorus, which limits phytoplankton growth in many lakes, is contemporaneous with increases in weight percent organic matter, carbon, nitrogen, $\delta^{13}C_{org,}$ and $\delta^{15}N$. Lakes heavily impacted by eutrophication typically have high fertilizer and sewage inputs, that are characterized by higher $\delta^{15}N$ values (Brenner et al., 1999) and high sediment $\delta^{13}C_{org}$ values (Schindler et al., 2008). Plots of $\delta^{13}C_{org}$ and $\delta^{15}N$ as well as $\delta^{15}N$ and C/N (**Figure 5-9)** show that this is an anomalous period in the context of the entire 17,000 year record.

Our conclusion is further supported by analysis of fecal 5β-stanols, including coprostinol and epi-coprostanol, which show an increase in concentration beginning around this period (**Figure 5-10**). These compounds can be used as indicators of fecal contamination in modern aquatic environments (Leeming and Nichols, 1996), and have been used as evidence of human occupation of a watershed (D'Anjou et al., 2012). Increases in these compounds suggest inputs of sewage to the lake, that is further supported by $\delta^{15}N$ values reaching as high as 11.5‰ in the uppermost sediments.

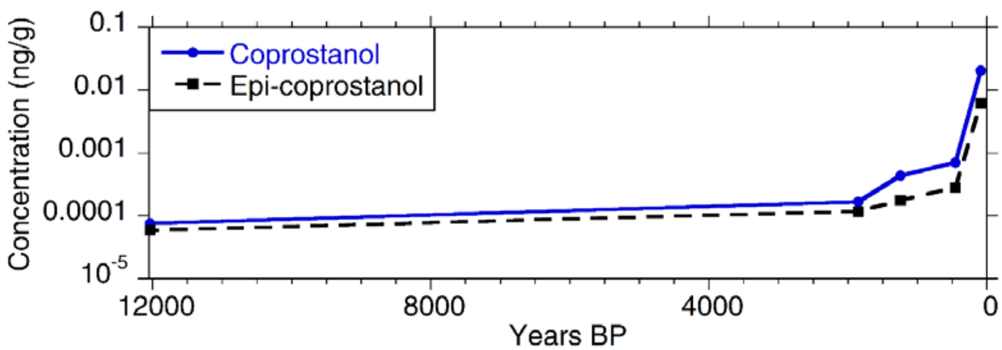

Figure 5-10- Concentrations of fecal 5β-stanols from Dian A-12 cores that begin to increase around 500 years BP.

The timing of these changes coincides closely with the initiation of the Qing Dynasty within the 95% confidence intervals of the age model (±160 years). This contrasts with previous study of a Yunnan lake, Xing Yun, which found an intensification of eutrophication beginning at 1400 AD with the Ming Dynasty, and a reduction in eutrophic conditions at 1700 AD with the

Qing Dynasty (see Chapter 2.0). However, the age of the upper portion of the Dian sediment cores is not as well constrained as the Xing Yun sediment cores due to fewer radiocarbon dates and the lack of a ^{210}Pb chronology (**Figure 5-3**).

Increases in carbonate precipitation of uniform thickness at all coring locations begins around 1560 AD, similar in timing to the other changes noted above. SEM photographs confirm that this is euhedral calcite around 2-3 μm in size and is unaffected by dissolution or etching (**Figure 5-7**). The largest increases in carbonate content from 13 to 23% take place from 1720 to 1820 AD. Historical documents from Kunming record that the lake completely dried out in 1764 AD (Sun et al., 1986). There are no indications in our proxy data or our transect cores (**Figure 5-4**) of a complete desiccation of the lake, however the increased amounts of carbonate material precipitated during this time may suggest a drop in lake level (Kelts and Hsu, 1978). Historical records suggest that the driver of this lake level change was due to natural climate variability although no other lake records in this region of Yunnan record desiccation or significant aridity during this time (see Chapters 2.0 and 5.0).

5.5 CONCLUSIONS

The results from Lake Dian provide 1) a new perspective on the climate in Southeast Asia as influenced by the ISM and 2) regional context for the spatial distribution of anthropogenic changes in watersheds in Yunnan. Though limited in our ability to definitively reconstruct lake levels with the series of transect cores from the southern basin, we tentatively find evidence for lower lake levels at 31 ka, similar to evidence of a weakened ISM from the Hulu Cave record. Additionally, there is evidence for a series of higher lake levels between 30 and 27 ka, 24.5 ka, and 20 to 15 ka. However, these results necessitate further investigation with additional radiocarbon dates and a wider range of proxy data.

The multi-proxy record from the A-12 cores show evidence for a relatively warm climate with enhanced lake primary productivity prior to 8.5 ka, likely associated with high summer insolation values and a strong ISM. Additionally, trace element geochemistry suggests a dry Younger Dryas event characterized by increased dust deposition from the Tibetan Plateau. By 8.5 ka, there is evidence for declining lake productivity and potentially lower lake levels associated with lower summer insolation values and a weak ISM. Further drops in lake level take place at 4 ka due to a drop in ISM strength that is observed in several other paleoclimate records. While this study is not of high enough resolution to capture rapid shifts in moisture or differentiate between the timing of shifts in the ISM and the EASM, this work adds to the spatial coverage of lake sediment paleoclimate records in Southeast Asia and broadly agrees with previous studies from the Tibetan Plateau (Berkelhammer et al., 2012; Bird et al., 2014; Morrill et al., 2006).

After 2 ka, changes in the Dian sediment record are characterized by anthropogenic impacts and largely correspond with recorded cultural and historical events. The initiation of human disturbance within the lake catchment matches closely to the introduction of terraced agriculture as well as other regional records that indicate the initiation of human disturbance around this period (see Chapter 2.0). The beginning of a trophic status shift in the lake is recorded ~1,000 years later and is likely associated with increased population pressure and rice agriculture. The modern-day impacts associated with intensive agriculture, fertilizer use, and sewage runoff from the city of Kunming are observed in the uppermost sediments. This study adds to a growing number of records that show early human impacts on the Yunnan Plateau that are equal in magnitude to post-industrial impacts.

6.0 CHENGHAI LAKE

The Isotopic Response of Lake Chenghai to Hydrologic Modification from Human Activity

The human modification of lake system hydrology is a widespread feature of the industrial era; however, these anthropogenic impacts have existed for thousands of years in regions of the world with long histories of human occupation. Here, we document the isotopic and geochemical response of a lake in southwestern China to the construction of a dam using geochemical analyses of lake sediment. The Chenghai record shows evidence of land use change by at least 1100 AD characterized by an increased flux of terrestrial organic matter and sediment rich in metals such as lead, copper, and iron. Landscape stabilization occurred from 1360 to 1700 AD. The stable isotopic composition of authigenic aragonite shifts toward higher values indicative of lower lake levels in response to the intentional manipulation of natural hydrology at 1690 AD. Trace element geochemistry and organic matter proxies also reveal rapid limnological variations. Similar to what has been observed in other lakes in this region of the world, we find that these changes closely coincide with shifts in natural climate variability, highlighting the complex, interconnected nature of human-environment interactions. This study demonstrates the importance of historical and cultural context in the interpretation of lake sediment records with substantial human settlement proximal to the lake system.

To reconstruct changes in land-use and lake-level management, we rely on measurements of the oxygen and carbon isotopic composition of authigenic aragonite ($\delta^{18}O$ and $\delta^{13}C$), the concentration and isotopic composition of organic matter (C/N, $\delta^{13}C_{org,}$ $\delta^{15}N$), the concentrations of weakly bound metals in sediment, and magnetic susceptibility. We use these analyses to investigate the timing and magnitude of environmental changes at Chenghai in the context of coincident anthropogenic activities. This multi-proxy approach allows us to characterize the nature of pre-industrial human disturbance to watersheds in southwestern China as well as the isotopic response of a lake to the intentional manipulation of hydrologic balance.

6.1 REGIONAL SETTING

Chenghai is located in Yunnan Province of China (**Figure 6-1**) where the closest city with meteorological records is Lijiang (**Figure 6-1**), approximately 50 km to the northwest. The climate is heavily influenced by the Asian Summer Monsoon (ASM), with 80% of precipitation falling between the months of June-September (**Table 6-1**). Temperatures are generally stable, ranging between 6 and 18°C (**Table 6-1**). Chenghai is a large and deep lake (maximum depth of 35 m) that was formed as a pull-apart basin during the Pleistocene (**Figure 6-1**) and sedimentary deposits in Chenghai are estimated to be 1,000 m thick (Wang et al., 1998). The bedrock in the Chenghai catchment is primarily Permian basalt with extensive deposits of Quaternary alluvium to the south (Dearing et al., 2008; Bureau of Geology and Mineral Resources of Yunnan Province, 1990).

Chenghai is less than 100 km away from the town of Jianchuan, the home of the Neolithic and Bronze Age site Haimenkou (Chiou-Peng, 2009). Haimenkou is the largest

Neolithic (ca. 1500 BC) site in China and has the largest Neolithic wooden structure ever discovered (Yao, 2010). Wheat, millet, and rice remains have also been found at this site, suggesting a wide range of agricultural practices in conjunction with large, permanent settlements (Yao, 2010). Haimenkou is also possibly the earliest site of copper-based metallurgy in western Yunnan, dating to ~1500 BC; a study of nearby Erhai Lake found evidence to support the advent of copper-based metallurgy at around this time (see Chapter 4.0). Further historical records pertaining to human activities around Chenghai are relatively limited; however, in 1690 AD, a dam was constructed upstream of Chenghai which led to lower lake levels. In 1942 AD the population around Chenghai increased and was accompanied by an expansion of agricultural activities and fertilizer use (Jinglu et al., 2004).

Chenghai is a closed basin, meaning that it is only fed by precipitation and has limited groundwater throughflow (Jinglu et al., 2004). The stable isotopic composition of the lake water, as well as high concentrations of ions such as Mg^{2+} and Na^{+}, suggests that the lake primarily loses water through evaporation (Whitmore et al., 1997). Stable oxygen isotopic composition of the lake water samples collected in the summer of 2012 average -1.58‰ VSMOW (**Figure 1-3**), ~8‰ higher than the average weighted oxygen isotope composition for Lijiang (**Table 6-1**). While Lijiang is the city with the closest weather station to Chenghai, it is situated 1000 m higher than the lake and the oxygen isotopes in precipitation may have lower values than the precipitation that actually falls on Chenghai. Nonetheless, the water samples collected from Chenghai plot far to the right of the Global Meteoric Water Line (GMWL) (**Figure 1-3**) and strongly suggest that Chenghai lake water is heavily modified by evaporative enrichment.

Table 6-1- Monthly average temperature, precipitation, and oxygen isotope values at Lijiang (26°53’N, 100°14’E, 2400 m).

	Jan	Feb	Mar	April	May	June	July	Aug	Sept	Oct	Nov	Dec
Average Temperature (°C) (Lawrimore et al., 2011)	6.06	7.54	10.33	13.35	16.56	17.92	17.94	17.23	15.95	13.22	9.21	6.56
Average Precipitation (mm) (Peterson and Vose, 1997)	2.21	5.75	11.89	16.70	59.72	170.46	245.01	214.21	150.07	72.42	11.47	3.20
$\delta^{18}O$ (‰VSMOW) (Bowen, 2013)	-6.4	-4.7	-5.7	-4.7	-6.1	-8.0	-10.6	-11.1	-10.9	-10.3	-8.8	-7.1

Average weighted $\delta^{18}O$ (‰VSMOW) = -9.76

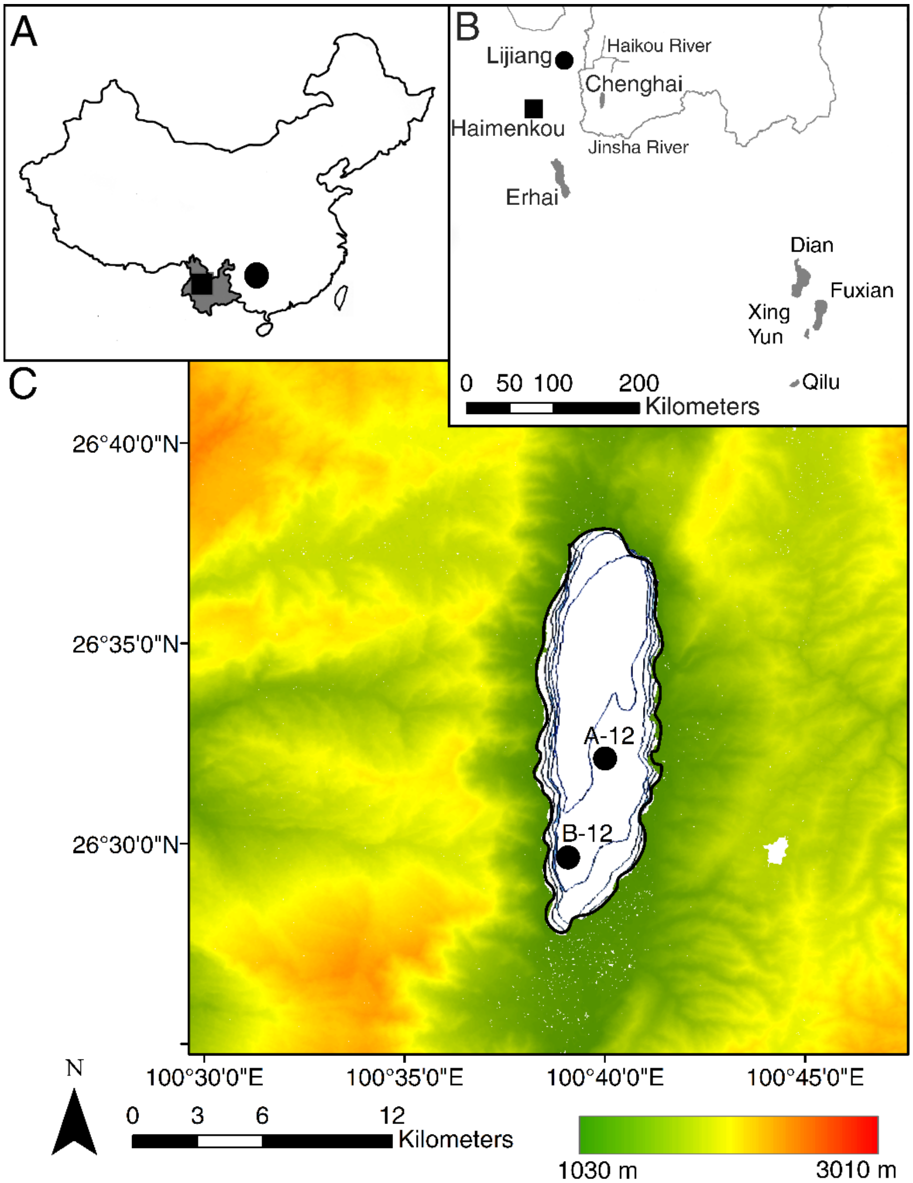

Figure 6-1- A- Locations of Chenghai Lake (square) and Dongge Cave (circle); B- Locations of Yunnan lakes mentioned in text as well as the city of Lijiang and the archaeological site Haimenkou; C- Map of Chenghai Lake with shaded topographic relief from ASTER Global DEMs. Coring locations indicated by black circles. Bathymetric data (10 meter contour intervals) from Wan et al., 2005.

ASTER global digital elevation maps (DEMs) indicate that the topographic relief around Chenghai is quite steep, making it prone to lake level change in response to hydrologic forcing (**Figure 6-1C**). A bathymetric map of Chenghai shows that dramatic changes in lake level (10-20 m) occur over very small distances (<0.5 km) (**Figure 6-1C)**. A change in bathymetric characteristics (such as surface area to volume ratio) will change the proportion of water lost through evaporation, thus changing the isotopic composition of the lake water (Steinman and Abbott, 2013). Historical records suggest that prior to 1690 AD the lake was a throughflow system, linking the Haikou River with the Jinsha River (Wan et al., 2005). After 1690 AD, dams were built upstream of the lake and the Haikou River stopped flowing (Jinglu et al., 2004; Wan et al., 2005) (**Figure 6-1**). Historical records indicate that between 1690 and 1980 AD, Chenghai dropped 38 m due to the dam construction (Wan et al., 2005). More recent observations have recorded drops in lake level of 5 m from 1960 to 1990 AD (Whitmore et al., 1997). While a drop of ~40 m over the span of 300 years is both substantial and rapid, DEMs confirm that if the lake were 30 m higher than present day levels, Chenghai would be an open basin lake, with significant throughflow to the south. Additionally, substantial deposits of Quaternary alluvium extend several kilometers to the south of Chenghai (Bureau of Geology and Mineral Resources of Yunnan Province, 1990), further evidence that the lake was once likely much higher and an open basin.

There have been multiple previous studies of Chenghai, though many of them have suffered from several limitations: most notably, limited chronologies relying only on ^{210}Pb ages to constrain the age of the sediments (Chen et al., 2002; Jinglu et al., 2003; Wang et al., 2002; Zhu et al., 2011). One study had a single AMS radiocarbon date from deeper sediment, but a single date makes it hard to constrain the timing of abrupt changes in isotopic geochemistry as well as sedimentation rates (Jinglu et al., 2004). Despite these limitations, these records demonstrate substantial variation in the stable isotopic composition of both organic matter and authigenic carbonates over less than a meter of sediment (Chen et al., 2002; Jinglu et al., 2004; Wang et al., 2002). An additional limitation is that the stable isotopic composition was measured on bulk carbonate material, which likely contained shell fragments subject to vital or biological effects (Leng and Marshall, 2004), and sampling was performed at a low resolution (~5 cm). Of further concern, the oxygen stable isotopic composition of this carbonate material shifts towards lower values over the last 120 years, which is unexpected due to observations that lake levels have dropped over this time period (Whitmore et al., 1997). A previous study also included an analysis of the concentrations of blue-green algae pigments and concluded that following the construction of the dam upstream in 1690 AD, slight increases in primary productivity took place (Jinglu et al., 2004). However, the most substantial changes and the switch from oligotrophic to eutrophic lake status took place more recently, around 1940 AD and this eutrophication intensified by 1984 AD (Jinglu et al., 2004). Our study expands upon this previous work with a longer sediment core of 123 cm, an improved radiocarbon chronology, and a higher-resolution, multi-proxy dataset that demonstrates the limnological consequences associated with the construction of an upstream dam.

6.2 MATERIALS AND METHODS

6.2.1 Core Collection

Two cores were collected from Chenghai using a UWITEC coring system with removable polycarbonate tubes. The A-12 core was collected at a water depth of 27 m and measures 123 cm (26°32’01’’N, 100°40’06’’E) (**Figure 6-1)**. The upper 30 cm were extruded in the field at 1 cm intervals and used for ^{210}Pb dating. The B-12 core was collected at a water depth of 20 m and measures 108 cm (26°29’18’’N, 100°39’05’’E) (**Figure 6-1)**. The upper 10 cm were extruded in the field at 1 cm intervals and used for ^{210}Pb dating. We focus our analysis on the A-12 core as it is the longest recovered sedimentary record and is closest to the deepest part of the lake.

6.2.2 Age Control

Radiocarbon ages were measured on four terrestrial macrofossils, including charcoal and leaves. Samples were analyzed at Keck Center for Accelerator Mass Spectrometry at the University of California Irvine. Prior to analysis, samples were pretreated using a standard acid, base, acid procedure (Abbott and Stafford, 1996). The resulting ages were calibrated using CALIB 7.0 and the INTCAL13 calibration curve (Reimer et al., 2013). The upper 19 cm of the A-12 core was lyophilized and analyzed for ^{210}Pb and ^{214}Pb activities by direct gamma (γ) counting in a broad energy germanium detector (Canberra BE-3825) at the University of Pittsburgh.

6.2.3 Geochemistry

Water content and bulk density were measured at 2 cm intervals using 1 cm^3 samples. Weight percent organic matter and carbonate content within these same samples was determined by loss-on-ignition (LOI) analysis at 550°C and 1000°C, respectively (Dean, 1974). Sediment core magnetic susceptibility was measured on split cores using a Bartington® Instruments Ltd. ME2EI surface-scanning sensor equipped with a TAMISCAN-TSI automatic logging conveyer. Samples for X-ray diffraction (XRD) analysis were taken every 50 cm, lyophilized, and ground by hand. The samples were prepared as back-filled cavity mounts and analyzed using a Phillips X'Pert MPD diffractometer.

Cores were sampled continuously at 0.5-cm intervals for analysis of the oxygen and carbon isotopic composition of aragonite minerals. Samples were disaggregated with 7% H_2O_2 and sieved through a 63-µm screen to remove biological carbonates derived from ostracod and gastropod shells. Samples were soaked in a 50% bleach and 50% DI water mixture for 6-8 hours, rinsed, and lyophilized. Aragonite samples were reacted in ~100% phosphoric acid at 90°C and measured using a dual-inlet GV Instruments, Ltd. (now Isoprime, Ltd) IsoPrime™ stable isotope ratio mass spectrometer and MultiPrep™ inlet module at the Regional Stable Isotope Laboratory for Earth and Environment Science Research at the University of Pittsburgh. Oxygen and carbon isotope results are expressed in conventional notation as the per mil deviation from the Vienna Peedee Belemnite standard- $\delta^{18}O$ (‰ VPDB) and $\delta^{13}C$ (‰ VPDB). One sigma analytical uncertainties are within ±0.10‰ for both isotopes. Replicate measurements of $\delta^{18}O$ and $\delta^{13}C$ had an average standard deviation of 0.10‰ and 0.05‰, respectively.

Weight percent nitrogen and carbon, nitrogen and carbon isotopic composition, and the atomic C/N ratio were measured at 4-cm intervals. Samples were covered in 1 M HCl for 24 hours to dissolve carbonate minerals and rinsed with water. Samples were then lyophilized and analyzed at the Regional Stable Isotope Laboratory for Earth and Environment Science Research at the University of Pittsburgh using a Eurovector Elemental Analyzer and Isoprime Dual Inlet Isotope Ratio Mass Spectrometer. Organic carbon isotopes are expressed in conventional notation as the per mil deviation from the Vienna Peedee Belemnite standard- $\delta^{13}C_{org}$ (‰ VPDB) whereas nitrogen isotopes are reported relative to atmospheric N_2- $\delta^{15}N$ (‰). One sigma analytical uncertainties are within ±0.14‰ for $\delta^{13}C_{org}$ and ±0.20‰ for $\delta^{15}N$. Replicate measurements of $\delta^{13}C_{org}$ and $\delta^{15}N$ had an average standard deviation of 0.30‰ and 0.5‰, respectively.

Weakly sorbed metal concentrations were measured at 3-cm intervals. All samples were lyophilized and homogenized prior to analysis. Elements were extracted by reacting samples with 10 mL of 1 M HNO_3 for ~24 hours (Graney et al., 1995). The supernatant was extracted and diluted before measurement on an inductively coupled plasma mass spectrometer (ICP-MS) at the University of Pittsburgh. Blanks were run every 10 samples to check for bleed through and concentrations arising from memory effects were consistently below detection limits. Duplicates were run every 10 samples and were generally within 10% of each other.

6.3 RESULTS

6.3.1 Geochronology

Radiocarbon ages were measured on four terrestrial macrofossils, with one excluded from the age model (**Table 6-2)**. This date was excluded since it was an age reversal- it is older than would be expected on the basis of the three other radiocarbon ages. This may be because the date was comprised of mixed material (charcoal and a leaf). Given that this date is older than would be expected on the basis of the three other radiocarbon ages, we have chosen to exclude this date. The large age ranges on the radiocarbon dates from 55.5 and 107.75 cm are due to uncertainty in the radiocarbon calibration curve (Reimer et al., 2009). The upper 19 cm of the core were dated using the constant rate of supply (CRS) ^{210}Pb age model method (**Table 6-3)** (Appleby and Oldfield, 1983). On the basis of ^{210}Pb dating as well as three AMS radiocarbon dates, a smooth spline age model was produced using *clam* 2.1 code (Blaauw, 2010) in the statistical software package, "R" (R Core Development Team, 2008) (**Figure 6-1)**. Uncertainty in the age model is generally ±150 years. The 123 cm of collected core spans the last 900 years.

Table 6-2- AMS radiocarbon dates for samples from Chenghai Core A-12.

UCI Number	Composite Core Depth (cm)	Material	^{14}C age (BP)	Error ±	Median Probability Calibrated Age (yr AD)	2σ Calibrated Age Range (yr AD)
116867	55.5	Charcoal and leaf	185	20	1769	1952-1663
*116868	67.5	Charcoal and leaf	425	20	1450	1482-1434
122326	107.75	Wood and charcoal	400	15	1462	1609-1444
122327	119	Grass and charcoal	845	20	1198	1252-1161

*denotes date excluded from age model

Table 6-3- Down-core ^{210}Pb activities, ^{214}Pb activities, cumulative weight, and CRS sediment ages from Chenghai Core A-12.

Depth (cm)	^{210}Pb activity, Bq-g^{-1}	1σ Error ^{210}Pb activity	^{214}Pb activity, Bq-g^{-1}	1σ Error ^{214}Pb activity	Cumulative Weight, g cm^{-2}	CRS age (yr AD/BC)	1σ Error Age
2.0-3.0	0.1410	0.0165	0.0433	0.0035	0.3465	2008	1.94
4.0-5.0	0.1170	0.0131	0.0421	0.0032	0.8142	2004	2.11
6.0-7.0	0.1110	0.0138	0.0330	0.0030	1.3284	1999	2.38
8.0-9.0	0.0946	0.0107	0.0284	0.0022	1.9650	1991	2.80
10.0-11.0	0.0843	0.0107	0.0300	0.0027	2.7930	1981	3.63
12.0-13.0	0.0755	0.0090	0.0314	0.0023	3.7985	1966	5.27
14.0-15.0	0.0509	0.0075	0.0367	0.0028	5.1036	1957	6.17
16.0-17.0	0.0564	0.0083	0.0347	0.0028	6.3755	1935	10.39

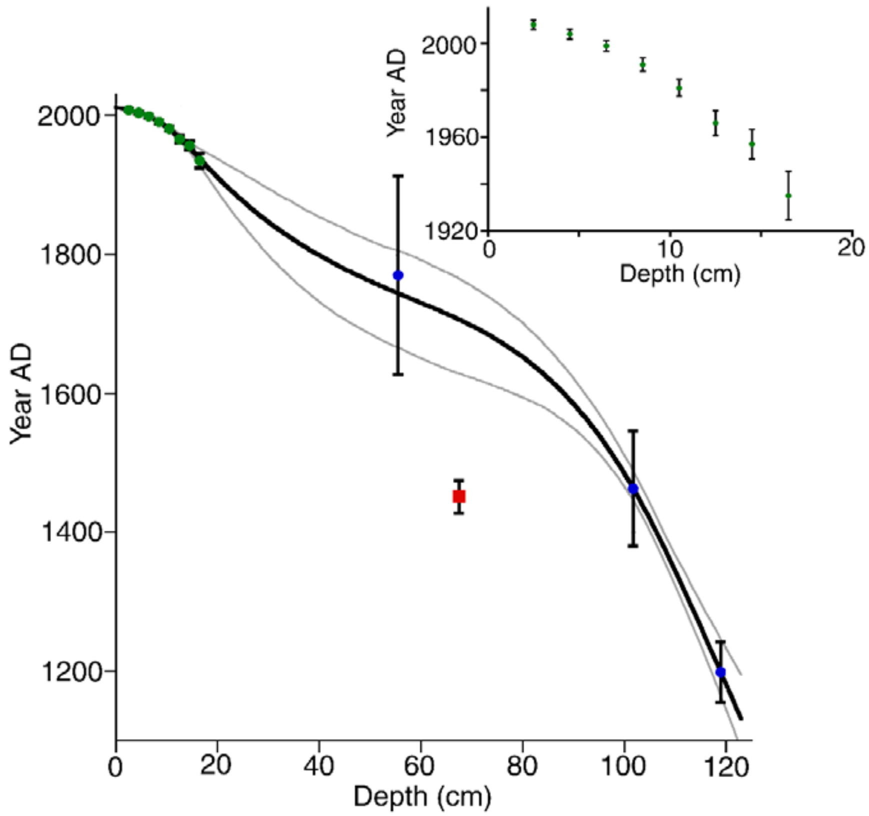

Figure 6-2- Age-depth model with 95% confidence intervals. ^{210}Pb dates (green circles), radiocarbon dates (blue squares), excluded radiocarbon date (red circle), all with 2 sigma error bars. ^{210}Pb dates with 2-sigma error bars in inset.

6.3.2 Geochemistry

The entire 123 cm of the core is composed of reddish, fine-grained clay, similar in composition to what has been found in the upper sections of sediment cores from other Yunnan lakes (see Chapters 2.0 and 5.0). These sediments have relatively high concentrations of iron (between 1-2%) and quartz. Scanning electron microscopy (SEM) and X-ray diffraction (XRD) samples taken evenly spaced down the core indicate that the primary carbonate mineral is authigenic aragonite (**Figure 6-3)** that ranges between 5 and 10% down the length of the core.

Jinglu et al., 2004 found calcite in the Chenghai cores via XRD analysis; however, we have both XRD peaks and SEM pictures down the entire length of the core confirming the presence of aragonite and the absence of calcite. Moreover, given the high magnesium concentrations observed in the Chenghai surface waters (Mg/Ca ratio ~ 12) (Whitmore et al., 1997), the presence of aragonite is not unexpected.

A- Chenghai A12 Core, 40 cm

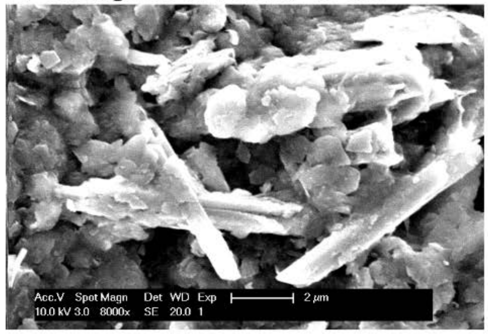

B- Chenghai A12 Core, 80 cm

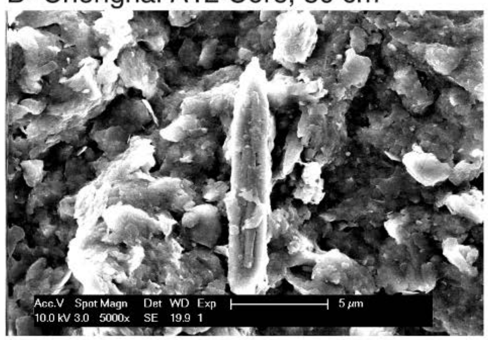

C- Chenghai A12 Core, 120 cm

Figure 6-3- Scanning electron microscopy (SEM) images of euhedral aragonite from Chenghai A-12 cores.

6.3.2.1 Unit I- 1150-1360 AD

Between 1150 and 1360 AD, sedimentation rates are stable at 0.06 cm/year. Oxygen and carbon isotopes exhibit high covariance, with an R^2 value of 0.80 (**Figure 6-4**). Additionally, oxygen and carbon isotopes of aragonite show a gradual trend towards higher values, from -7.0‰ to -6.4‰ and 0.0‰ to +1.7‰, respectively (**Figure 6-5**). Carbon isotope values shift towards lower values from +1.7‰ to +0.3‰ in the last 50 years of Unit I. The composition and isotopic signature of the organic matter is relatively stable with an average C/N ratio of 6.8, $\delta^{13}C_{org}$ value of -24.4‰, and $\delta^{15}N$ value of +3.7‰. Concentrations of copper are highest at the base of the core peaking at 61 μg/g, as do several other metals (Al, Co, Fe, Ti, and Zn- **Figure 6-6**). Magnetic susceptibility values display similar trends with a maximum of 543 10^{-5} m^3/kg at the base of the core. Concentrations of Pb exhibit different variations, remaining low and averaging 14±0.2 μg/g. Weight percent organic matter and aragonite are relatively constant throughout the entirety of the record, ranging between 7-10% and 5-10%, respectively.

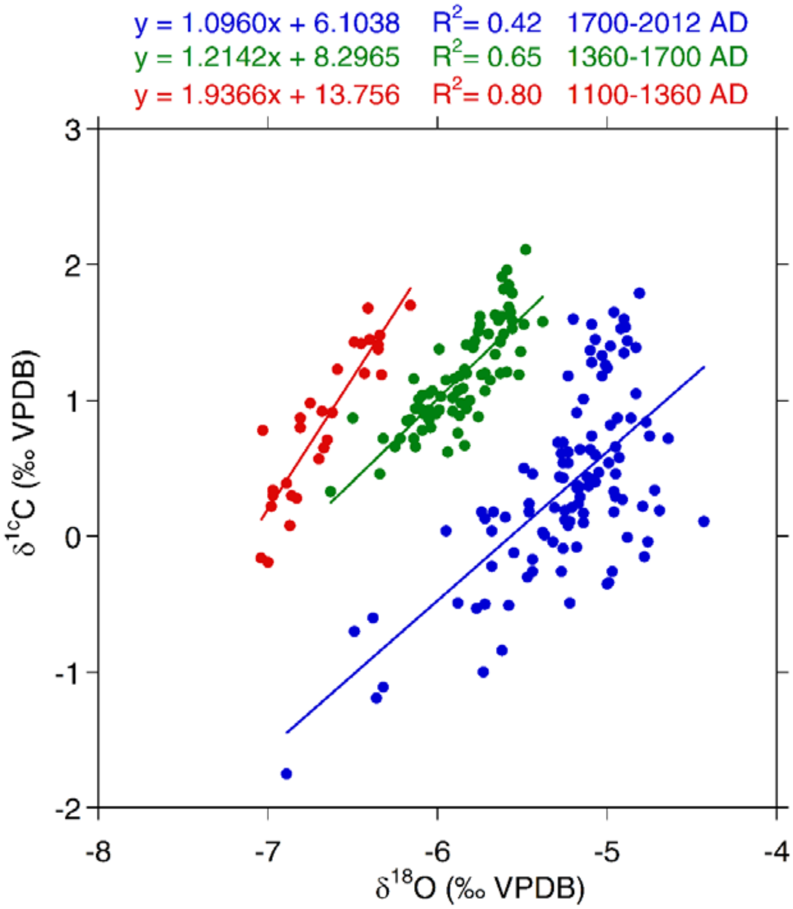

Figure 6-4- Isotopic covariance of Chenghai for three time periods; Unit I (1100-1360 AD) in red, Unit II (1360-1700 AD) in green, and Unit III (1700-2012 AD) in blue.

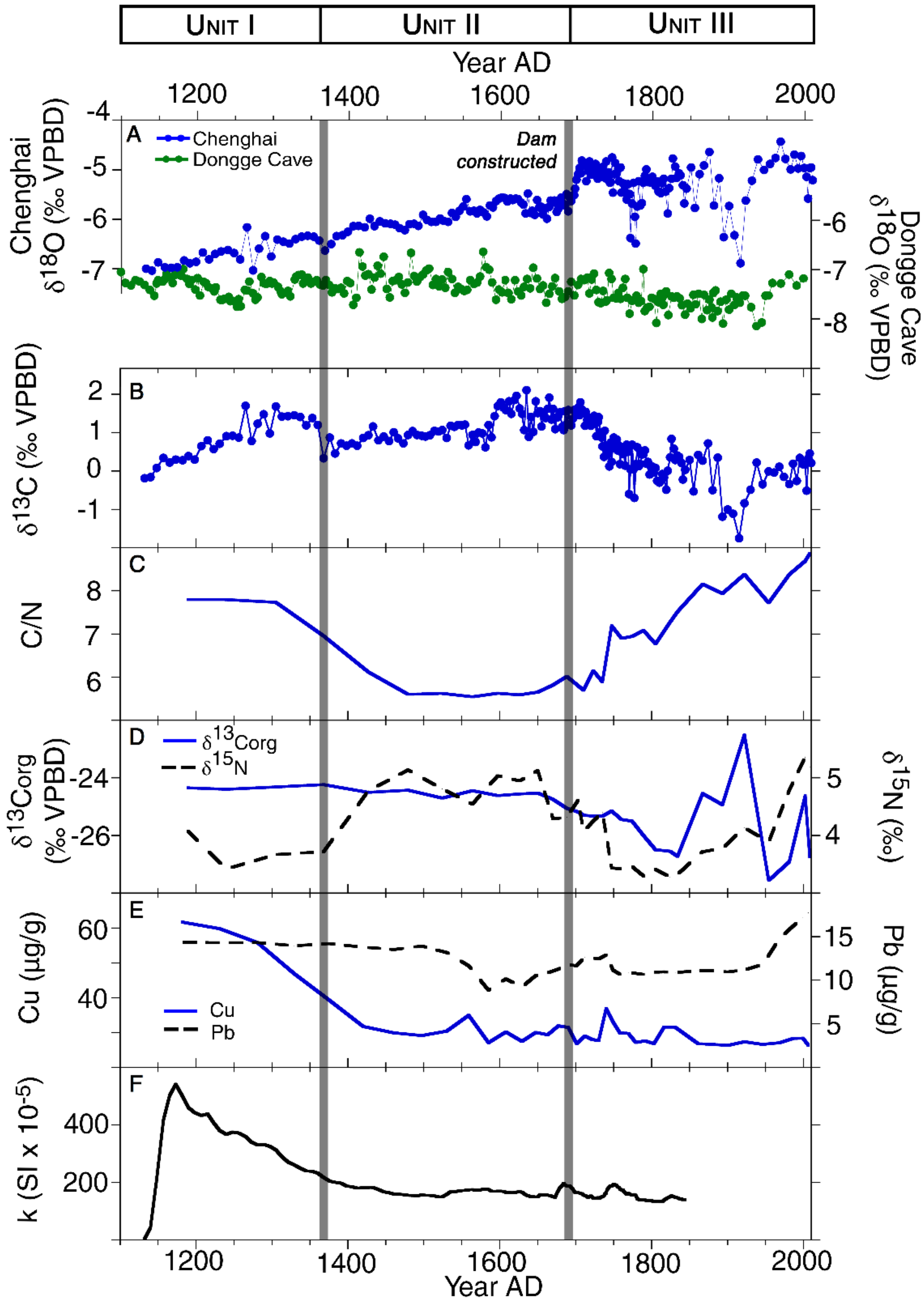

Figure 6-5- A- Oxygen isotopic composition of aragonite from Chenghai in blue, oxygen isotopic composition from Dongge Cave in green; C- Carbon isotopic composition of aragonite; C- Carbon to nitrogen ratio; D- Carbon isotopic composition of organic matter (blue solid line), nitrogen isotopic composition of organic matter (black dotted line); E- Concentration of copper (blue solid line), concentration of lead (black dotted line); F- Magnetic susceptibility.

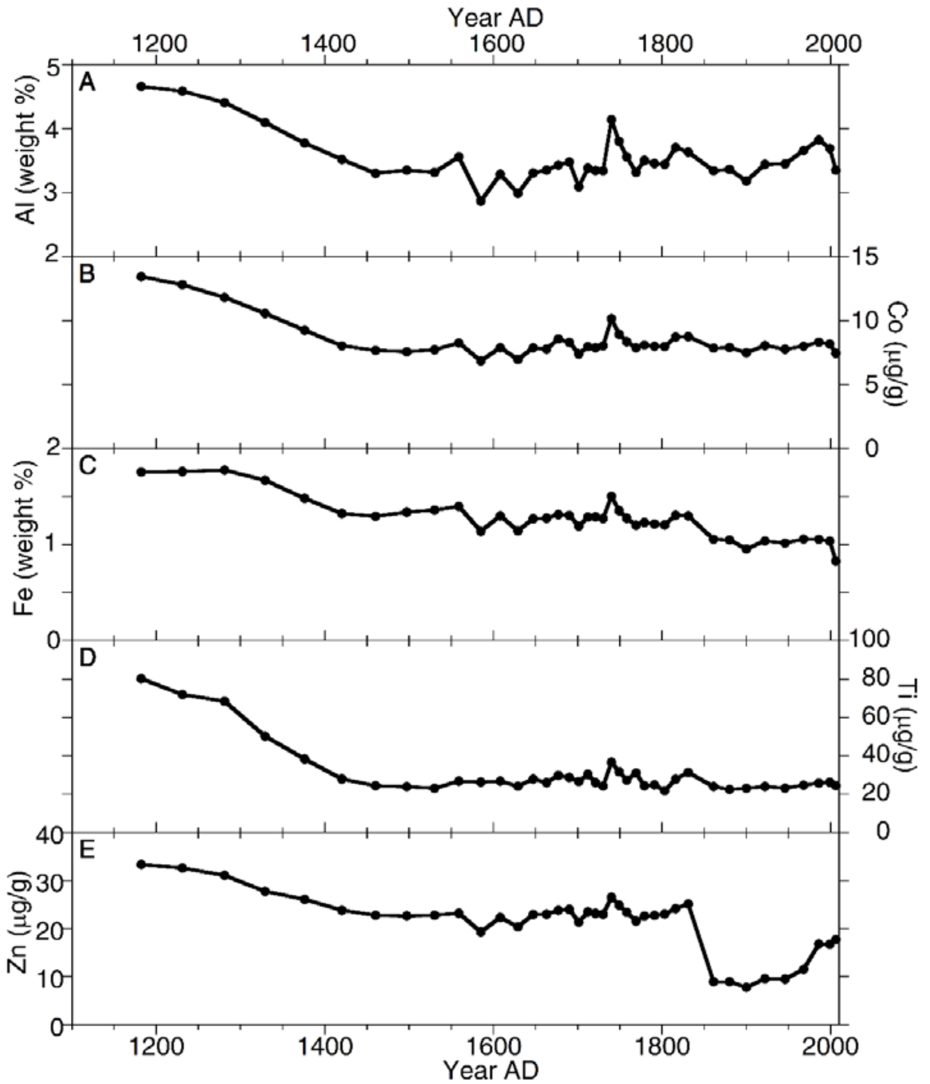

Figure 6-6- Concentrations of weakly bound metals from Chenghai. A) Al, B) Co, C) Fe, D) Ti, E) Zn.

6.3.2.2 Unit II- 1360-1700 AD

Sedimentation rates increase slightly to 0.10 cm/year and the most substantial changes during this unit occur in the $\delta^{18}O$ and $\delta^{13}C$ values. Carbon isotope values slowly increase to +2.0‰ and oxygen isotope values continue to slowly increase by ~1‰ from -6.4‰ to -5.5‰ (**Figure 6-5**). Oxygen and carbon isotopes exhibit slightly lower covariance, with an R^2 value of 0.65 (**Figure 6-4**). Organic carbon isotope values are stable at -24.6‰. Other variables in Unit II decline to a minimum at 1570 AD including C/N (4.5), copper (Cu) concentrations (27 µg/g), and magnetic susceptibility (between 150 10^{-5} m^3/kg), while $\delta^{15}N$ values increase to a maximum of +5.1‰ and remain generally high during the middle of this time unit. Lead (Pb) concentrations decrease slightly and become more variable during this interval, declining to an average of 12±2 µg/g.

6.3.2.3 Unit III- 1700 AD-present

From 1700 to 1830 AD, there are shifts of +1.5‰ in $\delta^{18}O$, -2‰ in $\delta^{13}C$, -2‰ in $\delta^{13}C_{org}$, and -1.5‰ in $\delta^{15}N$ (**Figure 6-5**). Sedimentation rates also increase 3-fold to 0.30 cm/year. After 1700 AD, the isotopic variability in the aragonite isotopes increases, with high year-to-year variability. Covariance between oxygen and carbon isotopes decreases slightly to an R^2 value of 0.42 (**Figure 6-4**). A negative isotopic excursion occurs from 1890-1930 AD; $\delta^{18}O$ values shift by -1.5‰, $\delta^{13}C$ values shift by -2.5‰, $\delta^{13}C_{org}$ values shift by +4‰, and $\delta^{15}N$ values shift by +1‰. By 1940 AD, these isotopes return to their pre-excursion values, with the exception of $\delta^{15}N$ which increases to +5‰. Magnetic susceptibility and concentrations of both Cu and Pb remain roughly the same. Carbon to nitrogen ratios steadily increase throughout Unit III to a maximum of 7.9. Concentrations of Pb increase to 18 μg/g within the last 40 years consistent with the use of leaded gasoline.

6.4 DISCUSSION

6.4.1 Isotopic Interpretation

Chenghai water samples suggest that a large portion of lake water is lost through evaporation (**Figure 1-3**), so lake water isotope values should reflect the balance between precipitation and evaporation (P/E). One challenge with this approach is in differentiating between changes in lake level due to human modification as opposed to changes in precipitation-evaporation balance from natural variability associated with the ASM. Variations in the isotopic composition of precipitation are recorded in speleothem carbonate stable isotopes at Dongge Cave in the Guizhou province, ~500 km east of Chenghai (Wang et al., 2005) (**Figure 6-1**) and can be used as a comparative dataset for this study to control for lake water isotope changes that are due to monsoonal variation. We use the Dongge Cave record as our primary comparative dataset because of the cave's proximity to Chenghai, the similarity in climate (**Tables 6.1 and 6.4**), and the well-dated, high-resolution nature of the record. The difference between Lijiang and Dongge Cave annual weighted $\delta^{18}O$ means of modern rainfall are offset by ~1.5‰ (**Tables 6.1 and 6.4**).

Table 6-4- Monthly average temperature, precipitation, and oxygen isotope values at Dongge Cave (25°17’N, 108°50’E, 680 m) (Dykoski et al., 2005).

	Jan	Feb	Mar	April	May	June	July	Aug	Sept	Oct	Nov	Dec
Average Temperature (°C)	5.2	9.9	11.3	16.3	19.7	22.1	23.5	22.8	20.8	16.4	11.4	7.2
Average Precipitation (mm)	29.8	36.7	55.7	135.7	237.8	305.4	324.2	292.3	124.8	116.4	61.8	32.5
$\delta^{18}O$ (‰VSMOW)	-4.72	-3.45	-4.47	-2.82	-5.16	-7.99	-12.42	-9.67	-12.48	-10.06	-6.99	-5.43

Average weighted $\delta^{18}O$ (‰VSMOW) = -8.33

We calculated the theoretical $\delta^{18}O$ value of aragonite using **Equation 6-1**:

$$1000 ln\alpha(\text{Aragonite-H}_2\text{O}) = 17.88(10^3 T^{-1}) - 31.14$$

Equation 6.1 (Kim et al., 2007)

where T = 31.2°C, the maximum August water temperature of Chenghai (Wan et al., 2005). Given the observed $\delta^{18}O$ value of -1.63‰ VSMOW from the water sample collected in 2009, the $\delta^{18}O$ value of aragonite precipitated in or around August should be -5.34‰ VPDB. This value is very close to the $\delta^{18}O$ value of aragonite in the surface sediments (-5.55‰). Since the images obtained using the SEM display euhedral aragonite down the entire length of the core and these calculations suggest that the aragonite is precipitating in equilibrium with the water column, we interpret the $\delta^{18}O$ values to primarily reflect changes in lake water balance.

6.4.2 Unit I- Anthropogenic Disturbance

The geochemical and isotopic shifts in Unit I can be primarily attributed to anthropogenic rather than natural factors. The color, composition, and geochemical variations observed in these sediments are similar to both catchment soils and those of sediment cores from other Yunnan lakes such as Qilu, Xing Yun, and Dian (**Figure 6-1**) that have been heavily impacted by anthropogenic activities (Brenner et al., 1991; Hillman et al., 2014; Sun et al., 1986; Whitmore et al., 1994a). While our sediment core does not extend back far enough to capture low, stable, background inputs of variables such as Cu or magnetic susceptibility, we interpret the high values of these parameters at 1150 AD to indicate human disturbance within the catchment. Given the long history of activities such as copper metallurgy at nearby archaeological sites

(Chiou-Peng, 2009; Hillman et al., 2015; Yao, 2010), it is likely that these activities contributed to a variety of metal loadings on the landscape through atmospheric transport that later entered the lake system via erosion. There are few historical records in this region of Yunnan that aid in the interpretation of these variables, and thus the timing of the initial anthropogenic impact on the lake is unclear. We hypothesize that a major change in land-use, such as clearance for agricultural activity, may have occurred sometime prior to 1150 AD leading to erosion and transport of a large amount of clastic material into the lake. This interpretation is supported by slightly higher C/N ratios than subsequent units (**Figure 6-5**), suggesting an increased proportion of terrestrial organic matter in the sediments (Meyers, 1994).

Previous studies of the Chenghai oxygen and carbon isotope record did not extend back as far as our Unit I interval (Chen et al., 2002; Jinglu et al., 2004). We interpret the $\delta^{18}O$ and $\delta^{13}C$ values in Unit I to indicate that the lake was a closed basin system during this period. While historical observations suggest that Chenghai was not a closed basin until dams were constructed in 1690 AD (Wan et al., 2005), we suggest an alternative hypothesis that Chenghai has been hydrologically closed since at least 1150 AD. The high degree of isotopic covariability between $\delta^{18}O$ and $\delta^{13}C$ values (R^2=0.80) (**Figure 6-4**) is usually interpreted to represent hydrologically closed conditions (Li and Ku, 1997; Talbot, 1990). Additionally, the $\delta^{18}O$ values of Chenghai at 1150 AD (-7.0‰) are very close to the $\delta^{18}O$ values of the Dongge Cave record at 1150 AD (-7.2‰) (**Figure 6-5**), but the annual weighted $\delta^{18}O$ means of modern rainfall are offset by ~1.5‰ (**Tables 6.1 and 6.4**). This suggests that if Chenghai were an open basin, $\delta^{18}O$ values should actually be 1.5‰ more negative than what we observe based on modern meteorological data.

While DEMs indicate that Chenghai was once likely a throughflow system, linking the Jinsha and Haikou Rivers, it is not clear how long ago this may have been. It is possible that the Haikou River throughflow was restricted prior to 1690 AD and that Chenghai had been lowering for some time beforehand; historical records before 1690 AD are lacking on such details. Alternatively, if Haikou River throughflow was not limited, Chenghai may have behaved as a closed basin system dominated by evaporation due to minimal surficial outflow. In closed basin lakes, shifts in oxygen isotopes towards higher values are traditionally interpreted to represent increased evaporation and/or less precipitation (Talbot, 1990). The Little Ice Age (LIA) is a time period of known aridity (Morrill et al., 2003) and cooler temperatures (Mann et al., 2009) Southwestern China; however, the timing of the LIA does not match closely with the observed changes in Unit I. While the initiation of the LIA in Asia is spatially and temporally variable (Morrill et al., 2003), changes are usually observed beginning ~1300 AD, by which time Chenghai $\delta^{18}O$ values already display a significant positive trend. Furthermore, the sustained, long-term trend towards higher $\delta^{18}O$ values throughout the entire 900 year record suggests that climatic variability is not the primary cause of this shift.

Analysis of authigenic calcite and other proxies from Xing Yun lake sediment, also in Yunnan Province (**Figure 6-1**), found that a long-term gradual trend towards lower lake levels beginning at 500 AD also could not be explained by climate variability and was the result of human modification of the catchment, which had a substantial influence on water balance (see Chapter 2.0). The Chenghai record does not extend back in time far enough to determine when the initial change in water balance occurred nor how abrupt this transition might have been. However, both the geochemical and isotopic variations throughout Unit I suggest the primary driver of change was anthropogenic activity, possibly related to the expansion of agriculture.

Future work is required to extend this sediment core record further back in time to capture the timing and magnitude of the initiation of this human disturbance.

6.4.3 Unit II- Landscape Stability

The slow and steady decrease in $\delta^{18}O$ values suggests the continued, gradual lowering of lake level (**Figure 6-5**) which may have resulted in part from catchment water diversion for agriculture. This time period does encompass the LIA, which resulted in increased aridity due to reduced monsoon strength (Morrill et al., 2003), and may have contributed to lower lake levels as well as the need for freshwater resources to sustain agriculture. Without a more regional paleoclimate record or more extensive historical records, it is difficult to more confidently attribute these changes to any one variable, highlighting the challenges of disentangling the roles of climate variability from anthropogenic manipulation. Small decreases in $\delta^{13}C$ values take place, causing the covariability to slightly drop through this interval (**Figure 6-4**). The $\delta^{18}O$, $\delta^{13}C$, and $\delta^{13}C_{org}$ values through Unit II agree with previous work done on Chenghai in the context of age model uncertainty (Jinglu et al., 2004) (**Figure 6-7**).

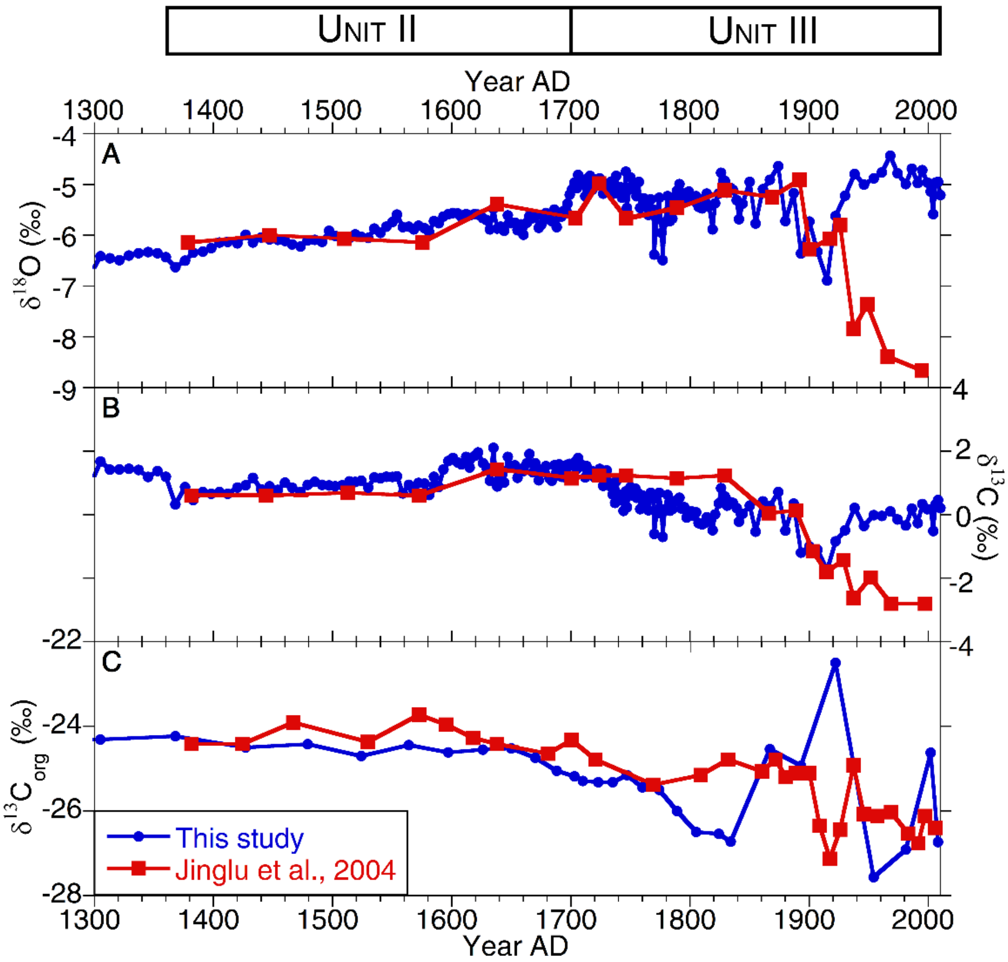

Figure 6-7- Comparison between our study (blue circles) and Jinglu et al., 2004 (red squares). A) $\delta^{18}O$, B) $\delta^{13}C$, C) $\delta^{13}C_{org}$. There is good relatively agreement between this study and the previous study prior to 1900 AD.

Magnetic susceptibility, Cu, and C/N values, which were high, begin to decline in Unit I with further, more substantial declines in Unit II. This suggests less erosional input and less terrestrial organic matter delivery to the lake. We hypothesize that this resulted from a period of landscape stabilization from the previous intensive land use change of Unit I, though the sedimentology (color, grain size, etc.) does not noticeably change. These changes may have been balanced by an increase in aquatic primary productivity, demonstrated by lower C/N ratios and higher $\delta^{15}N$ values, though the absolute values of these changes are relatively small (2 and 1.5‰, respectively). Notably there is no accompanying change in $\delta^{13}C_{org}$ values. While $\delta^{15}N$ and C/N are negatively correlated with an R^2 value of 0.53, $\delta^{13}C_{org}$ and C/N display no relationship (**Figure 6-8)**. This implies that $\delta^{15}N$ values are influenced by the source of organic matter with more positive values occurring when the aquatic flux of organic matter is high. Conversely, $\delta^{13}C_{org}$ values are controlled by more factors than simply the source of organic matter, perhaps explaining why there is no concomitant shift in $\delta^{13}C_{org}$ values with $\delta^{15}N$ and C/N. The $\delta^{13}C_{org}$ values may be more strongly influenced by variables such as carbon cycling within the lake and primary productivity.

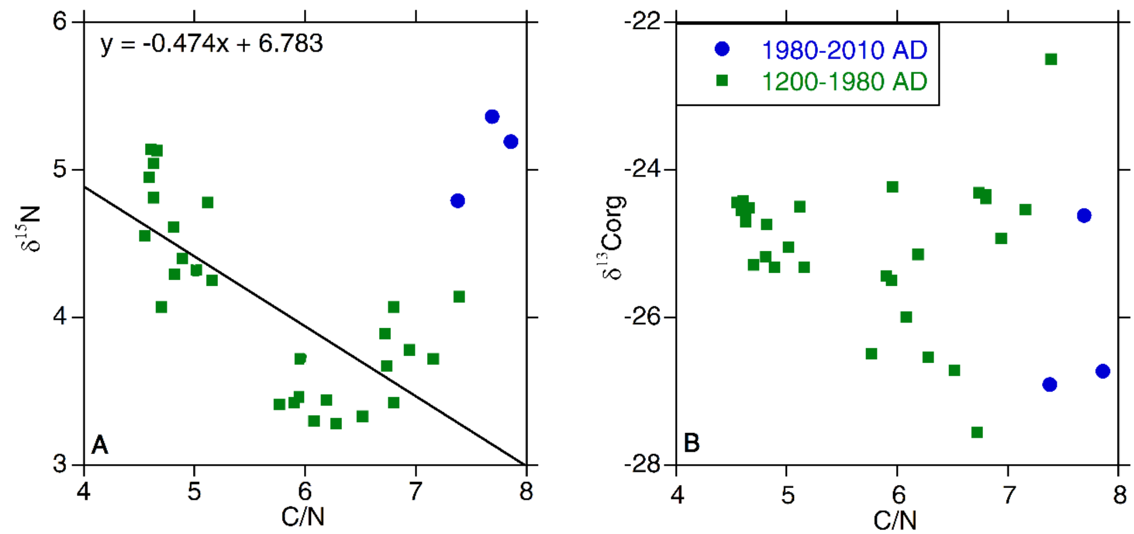

Figure 6-8- A) C/N versus $\delta^{15}N$ with a linear regression (R_2 = 0.53, $p < 0.001$). Data from 1980-2010 AD has anomalously high C/N and $\delta^{15}N$ values and was excluded from the regression; B) C/N versus $\delta^{13}C_{org}$ showing no relationship.

6.4.4 Unit III- Hydrologic modification

The substantial increase in sedimentation and the isotopic shifts that take place at 1700 AD (**Figure 6-5**) coincide closely with the construction of a dam upstream of the lake at 1690 AD (Jinglu et al., 2004; Wan et al., 2005). After the dam was constructed, historical records indicate the Haikou River stopped flowing through the lake (Wan et al., 2005), causing Chenghai to receive water only from precipitation as groundwater throughflow is limited (Jinglu et al., 2004). Our record shows that this hydrologic modification caused the lake level decline to temporarily accelerate and changed the lake water budget such that an even larger proportion of water loss occurred via evaporation, causing higher oxygen isotope values. The high variability in both $\delta^{18}O$ and $\delta^{13}C$ values throughout Unit III suggest that lake levels fluctuated over short periods of time (Steinman et al., 2010). It is difficult to assess the validity of the historical observations that suggest that Chenghai dropped by 40 m from this period at ~1690 AD to present (Wan et al., 2005). While our oxygen isotope record certainly suggests that substantial water loss occurred, a considerable, sustained drop of 40 m seems unlikely. If such a large lake level decline did occur, a shift larger than +1.5‰ in oxygen isotope values should be present in the sediment record, and 2) a long-term, monotonic trend towards higher $\delta^{18}O$ values throughout the whole of Unit III should be present. The high variability and the return to lower oxygen isotope values later in Unit III (ca. 1890 AD) suggests that while lake levels did decline, they did not do so continuously throughout after the dam was constructed.

The trend toward lower $\delta^{13}C$ values beginning at 1700 AD may be due to the oxidation and dissolution of organic matter at the shoreline influencing the dissolved inorganic carbon (DIC) pool. Both terrestrial and aquatic organic matter, being relatively depleted in ^{13}C, would have been exposed due to lake level decline. This organic matter could have oxidized and produced isotopically light CO_2 which then percolated into the lake and became incorporated into the DIC pool (Hammarlund et al., 1997). Although groundwater throughflow is limited in the Chenghai system, plant respiration and CO_2 exchange within the soil may still influence the carbon isotopic signature of inputs to the lake. The covariance of aragonite $\delta^{13}C$ and $\delta^{18}O$ values in Unit III is lower ($R^2 = 0.42$) than the Unit I (**Figure 6-4**), which is likely a result of the above explained mechanism rather than a wetter climate resulting in hydrologically open basin conditions.

It is also at 1700 AD that $\delta^{13}C_{org}$ and $\delta^{15}N$ values decrease and C/N ratio increases, both suggesting a slightly increased proportion of terrestrial organic matter delivery to the lake sediments (Meyers, 1994). While these C/N ratios are still well within the range of values expected for aquatic organic matter, the small change does suggest that more terrestrial organic matter was transported to the coring site due to lake level decline. Newly exposed sediment at the shoreline would have consisted of both terrestrial and aquatic organic matter, thus explaining why C/N ratios do not display a larger shift. Small increases in metal concentrations (Cu- **Figure 6-5**, Al and Fe- **Figure 6-6)** may also indicate increased clastic input associated with this lake level change.

Taken together, the isotopic shifts in both organic matter and aragonite that take place at 1890 AD suggest increased primary productivity and higher lake levels, possible due to the precipitation and warmer temperatures associated with the termination of the LIA. Since there are no historical indications of anthropogenic manipulation of lake hydrology at this time, we believe that the observed changes at 1890 AD in the Chenghai record are primarily driven by natural climate variability. In light of the potential for substantial spatial heterogeneity in precipitation due to orographic effects, the decline at 1890 in $\delta^{18}O$ values at Chenghai may represent the local expression of the overall return to wetter conditions for the Southwestern Yunnan region exhibited by the Dongge Cave record (Wang et al., 2005) (**Figure 6-5**). The lack of a concomitant change in C/N ratios or $\delta^{15}N$ values suggests that the source of organic matter did not change and that the shift in $\delta^{13}C_{org}$ values may be due to increased productivity associated with warmer temperatures. Weight percent organic matter does begin to increase around this time (**Figure 6-9**).

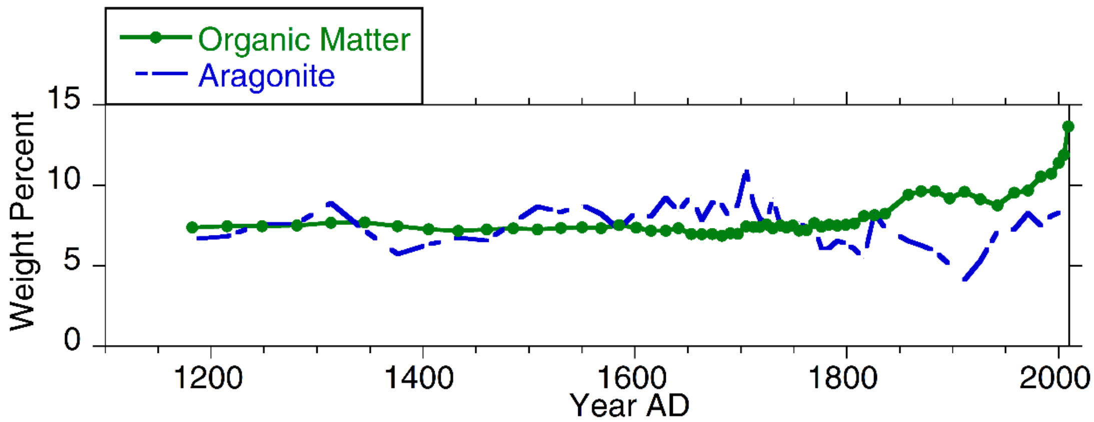

Figure 6-9- Weight percent organic matter estimated from LOI 550 (green circles) and weight percent aragonite estimated from LOI 1000 (dashed blue line).

The oxygen and carbon isotope records presented here are largely consistent with a previous study of Chenghai (Jinglu et al., 2004), albeit the resolution of our record is higher and consequently exhibits greater high frequency variability (**Figure 6-7**). For example, this previous study of Chenghai also recorded a shift in $\delta^{18}O$ of +1‰ at 1700 AD, a shift of -2‰ at 1900 AD, and a shift in $\delta^{13}C$ of -3‰ at 1900 AD. However, there are notable differences in the carbon isotopic composition of organic matter reported by our study and this prior investigation, in that Jinglu et al. (2004) only observed a -2‰ shift in $\delta^{13}C_{org}$ values at 1600 AD instead of the -4‰ shift we measured. Additionally, while we observe a +5‰ shift beginning at 1840 AD, Jinglu et al., 2004 observed a -3‰ shift. They noted that this was inconsistent with an increase in blue-green algal pigments, such as oscillaxanthin and myxoxanthophyll, which were interpreted to represent a more eutrophic phytoplankton assemblage (Jinglu et al., 2004). Reasons for the difference between the results presented here and the previous one are unclear; the broad agreement of oxygen and carbon isotopes of aragonite suggest that it is not due to disparity in age models. The sediment core analyzed in Jinglu et al., 2004 was taken closer to the deepest part of the lake, which may have had differing amounts and types of organic matter than our coring location. Given the dramatic lake level fluctuations that have taken place within the last several hundred years, the remobilization of organic matter from the shoreline and catchment may, in part, contribute to some of these differences.

Lastly, the higher nitrogen isotope values after 1930 AD are due to the expansion of agriculture and increased fertilizer use in the lake catchment, which was documented by Jinglu et al., 2004. This precipitated a shift in the trophic status of the lake as well as lower lake levels due to catchment water diversion for rice agriculture. Further increases in weight percent organic matter also occur around the same time (**Figure 6-9**). Our data through this interval differs significantly from the previous studies of Chenghai, which documented lower $\delta^{18}O$ and $\delta^{13}C$ values of 1-2‰ in the upper 10-15 cm of the sediment core (Chen et al., 2002; Jinglu et al., 2004). This is unexpected given that lake level has recently declined (Whitmore et al., 1997), which should have driven $\delta^{18}O$ and $\delta^{13}C$ values towards higher (rather than lower) values. This assertion is further supported by the increase in the concentration of dissolved ions such as Mg^{2+}, Na^{+}, and Fe^{3+} and the overall lake salinity. The highest $\delta^{18}O$ values of the entire record occur in this last 50 years, signifying the lowest lake levels of the past 900 years and the sensitivity of the lake to recent climate change.

6.5 CONCLUSION

This study records substantial anthropogenic impacts to Chenghai Lake as a result of land use changes and catchment modification beginning by at least 1150 AD. The observed changes in $\delta^{18}O$ of authigenic aragonite demonstrate that the isotopic response of a lake to intentional, anthropogenic modification is similar to what would be expected for lower lake levels due to natural climate variability, that is, a shift towards higher $\delta^{18}O$ values due to evaporative enrichment resulting from negative precipitation-evaporation balance anomalies. The consequences of this anthropic activity can also be seen in the organic carbon cycle of the lake, as more terrestrial organic matter washed into the lake resulting from lake level lowering. This study underscores the idea that accurate interpretations of records of environmental variability in regions of the world where humans have settled in large numbers require historical and archaeological context. Furthermore, in such a setting where environmental geochemistry can be influenced by a myriad of factors, a multi-proxy approach can aid in disentangling the impacts of anthropogenic changes from more “natural” climate variability. This study adds to a growing number of paleolimnological studies in Yunnan that document substantial human-induced changes to lakes and their watersheds throughout the last several thousand years (Brenner et al., 1991; Whitmore et al., 1994a).

7.0 CONCLUSIONS

7.1 THE NATURE OF ANTHROPOGENIC IMPACTS TO YUNNAN LAKES

In answer to research question 1- **"To what extent can modern industrial pollution, eutrophication, land use change, and hydrologic modification of lakes on the Yunnan Plateau be regarded as a continuation of earlier human activities?"**, we find substantial evidence that the four Yunnan lakes investigated in this study have been influenced by anthropogenic activity for millennia. Moreover, the scale of such pre-industrial modifications are either equal or greater in magnitude than modern-day impacts.

Based on the geochemical nature of the observed anthropogenic impacts, we can divide the four Yunnan lakes into two groups: 1) Xing Yun, Dian, and Chenghai; 2) Erhai. Broadly speaking, the changes recorded in lake sediments from Group 1 include:

- Increased deposition of fine-grained, iron-rich, red clay
- Increased concentrations of elements such as iron and aluminum
- Increased magnetic susceptibility values
- Increased weight percentage of organic carbon and nitrogen
- Higher $\delta^{13}C_{org}$ and $\delta^{15}N$ values

These characteristics arise from two processes associated with land use change: 1) increased soil erosion from the lake catchment and subsequent sediment accumulation in the lake basin and 2) increased nutrient loading arising from agriculture and sewage causing cultural eutrophication of the lake.

The timing of these changes in similar at both Xing Yun and Dian- between 200 and 500 AD. Unfortunately, the sediment core from Chenghai does not extend far enough to capture the initiation of these sediment changes. At the very least we can conclude that since 1150 AD, substantial anthropogenic impacts have occurred at Chenghai. While the timing of changes at Xing Yun and Dian is similar, the shifts seen in Dian are not as dramatic or dynamic as the ones seen in Xing Yun. Dian is a much larger lake than Xing Yun with a surface area and catchment area approximately 10 times larger. Dian likely responds less sensitively to changes occurring in the watershed and perturbations must be of a larger magnitude to be recorded. Alternatively, the observed differences in the variables may be due to lower sedimentation rates in Dian (averaging 0.07 cm/year over the last 1,800 years in the A-12 cores) compared to Xing Yun (averaging 0.13 cm/year over the last 1,500 years) and consequent lower sampling resolution.

Erhai is the only lake in Group 2 where the anthropogenic impact is generally characterized only by an increased concentration of heavy metals such as lead, zinc, cadmium, silver, and copper. These impacts arise from a combination of two processes: 1) land use change arising from agriculture and 2) atmospheric pollution associated with silver smelting. Initial disturbance in the form of increased sediment accumulation and concentrations of metals takes place between 250 and 400 AD associated with agricultural activities. However, from 1100-1300 AD, the increased concentrations of metals likely occurs due to atmospheric pollution.

Unlike the lakes in Group 1, the timing of these two processes do not appear to be directly connected.

The division of these two groups does not fall out along geographic boundaries (east/west) or physical lake characteristics (**Table 1-1**). This is contrary to the initial hypothesis that the magnitude and/or timing of anthropogenic impacts might span a geographic gradient since archaeological and historical records suggest that the eastern and western parts of Yunnan have had differing cultural traditions (Elvin et al., 2002; Higham, 1996). Additionally, the hypothesis that Xing Yun and Chenghai would be the most disturbed lake-catchment systems was disproven since all lakes appear to be equally impacted by human activity.

The difference between Group 1 and 2 is likely due to the differing catchment soil types since Erhai is surrounded by lithosols whereas Xing Yun, Dian, and Chenghai are surrounded by chromic luvisols (Fengrang, 1990) (**Figure 7-1)**. Lithosols are shallow and underdeveloped soils comprised mostly of rock fragments (Canarache et al., 2006) that limits the potential for catchment soil accumulation within the Erhai basin. By contrast, chromic luvisols are characterized by clay accumulation due to moderate amounts of weathering of limestone and are often reddish in color (International Soil Reference and Information Centre). The defining characteristic of Group 1 lakes is the accumulation of these chromic luvisols in the lake basin.

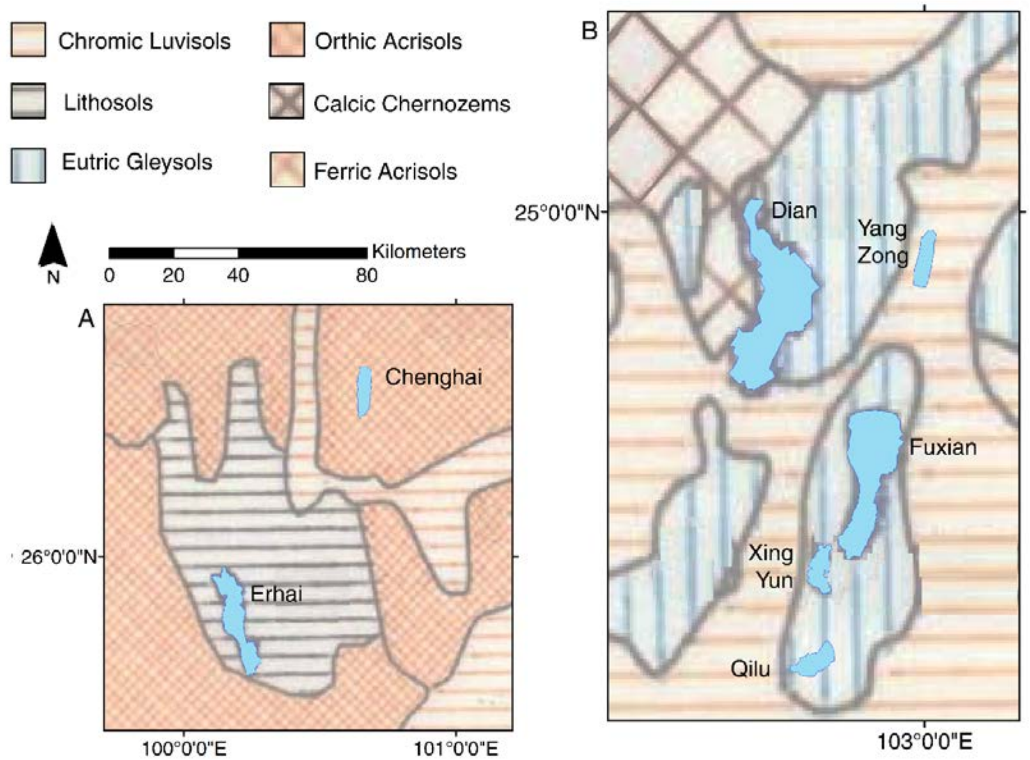

Figure 7-1- Soil map of A) Western Yunnan and B) Eastern Yunnan. Adapted from Fengrang, 1990.

A key finding of this research is that pre-industrial land use change has dramatically altered the geomorphology of southwestern China; this has important implications for the mobilization of sediments contaminated with heavy metals. As deforestation and land use change has already led to soil loss within many lake catchments in Yunnan, the mobility of this soil, likely high in concentrations of lead, silver, zinc, etc., may lead to further modern contamination problems.

Despite documented land use change, both pre-industrial (Elvin et al., 2002; Shen et al., 2006) and modern (Wang et al., 2004), Erhai does not display signs of cultural eutrophication like the Group 1 lakes. While the isotopic composition of organic matter was not measured, Erhai sediments do not display increased concentrations of phosphorus like Xing Yun, Dian, and

Chenghai. This may be due to the lack of fine-grained clays in the Erhai catchment that can contribute a significant portion of bioavailable phosphorus to lakes through adsorption and can result in nutrient loading and eutrophication (Nowlin et al., 2005).

The timing of initial human disturbance at lakes Xing Yun, Dian, and Erhai appears to be quite similar (between 200 and 500 AD). However, the intensification of this disturbance occurs at slightly different times and matches closely with known historical and cultural changes- between 1100 and 1300 AD at Erhai and Xing Yun with the establishment of the Yuan Dynasty (the Mongols) and between 1500 and 1700 AD at Dian and Chenghai with the establishment and decline of both the Ming and Qing Dynasties. Both these periods encompass significant cultural changes and political upheaval.

The Mongols (ca. 1271-1368 AD) invaded Yunnan and formally annexed it, nominally making it part of Chinese territory (Giersch, 2009). This was accompanied by extensive building, land reclamation, and water works projects such as canals that fundamentally altered Yunnan lake hydrology (Herman, 2002; Sun et al., 1986). When the Mongol Dynasty declined and the Ming Dynasty (ca. 1368-1644 AD) replaced it, mining activity increased in Yunnan and Han immigrants began settling in the province (Yang, 2009). These Han immigrants brought iron plows with them and began extensively clearing land for the expansion of agriculture (Marks, 2012). Adding to the political upheaval, water shortages were noted during the early Ming Dynasty followed by slope instabilities and erosional problems in the late Ming (Elvin et al., 2002). These environmental problems intensified during the Qing Dynasty (ca. 1644-1911 AD) (Elvin et al., 2002) as Han immigrants were able to push into mountainous areas previously only accessed by the native populations, began practicing slash and burn agriculture with new crops, and expanded mining activity (Giersch, 2009; Yang, 2009). We suggest that the observed intensification of anthropogenically-driven lake-catchment changes is tightly coupled to the political and social changes taking place.

7.2 ISM VARIABILITY RECORDED IN YUNNAN LAKES

Only sediments from Xing Yun and Dian are old enough to extend beyond the influence of human modification, record natural environmental change, and address research question 2- “**What is the timing and nature of abrupt shifts in moisture associated with Indian Summer Monsoon (ISM) variability in the Pleistocene and Holocene?”**. These records have extended the spatial resolution of terrestrial hydroclimate variability of the ISM, that was previously limited to mostly short, non-continuous speleothem records (Berkelhammer et al., 2010; Fleitmann et al., 2003; Neff et al., 2001; Sinha et al., 2007) and ice caps (Thompson et al., 1989; Thompson et al., 1998).

Elemental concentrations of Xing Yun sediments, which are at least 50,000 years old, track changes in insolation, suggesting that the geochemical signal is primarily driven by weathering and erosion resulting from precipitation associated with monsoonal variability. This simple relationship breaks down from 42,000 to 35,000 years BP during Marine Isotope Stage 2 when Northern Hemisphere glaciers were extensive and likely caused the monsoon system to weaken significantly (deMenocal and Rind, 1993). The preliminary results of the transect core study at Dian also indicate low lake levels at 31-30 ka possibly due to a weakened ISM.

One of the most abrupt events in the past 20,000 years was the Younger Dryas cold event that caused a weakening of the entire monsoon system (Sinha et al., 2005; Wang et al., 2005; Wang et al., 2001) and was recorded in Dian sediments as an increase in dust arriving from the

Tibetan Plateau. An unconformity in Xing Yun sediments prevented this event from being recorded. The Holocene portion of the Xing Yun and Dian records are somewhat similar- both records suggest a sustained gradual trend towards lower lake levels beginning around 8,000 to 7,000 years BP. Further drops in lake level take place at 5,500 years BP in Xing Yun and 4,000 years BP in Dian associated with declining summer insolation. Other studies have suggested the possibility of this abrupt shift in aridity being linked with either North Atlantic cooling (Bond et al., 1997) or more frequent ENSO events (Moy et al., 2002), that has the general effect of weakening the ISM.

One notable difference between Xing Yun and Dian is the limnological response to declining summer insolation throughout the Holocene. At Xing Yun, C/N gradually declines while $\delta^{13}C_{org}$ and $\delta^{15}N$ values gradually increase, suggesting less terrestrial organic matter input as lake levels steadily dropped. However at Dian, we observe the opposite trend with gradually increasing C/N and decreasing $\delta^{13}C_{org}$ and $\delta^{15}N$ values indicative of more terrestrial organic matter being delivered to the lake as shelf areas became exposed. This may be due to the large differences in limnological characteristics. Dian is much larger in lake surface area, catchment surface area, and shoreline distance and has more potential shelf area exposure as lake levels drop.

All of these findings agree well with numerous previous findings that Northern Hemisphere monsoonal systems respond to forcing from average summer insolation (Cheng et al., 2012a) and that several abrupt shifts in monsoon strength took place over the Holocene in conjunction with North Atlantic cooling events (Morrill et al., 2003). Other lake sediment records from the Tibetan Plateau such as Paru Co (Bird et al., 2014) and Ahung Co (Morrill et al., 2006) appear to agree particularly well with the Xing Yun record. What Dian and Xing Yun reveal in the context of previous paleoclimate studies is that changes in the strength of the entire Asian Summer Monsoon system are broadly coherent from the Tibetan Plateau, through Yunnan, and across to central and eastern China. This geographic extent covers not just the ISM but also the EASM and yet changes in the two systems appear to be mostly coherent in terms of both character and timing, as has been noted by other researchers. The initial hypothesis was that differences in the timing of shifts between the ISM and EASM would be apparent. However, at this time, our records are neither well-dated enough nor sampled at a high enough resolution to determine this and this is a direction of future research.

7.3 LINKING HUMAN AND ENVIRONMENTAL CHANGE

We can learn from these four Yunnan lakes that an appropriate historical and archaeological context must be applied to the interpretation of lake sediment records in regions of the world with long histories of human occupation. Lacking this context, the analysis of variables such as oxygen isotopes of carbonate materials, carbon and nitrogen isotopes of organic matter, and trace element geochemistry becomes challenging, if not impossible. How much weight should be assigned to natural climate change to account for shifts in these variables? If shifts in these variables can be attributed to human activity, what type of activity can account for the nature of the observed changes? These questions can only be approached with an integrated, interdisciplinary framework (**Figure 7-2)**. For example, previous work at Xing Yun by Hodell et al., 1999 observed many of the same shifts in lake hydrologic balance that this study found. However, they were incorrectly attributed to natural climate variability rather than anthropogenic manipulation. Furthermore, lacking an appropriate historical context, the shifts in hydrologic balance observed at Chenghai may appear to be climatically driven when instead they are the result of dam construction. A recognition and understanding of how human activities may impact and/or bias paleoclimate records requires further work using this integrated framework.

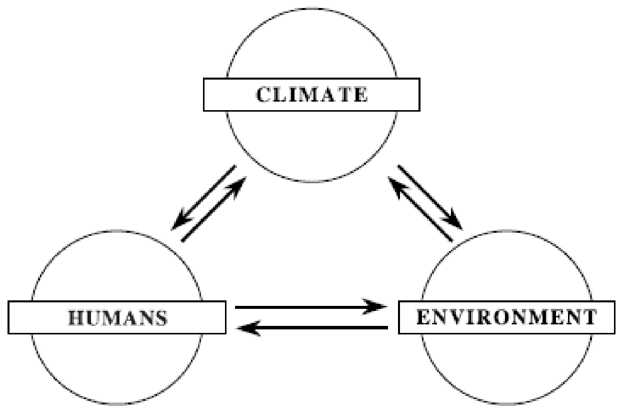

Figure 7-2- The conceptual framework integrating humans, climate, and the environment (Brenner et al., 2002).

In regards to research question 3- "**What role has hydroclimatic change played in human settlement and subsistence practices?"**, we determined that anthropogenic modification of lake hydrological balance prior to the 20th century was substantial. We may speculate that this was driven by the need for control of vital freshwater resources for agriculture, possibly in response to hydroclimate variability, but we cannot definitively make this link due to the lack of appropriate archaeological and historical context. Similar to previous researchers (Binford et al., 2000; Buckley et al., 201; Cullen et al., 2000; Hodell et al., 2001; Zhang et al., 2008a), we find that making the connection between climate change and social change is often limited by a lack of unambiguous proxy data wherein anthropogenically driven shifts can be straightforwardly separated from natural climate variability. As climate, especially monsoonally driven climate, is spatially variable, we also find that a lack of nearby paleoclimate records presents chronological control challenges that other past human-environmental studies have been challenged by. The possibility of new, independent lines of evidence, such as the abundance of fecal 5β-stanols (organic compounds deriving from feces of higher mammals) as an estimate for human populations (D'Anjou et al., 2012) or the use of the hydrogen isotopic composition of terrestrial leaf waxes, unaffected by human influence but abundant in lakes as recorders of the isotopic composition of precipitation (Sachse et al., 2012), may resolve these challenges in the future.

Future work beyond this dissertation is to enhance regional models of human-environmental interactions by increasing the spatial resolution of sediment cores to other lakes such as Qilu, Yang Zong, or Lugu (**Figure 1-1**) and extend the temporal resolution in lakes such as Chenghai. Additionally, the possibility of utilizing techniques such as the abundance of fecal 5β-stanols coupled to estimates of hydroclimate change in the same sediment sequence offers great potential to make a direct link between drivers of eutrophication and hydrologic change. The ultimate aim of future research is to develop widely applicable analytical frameworks that can be employed in other regions around the world.

BIBLIOGRAPHY

Abbott, M.B., Stafford, T.W., 1996. Radiocarbon Geochemistry of Modern and Ancient Arctic Lake Systems, Baffin Island, Canada. Quaternary Research 45, 300-311.

Abbott, M.B., Wolfe, A.P., 2003. Intensive pre-Incan metallurgy recorded by lake sediments from the Bolivian Andes. Science 301, 1893-1895.

Abram, N.J., Gagan, M.K., Cole, J.E., Hantoro, W.S., Mudelsee, M., 2008. Recent intensification of tropical climate variability in the Indian Ocean. Nature Geoscience 1, 849-853.

Abram, N.J., Gagan, M.K., Liu, Z., Hantoro, W.S., McCulloch, M.T., Suwargadi, B.W., 2007. Seasonal characteristics of the Indian Ocean Dipole during the Holocene epoch. Nature 445, 299-302.

Abram, N.J., McGregor, H.V., Gagan, M.K., Hantoro, W.S., Suwargadi, B.W., 2009. Oscillations in the southern extent of the Indo-Pacific Warm Pool during the mid-Holocene. Quaternary Science Reviews 28, 2794-2803.

Allard, F., 1998. Stirrings at the Periphery: History, Archaeology, and the Study of Dian. International Journal of Historical Archaeology 2.

Allen, C.R., Gillespie, A.R., Han, Y., Sieh, K.E., Zhang, B., Zhu, C., 1984. Red River and associated faults, Yunnan Province, China: Quaternary geology, slip rates, and seismic hazard. Geological Society of America Bulletin 95, 685-700.

Allen, C.R., Zhuoli, L., Hong, Q., Xueze, W., Huawei, Z., Weishi, H., 1991. Field study of a highly active fault zone: The Xianshuihe fault of southwestern China. Geological Society of America Bulletin 103, 1178-1199.

Amundson, R., Austin, A.T., Schuur, E.A., Yoo, K., Matzek, V., Kendall, C., Uebersax, A., Brenner, D., Baisden, W.T., 2003. Global patterns of the isotopic composition of soil and plant nitrogen. Global Biogeochemical Cycles 17, 1031.

Appleby, P., Oldfield, F., 1983. The assessment of ^{210}Pb data from sites with varying sediment accumulation rates. Hydrobiologia 103, 29-35.

Araguás-Araguás, L., Froehlich, K., Rozanski, K., 1998. Stable isotope composition of precipitation over southeast Asia. Journal of Geophysical Research 103, 28721.

Berger, A.L., 1978. Long-Term Variations of Daily Insolation and Quaternary Climatic Changes. Journal of Atmospheric Science 35, 2362-2367.

Berkelhammer, M., Sinha, A., Mudelsee, M., Cheng, H., Edwards, R.L., Cannariato, K.G., 2010. Persistent multidecadal power of the Indian Summer Monsoon. Earth and Planetary Science Letters 290, 166-172.

Berkelhammer, M., Sinha, A., Stott, L.D., Cheng, H., Pausata, F.S.R., Yoshimura, K., 2012. An Abrupt Shift in the Indian Monsoon 4000 Years Ago. American Geophysical Union.

Beyer, W.N., Auget, D.J., Morton, A., Campbell, J.K., LeCaptain, L., 1998. Lead Exposure of Waterfowl Ingesting Coeur d'Alene River Basin Sediments. Journal of environmental quality 27, 1533-1538.

Bindler, R., Yu, R., Hansson, M., Claben, N., Karlsson, J., 2012. Mining, Metallurgy and the Historical Origin of Mercury Pollution in Lakes and Watercourses in Central Sweden. Environmental Science and Technology 46, 7984-7991.

Binford, M.W., Brenner, M., Whitmore, T.J., Higuera-Gundy, A., Deevey, E.S., Leyden, B.W., 1987. Ecosystem, paleoecology, and human disturbance in subtropical and tropical Americ. Quaternary Science Reviews 6, 115-128.

Binford, M.W., Kahl, J.S., Norton, S.A., 1993. Interpretation of ^{210}Pb profiles and verification of the CRS dating model in PIRLA project lake sediment cores. Journal of Paleolimnology 9, 275-296.

Binford, M.W., Kolata, A.L., Brenner, M., Janusek, J.W., Seddon, M.T., Abbott, M., Curtis, J.H., 2000. Climate Variation and the Rise and Fall of an Andean Civilization. Quaternary Research 47, 235-248.

Bird, B.W., Polisar, P.J., Lei, Y., Thompson, L.G., Yao, T., Finney, B.P., Bain, D.J., Pompeani, D.P., Steinman, B.A., 2014. A Tibetan lake sediment record of Holocene Indian summer monsoon variability. Earth and Planetary Science Letters 399, 92-102.

Blaauw, M., 2010. Methods and code for “classical” age-modeling of radiocarbon sequences. Quaternary Geochronology 5, 512-518.

Boës, X., Rydberg, J., Martinez-Cortizas, A., Bindler, R., Renberg, I., 2011. Evaluation of conservative lithogenic elements (Ti, Zr, Al, and Rb) to study anthropogenic element enrichments in lake sediments. Journal of Paleolimnology 46, 75-87.

Bond, G., Showers, W., Cheseby, M., Lotti, R., Almasi, P., DeMenocal, P.B., Priore, P., Cullen, H., Hajdas, I., Bonani, G., 1997. A Pervasive Millennial-Scale Cycle in North Atlantic Holocene and Glacial Climates. Science 278, 1257-1266.

Bowen, G.J., 2013. The Online Isotopes in Precipitation Calculator, version 2.2. http://www.waterisotopes.org.

Boyle, J.F., 2002. Inorganic Geochemical Methods in Palaeolimnology, in: Last, W.M., Smol, J.P. (Eds.), Tracking Environmental Change Using Lake Sediments. Kluwer Academic Publishers, Dordrecht, The Netherlands.

Bray, F., 1986. The Rice Economies. Basin Blackwell Inc., New York.

Brenner, M., 1983. Paleolimnology of the Petén Lake district, Guatemala. II. Mayan population density and sediment and nutrient loading of Lake Quexil. Hydrobiologia 103, 205-210.

Brenner, M., Dorsey, K., Xueliang, S., Zuguan, W., Ruihua, L., Binford, M.W., Whitmore, T.J., Moore, A.M., 1991. Paleolimnology of Qilu Hu, Yunnan Province, China. Hydrobiologia 214, 333-340.

Brenner, M., Rosenmeier, M.F., Hodell, D.A., Curtis, J.H., 2002. Paleolimnology of the Maya Lowlands. Ancient Mesoamerica 13, 141-157.

Brenner, M., Whitmore, T.J., Curtis, J.H., Hodell, D.A., Schelske, C.L., 1999. Stable isotope ($\delta^{13}C$ and $\delta^{15}N$) signatures of sedimented organic matter as indicators of historic lake trophic state. Journal of Paleolimnology 22, 205-221.

Broecker, W., Bond, G., Klas, M., Clark, E., McManus, J., 1992. Origin of the northern Atlantic's Heinrich events. Climate Dynamics 6, 265-273.

Buckley, B.M., Anchukaitis, K.J., Penny, D., Fletcher, R., Cook, E.R., 201. Climate as a Contributing Factor in the DEmise of Angkor, Cambodia. Proceedings of the National Academy of Sciences of the United States of America 107, 6748-6752.

Bureau of Geology and Mineral Resources of Yunnan Province, 1990. Regional geology of Yunnan Province. Geological Publishing House, Beijing.

Cai, Y., An, Z., Cheng, H., Edwards, R.L., Kelly, M.J., Liu, W., Wang, X., Shen, C.C., 2006. High-resolution absolute-dated Indian Monsoon record between 53 and 36 ka from Xiaobailong Cave. Geology 5, 512-518.

Cai, Y., Zhang, H., Cheng, H., An, Z., Lawrence Edwards, R., Wang, X., Tan, L., Liang, F., Wang, J., Kelly, M., 2012. The Holocene Indian monsoon variability over the southern Tibetan Plateau and its teleconnections. Earth and Planetary Science Letters 335-336, 135-144.

Camarero, L., Masque, P., Devos, W., Ani-Ragolta, I., Catalan, J., Moor, H.C., Pla, S., Sanchez-Cabeza, J.A., 1998. Historical Variations in Lead Fluxes in the Pyrenees (Northeast Spain) from a Dated Lake Sediment Core. Water, Air, and Soil Pollution 105, 436-449.

Canarache, A., Vintila, I.I., Munteanu, I., 2006. Elsevier's Dictionary of Soil Science: Definitions in English with French, German, and Spanish word translations. Elsevier.

Carson, J.F., Whitney, B.S., Mayle, F.E., Iriarte, J., Prumers, H., Soto, J.D., Watling, J., 2014. Environmental impact of geometric earthwork construction in pre-Columbian Amazonia. Proceedings of the National Academy of Sciences of the United States of America 111, 10497-10502.

Center for International Earth Science Information Network, 2000. China Population Density, Gridded Population of the World (GPW), Version 2. CIESIN, Palisades, NY.

Chang, X., Zhu, B., 2002. Isotope Geochemistry of the Dongchuan Copper Deposit, Yunnan, SW China: Stratigraphic Chronology and Application of Lead Isotopes in Geochemical Exploration. Chinese Journal of Geochemistry 21, 65-72.

Chen, J., Wan, G.J., Wang, F., Zhang, D.D., Huang, R., Zhang, F., Schmidt, R., 2002. Environmental Records of Carbon in Recent Lake Sediments. Science in China Series D 45, 875-884.

Chen, X., Chen, F., Zhou, A., Huang, X., Tang, L., Wu, D., Zhang, X., Yu, J., 2014. Vegetation history, climatic changes and Indian summer monsoon evolution during the Last Glaciation (36,400–13,400 cal yr BP) documented by sediments from Xingyun Lake, Yunnan, China. Palaeogeography, Palaeoclimatology, Palaeoecology 410, 179-189.

Cheng, H., Sinha, A., Wang, X., Cruz, F.W., Edwards, R.L., 2012a. The Global Paleomonsoon as seen through speleothem records from Asia and the Americas. Climate Dynamics 39, 1045-1062.

Cheng, Y., Mao, J., Rusk, B., Yang, Z., 2012b. Geology and genesis of Kafang Cu–Sn deposit, Gejiu district, SW China. Ore Geology Reviews 48, 180-196.

Chiou-Peng, T., 2008. Dian Bronze Art: Its Source and Formation. Bulletin of the Indo-Pacific Prehistory Association 34-43.

Chiou-Peng, T., 2009. Incipient metallurgy in Yunnan: new data for old debates, in: Mei, J., Rehren, T. (Eds.), Metallurgy and Civilisation: Eurasia and Beyond. Archetype, London.

Chiou-Peng, T., 2011. The Technical History of Early Asian Kettledrums, in: Bunker, E., Latchford, D. (Eds.), Khmer Bronze Masterpieces:new interpretations of the past. Art Media Resources, Chicago, pp. 17-25.

Clemens, S.C., Prell, W.L., Sun, Y., 2010. Orbital-scale timing and mechanisms driving Late Plesitocene Indo-Asian summer monsoons: Reinterpreting cave speleothem $\delta^{18}O$. Paleoceanography 25.

Cohen, A.S., 2003. Paleolimnology: The History and Evolution of Lake Systems. Oxford University Press, Yew York.

Cook, C.G., Jones, R.T., Langdon, P.G., Leng, M.J., Zhang, E., 2011. New insights on Late Quaternary Asian palaeomonsoon variability and the timing of the Last Glacial Maximum in southwestern China. Quaternary Science Reviews 30, 808-820.

Cook, C.G., Leng, M.J., Jones, R.T., Langdon, P.G., Zhang, E., 2012. Lake ecosystem dynamics and links to climate change inferred from a stable isotope and organic palaeorecord from a mountain lake in southwestern China (ca. 22.6–10.5 cal ka BP). Quaternary Research 77, 132-137.

Cooke, C.A., Balcom, P.H., Biester, H., Wolfe, A.P., 2009. Over three millennia of mercury pollution in the Peruvian Andes. Proceedings of the National Academy of Sciences of the United States of America 106, 8830–8834.

Cosford, J., Qing, H., Yuan, D., Zhang, M., Holmden, C., Patterson, W., Hai, C., 2008. Millennial-scale variability in the Asian monsoon: Evidence from oxygen isotope records from stalagmites in southeastern China. Palaeogeography, Palaeoclimatology, Palaeoecology 266, 3-12.

Craine, J.M., Elmore, A.J., Aidar, M.P., Bustamante, M., Dawson, T.E., Hobbie, E.A., Kahmen, A., Mack, M.C., McLauchlan, K.K., Michelsen, A., Nardoto, G.B., Pardo, L.H., Penuelas, J., Reich, P.B., Schuur, E.A., Stock, W.D., Templer, P.H., Virginia, R.A., Welker, J.M., Wright, I.J., 2009. Global patterns of foliar nitrogen isotopes and their relationships with climate, mycorrhizal fungi, foliar nutrient concentrations, and nitrogen availability. New Phytologist 183, 980-992.

Cui, J., 2014, personal communication.

Cui, J., Wu, X., 2008. Provenance Study of Bronze Artifacts Unearthed from Yunnan Province, China and Vietnam (*in Chinese*). Wenwu Press.

Cullen, H.M., deMenocal, P.B., Hemming, S., Hemming, G., Brown, F.H., Guilderson, T., Sirocko, F., 2000. Climate change and the collapse of the Akkadian empire: Evidence from the deep sea. Geology 28, 379-382.

D'Anjou, R.M., Bradley, R.S., Balascio, N.L., Finkelstein, D.B., 2012. Climate impacts on human settlement and agricultural activities in northern Norway revealed through sediment biogeochemistry. Proceedings of the National Academy of Sciences of the United States of America 109, 20332-20337.

Dai, Z., Zhang, Z., 1998. A brief excavation report on the Chongzipipo ore smelting site at Gejiu (*in Chinese*). Yunnan Wenwu 46, 8-10.

Davidson, W., 1993. Iron and manganese in lakes. Earth-Science Reviews 34, 119-163.

Dayem, K.E., Molnar, P., Battisti, D.S., Roe, G.H., 2010. Lessons learned from oxygen isotopes in modern precipitation applied to interpretation of speleothem records of paleoclimate from eastern Asia. Earth and Planetary Science Letters 295, 219-230.

Dean, W.E., 1974. Determination of carbonate and organic matter in calcareous sediments and sedimentary rocks by loss on ignition: comparison with other methods. Journal of Sedimentary Petrology 44, 242-248.

Dean, W.E., 1999. The carbon cycle and biogeochemical dynamics in lake sediments. Journal of Paleolimnology 21, 375-393.

Dearing, J.A., 1999. Environmental Magnetic Susceptibility Using the Bartington MS2 System, 2nd ed.

Dearing, J.A., Jones, R.T., Shen, J., Yang, X., Boyle, J.F., Foster, G.C., Crook, D.S., Elvin, M.J.D., 2008. Using multiple archives to understand past and present climate–human–environment interactions: the lake Erhai catchment, Yunnan Province, China. Journal of Paleolimnology 40, 3-31.

Deevey, E.S., Gross, M.S., Hutchinson, G., Kraybill, H.L., 1954. The natural C14 contents of materials from hard-water lakes. Geology 40, 285-288.

deMenocal, P.B., Rind, D., 1993. Sensitivity of Asian and African Climate to Variations in Seasonal Insolation, Glacial Ice Cover, Sea Surface Temperature, and Asian Orography. Journal of Geophysical Research 98, 7265-7287.

DiNezio, P.N., Tierney, J.E., 2013. The effect of sea level on glacial Indo-Pacific climate. Nature Geoscience 6, 485-491.

Downing, J.A., McCauley, E., 1992. The nitrogen: phosphorus relationship in lakes. Limnology and Oceanography 37, 936-945.

Durand, J.D., 1960. The Population Statistics of China, A.D. 2-1953. Population Studies 13, 209-256.

Dykoski, C., Edwards, R., Cheng, H., Yuan, D., Cai, Y., Zhang, M., Lin, Y., Qing, J., An, Z., Revenaugh, J., 2005. A high-resolution, absolute-dated Holocene and deglacial Asian monsoon record from Dongge Cave, China. Earth and Planetary Science Letters 233, 71-86.

Elliott, E.M., Brush, G.S., 2006. Sedimented Organic Nitrogen Isotopes in Freshwater Wetlands Record Long-Term Changes in Watershed Nitrogen Source and Land Use. Environmental Science and Technology 40, 2910-2916.

Elvin, M.J.D., Crook, D.S., Shen, J., Jones, R.T., Dearing, J.A., 2002. The Impact of Clearance and Irrigation on the Environment in the Lake Erhai Catchment from the Ninth to the Nineteenth Century. East Asian History 23, 1-60.

England, P., Molnar, P., 1990. Right-lateral shear and rotation as the explanation for strike-slip faulting in eastern Tibet. Nature 334, 140-142.

Fengrang, Z., 1990. Soil Map of the People's Republic of China, in: FAO/UNSECO Soil Map of the World. State Land Administration, China, Beijing Agricultural University.

Ferrat, M., Weiss, D.J., Strekopytov, S., Dong, S., Chen, H., Najorka, J., Sun, Y., Gupta, S., Tada, R., Sinha, R., 2011. Improved provenance tracing of Asian dust sources using rare earth elements and selected trace elements for palaeomonsoon studies on the eastern Tibetan Plateau. Geochimica et Cosmochimica Acta 75, 6374-6399.

Fleitmann, D., Burns, S., Mudelsee, M., Neff, U., Kramers, J., Mangini, A., Matter, A., 2003. Holocene Forcing of the Indian Monsoon Recorded in a Stalagmite from Southern Oman. Science 300, 1737-1739.

Fleitmann, D., Burns, S.J., Mangini, A., Mudelsee, M., Kramers, J., Villa, I., Neff, U., Al-Subbary, A.A., Buettner, A., Hippler, D., Matter, A., 2007. Holocene ITCZ and Indian monsoon dynamics recorded in stalagmites from Oman and Yemen (Socotra). Quaternary Science Reviews 26, 170-188.

Fuller, D.Q., 2012. Pathways to Asian Civilizations: Tracing the Origins and Spread of Rice and Rice Cultures. Rice 4, 78-92.

Gallon, C., Tessier, A., Gobeil, C., Alfaro-De La Torre, M.C., 2004. Modeling diagenesis of lead in sediments of a Canadian Shield lake. Geochimica et Cosmochimica Acta 68, 3531-3545.

Galman, V., Rydberg, J., Bigler, C., 2009. Decadal diagenetic effects on $\delta^{13}C$ and $\delta^{15}N$ studied in varved lake sediment. Limnology and Oceanography 54, 917-924.

Galman, V., Rydberg, J., de-Luna, S.S., Bindler, R., Renberg, I., 2008. Carbon and nitrogen loss rates during aging of lake sediment: Changes over 27 years studied in varved lake sediment. Limnology and Oceanography 53, 1076-1082.

Gasse, F., Fontes, J.C., Van Campo, E., Wei, K., 1996. Holocene environmental changes in Bangong Co basin (Western Tibet). Part 4: Discussion and conclusions. Palaeogeography, Palaeoclimatology, Palaeoecology 120, 79-92.

Giersch, 2009. Asian borderlands: the transformation of Qing China's Yunnan frontier. Harvard University Press, Boston.

Golas, P.J., 1999. Science and Civilisation in China: Volume 5- Chemistry and Chemical Technology, Part 13- Mining. Cambridge University Press, Cambridge.

Graney, J., Halliday, A., Keeler, G., Nriagu, J., Robbins, J., Norton, S., 1995. Isotopic record of lead pollution in lake sediments from the northeastern United States. Geochemica et Cosmochimica Acta 59, 1715-1728.

Gu, Z., Liu, J., Yuan, B., Liu, T., Liu, R., Liu, Y., Zhang, G., 1993. The changes in monsoon influence in the Qinghai-Tibetan Plateau during the past 12,000 years. Geochemical evidence from the L. Selin sediments. Chinese Science Bulletin 38, 61-64.

Guo, J.Y., Wu, F.C., Liao, H.Q., Zhao, X.L., Li, W., Wang, J., Wang, L.F., Giesy, J.P., 2013. Sedimentary record of polycyclic aromatic hydrocarbons and DDTs in Dianchi Lake, an urban lake in Southwest China. Environmental science and pollution research international 20, 5471-5480.

Gupta, A.K., Anderson, D.M., Overpeck, J.T., 2002. Abrupt changes in the Asian southwest monsoon during the Holocene and their links to the North Atlantic Ocean. Nature 421.

Hamilton-Taylor, J., Davison, W., 1978. Redox-Driven Cycling of Trace Elements in Lakes, in: Lerman, A., Imboden, D.M., Gat, J.R. (Eds.), Physics and Chemistry of Lakes, 2nd ed. Springer-Verlag, New York.

Hammarlund, D., Aravena, R., Bernekow, L., Buchardt, B., Possnert, G., 1997. Multi-component carbon isotope evidence of early Holocene environmental change and carbon-flow pathways from a hard-water lake in northern Sweden. Journal of Paleolimnology 18, 219-233.

Han, R., Ke, J., 2007. History of Technology in China: Mining and Ore Processing (*in Chinese*). Science Press, Beijing.

Herman, J., 2002. The Mongol Conquest of Dali: The Failed Second Front, in: Cosmo, N.D. (Ed.), Warfare in Inner Asian History (500-1800). Brill, Boston.

Herzschuh, U., 2006. Palaeo-moisture evolution in monsoonal Central Asia during the last 50,000 years. Quaternary Science Reviews 25, 163-178.

Higham, C., 1996. The Bronze Age of Southeast Asia. Cambridge University Press, Cambridge.

Higham, C., Higham, T., Ciarla, R., Douka, K., Kijngam, A., Rispoli, F., 2011. The Origins of the Bronze Age of Southeast Asia. Journal of World Prehistory 24, 227-274.

Hillman, A.L., Abbott, M.B., Yu, J.Q., Bain, D.J., Chiou-Peng, T., 2015. The Environmental Legacy of Copper Metallurgy and Mongol Silver Smelting Recorded in Yunnan Lake Sediments.

Hillman, A.L., Yu, J., Abbott, M.B., Cooke, C.A., Bain, D.J., Steinman, B.A., 2014. Rapid environmental change during dynastic transitions in Yunnan Province, China. Quaternary Science Reviews 98, 24-32.

Hodell, D.A., Brenner, M., Curtis, J.H., Guilderson, T., 2001. Solar Forcing of Drought Frequency in the Maya Lowlands. Science 292, 1367-1370.

Hodell, D.A., Brenner, M., Kanfoush, S.L., Curtis, J.H., Stoner, J.S., Xueliang, S., Yuan, W., Whitmore, T.J., 1999. Paleoclimate of Southwestern China for the Past 50,000 yr Inferred from Lake Sediment Records. Quaternary Research 52, 369-380.

Hodell, D.A., Schelske, C.L., 1998. Production, Sedimentation, and Isotopic Composition of Organic Matter in Lake Ontario. Limnology and Oceanography 43, 200-214.

Hollander, D.J., McKenzie, J.A., Ten Haven, H.L., 1992. A 200 year sedimentary record of progressive eutrophication in Lake Greifen (Switzerland): implications for the origin of organic-carbon-rich sediments. Geology 20, 825-829.

Hou, Z., Zaw, K., Pan, G., Mo, X., Xu, Q., Hu, Y., Li, X., 2007. Sanjiang Tethyan metallogenesis in S.W. China: Tectonic setting, metallogenic epochs and deposit types. Ore Geology Reviews 31, 48-87.

Hu, C., Henderson, G.M., Huang, J., Xie, S., Sun, Y., Johnson, K.R., 2008. Quantification of Holocene Asian monsoon rainfall from spatially separated cave records. Earth and Planetary Science Letters 266, 221-232.

Huybers, P., Wunch, C., 2004. A depth-derived Pleistocene age model: Uncertainty estimates, sedimentation variability, and nonlinear climate change. Paleoceanography 19, PA1028.

Hyodo, M., Yoshihara, A., Kashiwaya, K., Okimura, T., Masuzawa, T., Nomura, R., Tanaka, S., Xing, T.B., Qing, L.S., Jian, L.S., 1999. A Late Holocene geomagnetic secular variation record from Erhai Lake, southwest China. Geophysical Journal International 136, 784-790.

IAEA/WMO, 2014. Global Network of Isotopes in Precipitation. The GNIP Database. www.iaea.org/water.

International Soil Reference and Information Centre, Majors Soils of the World- Luvisols.

Ito, E., 2001. Application of Stable Isotope Techniques to Inorganic and Biogenic Carbonates, in: Last, W.M., Smol, J.P. (Eds.), Tracking Environmental Change Using Lake Sediments. Volume 2: Physical and Geochemical Methods. Kluwer Adaemic Publishers, Dordrecht, The Netherlands.

Jin, Z., Li, X., Zhang, B., Han, Y., Zheng, G., 2013. Geochemical records in Holocene lake sediments of northern China: Implication for natural and anthropogenic inputs. Quaternary International 304, 200-208.

Jinglu, W., Gagan, M.K., Xuezhong, J., Weilan, X., Sumin, W., 2004. Sedimentary geochemical evidence for recent eutrophicatio of Lake Chenghai, Yunnan, China. Journal of Paleolimnology 32, 85-94.

Jinglu, W., Sumin, W., Weilan, X., 2003. Isotopic Tracing of Trophication Processes over the Last Millennia on Lake Chenghai. Chinese Journal of Geochemistry 22, 271-279.

Kamitani, M., Okumura, K., Teraoka, Y., Miyano, S., Watanabe, Y., 2007. Mineral Resources Map of East Asia. Geological Survey of Japan, AIST.

Kearney, P., Klepeis, K.A., Vine, F.J., 2009. Global Tectonics. Wiley-Blackwell, West Sussex, UK.

Kelts, K.R., Hsu, K.J., 1978. Freshwater Carbonate Sedimentation, in: Lerman, A. (Ed.), Lakes: Chemistry, Geology, Physics. Springer-Verlag, New York.

Kendall, C., Elliott, E.M., Wankel, S.D., 2007. Tracing anthropogenic inputs of nitrogen to ecosystems, in: Lajtha, K., Michener, R.H. (Eds.), Stable Isotopes in Ecology and Environmental Science, 2nd ed. Blackwell Scientific Publications.

Kim, S.-T., O'Neil, J.R., 1997. Equilibrium and nonequilibrium oxygen isotope effects in synthetic carbonates. Geochemica et Cosmochimica Acta 61, 3461-3475.

Kim, S.-T., O'Neil, J.R., Hillaire-Marcel, C., Mucci, A., 2007. Oxygen isotope fractionation between synthetic aragonite and water: Influence of temperature and Mg2+ concentration. Geochemica et Cosmochimica Acta 71, 4704-4715.

King, R.W., Shen, F., Burchfiel, B.C., Royden, L.H., Wang, E., Chen, Z., Liu, Y., Zhang, X.-Y., Zhao, J.-X., Li, Y., 1997. Geodetic measurement of crustal motion in southwest China. Geology 25, 179-182.

Kottek, M., Grieser, J., Beck, C., Rudolf, B., Rubel, F., 2006. World map of the Koppen-Geiger climate classification updated. Meteorologische Zeitschrift 15, 259-263.

Krishnan, R., Sugi, M., 2003. Pacific decadal oscillation and variability of the Indian summer monsoon rainfall. Climate Dynamics 21, 233-242.

Kumar, K.K., Rajagopalan, B., Cane, M.A., 1999. On the Weakening Relationship Between the Indian Monsoon and ENSO. Science 284, 2156.

Lal, M., Nozawa, T., Emori, S., Harasawa, H., Takahashi, K., Kimoto, M., Abe-Ouchi, A., Nakajima, T., Takemura, T., Numaguti, A., 2011. Future climate change: Implications for Indian summer monsoon and its variability. Current Science 81, 1196-1207.

Lawrimore, J.H., Menne, M.J., Gleason, B.E., Williams, C.N., Wuertz, D.B., Vose, R.S., Rennie, J., 2011. An overview of the Global Historical Climatology Network monthly mean temperature data set, version 3. Journal of Geophysical Research 116.

Lecce, S., Pavlowsky, R., Schlomer, G., 2007. Mercury contamination of active channel sediment and floodplain deposits from historic gold mining at Gold Hill, North Carolina, USA. Environmental Geology 55, 113-121.

Lee, C.S.L., Qi, S.-H., Zhang, G., Luo, C.-L., Zhao, L.Y.L., Li, X.-D., 2008. Seven Thousand Years of Records on the Mining and Utilization of Metals from Lake Sediments in Central China. Environmental Science and Technology 42, 4732–4738.

Lee, J., 1982. Food Supply and Population Growth in Southwest China, 1250-1850. The Journal of Asian Studies 41, 711-746.

Leeming, R., Nichols, P.D., 1996. Concentrations of coprostanol that correspond to existing bacterial indicator guideline limits. Water research 30, 2997-3006.

LeGrande, A.N., Schmidt, G.A., 2009. Sources of Holocene variability of oxygen isotopes in paleoclimate archives. Climate of the Past 5, 441-455.

Leng, M.J., Marshall, J.D., 2004. Palaeoclimate interpretation of stable isotope data from lake sediment archives. Quaternary Science Reviews 23, 811-831.

Li, H.-C., Ku, T.-L., 1997. $\delta^{13}C$-$\delta^{18}O$ covariance as a paleohydrological indicator for closed-basin lakes. Palaeogeography, Palaeoclimatology, Palaeoecology 133, 69-80.

Li, R., Dong, M., Zhao, Y., Zhang, L., Cui, Q., He, W., 2007. Assessment of water quality and identification of pollution sources of plateau lakes in Yunnan (China). Journal of environmental quality 36, 291-297.

Li, X., Walker, D., 1986. The plant geography of Yunnan Province, southwest China. Journal of Biogeography 13, 367-397.

Lima, A.L., Hubeny, J.B., Reddy, C.M., King, J.W., Hughen, K.A., Eglinton, T.I., 2005. High-resolution historical records from Pettaquamscutt River basin sediments: 1. ^{210}Pb and varve chronologies validate record of ^{137}Cs released by the Chernobyl accident. Geochimica et Cosmochimica Acta 69, 1803-1812.

Lin, S., Qiao, Y., Walker, D., 1986. Late Pleistocene and Holocene vegetation history at Xi Hu, Er Yuan, Yunnan Province, southwest China. Journal of Biogeography 13, 419-440.

Lister, G.S., Kelts, K.R., Zao, C.K., Yu, J.Q., Niessen, F., 1991. Lake Qinghai, China: closed-basin like levels and the oxygen isotope record for ostracoda since the latest Pleistocene. Palaeogeography, Palaeoclimatology, Palaeoecology 84, 141-162.

Liu, W., Li, S., Bu, H., Zhang, Q., Liu, G., 2012. Eutrophication in the Yunnan Plateau lakes: the influence of lake morphology, watershed land use, and socioeconomic factors. Environmental science and pollution research international 19, 858-870.

Liu, W., Zhang, Q., Liu, G., 2010. Lake eutrophication associated with geographic location, lake morphology and climate in China. Hydrobiologia 644, 289-299.

Liu, Z., Wen, X., Brady, E.C., Otto-Bliesner, B., Yu, G., Lu, H., Cheng, H., Wang, Y., Zheng, W., Ding, Y., Edwards, R.L., Cheng, J., Liu, W., Yang, H., 2014. Chinese cave records and the East Asia Summer Monsoon. Quaternary Science Reviews 83, 115-128.

Lu, D., Wang, D., 1998. Metallurgy and Metal Artifacts in Ancient China (*in Chinese*). Shanxi Science and Technology Press.

Lu, S., Wang, S., Chen, Y., 2015. Palaeopedogenesis of red palaeosols in Yunnan Plateau, southwestern China: Pedogenical, geochemical and mineralogical evidences and palaeoenvironmental implication. Palaeogeography, Palaeoclimatology, Palaeoecology 420, 35-48.

MacDonald, D.D., Ingersoll, C.G., Berger, T.A., 2000. Development and Evaluation of Consensus-Based Sediment Quality Guidelines for Freshwater Ecosystems. Enviranrnental Contamination and Toxicology 39, 20-31.

Maher, B.A., Thompson, R., 2012. Oxygen isotopes from Chinese caves: records not of monsoon rainfall but of circulation regime. Journal of Quaternary Science 27, 615-624.

Mann, M.E., Zhang, Z., Rutherford, S., Bradley, R., Hughes, M.K., Shindell, D., Ammann, C., Faluvegi, G., Ni, F., 2009. Global Signatures and Dynamical Origins of the Little Ice Age and Medieval Climate Anomaly. Science 326, 1256-1260.

Marchitto, T.M., Muscheler, R., Ortiz, J.D., Carriquiry, J.D., van Geen, A., 2010. Dynamical response of the tropical Pacific Ocean to solar forcing during the early Holocene. Science 330, 1378-1381.

Marcott, S.A., Shakun, J.D., Clark, P.U., Mix, A.C., 2013. A Reconstruction of Regional and Global Temperature for the Past 11,300 Years. Science 339, 1198-1201.

Marks, R.B., 2012. China Its Environment and History. Rowman and Littlefield Publishers, Inc., Lanham, Maryland.

McKenzie, J.A., 1985. Carbon isotopes and productivity in the lacustrine and marine environment, in: Stumm, W. (Ed.), Chemical Processes in Lakes. Wiley, New York.

Meng, C.-Y., Li, W.Y.L., 1970. Geologic Map of the Republic of China. Chinese Petroleum Corporation.

Meyers, P., 1994. Preservation of elemental and isotopic source identification of sedimentary organic matter. Chemical Geology 114, 289-302.

Meyers, P., Laillier-verges, E., 1999. Lacustrine sedimentary organic matter records of Late Quaternary paleoclimates. Journal of Paleolimnology 21, 345-372.

Min, R., 2013. An Overview of the Haimenkou site in Jianchuan (*in Chinese*). Xueyuan 15, 6-9.

Molnar, P., Tapponnier, P., 1975. Cenozoic Tectonics of Asia: Effects of a Continental Collison. Science 189, 419-426.

Morrill, C., Overpeck, J.T., Cole, J.E., 2003. A synthesis of abrupt changes in the Asian summer monsoon since the last deglaciation. The Holocene 13, 465-476.

Morrill, C., Overpeck, J.T., Cole, J.E., Liu, K.-b., Shen, C., Tang, L., 2006. Holocene variations in the Asian monsoon inferred from the geochemistry of lake sediments in central Tibet. Quaternary Research 65, 232-243.

Moy, C.M., Seltzer, G.O., Rodbell, D.T., Anderson, D.M., 2002. Variability of El Nino Southern Oscillation activity at millennial timescales during the Holocene epoch. Nature 402, 162-165.

Murowchick, R.E., 1989. The Ancient Bronze Metallurgy of Yunnan and its Environs: Development and Implications, Anthropology. Harvard University, Ann Arbor, Michigan, p. 490.

Needham, J., Gwei-Djen, L., 1971. Science and Civilisation in China: Volume 4- Physics and Physical Technology, Part 2- Spagyrical Discovery and Invention: Magisteries of Gold and Immortality. Cambridge University Press, Cambridge.

Neff, U., Burns, S., Mangini, A., Mudelsee, M., Fleitmann, D., Matter, A., 2001. Strong coherence between solar variability and the monsoon in Oman between 9 and 6 kyr ago. Nature 411, 290-293.

Nowlin, W.H., Evarts, J.L., Vanni, M.J., 2005. Release rates and potential fates of nitrogen and phosphorus from sediments in a eutrophic reservoir. Freshwater Biology 50, 301-322.

Nriagu, J., 1989. A global assessment of natural sources of atmospheric trace metals. Nature 338, 47-49.

O'Hara, S.L., Street-Perrott, F.A., Burt, T.B., 1993. Accelerated soil erosion around a Mexican highland lake caused by prehistoric agriculture. Nature 362, 48–51.

Peterson, T.C., Vose, R.S., 1997. An overview of the Global Historical Climatology Network temperature database. Bulletin of the American Meteorlogical Society 78, 2837-2849.

Pirajno, F., 2013. The Geology and Tectonic Settings of China's Mineral Deposits. Springer, New York.

Polissar, P.J., Freeman, K.H., 2010. Effects of aridity and vegetation on plant-wax δD in modern lake sediments. Geochimica et Cosmochimica Acta 74, 5785-5797.

Pompeani, D.P., Abbott, M., Steinman, B., Bain, D.J., 2013. Lake Sediments Record Prehistoric Lead Pollution Related to Early Copper Production in North America. Environmental Science and Technology 47, 5545-5552.

Reimann, C., De Caritate, P., 2000. Intrinsic Flaws of Element Enrichment Factors (EFs) in Environmental Geochemistry. Environmental Science and Technology 34, 5084-5091.

Reimer, P., Baillie, M., Bard, E., Bayliss, A., Beck, J., Blackwell, P., Ramsey, C., Buck, C., Burr, G., Edwards, R., Friedrich, M., Grootes, P., Guilderson, T., Hajdas, T., Hogg, A., Hughen, K., Kaiser, K., Kromer, B., McCormac, F., Manning, S., Reimer, R., Richards, D., Southon, J., Talamo, S., Turney, C., van der Plicht, J., Weyhenmeyer, C., 2009. IntCal09 and Marine09 radiocarbon age calibration curves, 0-50,000 years cal BP. Radiocarbon 51, 1111-1150.

Reimer, P.J., Bard, E., Bayliss, A., Beck, J.W., Blackwell, P.G., Ramsey, C.B., Buck, C.E., Cheng, H., Edwards, R.L., Friedrich, M., Grootes, P.M., Guilderson, T.P., Haflidason, H., Hajdas, I., Hatté, C., Heaton, T.J., Hoffmann, D.L., Hogg, A.G., Hughen, K.A., Kaiser, K.F., Kromer, B., Manning, S.W., Niu, M., Reimer, R.W., Richards, D.A., Scott, E.M., Southon, J.R., Staff, R.A., Turney, C.S.M., Plicht, J.v.d., 2013. INTCAL13 and Marine 13 Radiocarbon Age Calibration Curves 0–50,000 years CAL BP. Radiocarbon 55, 1869-1887.

Rein, B., Lückge, A., Reinhardt, L., Sirocko, F., Wolf, A., Dullo, W.-C., 2005. El Niño variability off Peru during the last 20,000 years. Paleoceanography 20.

Renberg, I., Persson, M.W., Emteryd, O., 1994. Pre-industrial atmospheric lead contamination detected in Swedish lake sediments. Nature 368, 323-326.

Rosenmeier, M.F., Hodell, D.A., Brenner, M., Curtis, J.H., Guilderson, T.P., 2002. A 4000-Year Lacustrine Record of Environmental Change in the Southern Maya Lowlands, Petén, Guatemala. Quaternary Research 57, 183-190.

Royden, L.H., Burchfiel, B.C., van der Hilst, R.D., 2008. The Geological Evolution of the Tibetan Plateau. Science 321, 1054-1058.

Sachse, D., Billault, I., Bowen, G.J., Chikaraishi, Y., Dawson, T.E., Feakins, S.J., Freeman, K.H., Magill, C.R., McInerney, F.A., van der Meer, M.T.J., Polissar, P., Robins, R.J., Sachs, J.P., Schmidt, H.-L., Sessions, A.L., White, J.W.C., West, J.B., Kahmen, A., 2012. Molecular Paleohydrology: Interpreting the Hydrogen-Isotopic Composition of Lipid Biomarkers from Photosynthesizing Organisms. Annual Review of Earth and Planetary Sciences 40, 221-249.

Schelske, C.L., Hodell, D.A., 1995. Using Carbon Isotopes of Bulk Sedimentary Organic Matter to Reconstruct the History of Nutrient Loading and Eutrophication in Lake Erie. Limnology and Oceanography 40, 918-929.

Schindler, D.W., Wolfe, A.P., Vinebrooke, R., Crowe, A., Blais, J.M., Miskimmin, B., Freed, R., Perren, B., 2008. The cultural eutrophication of Lac la Biche, Alberta, Canada: a paleoecological study. Canadian Journal of Fisheries and Aquatic Sciences 65, 2211-2223.

Schoenbohm, L.M., Burchfiel, B.C., Liangzhong, C., Jiyun, Y., 2006. Miocene to present activity along the Red River fault, China, in the context of continental extrusion, upper-crustal rotation, and lower-crustal flow. Geological Society of America Bulletin 118, 672-688.

Searle, M.P., Yeh, M.W., Lin, T.H., Chung, S.L., 2010. Structural constraints on the timing of left-lateral shear along the Red River shear zone in the Ailao Shan and Diancang Shan Ranges, Yunnan, SW China. Geosphere 6, 316-338.

Shen, J., Jones, R.T., Yang, W., Dearing, J.A., Wang, S., 2006. The Holocene vegetation history of Lake Erhai, Yunnan province southwestern China: the role of climate and human forcings. The Holocene 16, 265-276.

Shen, J., Yang, L., Yang, X., Matsumoto, R., Tong, G., Zhu, Y., Wang, S., 2005. Lake sediment records on climate change and human activities since the Holocene in Erhai catchment, Yunnan Province, China. Science in China Series D 48, 353.

Sinha, A., Cannariato, K.G., Stott, L.D., Cheng, H., Edwards, R.L., Yadava, M.G., Ramesh, R., Singh, I.B., 2007. A 900-year (600 to 1500 AD) record of the Indian summer monsoon precipitation from the core monsoon zone of India. Geophysical Research Letters 34.

Sinha, A., Cannariato, K.G., Stott, L.D., Li, H.-C., You, C.-F., Cheng, H., Edwards, R.L., Singh, I.B., 2005. Variability of Southwest Indian summer monsoon precipitation during the Bølling-Ållerød. Geology 33, 813-816.

Song, Z., Zhang, J., Jiang, X., Wang, C., Xie, Z., 2013. Population structure of an endemic gastropod in Chinese plateau lakes: evidence for population decline. Freshwater Science 32, 450-461.

Steinman, B., Rosenmeier, M.F., Abbott, M.B., Bain, D.J., 2010. The isotopic and hydrologic response of small, closed basin lakes to climate forcing from predictive models: application to paleoclimate studies in the upper Columbia River basin. Limnology and Oceanography 55, 2231-2245.

Steinman, B.A., Abbott, M.B., 2013. Isotopic and hydrologic responses of small, closed lakes to climate variability: Hydroclimate reconstructions from lake sediment oxygen isotope records and mass balance models. Geochimica et Cosmochimica Acta 105, 342-359.

Stott, L.D., Cannariato, K.G., Thunell, R., Haug, G.H., Koutavas, A., Lund, S., 2004. Decline of surface temperature and salinity in the western tropical Pacific Ocean in the Holocene epoch. Nature 431, 52-59.

Stott, L.D., Timmerman, A., Thunell, R., 2007. Southern Hemisphere and Deep-Sea Warming Led Deglacial Atmospheric CO2 Rise and Tropical Warming. Science 318.

Sun, X., Wu, Y., Qiao, Y., Walker, D., 1986. Late Pleistocene and Holocene Vegetation History at Kunming, Yunnan Province, Southwest China. Journal of Biogeography 13, 441-476.

Talbot, M.R., 1990. A review of the palaeohydrological interpretation of carbon and oxygen isotopic ratios in primary lacustrine carbonates. Chemical Geology 80, 261-279.

Talbot, M.R., 2001. Nitrogen Isotopes in Paleolimnology, in: Last, W.M., Smol, J.P. (Eds.), Tracking Environmental Change Using Lake Sediments: Volume 2 Physical and Geochemical Methods. Kluwer Academic Publishers, Dordrecht, The Netherlands.

Talbot, M.R., Livingstone, D.A., Palmer, P.G., Maley, J.M., Melack, G., Delibrias, G., Guilliksen, S., 1984. Preliminary results from sediment cores from Lake Bosumtwi, Ghana. Palaeoecology of Africa 16, 173-192.

Taylor, R.E., 1978. Radiocarbon Dating: An Archaeological Perspective, Archaeological Chemistry II. American Chemical Society, pp. 33-69.

R Core Development Team, 2008. R: A language and environment for statistical computing.

Thomas, E.K., Huang, Y., Morrill, C., Zhao, J., Wegener, P., Clemens, S.C., Colman, S.M., Gao, L., 2014. Abundant C4 plants on the Tibetan Plateau during the Lateglacial and early Holocene. Quaternary Science Reviews 87, 24-33.

Thompson, L.G., Mosley-Thompson, E., Davis, M.E., Bolzan, J.F., Dai, J., Yao, T., Gundestrup, N., Wu, X., Klein, L., Xie, Z., 1989. Holocene--Late Pleistocene Climatic Ice Core Records from Qinghai-Tibetan Plateau. Science 246, 474-477.

Thompson, L.G., Yao, T., Davis, M.E., Henderson, K.A., Mosley-Thompson, E., Lin, P.-N., Beer, J., Synal, H.-A., Cole-Dai, J., Bolzan, J.F., 1998. Tropical Climate Instability: The Last Glacial Cycle from a Qinghai-Tibetan Ice Core. Science 276, 1821-1825.

Tokalioğlu, S., Kartal, S., Elci, L., 2000. Determination of heavy metals and their speciation in lake sediments by flame atomic absorption spectrometry after a four-stage sequential extraction procedure. Analytica Chimica Acta 413, 33-40.

Trimble, S.W., 1983. A Sediment Budget for Coon Creek Basin in the Driftless Area, Wisconsin. American Journal of Science 283, 454-474.

Turner, A.G., Annamalai, H., 2012. Climate change and the South Asian summer monsoon. Nature Climate Change 2, 587-595.

Wan, G.J., Chen, J.A., Wu, F.C., Xu, S.Q., Bai, Z.G., Wan, E.Y., Wang, C.S., Huang, R.G., Yeager, K.M., Santschi, P.H., 2005. Coupling between $^{210}Pb_{ex}$ and organic matter in sediments of a nutrient-enriched lake: An example from Lake Chenghai, China. Chemical Geology 224, 223-236.

Wan, J., 2013. Prehistoric cultures in the Canger Area (*in Chinese*). Wenwu Press, Beijing.

Wang, B., Clemens, S.C., Liu, P., 2003. Contrasting the Indian and East Asian monsoons: implications on geologic timescales. Marine Geology 201, 5-21.

Wang, E., Burchfiel, B.C., 1997. Interpretation of Cenozoic tectonics in the right-lateral accommodation zone between the Ailao Shan shear zone and the Eastern Himalaya syntaxis. International Geology Review 39, 191-219.

Wang, E., Burchfiel, B.C., Royden, L.H., Liangzhong, C., Jishen, C., Wenxin, L., Zhiliang, C., 1998. Late Cenozoic Xianshuihe-Xiaojiang, Red River, and Dali fault systems of southwestern Sichuan and central Yunnan, China: Special Paper of the Geological Society of America, Geological Society of America.

Wang, F., Wan, G.J., Liu, C., Xu, S.Q., 2002. The Correlation of Inorganic C, O Isotopic Values for Lake Chenghai Sediments and Its Environmental Implications. Chinese Journal of Geochemistry 21, 186-192.

Wang, J., 1994. Chorography of Jiangchuan County (*in Chinese*). Publishing House of Yunnan Province, Kunming.

Wang, L., Li, J., Lu, H., Gu, Z., Rioual, P., Hao, Q., Mackay, A.W., Jiang, W., Cai, B., Xu, B., Han, J., Chu, G., 2012a. The East Asian winter monsoon over the last 15,000 years: its links to high-latitudes and tropical climate systems and complex correlation to the summer monsoon. Quaternary Science Reviews 32, 131-142.

Wang, Q., Yang, X., Anderson, N.J., Zhang, E., Li, Y., 2014. Diatom response to climate forcing of a deep, alpine lake (Lugu Hu, Yunnan, SW China) during the Last Glacial Maximum and its implications for understanding regional monsoon variability. Quaternary Science Reviews 86, 1-12.

Wang, R., Dearing, J.A., Langdon, P.G., Zhang, E., Yang, X., Dakos, V., Scheffer, M., 2012b. Flickering gives early warning signals of a critical transition to a eutrophic lake state. Nature 492, 419-422.

Wang, X., Yu, S., Huang, G.H., 2004. Land allocation based on integrated GIS-optimization modeling at a watershed level. Landscape and Urban Planning 66, 61-74.

Wang, Y., Cheng, H., Edwards, R.L., He, Y., Kong, X., An, Z., Wu, J., Kelly, M.J., Dykoski, C.A., Li, X., 2005. The Holocene Asian monsoon: links to solar changes and North Atlantic climate. Science 308, 854-857.

Wang, Y., Cheng, H., Edwards, R.L., Kong, X., Shao, X., Chen, S., Wu, J., Jiang, X., Wang, X., An, Z., 2008. Millennial- and orbital-scale changes in the East Asian monsoon over the past 224,000 years. Nature 451, 1090-1093.

Wang, Y.J., Cheng, H., Edwards, R.L., An, Z.S., Wu, J.Y., Shen, C.C., Dorale, J.A., 2001. A high-resolution absolute-dated late Pleistocene Monsoon record from Hulu Cave, China. Science 294, 2345-2348.

Weiss, D.J., Shotyk, W., Appleby, P., Kramers, J., Cheburkin, A.K., 1999. Atmospheric Pb Deposition since the Industrial Revolution Recorded by Five Swiss Peat Profiles: Enrichment Factors, Fluxes, Isotopic Composition, and Sources. Environmental Science and Technology 33, 1340-1352.

White, J.C., Hamilton, E.G., 2009. The Transmission of Early Bronze Technology to Thailand: New Perspectives. Journal of World Prehistory 22, 357-397.

Whitmore, T.J., Brenner, M., Engstrom, D.R., Xueliang, S., 1994a. Accelerated soil erosion in watersheds of Yunnan Province, China. Journal of Soil and Water Conservation 49, 67-72.

Whitmore, T.J., Brenner, M., Jiang, Z., Curtis, J.H., Moore, A.M., Engstrom, D.R., Yu, W., 1997. Water quality and sediment geochemistry in lakes of Yunnan Province, southern China. Environmental Geology 32, 45-55.

Whitmore, T.J., Brenner, M., Xueliang, S., 1994b. Environmental implications of the late Quaternary diatom history from Xingyun Hu, Yunnan Province, China, in: Kociolek, J. (Ed.), Proceedings of the 11th International Diatom Symposium. California Academy of Sciences.

Wright, H., Mann, D., Glaser, P., 1984. Piston corers for peat and lake sediments. Ecology 65, 657-659.

Xu, S.Q., Zheng, G., 2003. Variations in radiocarbon ages of various organic fractions in core sediments from Erhai Lake, SW China. Geochemical Journal 37, 135-144.

Xue, B., Wu, L., 2002. Studies of Historical Data Concerning Exploitation of Silver (Lead)- Zinc Deposits in Yunnan Province and Some Opinions on Further Mineral Exploration (*in Chinese*). Mineralium Deposita 21, 298-303.

Xue, C., Zeng, R., Liu, S., Chi, G., Qing, H., Chen, Y., Yang, J., Wang, D., 2007. Geologic, fluid inclusion and isotopic characteristics of the Jinding Zn–Pb deposit, western Yunnan, South China: A review. Ore Geology Reviews 31, 337-359.

Yancheva, G., Nowaczyk, N.R., Mingram, J., Dulski, P., Schettler, G., Negendank, J.F., Liu, J., Sigman, D.M., Peterson, L.C., Haug, G.H., 2007. Influence of the intertropical convergence zone on the East Asian monsoon. Nature 445, 74-77.

Yang, B., 2009. Between winds and clouds: the making of Yunnan (second century BCE to twentieth century CE). Columbia University Press, New York.

Yang, X., Shen, J., Jones, R.T., Wang, S., Tong, G., Zhang, Z., 2005. Pollen evidence of early human activities in Erhai basin, Yunnan Province. Chinese Science Bulletin 50, 568-577.

Yang, Y.H., Zhou, F., Guo, H.C., Sheng, H., Liu, H., Dao, X., He, C.J., 2010. Analysis of spatial and temporal water pollution patterns in Lake Dianchi using multivariate statistical methods. Environmental monitoring and assessment 170, 407-416.

Yao, A., 2010. Recent Developments in the Archaeology of Southwestern China. Journal of Archaeological Research 18, 203-239.

Yao, A., Zhilong, J., 2012. Rediscovering the settlement system of the “Dian” kingdom, in Bronze Age southern China. Antiquity 86, 353-367.

Yu, G., Harrison, S.P., Xu, B., 2001. Lake status records from China: Data Base Documentation.

Yu, G., Xue, B., Liu, J., Chen, X., 2003. LGM lake records from China and an analysis of climate dynamics using a modelling approach. Global and Planetary Change 38, 223-256.

Yunnan Provincial Institute of Cultural Relics and Archaeology, 2009a. Excavation of the Yinsuodao site at Haidong in Dali City (*in Chinese*). Kaogu 8, 23-41.

Yunnan Provincial Institute of Cultural Relics and Archaeology, 2009b. The Third excavation of the Haimenkou site in Jianchuan (*in Chinese*). Kaogu 8, 3-22.

Yuan, D., Cheng, H., Edwards, R.L., Dykoski, C.A., Kelly, M.J., Zhang, M., Qing, J., Lin, Y., Wang, Y., Wu, J., Dorale, J.A., An, Z., Cai, Y., 2004. Timing, duration, and transitions of the last interglacial Asian monsoon. Science 304, 575-578.

Zeng, H.-A., Wu, J.-L., 2009. Sedimentary Records of Heavy Metal Pollution in Fuxian Lake, Yunnan Province, China: Intensity, History, and Sources. Pedosphere 19, 562-569.

Zhang, H., Li, S., Feng, Q., Zhang, S., 2010. Environmental change and human activities during the 20^{th} century reconstructed from the sediment of Xingyun Lake, Yunnan province, China. Quaternary International 212, 14-20.

Zhang, J., Chen, F., Holmes, J.A., Li, H., Guo, X., Wang, J., Li, S., Lü, Y., Zhao, Y., Qiang, M., 2011. Holocene monsoon climate documented by oxygen and carbon isotopes from lake sediments and peat bogs in China: a review and synthesis. Quaternary Science Reviews 30, 1973-1987.

Zhang, P., Cheng, H., Edwards, R.L., Chen, F., Wang, Y., Yang, X., Liu, J., Tan, M., Wang, X., Liu, J., An, C., Dai, Z., Zhou, J., Zhang, D., Jia, J., Jin, L., Johnson, K.R., 2008a. A Test of Climate, Sun, and Culture Relationships from an 1810-Year Chinese Cave Record. Science 322, 940-942.

Zhang, Q., Wang, D., Zhu, X., Zhang, Z., Zhu, C., 2009. Lead isotopic systematics for native copper-chalcocite mineralization in basaltic lavas of the Emeishan large igneous province, SW China: Implications for the source of copper. Chinese Journal of Geochemistry 28, 1-18.

Zhang, Q., Zhu, X., Zhang, Z., 2006. Lead isotopic composition and lead source of the Tongchanghe basalt-type native copper-chalcocite deposit in Ninglang, western Yunnan, China. Chinese Journal of Geochemistry 25, 112-121.

Zhang, X., Wang, Y., Lei, H., 1996. Authigenic mineralogy, depositional environments and evolution of fault-bounded lakes of the Yunnan Plateau, south-western China. Sedimentology 43, 367-380.

Zhang, Y., Gao, X., Zhong, Z., Deng, X., Peng, B., 2008b. Comprehensive evaluation of heavy metal contamination of sediment in Lake Dianchi by using modified AHP method and ^{137}Cs dating. Frontiers of Environmental Science & Engineering in China 2, 370-379.

Zhang, Z., 2000. History of Yunnan Metallurgy (*in Chinese*). Yunnan Fine Arts Publishing House, Kunming.

Zhang, Z., Zhao, M., Yang, X., Wang, S., Jiang, X., Oldfield, F., Eglinton, G., 2004. A hydrocarbon biomarker record for the last 40 kyr of plant input to Lake Heqing, southwestern China. Organic Geochemistry 35, 595-613.

Zhisheng, A., Clemens, S.C., Shen, J., Qiang, X., Jin, Z., Sun, Y., Prell, W.L., Luo, J., Wang, S., Xu, H., Cai, Y., Zhou, W., Liu, X., Liu, W., Shi, Z., Yan, L., Xiao, X., Chang, H., Wu, F., Ai, L., Lu, F., 2011. Glacial-interglacial Indian summer monsoon dynamics. Science 333, 719-723.

Zhou, C., Wei, C., Guo, J., Li, C., 2001. The Source of Metals in the Qilinchang Zn-Pb Deposit, Northeastern Yunnan, China: Pb-Sr Isotope Constraints. Economic Geology 96, 583-598.

Zhou, W., Martinón-Torres, M., Chen, J., Liu, H., Li, Y., 2012. Distilling zinc for the Ming Dynasty: the technology of large scale zinc production in Fengdu, southwest China. Journal of Archaeological Science 39, 908-921.

Zhu, Z., Chen, J.a., Zeng, Y., Li, H., Yan, H., Ren, S., 2011. Research on the carbon isotopic composition of organic matter from Lake Chenghai and Caohai Lake sediments. Chinese Journal of Geochemistry 30, 107-113.